THE EFFECTS OF A VORTEX FIELD ON FLAMES WITH FINITE REACTION RATES

Thesis by
Olin Perry Norton

In Partial Fulfillment

of the Requirements for the Degree of

Doctor of Philosophy

California Institute of Technology

Pasadena, California

1983

(Submitted August 9, 1982)

ACKNOWLEDGEMENTS

First, I would like to thank my thesis advisor, Dr. Frank E. Marble, for direction and encouragement in this work. The numerical work in this thesis would not have been possible had not the Space and Defense Systems Group of TRW made available their extensively modified version of the BLOTTNER program. The program was converted to run on the Caltech computer by Kiku Matsumoto of the computing center staff. I am also indebted to Dr. J. E. Broadwell for extensive discussions on the *HF* reaction system and the use of the computer program.

The text was prepared on the word processor system with the advice and assistance of the staff of the computing center and Drs. Malladi Subbaiah, Chris Catherasoo, Ben Conner, Ann Karagozian, and K. Ravi Chandar.

The author's graduate study has been supported by a fellowship from the National Science Foundation and by various assistantships from the California Institute of Technology. This research has been supported in part by grants from the United States Air Force (AFOSR-80-0265) and the National Aeronautics and Space Administration (NAG-3-70).

Finally, encouragement and moral support from my parents, John and Jean Norton, family, and friends were especially welcome. The author thanks Dorothy Eckerman for her friendship, encouragement, and willingness to listen.

ABSTRACT

A diffusion flame, supported by a one-step chemical reaction, is initiated along the horizontal axis between a fuel occupying the upper half-plane and an oxidizer below. Simultaneously, a vortex of circulation Γ is established at the origin. As time progresses the flame is extended and "wound up" by the vortex flow field. The effect of distortion of the flame is locally described by the time-dependent straining of a one-dimensional flame. The rate of chemical reaction is represented by the characteristic chemical reaction time, t_{ch}, of the system. The combustion field then consists of a totally reacted core region and an external flame region consisting of a pair of spiral arms extending off at large radii toward their original positions.

The presence of the vortex increases the rate of fuel consumption of the flame. For large values of $\frac{\Gamma}{D}$, the augmentation of fuel consumption due to the vortex is proportional to $\rho\Gamma^{\frac{2}{3}}D^{\frac{1}{3}}$, and is a function of $\frac{t}{t_{ch}}$ which approaches a constant value as $t \to \infty$. The growth of the fuel consumption rate from zero to its steady value for large times is governed by the time scale t_{ch}. If the products of combustion occupy more volume than the original reactants, then the spiral flame will appear as an unsteady volume dilitation for times on the order of the chemical time. An unsteady volume dilitation acts as an acoustic source, so the interaction of a vortex and a diffusion flame is shown to result in the generation of a pressure pulse; the peak pressure occurring after a delay proportional to the chemical time, and the strength of the pulse proportional to $\Gamma^{\frac{2}{3}}D^{\frac{1}{3}}$ and inversely proportional to $\sqrt{t_{ch}}$.

These results are valid for hypergolic reaction systems in which the reactant temperature does not significantly effect the rates of the chemical

reactions. For systems described as having "large activation energy", the rates are strongly temperature dependent and another description is appropriate. For these systems, a vortex established on an already ignited flame exhibits, in addition to the features described above, an extinct core of unburned reactants if the circulation of the vortex is large.

The results provide the fundamental structure for the mechanism of combustion instability proposed by Rogers and Marble in 1956.

TABLE OF CONTENTS

LIST OF FIGURES AND TABLES

LIST OF MATHEMATICAL SYMBOLS

Lower Case Roman Letters

Symbol	Description
a	distance from vortex to flame
c	speed of sound
c_p	specific heat
d	initial flame spacing
k	reaction rate, usually a function of temperature
k_b	backward reaction rate
k_f	forward reaction rate
k_0	a constant in the Arrhenius reaction rate expression, equation 3.25
l	a measure of distance along the flame
$\dot{m}$	rate of fuel consumption per unit area of flame surface
$\dot{m}_0$	in chapter six, the value of $\dot{m}$ as if only one flame were present, ignoring interactions with adjacent flames
p	$\Gamma t/\pi r^2$; dimensionless time
p'	$\Gamma t'/\pi r^2$
p^*	$\Gamma t^*/\pi r^2$
p_{ch}	$\Gamma t_{ch}/\pi r^2$
q	$\Gamma^{\frac{2}{3}} D_0^{\frac{1}{3}} t/\pi r^2$; dimensionless time
q'	$\Gamma^{\frac{2}{3}} D_0^{\frac{1}{3}} t'/\pi r^2$
q^*	$\Gamma^{\frac{2}{3}} D_0^{\frac{1}{3}} t^*/\pi r^2$
q_{ch}	$\Gamma^{\frac{2}{3}} D_0^{\frac{1}{3}} t_{ch}/\pi r^2$

r	radius; the distance from the vortex to a given piece of the flame
r^*	the time-dependent radius of the burned-out core
r_{arms}	the radius of the spiral flame structure
r_{ext}	the time-dependent radius of the extinct core
$r_{ext\ max}$	the maximum extent of the extinct core
r_0	the initial value of r
t	time
t'	the time when $\bar{\tau}$ exceeds t_{ch}
t''	a dummy variable of integration
$\hat{t}$	$\pi a^2/\Gamma^{\frac{2}{3}} D_0^{\frac{1}{3}}$; the characteristic time for the influence of the vortex to spread a distance a
$\tilde{t}$	in chapter six, the time at which $\frac{\delta}{\Delta}$ exceeds $\sqrt{\pi/2}/4$
$_*t$	$\frac{t}{t_{ch}}$; dimensionless time
t^*	the time at which the fuel at a given radius is exhausted; the burnout time
t_{ch}	the characteristic chemical time
t_{diff}	the characteristic time required for reactants to diffuse into the reaction zone
t_{ext}	the time when extinction occurs at a given radius
$t_{ext\ max}$	the time when the extinct core reaches its maximum radius
t_{min}	in chapter eight, the time when $\bar{\tau}$ reaches a minimum
t_{osc}	in chapter seven, the period of acoustic oscillations
t_0	in chapter eight, the initial age of the flame before straining begins

u	x component of velocity
u_i	x component of the flux of the i^{th} species
u_n	in the numerical solutions of chapter four, the value of u at y_n
u_r	r component of velocity
u_θ	θ component of velocity
v	y component of velocity
v_{Di}	the part of v^i due to molecular diffusion of the i^{th} species relative to the bulk fluid
v_i	y component of the flux of the i^{th} species
μ_f	coefficient for power-law dependence of reaction intensity w on the concentration of fuel
w	local reaction intensity; the rate of consumption of reactants and creation of products due to chemical reaction
w_i	rate of creation or destruction of the i^{th} species due to chemical reaction
w_o	rate of consumption of oxidizer
x	usually, the coordinate axis parallel to the flame surface; in chapter seven, the distance from the vortex line to an observer
y	the coordinate axis normal to the flame surface
y'	dummy variable of integration
y_n	in the numerical calculations of chapter four, the value of y at the n^{th} mesh point
z	in chapter seven, distance measured along the axis of the vortex

Upper Case Roman Letters

Symbol	Description
A_n	n^{th} Fourier coefficient

C	volume of reaction products in the burned-out core
$\dot{C}$	rate of growth of the volume of reaction products in the burned-out core
D	molecular diffusivity
D_0	constant reference value of D
F_0, F_1, F_2	numerical coefficients which describe the temperature dependence of the forward reactions listed in table 4.1, see equation 4.1
G_0, G_1, G_2	numerical coefficients which describe the temperature dependence of the backward reactions listed in table 4.1, see equation 4.2
K	the equilibrium coefficient
L	length
$\dot{M}$	the increase in the rate of fuel consumption attributed to the vortex
$P - P_0$	in the acoustic calculations of chapter seven, the pressure increase due to the unsteady rate of fuel consumption of the vortex-flame interaction
$(P - P_0)_{max}$	in the acoustic calculations of chapter seven, the maximum intensity of the pressure pulse
Q	the rate at which volume is being created by the vortex-flame interaction
$\dot{Q}$	the time derivative of Q
R	remainder term
Re	$\Gamma/2\pi\nu$; Reynolds number of the vortex
Sc	ν/D; the Schmidt number
T	temperature
T_a	a measure of the activation energy of a reaction, see equation 3.25
T_f	the adiabatic flame temperature
T_∞	the constant temperature of both reactants far from the flame

U	in the mixing layer problem, the equal velocities of the upper and lower streams, may be a function of x
U_0	freestream velocity for mixing layers in which the two streams have constant and equal velocities
Y_A	mass fraction of species A
Y_B	mass fraction of species B
Y_f	fuel mass fraction
$Y_{f\infty}$	constant fuel mass fraction far from the flame
Y_i	ρ_i/ρ; mass fraction of the i^{th} species
Y_o	oxidizer mass fraction
$Y_{o\infty}$	constant oxidizer mass fraction far from the flame

Lower Case Greek Letters

Symbol	Description
α	ratio of the final volume of combustion products to the original volume of the reactants
β	$t_{ch}/\hat{t}$
γ	$\zeta/\sqrt{D_0\bar{\tau}}$; similarity coordinate
${}_*\gamma$	${}_*\zeta/\sqrt{{}_*\bar{\tau}}$; dimensionless similarity coordinate
δ	$\sqrt{D_0\bar{\tau}}$; flame thickness
δ_0	in chapter eight, the initial thickness of the flame before straining begins
δl	a small increment in l
$\delta\lambda$	a small increment in λ
ε	the strain rate, usually a function of time
${}_*\varepsilon$	εt_{ch}; dimensionless strain rate
ζ	$\xi\, e^{\int_0^t \varepsilon(t'')\, dt''}$; transformed y coordinate

$_*\zeta$ $\zeta/\sqrt{D_0 t_{ch}}$; dimensionless ζ

η $\pi^{\frac{1}{2}} r/\Gamma^{\frac{1}{3}} D_0^{\frac{1}{6}} t^{\frac{1}{2}}$; transformed radius

η^* $\pi^{\frac{1}{2}} r^*/\Gamma^{\frac{1}{3}} D_0^{\frac{1}{6}} t^{\frac{1}{2}}$; transformed radius of the burned-out core

θ angular coordinate of a given piece of the flame, in polar coordinates, see figure 2.3

θ^* the angle at which the burned-out core intersects the original flame position, see figure 5.7

θ_0 initial angular coordinate of a given piece of the of the flame

κ the curvature of the flame surface

λ a Lagrangian coordinate which identifies a particular piece of the flame; in chapter one, the position of a given piece of flame, given by r and θ, is considered to be a function of λ and t

λ^* the value of λ corresponding to the burned-out core radius; see figure 5.7

μ_f indicates dependence of w upon oxidizer concentration in a more general rate expression considered by Carrier *et al.*

μ_o indicates dependence of w upon oxidizer concentration in a more general rate expression considered by Carrier *et al.*

μ_T coefficient for power-law dependence of reaction rate on temperature; see equation 3.25

ν kinematic viscosity

ξ $\int_0^y \frac{\rho(y')}{\rho_0} dy'$; Howarth-transformed y coordinate

$_*\xi$ $\xi/\sqrt{D_0 t_{ch}}$; dimensionless ξ coordinate

ξ_{flame} the location of the thin reation zone in the ξ coordinate

ρ	bulk fluid density
ρ_i	concentration of species i
ρ_0	a constant reference value of the density, evaluated far from the flame
σ	the increase in flame surface caused by the vortex
τ	found from the equation $\frac{d\tau}{dt} = e^{2\int_0^t \varepsilon(t'')\,dt''}$; transformed time coordinate
${}_*\tau$	τ/t_{ch}; dimensionless τ
$\bar{\tau}$	$\tau\, e^{-2\int_0^t \varepsilon(t'')\,dt''}$; transformed time
${}_*\bar{\tau}$	$\bar{\tau}/t_{ch}$; dimensionless $\bar{\tau}$
$\bar{\tau}_{ext}$	in chapter eight, extinction occurs when $\bar{\tau}$ falls below this critical value
$\bar{\tau}_{min}$	in chapter eight, $\bar{\tau}$ decreases to a minimum and thereafter increases; $\bar{\tau}_{min}$ is this minimum value of $\bar{\tau}$
φ	$Y_f - Y_0$; Schvab-Zeldovitch variable
φ_1	$Y_A - Y_B$; Schvab-Zeldovitch variable
φ_2	$Y_A + Y_B + Y_C$; Schvab-Zeldovitch variable
φ_3	$Y_C - \Theta$; Schvab-Zeldovich variable
φ_4	Y_C; Schvab-Zeldovitch variable
ψ	$\frac{\pi\xi}{d} e^{-\int_0^t \varepsilon(t'')\,dt''}$; transformed variable of integration in equation 6.22
ω	frequency

Upper Case Greek Letters

Symbol	Description
Γ	the circulation of the vortex
ΔH	heat release of the reaction

Θ	dimensionless temperature defined by equation 8.1
$\hat{\Theta}_a$	T_a made dimensionless by $\frac{\Delta H}{c_p}$
$\hat{\Theta}_f$	T_f made dimensionless by $\frac{\Delta H}{c_p}$
$\hat{\Theta}_\infty$	T_∞ made dimensionless by $\frac{\Delta H}{c_p}$
Σ	flame density; surface area per unit volume

1. INTRODUCTION

The study of combustion, or of chemically reacting flows, may be conceptually divided into two parts: if the reactants are mixed before burning the process is referred to as a premixed flame, and if the reactants are initially separated and are transported to the reaction zone by molecular diffusion the process is referred to as a diffusion flame. This analysis is primarily concerned with diffusion flames.

Diffusion flames occur naturally in such primitive devices as candles, kerosene lamps, and wood fires. Technologically, diffusion flames constitute the main combustion mechanism in natural gas combustors, diesel engines, liquid spray combustion, and many types of chemical lasers.

Chemical reaction can occur only in regions where the reactants are intimately mixed on a molecular level, thus reaction in a laminar diffusion flame depends on simultaneous processes of interdiffusion and chemical reaction. Turbulence should increase the rate of reaction, because turbulent mixing augments the process of molecular diffusion. It has frequently been suggested (Damköhler (1939,1940), Shelkin (1943), Karlovitz *et al.* (1951), Scurlock and Grover (1952), and Marble and Broadwell (1977)) that some turbulent combustion processes may be described as a collection of laminar flame structures, which retain their identity but are distorted by the turbulence. This description is particularly suitable for at least the early phases of turbulent diffusion flames.

If one applies this idea to the problem of a single vortex interacting with an initially flat fuel-oxidizer interface, the velocity field will increase the total surface area of the flame. Thus, an increase in the total reaction rate would be expected, based on the increased area of the interface between the fuel and the

oxidizer. However, the increase in total surface area is the result of locally stretching each individual piece of the flame. This stretching may be expressed in terms of the strain rate, the proportional rate of increase of flame surface, a stretching of the flame sheet along the direction of the sheet which results in an inflow normal to the flame sheet. This velocity normal to the flame surface serves to augment the process of molecular diffusion, usually increasing the rate of reactant consumption per unit flame area. Thus, the velocity field will act to increase the overall reaction rate in two ways: by increasing the surface area of the flame, and by increasing the rate of reaction per unit area of flame surface.

To complicate matters, one finds that increasing the strain rate does not always increase the reactant consumption per unit flame area. Especially with strongly exothermic reactions with a chemical reaction rate which depends strongly on temperature, increasing the strain rate above a critical value causes the flame to go out. Even for reactions which do not show this abrupt extinction behavior, increasing the strain rate causes an increase in reactant consumption only to a certain point, with further increases in the strain rate causing a reduction in the reactant consumption rate per unit flame area.

Furthermore, creation of flame surface cannot continue without limit. Each flame surface really has a finite thickness, and if the flame surface area per unit volume were to increase indefinitely, then after a while the mean spacing between flame sheets would be less than the mean thickness of each sheet. Thus, one must include some mechanism to account for the influence of neighboring flames. This effect can be viewed another way, by noting that a given material volume contains only so much of each reactant. As the straining increases the flame area within this volume, and as these flames consume the reactants, eventually one reactant will be depleted. The rate of reaction must go

to zero when either reactant is depleted. Possibilities include: a flame shortening mechanism, which would offset the creation of flame surface due to straining with a flame destruction term, or an attenuation mechanism, which would express the diminution of the reactant consumption rate of each flame as a function of either closeness to its neighbors or the local depletion of reactants.

These three ideas: the increase in flame surface area due to straining, the effect of local straining on the rate of reactant consumption per unit flame area, and the reduction in reactant consumption per unit flame surface area as a function of increasing flame density (or of local depletion of reactants) are the basis of the analysis to follow.

In many technological circumstances, including chemical lasers and conventional gas burners, it is important to increase the rate at which chemical reaction takes place. In the latter this is done to reduce the volume which must be devoted to combustion; in the former, rapid combustion is essential to preserve the non-equilibrium molecular states required for lasing. On the basis of the turbulent flame model described earlier, one may encourage rapid combustion through extension of the active interfacial area between fuel and oxidizer. This may be accomplished by the introduction of vortex structures into the flowing gas, by means of vortex generators or otherwise, so aligned as to stretch the interface.

Marble (1982) has solved the problem of an initially flat flame sheet on which a vortex has been established. The viscosity of the fluid was included, and the chemical reactions were assumed to be infinitely fast, so the reaction rate was controlled by diffusion. The solution consisted of a burned out core, containing hot combustion products, where all available reactants had been consumed. Outside of the core, the flame sheet formed spiral arms which

wrapped around the core at smaller radii and remained in their original positions at larger radii. The solution showed similarity, the radius of the core increasing like $\sqrt{t}$. Marble also found that the presence of the vortex increased the reactant consumption rate of the flame above what it would have been if the vortex had not been present. This augmentation of the reactant consumption rate was found to be constant, independent of time.

Marble found that if the circulation of the vortex were large, in particular if

$$Re\sqrt{Sc} > 50 \qquad 1.1$$

where the Reynolds number $Re \equiv \frac{\Gamma}{2\pi\nu}$ and the Schmidt number $Sc \equiv \frac{\nu}{D}$, Γ being the vortex circulation, ν the kinematic viscosity, and D the molecular diffusivity, then the increase in the reactant consumption rate was proportional to $\Gamma^{\frac{2}{3}}D^{\frac{1}{3}}$ and the core radius was proportional to $\left[\Gamma^{\frac{2}{3}}D^{\frac{1}{3}}t\right]^{\frac{1}{2}}$ Thus, for large Reynolds number vortices, the solution is independent of ν and depends not on D and Γ separately, but rather on the combined transport coefficient $\Gamma^{\frac{2}{3}}D^{\frac{1}{3}}$.

In addition, Karagozian (1982) has extended Marble's analysis to include the effect of axially straining the vortex in the third dimension. Karagozian has also considered the density change due to the heat release of the reaction and its effect on the fuel consumption rate.

In this work the assumption of infinitely fast chemistry will be relaxed. In addition, the case where the vortex is displaced from the flame by a finite distance will be considered. To simplify the analysis, instead of the viscous vortex of Marble, for this analysis a potential vortex shall be assumed. Additionally, numerical results will be given for the limit $\frac{\Gamma}{D} \to \infty$; these assumptions will correspond to the large Re limit investigated by Marble.

The extinction of flames by straining will be briefly discussed, but the calculations will be limited by an inability to describe the ignition process. Finally, the generation of an acoustic pulse by a flame rolled up by a vortex will be described, with possible applications to combustion generated noise and certain types of combustion instability.

2. FLAME KINEMATICS

2.1 Introduction

The problem is to describe the interaction of a vortex and a diffusion flame in two dimensions. The vortex lies at the origin of the coordinate system. Viscosity will be neglected, so the velocity field will be taken from the potential flow solution for an isolated vortex in a medium at rest. The flame will be represented by a line; initially a straight line which passes within a distance a of the vortex. Locally, the flame will be convected with the fluid, so each point on the line moves with the local fluid velocity. As a result, the initially flat flame will be wound into a spiral; increasing the flame surface area and locally straining the flame.

The analysis is based on two fundamental assumptions. The first is that the flame may be treated as a material surface which is convected by the velocity field, each piece of the flame moving with the local fluid velocity. This assumption is satisfied for diffusion flames with a stoichiometry of unity. The second is that the reactant consumption rate of the flame per unit surface area is given by the results of a one dimensional analysis of strained laminar diffusion flames, which will be given in the next chapter. Since the analysis will be based on one dimensional strained flames, the radius of curvature of the flame must be large compared to its thickness, and concentration and temperature gradients along the flame must be small compared to gradients normal to the flame. The validity of these assumptions, as well as the importance of viscosity, will be examined in chapter six. In this chapter, the winding up of an initially flat flame by a potential vortex will be traced, and the increase in flame area and the local flame straining which result will be calculated.

For convenience, the two reactants will often be referred to as "fuel" and "oxidizer". It is understood that the problem is in two dimensions, therefore one may refer to the length of the line representing the flame as the "flame area", and areas in the plane may be called "volumes". To obtain a true area or volume, one must multiply the results by a length in the direction normal to the plane.

The initially flat flame, distorted by the vortex, will be wound into a spiral. Figure 2.1 shows the resulting spiral when the offset distance a is zero. Thus, the surface area of the flame will be increased with time. One objective of this chapter is to calculate this increase. Furthermore, as shown in the figure, this increase in total flame area is accomplished by locally stretching each infinitesimal piece of the flame. In later chapters, the rate of local stretching will be related to the fuel consumption rate per unit area of flame, so another objective is to calculate the rate of local straining of the flame surface.

In order to examine a tiny piece of the flame in detail, consider a coordinate system attached to the piece of flame, translating and rotating as the flame moves. Let the coordinate system translate such that the same piece of flame is always at the origin, and rotate such that the x axis is always tangent to the flame at the origin. The y axis will always be perpendicular to the flame at the origin. (Figure 2.2) Locally expand the velocity field about the origin in the (x,y) coordinate system. The x velocity component is,

$$u(x,y) \approx u\Big]_{(0,0)} + \frac{\partial u}{\partial x}\Big]_{(0,0)} x + \frac{\partial u}{\partial y}\Big]_{(0,0)} y + \cdots \qquad 2.1a$$

and the y component is,

$$v(x,y) \approx v\Big]_{(0,0)} + \frac{\partial v}{\partial x}\Big]_{(0,0)} x + \frac{\partial v}{\partial y}\Big]_{(0,0)} y + \cdots \qquad 2.1b$$

Since the coordinate system has been chosen such that the origin moves with

the local fluid velocity, $u\big]_{(0,0)} = 0$ and $v\big]_{(0,0)} = 0$. The coordinate system rotates such that the x axis is tangent to the flame, so $\left.\frac{\partial v}{\partial x}\right]_{(0,0)} = 0$. The x component of the velocity is unimportant because of the assumption that the flame is locally one dimensional. Only the y velocity component is of interest. The remaining term $\left.\frac{\partial v}{\partial y}\right]_{(0,0)}$ is equal to the negative of $\left.\frac{\partial u}{\partial x}\right]_{(0,0)}$ from the continuity equation.

Now, consider two points on the flame. Let one be at the origin and the other on the x axis a small distance δl from the origin. Since each point moves at the local fluid velocity, the separation distance δl will increase with time according to

$$\varepsilon \equiv \frac{1}{\delta l}\frac{d\,\delta l}{dt} = \left.\frac{\partial u}{\partial x}\right]_{(0,0)} \qquad 2.2$$

Here, ε is the strain rate of the flame, defined as the rate of increase of flame length per unit length. Thus, the creation of flame surface by stretching the flame along the x axis can be related to the velocity component perpendicular to the flame surface, since $v(x,y) \approx \left.\frac{\partial v}{\partial y}\right]_{(0,0)} y = -\left.\frac{\partial u}{\partial x}\right]_{(0,0)} y = -\varepsilon y$. If ε is the rate of strain of the flame surface, then the velocity component perpendicular to the flame is $v = -\varepsilon y$.

The velocity field about a piece of flame has been approximated with the lowest order terms in a local expansion, which is valid only over a short distance. Karagozian (1982) has noted that this expansion of the velocity field about the flame is similar to the boundary layer approximation, and is valid if the flame is thin compared to the scale of variations within the flow field. In addition, the flame has been taken to be locally flat; the curvature of the flame has been neglected and the flame is assumed to lie along the x axis, rather than merely being tangent to it at the origin. This is allowable only if the radius of

curvature of the flame is large compared to the flame thickness. Finally, if the gradients of concentration and temperature in the x direction are small compared to those in the y direction, one can neglect convection and diffusion in x and approximate each piece of flame as if it were a one dimensional (concentrations and temperatures are functions of y and the time t), transiently strained (with a normal velocity component v equal to $-\varepsilon(t)\, y$) diffusion flame. Furthermore, the function $\varepsilon(t)$ may be found by computing a purely geometrical quantity, the local rate of extension of the line representing the flame, expressed as the rate of change of length per unit length.

In this chapter, the creation of flame surface area and the transient local strain rate ε will be calculated. Chapters three and four will address the problem of predicting the fuel consumption rate per unit flame area of a one-dimensional, transiently strained diffusion flame. If one approximates each piece of the flame as a one-dimensional strained flame, these results can be combined to yield a description of the fuel consumption rate due to the interaction of the vortex and the flame.

2.2 Flame Surface Area and Strain Rate

In order to examine the convection of the flame in the velocity field surrounding a potential vortex, introduce polar coordinates with the potential vortex at the origin. Use the Lagrangian coordinate λ to label each piece of the flame as it is convected by the vortex field. (See figure 2.3.) The position of the flame (r, θ) is then a function of λ and the time t. Since each piece of flame is transported with the local fluid velocity,

$$\frac{\partial r}{\partial t} = u_r = 0 \qquad 2.3a$$

$$\frac{\partial \theta}{\partial t} = \frac{u_\theta}{r} = \frac{\Gamma}{2\pi r^2}$$

2.3b

If the initial position of the flame at $t = 0$ is denoted by $(r_0(\lambda),\theta_0(\lambda))$, the solution to equations 2.3 is,

$$r(\lambda,t) = r_0(\lambda) \qquad 2.4a$$

$$\theta(\lambda,t) = \theta_0(\lambda) + \frac{\Gamma t}{2\pi r_0^2(\lambda)} \qquad 2.4b$$

At any time, the distance along the flame separating two points designated λ_1 and λ_2 is

$$\int_{\lambda_1}^{\lambda_2} dl = \int_{\lambda_1}^{\lambda_2} (dr^2 + r^2 d\theta^2)^{\frac{1}{2}} = \int_{\lambda_1}^{\lambda_2} \left[\left[\frac{\partial r}{\partial \lambda}\right]^2 + r^2\left[\frac{\partial \theta}{\partial \lambda}\right]^2\right]^{\frac{1}{2}} d\lambda \qquad 2.5$$

If $\delta\lambda = \lambda_2 - \lambda_1$ is small,

then its length is given by

$$\delta l = \left[\left[\frac{\partial r}{\partial \lambda}\right]^2 + r^2\left[\frac{\partial \theta}{\partial \lambda}\right]^2\right]^{\frac{1}{2}} \delta\lambda \qquad 2.6$$

From equation 2.2,

$$\varepsilon = \frac{\frac{\partial}{\partial t}\left[\left[\frac{\partial r}{\partial \lambda}\right]^2 + r^2\left[\frac{\partial \theta}{\partial \lambda}\right]^2\right]^{\frac{1}{2}}}{\left[\left[\frac{\partial r}{\partial \lambda}\right]^2 + r^2\left[\frac{\partial \theta}{\partial \lambda}\right]^2\right]^{\frac{1}{2}}} \qquad 2.7$$

substituting from equations 2.4,

$$\varepsilon = \frac{r_0^2\left[\frac{\Gamma t}{\pi r_0^3}\frac{dr_0}{d\lambda} - \frac{d\theta_0}{d\lambda}\right]\left[\frac{\Gamma}{\pi r_0^3}\frac{dr_0}{d\lambda}\right]}{\left[\frac{dr_0}{d\lambda}\right]^2 + r_0^2\left[\frac{\Gamma t}{\pi r_0^3}\frac{dr_0}{d\lambda} - \frac{d\theta_0}{d\lambda}\right]} \qquad 2.8$$

So far, the initial shape of the flame, given by $r_0(\lambda)$ and $\theta_0(\lambda)$, has not been specified. The initial flame is a straight line displaced from the origin by a

distance a, and let λ be measured as shown in figure 2.3. Then,

$$r_0(\lambda) = \sqrt{a^2 + \lambda^2} \qquad 2.9a$$

$$\theta_0(\lambda) = arctan(\frac{\lambda}{a}) \qquad 2.9b$$

Substituting equations 2.9, equation 2.5 for flame surface area becomes,

$$\int_{\lambda_1}^{\lambda_2} dl = \int_{\lambda_1}^{\lambda_2} \left[\left[\frac{\lambda}{r} \right]^2 + r^2 \left[\frac{a}{r^2} - \frac{\Gamma t}{\pi r^3} \frac{\lambda}{r} \right]^2 \right]^{\frac{1}{2}} d\lambda \qquad 2.10$$

and equation 2.8 becomes,

$$\varepsilon = \frac{1}{t} \frac{\left[\left[\frac{\Gamma t}{\pi r^2} \right] \frac{\lambda}{r} - \frac{a}{r} \right] \left[\left[\frac{\Gamma t}{\pi r^2} \right] \frac{\lambda}{r} \right]}{\left[\frac{\lambda}{r} \right]^2 + \left[\left[\frac{\Gamma t}{\pi r^2} \right] \frac{\lambda}{r} - \frac{a}{r} \right]^2} \qquad 2.11$$

The effect of the offset distance a is of interest. However, most of the analysis to follow will deal with the special case where $a = 0$. When the offset distance a is zero, equation 2.10 becomes

$$\int_{r_1}^{r_2} dl = 2 \int_{r_1}^{r_2} \left[1 + \left[\frac{\Gamma t}{\pi r^2} \right]^2 \right]^{\frac{1}{2}} dr \qquad 2.12$$

So the annulus $(r, r+dr)$ contains flame area $2\left[1+\left[\frac{\Gamma t}{\pi r^2}\right]^2\right]^{\frac{1}{2}} dr$. Again taking the special case $a = 0$, equation 2.11 becomes

$$\varepsilon = \frac{1}{t} \frac{\left[\frac{\Gamma t}{\pi r^2} \right]^2}{1 + \left[\frac{\Gamma t}{\pi r^2} \right]^2} \qquad 2.13$$

Now that the strain rate ε is known as a function of time, and the surface area of the flame is known, the objectives of this chapter have been reached. However, flame kinematics contains some more information which will be of use

later.

2.3 Flame Density and Spacing

The flame surface density Σ is defined as the surface area of flame per unit volume. Equivalently, in two dimensions the flame density is flame length per unit area. Flame density has units of reciprocal length. From the previous section, for the special case $\alpha = 0$ an annulus $(r, r+dr)$ contains flame area $2\left[1+\left[\frac{\Gamma t}{\pi r^2}\right]^2\right]^{\frac{1}{2}} dr$. The volume of this annulus is $2\pi r dr$, so the flame density Σ is

$$\Sigma = \frac{\left[1+\left[\frac{\Gamma t}{\pi r^2}\right]^2\right]^{\frac{1}{2}}}{\pi r} \qquad 2.14$$

Note that at any fixed radius r, the flame density increases with time. Eventually, as the flame becomes tightly wrapped around the origin, the flame surfaces will resemble concentric circles about the origin. When the flame structure consists of uniformly spaced parallel flames, the distance between flames Δ will be the reciprocal of the flame density.

$$\Delta = \frac{1}{\Sigma} = \frac{\pi r}{\left[1+\left[\frac{\Gamma t}{\pi r^2}\right]^2\right]^{\frac{1}{2}}} \qquad 2.15$$

For the outer arms of the flame, equation 2.15 does not have any meaning.

2.4 Flame Curvature

Another quantity which will be of interest later is the curvature of the flame surface. First, an equation for the flame surface is found. Taking the special case $\alpha = 0$, equations 2.9 may be substituted into equations 2.4 with $r_0 = \lambda$ and $\theta_0 = \pm \frac{\pi}{2}$ to yield an expression for θ as a function of r and t.

$$\theta = \frac{\Gamma t}{2\pi r^2} \pm \frac{\pi}{2} \qquad 2.16$$

The curvature κ of the line is found from elementary calculus, and the radius of curvature of the line is $\frac{1}{\kappa}$

$$\frac{1}{\kappa} = r \frac{\left[1 + \left[\frac{\pi r^2}{\Gamma t}\right]^2\right]^{\frac{3}{2}}}{\left|1 - \left[\frac{\pi r^2}{\Gamma t}\right]^2\right|} \qquad 2.17$$

2.5 Similarity

The repeated occurrence of the dimensionless $\frac{\Gamma t}{\pi r^2}$ suggests the existence of a similarity variable proportional to $\frac{r}{\sqrt{\Gamma t}}$, indicating that the shape of the spiral is independent of time, the only effect of increasing time being to increase the size of the spiral. The characteristic radius of the spiral may be defined as the radius at which the flame sheet has been rotated ninety degrees from its original position. Denoting the characteristic radius by r_{arms}, and choosing the upper arm of the spiral ($\theta_0 = \frac{\pi}{2}$), r_{arms} is the radius where $\theta = \pi$. From equation 2.16,

$$\frac{r_{arms}}{\sqrt{\Gamma t}} = \frac{1}{\pi} \qquad 2.18$$

Later developments will show that the region of interest in this analysis is the region $r << r_{arms}$, where most of the additional flame surface is being generated. In this region, equation 2.13 for the strain rate is approximately,

$$\varepsilon \sim \frac{1}{t} \qquad 2.19$$

and equation 2.14 for the flame spacing becomes

$$\Delta \sim \frac{\pi^2 r^3}{\Gamma t} \qquad 2.20$$

Equation 2.17 for the flame radius of curvature becomes

$$\frac{1}{\kappa} \sim r \qquad 2.21$$

The flame in this innermost region is tightly wrapped around the origin, so much so that the flame surfaces are nearly concentric circles.

In contrast, at large radii $r >> r_{arms}$ the flame arms are unstrained and lie near their original positions. This region will not be of interest in the analysis to follow.

2.6 Summary

The flame is a line which is transported at the local fluid velocity. Assuming the velocity field to be that of a potential vortex, an increase in flame surface area and a resultant local straining of the flame sheet were found. In the absence of viscosity, the distorted flame contour is similar at all times, such that $\frac{r}{\sqrt{\Gamma t}}$ is constant.

3. STRAINED LAMINAR DIFFUSION FLAMES

3.1 Introduction

Each piece of the complex flame structure shall be analysed as a one dimensional laminar diffusion flame which is strained at the rate ε. The strain rate will be a function of time, and the objective is to find $\dot{m}$, the time dependent reactant consumption rate per unit flame area. Fortunately, strained laminar diffusion flames have received a great deal of attention, and methods are already available. For a review of the subject, see Williams (1971).

3.2 Governing Equations

For chemically reacting flows, in addition to the usual equations of mass, momentum, and energy conservation, one obtains a conservation equation for each chemical species present (for more detail, see Williams (1965)). In two dimensional flow, the conservation equation for the i^{th} species is

$$\frac{\partial \rho_i}{\partial t} + \frac{\partial \rho_i u_i}{\partial x} + \frac{\partial \rho_i v_i}{\partial y} = w_i \qquad 3.1$$

Here ρ_i is the concentration (mass per unit volume) of the i^{th} chemical species. If Y_i is the mass fraction of species i, then $\rho_i = Y_i \rho$. The velocity of species i consists of the bulk fluid velocity plus the relative flux of species i due to diffusion. This is a one dimensional problem; concentrations and temperatures are taken to be independent of x. Therefore, $u_i = u$ and $v_i = v + v_{Di}$; no diffusion occurs in the x direction. The source term w_i represents the creation and destruction of species i due to chemical reactions. Clearly, $\sum_i Y_i = 1$ and $\sum_i w_i = 0$.

The momentum equation could be included at this point; however, the velocity field is already specified and the pressure is nearly constant across the

flame. Therefore, take the velocity to be $u = \varepsilon(t)\, x$. To simplify further, assume diffusion obeys Fick's law, $Y_i\, v_{Di} = -D\, \frac{\partial Y_i}{\partial y}$. To account for the variation of the diffusion coefficient and density with temperature, assume that $\rho^2 D = \rho_0^2 D_0$, where the zero subscript refers to a constant reference value, and use a Howarth transformation $\xi = \int_0^y \frac{\rho(y')}{\rho_0}\, dy'$ to yield (see Marble (1979))

$$\frac{\partial Y_i}{\partial t} - \varepsilon(t)\, \xi\, \frac{\partial Y_i}{\partial \xi} - D_0\, \frac{\partial^2 Y_i}{\partial \xi^2} = \frac{w_i}{\rho} \qquad 3.2$$

where all species have been assumed to have equal densities and diffusivities. The energy equation may be treated similiarly, with the result that if the specific heats of the species are constant and equal, the product of the density and the thermal conductivity is constant, the Lewis number is unity, and the viscous dissipation term is neglected, the temperature obeys the same equation as do the species mass fractions.

For boundary conditions, consider a diffusion flame which separates semi-infinite regions of reactants. Calling one reactant "fuel" and the other "oxidizer", the appropriate boundary conditions are $Y_f = Y_{f\infty}$, $Y_o = 0$, $T = T_\infty$ as $y \to +\infty$ and $Y_f = 0$, $Y_o = Y_{o\infty}$, $T = T_\infty$ as $y \to -\infty$. Here $Y_{f\infty}$ and $Y_{o\infty}$ are the constant mass fractions of fuel and oxidizer found at plus and minus infinity, respectively. The fuel and oxidizer streams have been taken to have the same temperatures, given by T_∞.

The initial conditions which will be used most often in the analysis are, at $t = 0$, $Y_f = Y_{f\infty}$, $Y_o = 0$, $T = T_\infty$ for all $y > 0$ and $Y_f = 0$, $Y_o = Y_{o\infty}$, $T = T_\infty$ for all $y < 0$. At times, these initial conditions will not be sufficient to "ignite" the flame. In those cases, a region of elevated temperature must be specified in the initial conditions to ensure a vigorously burning flame.

The situation described is that of a semi-infinite reservoir ($y > 0$) of fuel of constant composition and temperature separated from a similar region of oxidizer ($y < 0$) by an impermeable plate for $t < 0$. At $t = 0$, the plate vanishes and the two reactants diffuse into one another and react.

3.3 Experimental Configurations

Although the previous formulation allows the strain rate ε to be an arbitrary function of time, the laminar diffusion flames commonly produced in laboratories fall into one of two classes: the unstrained transient flame or the steady state strained flame.

In the unstrained transient flame configuration, fuel and oxidizer streams are flowing in the x direction with constant, equal velocities u. The reactants are kept from mixing by a splitter plate which ends at $x = 0$. Subsequently, for $x > 0$, the reactants interdiffuse and react. The boundary layer approximation, ignoring diffusion in the x direction compared to diffusion in the y direction, and the substitution $t = \frac{x}{u}$ leads directly to equation 3.2 with $\varepsilon(t) \equiv 0$. The experiments by Melvin *et al.* (1971) and by Phillips (1964) are of this type.

The other case, the steady state strained flame, is found analytically by setting the strain rate $\varepsilon(t)$ equal to a constant and examining the steady solutions which occur as $t \to \infty$. In the laboratory, this case may be approximated in several ways.

The "opposed jet diffusion flame" is produced by impinging two jets, one of fuel and the other of oxidizer, which are flowing in opposite directions. Ignoring viscosity, if y is the coordinate axis along the axes of the two jets, then $v = -\varepsilon y$ in the region between the two jets. The strain rate may be varied by changing the jet velocities or by changing the gap between the two jet exits. A flat, one dimensional flame may be produced where the two streams come together.

A detailed account of the production of one-dimensional strained laminar diffusion flames in the laboratory is found in the work of Hahn and Wendt (1981a,1981b) and Hahn (1979). Detailed measurements of temperature and species concentrations are given, and the results are compared to numerical calculations for methane-air flames. Hahn and Wendt also discuss the effect of the heat release of the flame on the velocity distribution; one result is that the flame acts as a source of vorticity. The experiment of Potter *et al.* (1960) is also based on the opposed jet diffusion flame.

The potential flow solution for two impinging jets is the same as that for a jet impinging on a wall at $y = 0$, and also for the flow in the neighborhood of the forward stagnation point of a blunt body. Therefore, a constant strain flame may be produced by blowing a jet of air against the surface of a liquid or gaseous fuel, as was done by Kent and Williams (1974), Krishnamurthy (1975), and Seshadri (1978). In addition, Tsuji and Yamaoka (1968) investigated the flame in the forward stagnation point region of a cylinder, with fuel injected through the porous wall of the cylinder. These configurations differ slightly from the previous analytical treatment. First, if viscosity is included, a boundary layer will form on the wall. Some investigators include viscosity and others do not. However, numerical calculations by Jain and Mukunda (1968) both including and neglecting the effects of viscosity do not show a significant effect on the combustion process. Secondly, the boundary conditions differ. For an oxidizer jet impinging on a surface of solid or liquid fuel, the boundary condition on the fuel side is applied at the wall instead at infinity, and includes the vaporization of the fuel at the wall surface. For injection of fuel through a porous wall, the flux of fuel at the wall is specified.

3.4 Limiting Cases

In general, the reactant consumption or production term $\frac{w_i}{\rho}$ is a function of species concentrations and the temperature. Most reactions of physical interest are the aggregate of many individual reactions involving intermediate reaction products. These complicated reaction systems are often approximated (see Williams (1971)) as a single step second order reaction,

$$fuel + oxidizer \rightarrow products$$

Since both reactants have been assumed to be of equal density, the appropriate rates of consumption of fuel and oxidizer are;

$$\frac{w_o}{\rho} = \frac{w_f}{\rho} = -kY_oY_f \qquad 3.3$$

Here k is the second order reaction rate constant, with units of reciprocal time. Clearly, a characteristic chemical reaction time t_{ch} may be defined which is proportional to $\frac{1}{k}$.

Friedlander and Keller (1963) considered the case of a steady unstrained diffusion flame of fixed thickness l, governed by the equations,

$$D_0 \frac{d^2Y_o}{dy^2} = kY_oY_f \qquad 3.4a$$

$$D_0 \frac{d^2Y_f}{dy^2} = kY_oY_f \qquad 3.4b$$

with boundary conditions $Y_o = Y_{o\infty}$ and $Y_f = 0$ at $y = \frac{l}{2}$, and $Y_o = 0$ and $Y_f = Y_{f\infty}$ at $y = -\frac{l}{2}$. Using the characteristic length l to make y dimensionless results in the appearance of the dimensionless number $\frac{kl^2}{D_0}$. Known as the Damköhler number, this group represents the ratio of the characteristic time

required (proportional to $\frac{l^2}{D_0}$) for the reactants to diffuse together to that required for already mixed reactants to react (proportional to $\frac{1}{k}$).

Thus two separate limiting cases may be distinguished; that where the chemical reaction term is negligible to lowest order (small Damköhler number), and that where the reaction is considered to be instantaneous and the rate of diffusion controls the rate of fuel consumption (large Damköhler number). In each case, perturbation methods may be used to find solutions for the rate of fuel consumption per unit flame area. These ideas have been applied to the stagnation point problem by Fendell (1965).

3.4.1 Fast Chemistry Solution

The solution for the case of a fast chemical reaction was first given by Burke and Schumann (1928). An infinitely fast chemical reaction rate implies chemical equilibrium everywhere. The reaction is taken to be just the forward reaction, thus fuel and oxidizer cannot coexist. The chemical reaction is confined to an infinitely thin flame sheet. On one side of the flame sheet, fuel diffuses toward the flame and on the other side oxidizer diffuses toward the flame. No oxidizer is found on the fuel side of the flame sheet, and no fuel is found on the oxidizer side. At the flame sheet itself, both the fuel concentration and the oxidizer concentration vanish. The flame sheet serves as a sink for both fuel and oxidizer. The rate of fuel consumption per unit area is equal to the rate of diffusion of fuel into the flame sheet, which is $\rho_0 D_0 \frac{\partial Y_f}{\partial \xi}$ evaluated at the flame sheet on the fuel side, $\xi = \xi^+_{flame}$. Likewise, the oxidizer consumption is given by $\rho_0 D_0 \frac{\partial Y_o}{\partial \xi}$ at $\xi = \xi^-_{flame}$. Obviously, the ratio of fuel consumption to oxidizer consumption must be in stoichiometric proportions, and this determines the flame position ξ_{flame}.

Assume, for convenience only, that $Y_{f\infty} = Y_{o\infty} = 1$, that fuel and oxidizer have equal diffusivities, and that they react in 1:1 proportions. The flame will then be symmetric about $\xi = 0$ and equation 3.2 becomes for $\xi > 0$

$$\frac{\partial Y_f}{\partial t} - \varepsilon(t)\,\xi\,\frac{\partial Y_f}{\partial \xi} - D_0\,\frac{\partial^2 Y_f}{\partial \xi^2} = 0 \qquad 3.5a$$

$$Y_o = 0 \qquad 3.5b$$

and for $\xi < 0$

$$Y_f = 0 \qquad 3.6a$$

$$\frac{\partial Y_o}{\partial t} - \varepsilon(t)\,\xi\,\frac{\partial Y_o}{\partial \xi} - D_0\,\frac{\partial^2 Y_o}{\partial \xi^2} = 0 \qquad 3.6b$$

with boundary conditions $Y_f(+\infty) = Y_o(-\infty) = 1$ and initial conditions at $t = 0$ of $Y_f = 1$ for $\xi > 0$ and $Y_o = 1$ for $\xi < 0$.

Following Carrier *et al.* (1975), use the coordinate transformations

$$\xi = \zeta\, e^{-\int_0^t \varepsilon(t'')\,dt''} \qquad 3.7$$

and

$$\frac{d\tau}{dt} = e^{2\int_0^t \varepsilon(t'')\,dt''} \qquad 3.8$$

Equation 3.8 may be integrated to yield τ as a function of time, if the correct initial condition, $\tau(0)$ is known. Regardless of what value is chosen, the substitutions 3.7 and 3.8 eliminate the convection term and thus equations 3.5a and 3.6b become

$$\frac{\partial Y_f}{\partial \tau} - D_0\,\frac{\partial^2 Y_f}{\partial \zeta^2} = 0 \qquad 3.9a$$

$$\frac{\partial Y_o}{\partial \tau} - D_0\,\frac{\partial^2 Y_o}{\partial \zeta^2} = 0 \qquad 3.9b$$

Together with the boundary and initial conditions these equations yield the

following solution

$$Y_f = erf\left[\frac{\zeta}{\sqrt{4D_0\tau}}\right] \qquad Y_o = 0 \qquad \text{for} \qquad \zeta > 0 \tag{3.10a}$$

$$Y_o = -erf\left[\frac{\zeta}{\sqrt{4D_0\tau}}\right] \qquad Y_f = 0 \qquad \text{for} \qquad \zeta < 0 \tag{3.10b}$$

Thus the fuel consumption rate per unit flame area may be found.

$$\dot{m} = \rho_0 D_0 \left.\frac{\partial Y_f}{\partial \xi}\right|_{\xi = 0^+} = \rho_0 \left[\frac{D_0}{\pi\tau}\right]^{\frac{1}{2}} e^{\int_0^t \varepsilon(t'')\,dt''} \tag{3.11}$$

From equations 3.10, the width of the diffusion zone is proportional to $\sqrt{D_0\tau}$ in ζ coordinates, or to $\sqrt{D_0\tau}\, e^{-\int_0^t \varepsilon(t')\,dt'}$ in ξ coordiates. (ξ differs from the physical coordinate y by only a Howarth transformation.)

The grouping $\tau\, e^{-2\int_0^t \varepsilon(t'')\,dt''}$ will occur often so give it the symbol $\bar{\tau}$.

$$\bar{\tau} \equiv \tau\, e^{-2\int_0^t \varepsilon(t'')\,dt''} \tag{3.12}$$

Rewrite equation 3.11 as

$$\dot{m} = \rho_0 \left[\frac{D_0}{\pi\bar{\tau}}\right]^{\frac{1}{2}} \tag{3.13}$$

and the characteristic thickness of the flame δ may be defined as

$$\delta \equiv \sqrt{D_0\bar{\tau}} \tag{3.14}$$

The characteristic diffusion time is proportional to $\frac{\delta^2}{D_0}$ which is equal to $\bar{\tau}$. Therefore, one may expect this solution to be valid as long as $\bar{\tau}$ is large compared to the characteristic chemical time.

Returning to the question of the proper initial condition for finding τ, note that the flame will be of zero thickness at $t = 0$ if $\tau(0) = 0$. Therefore, if the diffusion flame were initiated (by removing a partition between the reactants) at

$t = 0$, then τ should be zero at $t = 0$. Note that if $\tau = 0$, then $\bar{\tau} = 0$ also.

3.4.2 Extensions of the Burke-Schumann Solution

The previous analysis is completely independent of the chemical reactions which occur at the flame sheet, with one exception. The stoichiometry of the overall reaction specifies the ratio of fuel to oxidizer diffusing into the flame sheet. Marble (1979) has given the solution for an arbitrary fuel-oxidizer ratio, in addition to allowing for $Y_{o\infty}$ and $Y_{f\infty}$ not equal to one and for different diffusion coefficients for fuel and oxidizer. The nature of the solution is unchanged. For the unstrained case, one still obtains a similarity solution in which flame thickness is proportional to $\sqrt{t}$, and thus the fuel consumption rate is proportional to $\frac{1}{\sqrt{t}}$. In the case of an arbitrary strain rate, the same dependence of fuel consumption and flame thickness on $\bar{\tau}$ will be found, only the constants will be changed.

In the previous analysis, the chemical reaction was considered to be infinitely fast and to proceed only in the forward direction. One may ask how allowing reversible reactions and finite rate reactions changes the solutions, and whether the Burke-Schumann solution is recoverable in the limit.

If the equilibrium constant K (the ratio of the forward to the backward reaction rates) is included and the asymptotic limit $K >> 1$ is examined, the previous solution is recovered as the lowest order outer solution, and the reaction zone expands from a flame sheet of zero thickness to a thin boundary layer which may be analysed using singular perturbation analysis (see Fendell (1967) and Chung and Blankenship (1966)). Clarke (1968) and Clarke and Moss (1969) have analysed a system of four reactions which describe the hydrogen-oxygen diffusion flame, and discuss the effect of the reverse reactions on the flame structure.

If the requirement that the reaction be infinitely fast is relaxed, and the limit $k >> 1$ is examined (more accurately the limit of a large Damköhler number), again the Burke-Schumann solution is recovered as the lowest order outer solution. An inner solution describing the detailed structure of the reaction zone is also obtained. Fendell (1965) analysed a constant strain single step, second order reaction ($\frac{w}{\rho} = k Y_o Y_f$), and a more general overall reaction ($\frac{w}{\rho} = k Y_o^{\mu_o} Y_f^{\mu_f}$) has been considered by Carrier *et al.* (1975). A system of four reactions for the hydrogen-oxygen diffusion flame has been solved by Clarke (1969).

Thus, the Burke-Schumann solution is valid in the limit of a negligible backward reaction and a fast forward reaction. The elimination of the explicit time dependence of the strain rate in favor of the parameter $\bar{\tau}$ is valid only to lowest order in the limit of a large Damköhler number (see Carrier *et al.* (1975)).

3.4.3 The Slow Chemistry Limit

As an aid to understanding the behavior of a flame over the entire range of Damköhler numbers, the opposite limit may be explored; the small Damköhler number limit (see Fendell (1965) and Friedlander and Keller (1963)). The chemical reaction terms are neglected to lowest order, and concentration profiles of fuel and oxidizer are found. Then, the rate of conversion of fuel and oxidizer into product is calculated as a perturbation.

Ignoring the chemical production terms, equation 3.2 becomes

$$\frac{\partial Y_i}{\partial t} - \varepsilon(t)\, \xi\, \frac{\partial Y_i}{\partial \xi} - D_0\, \frac{\partial^2 Y_i}{\partial \xi^2} = 0 \qquad 3.15$$

with the same boundary and initial conditions as before. Once again the coordinate transformations given by equations 3.7 and 3.8 are used, and

similarity solutions for the fuel and oxidizer concentrations are found. They are

$$Y_f = \frac{1}{2} + \frac{1}{2} erf\left[\frac{\zeta}{\sqrt{4D_0\tau}}\right] \qquad 3.16a$$

$$Y_o = \frac{1}{2} - \frac{1}{2} erf\left[\frac{\zeta}{\sqrt{4D_0\tau}}\right] \qquad 3.16b$$

If the chemical reaction is a single step, second order reaction, then $\frac{w}{\rho} = k Y_o Y_f$. The fuel consumption per unit flame area is just w integrated across the thickness of the flame, or

$$\dot{m} = \int_{-\infty}^{+\infty} w \, dy \qquad 3.17$$

which becomes

$$\dot{m} = \int_{-\infty}^{+\infty} \rho k [\frac{1}{2} + \frac{1}{2} erf [\frac{\zeta}{\sqrt{4D_0\tau}}]][\frac{1}{2} + \frac{1}{2} erf [\frac{\zeta}{\sqrt{4D_0\tau}}]] \, dy \qquad 3.18$$

Since the chemical reaction is weak, then to lowest order $T = T_\infty$ across the flame. Thus ρ and k are to be evaluated at T_∞. Transforming the variable of integration yields

$$\dot{m} = \rho_0 k(T_\infty) \sqrt{D_0\tau} \, e^{-\int_0^t \varepsilon(t'')\, dt''} \int_{-\infty}^{+\infty} [\frac{1}{2} + \frac{1}{2} erf \frac{\gamma}{2}] [\frac{1}{2} - \frac{1}{2} erf \frac{\gamma}{2}] \, d\gamma \qquad 3.19$$

which gives the result

$$\dot{m} = \frac{\rho_0 k(T_\infty) \sqrt{2D_0\tau}}{\sqrt{\pi}} e^{-\int_0^t \varepsilon(t'')\, dt''} \qquad 3.20$$

Interestingly, the parameter $\bar{\tau}$ has appeared once again, for equation 3.20 may be rewritten as

$$\dot{m} = \left[\frac{2}{\pi}\right]^{\frac{1}{2}} \rho_0 k(T_\infty) \sqrt{D_0\bar{\tau}} \qquad 3.21$$

This result is more general than it first seems, since examination of equations 3.16 and 3.19 reveal that the proportionality of $\dot{m}$ to $\sqrt{\tau}$ is a result of

the similarity solutions for Y_f and Y_o. The reaction term w could be any arbitrary function of Y_f and Y_o, and the result would be the same; the overlap between the fuel and oxidizer profiles would be proportional to $\sqrt{D_0\bar{\tau}}$ and $\dot{m}$ would be proportional to the flame width. Just as before, the flame width δ may be defined as

$$\delta \equiv \sqrt{D_0\bar{\tau}} \qquad 3.22$$

and the appropriate diffusion time is proportional to $\frac{\delta^2}{D_0}$, which is equal to $\bar{\tau}$. The requirement that the Damköhler number $\frac{t_{diff}}{t_{ch}}$ be small is equivalent to requiring that $\frac{\bar{\tau}}{t_{ch}}$ be small.

3.5 The Proposed Model

In the limits as $\bar{\tau} >> t_{ch}$ and as $\bar{\tau} << t_{ch}$ the fuel consumption rate per unit flame area has been found to depend only on the parameter $\bar{\tau}$, regardless of what function the strain rate ε is of time. To lowest order,

$$\dot{m} \sim \rho_0 k(T_\infty) \left[\frac{2}{\pi}\right]^{\frac{1}{2}} \sqrt{D_0\bar{\tau}} \quad \text{for} \quad \bar{\tau} << t_{ch} \qquad 3.23a$$

$$\dot{m} \sim \rho_0 \left[\frac{D_0}{\pi\bar{\tau}}\right]^{\frac{1}{2}} \quad \text{for} \quad \bar{\tau} >> t_{ch} \qquad 3.23b$$

It must be stressed that the dependence exclusively on the parameter $\bar{\tau}$ is true only to lowest order, and is not true at all for $\frac{\bar{\tau}}{t_{ch}}$ of order one. Nevertheless, one requires a method of estimating the fuel consumption $\dot{m}$ for intermediate values of $\bar{\tau}$. One notes that equation 3.23a is an increasing function of $\bar{\tau}$ and that equation 3.23b is a decreasing function of $\bar{\tau}$. The two equations yield the same value for $\dot{m}$ if $\bar{\tau} = \frac{1}{\sqrt{2}\,k(T_\infty)}$. Recalling that the characteristic chemical

time of the system is proportional to $\frac{1}{k}$, defining $t_{ch} \equiv \frac{1}{\sqrt{2}\, k(T_\infty)}$ enables equations 3.23 to be written as

$$\dot{m} \sim \frac{\rho_0}{t_{ch}} \left[\frac{D_0 \bar{\tau}}{\pi}\right]^{\frac{1}{2}} = \rho_0 \left[\frac{D_0}{\pi \bar{\tau}}\right]^{\frac{1}{2}} \left[\frac{\bar{\tau}}{t_{ch}}\right] \quad \text{for} \quad \bar{\tau} << t_{ch} \qquad 3.24a$$

$$\dot{m} \sim \rho_0 \left[\frac{D_0}{\pi \bar{\tau}}\right]^{\frac{1}{2}} \quad \text{for} \quad \bar{\tau} >> t_{ch} \qquad 3.24b$$

The chemical time t_{ch} has been chosen such that if $\bar{\tau} < t_{ch}$, the value of $\dot{m}$ from equation 3.24a is less than that from 3.24b, therefore the reaction may be thought of as being reaction limited. For $\bar{\tau} > t_{ch}$, the term diffusion limited is appropriate, since equation 3.24b predicts a lower value for $\dot{m}$ than does equation 3.24a. At $\bar{\tau} = t_{ch}$ the two equations agree.

The formulation which will be used for the bulk of this work is the following: Given ε as a function of time, calculate $\bar{\tau}$ as a function of time using equations 3.8 and 3.12. Then, for values of $\frac{\bar{\tau}}{t_{ch}}$ less than one, calculate $\dot{m}$ using equation 3.24a. If $\frac{\bar{\tau}}{t_{ch}}$ is greater than one, use equation 3.24b to find $\dot{m}$. The accuracy of this method will be discussed in chapter four.

3.6 The Effects of Activation Energy

The previous discussion presumes that a continuous transition exists between the small Damköhler number and the large Damköhler number regimes. In some cases this is true; see Williams (1971) and chapter four of this thesis. In other cases it is not. If the reaction is strongly exothermic and the reaction rate depends strongly on temperature, more than one solution may exist at a given Damköhler number (see Williams (1971)).

Before proceeding further, it is necessary to mention results for the flame

temperature profile. For small Damköhler numbers, to lowest order the reaction is neglected, so $T = T_\infty$ across the flame. Higher order terms show that the maximum temperature which occurs in the middle of the flame increases as the Damköhler number increases (Fendell (1965)). In the large Damköhler number limit, the Burke-Schumann solution yields a temperature profile which reaches a sharp peak at the flame sheet. If the Lewis number is equal to unity, then the maximum temperature is equal to the adiabatic flame temperature T_f, the temperature which would be obtained if fuel and oxidizer were mixed in stoichiometrically correct proportions in an adiabatic reservoir (Marble (1979)). As one might expect, higher order terms show that T_{max} decreases as the Damköhler number decreases.

3.6.1 Steady State Solutions

The case usually considered is the steady state strained flame, characterized by a constant value of the strain rate ε. (In this case $\bar{\tau} = \frac{1}{2\varepsilon}$.) The characteristic time of the flow field is thus proportional to $\frac{1}{\varepsilon}$. The definition of a characteristic chemical time is more difficult. The previous definition, that t_{ch} is proportional to $\frac{1}{k}$, only makes sense if k is nearly constant. The reaction rate k is usually a function of temperature, most often a function of the Arrhenius form,

$$k = k_0 \left[\frac{T}{T_\infty}\right]^{\mu_T - 1} e^{-\frac{T_a}{T}} \qquad 3.25$$

where k_0, μ_T, and T_a are constants. Obviously, k_0 has units of reciprocal time, so usually the Damköhler number is defined (see Friedlander and Keller (1963), for example) as $\frac{k_0}{\varepsilon}$.

This choice of a chemical time is convenient, since k_0 and ε are known quantities, but it is not necessarily the best choice. As pointed out by Williams (1971), the reaction rate is of greatest importance in the region of highest temperature, therefore the reaction rate k evaluated at $T = T_{max}$ should be used as the characteristic chemical time of the system. This introduces a complication, since T_{max} is not known *a priori*.

The existence of multiply valued solutions can be argued intuitively. For instance, let the strain rate ε be some intermediate value. If one guesses that the large Damköhler number solution were valid, then $T_{max} \approx T_f$. The reaction rate k should then be evaluated at T_f. On the other hand, had one guessed that the Damköhler number would be small, then $T_{max} \approx T_\infty$, and k should be evaluated at T_∞. This gives rise to multiply valued solutions if $k(T_f)$ is much larger than $k(T_\infty)$. In such a case, a value of ε could be chosen such that $\frac{k(T_f)}{\varepsilon} >> 1$, which would justify the assumption that $T_{max} \approx T_f$, while at the same time $\frac{k(T_\infty)}{\varepsilon} << 1$, which would justify setting $T_{max} \approx T_\infty$.

3.6.1.1 Ignition and Extinction

Fendell (1965) analysed the stagnation flow problem, using asymptotic analyses for both large and small Damköhler numbers as well as numerical solutions for intermediate values. He found that a graph of T_{max} versus the Damköhler number based on k_0 forms an S shape. The lower branch of the S is described by the small Damköhler number (or "slow chemistry" or "frozen flow") solution and the upper branch is described by the large Damköhler number (or "fast chemistry" or "equilibrium flow" or "Burke-Schumann") solution. The most interesting feature of Fendell's solution is the existence of three solutions for certain choices of the strain rate ε.

As a consequence, if a flame is burning well on the upper branch of the S, and the strain rate is slowly increased, eventually a critical value of the strain rate is reached. If the strain is increased further, the lower branch of the S is the only possible steady solution. This defines an extinction condition. Similiarly, one can define an ignition condition, a critical Damköhler number where the system will jump from the lower branch to the upper.

Zeldovitch (1951) analysed the thin reaction zone imbedded in the Burke-Schumann flame by means of order of magnitude estimates. Reasoning that the reaction zone must increase in thickness if the fuel consumption rate is to increase, Zeldovitch saw that this would also lower the flame temperature in the reaction zone. If the reaction rate were a strong function of temperature, the fuel consumption rate as a function of reaction zone thickness would increase at first, reach a maximum, and then decrease. Therefore, the capacity of the reaction zone to consume fuel is limited. Later, Liñan (1963) more accurately analyzed the inner reaction zone. He too found indications that the inner reaction zone has a limited capacity to consume fuel.

These results of Zeldovitch and Liñan can be used to intuitively explain the extinction process. For a constant strain flame, the Burke-Schumann solution predicts that $\dot{m}$ should increase as $\sqrt{\varepsilon}$ as ε is increased. The Burke-Schumann calculation of $\dot{m}$ is just the rate at which the outer diffusion zones convect and diffuse reactants into the inner reaction zone. If the strain rate ε were too large, and the outer regions of the flame pump fuel and oxidizer into the inner reaction zone beyond the capacity of the inner zone to consume these increased fluxes, the temperature of the flame would fall and the flame would go out.

3.6.1.2 Stability

Williams (1971) reports that most investigators believe the middle branch

to be unstable. This is intuitively plausible, since a small increase in flame temperature will increase the rate of fuel consumption and thereby increase the rate of heat release by the flame. Similiarly, a decrease in flame temperature should cause a decrease in the heat release rate of the flame. Stability analyses by Kirkby and Schmitz (1966) and by Schmitz (1967) suggest that the middle branch is unstable as also are adjacent regions of the upper and lower branches (*i.e.* the instability boundaries do not precisely correspond to points of vertical tangency on the S curve). The boundary conditions used in these analyses do not correspond to either the stagnation point problem or to the opposed jet diffusion flame. Consequently, for the cases of interest the question of stability has not been definitely answered.

3.6.1.3 Activation Energy Asymptotics

If one wants analytical expressions for the critical ignition and extinction Damköhler numbers, the asymptotic limits of large and small Damköhler numbers are clearly inappropriate, since the multivaluedness occurs at intermediate values of the Damköhler number. In addition, the asymptotic formulas fail completely in near the ignition and extinction points (Fendell (1965)). Williams (1971) suggested the limit of large activation energy ($T_a \to \infty$). The analysis was carried out by Liñan (1974). In Liñan's analysis, all temperatures were nondimensionalized by the heat released by the reaction, $\frac{\Delta H}{c_p}$, resulting in the dimensionless ambient temperature $\hat{\Theta}_\infty$, the dimensionless activation energy $\hat{\Theta}_a$, and the dimensionless flame temperature $\hat{\Theta}_f = \hat{\Theta}_\infty + \frac{1}{2}$. The limit $\frac{\hat{\Theta}_f}{\hat{\Theta}_\infty^2} \to \infty$ was taken. Liñan found that if the Damköhler number were defined as $\frac{k_0}{\varepsilon}$, then the critical value required for ignition is

$$\left[\frac{k_0}{\varepsilon}\right]_{ign} \sim 2.5925 \left[\frac{\hat{\Theta}_\infty^2}{\hat{\Theta}_f}\right] e^{\frac{\hat{\theta}_f}{\hat{\theta}_\infty}} \qquad 3.26$$

and for extinction is

$$\left[\frac{k_0}{\varepsilon}\right]_{ext} \sim \frac{0.85}{2\pi} \left[\frac{\hat{\Theta}_a}{\hat{\Theta}_f^2}\right]^3 e^{\frac{\hat{\theta}_a}{\hat{\theta}_f}} \qquad 3.27$$

Liñán performed the analysis allowing the two reactants to be at different temperatures and in different concentrations, but his results have been simplified here for the case of both reactants initially at T_∞ and with initial mass fractions of unity.

The analysis was performed by Liñán for the opposed jet geometry, but it has been extended to the stagnation flow problem by Krishnamurthy *et al.* (1976).

3.6.1.4 Numerical Results

In addition to the numerical results by Fendell (1965) and by Jain and Mukunda (1968) exhibiting the S shaped curve for single step reactions, Marathe *et al.* (1977) have numerically studied a system of four reactions for the reaction of hydrogen and oxygen. Their results show that the upper branch ceases to exist for too large a strain rate. In addition, a single step reaction is found which duplicates the extinction criteria found for the system of four reactions.

3.6.1.5 Experimental Results

The extinction of laminar diffusion flames by increasing the strain rate has been observed. In an early experiment, Potter *et al.* (1960) established opposed jet diffusion flames using air and several gaseous fuels. They found that a nearly one dimensional flame could be established between the two jets

for low flow rates, but the center of the flame sheet would disappear if the flow rate were increased too much. An explanation was attempted based on the "apparent flame strength" theory of Spalding (1954). Their actual numerical results are not of interest here (the experiments were done using parabolic exit velocity profiles for the jets since uniform profiles produced results which were dependent on the distance between the two jets), yet the results are of qualitative interest, since they show that extinction may result from increasing flow rates.

Tsuji and Yamaoka (1968) performed experiments by blowing air over a cylinder with porous walls through which fuel (either methane or propane) was injected. The velocity gradient in the forward stagnation point region is increased by increasing the freestream velocity. The results show extinction of the flame in this region as the strain rate is increased.

Many experiments have been done demonstrating extinction in the stagnation point flow obtained by impinging an air (often diluted with nitrogen) jet on the surface of a liquid or gaseous fuel. Increasing the air jet velocity increases the velocity gradients (and hence the strain rates) in the stagnation point flow above the fuel. The adiabatic flame temperature may be controlled by varying the the dilution of air by nitrogen. (see Seshadri (1978), Kent and Williams (1974), and Krishnamurthy (1975)) The results of Tien *et al.* (1978) show the burning rate of a solid fuel (polymethyl methacrylate) increases as $\sqrt{\varepsilon}$ with increasing strain rate ε until suddenly the flame goes out.

Experimental evidence for the existence of the ignition point is absent. The ignition mechanism (see Liñan and Crespo (1976)) depends on the small reaction rate at $T = T_\infty$ slowly reacting the fuel and oxidizer, causing heat to be released, which slowly increases the temperature in the "flame". Eventually, if the strain rate is small enough, a temperature runaway occurs, causing the

flame to jump from the lower to the upper branch. The problem with the ignition mechanism is that it depends on the reaction rate of the fuel and oxidizer at T_∞. The reaction rate of hydrocarbon fuels at ordinary room temperatures is certainly very small, but Arrhenius expressions which accurately express reaction rates at typical flame temperatures cannot be accurately extrapolated down to room temperatures. On this basis, and in view of the lack of experimental confirmation, the ignition point will be ignored in this analysis. The flame behavior will consist of a strongly burning branch where fuel consumption is given by equation 3.23b, and which ceases to exist below a critical Damköhler number. The lower branch of the solution will be taken to be a "flame" where fuel and oxidizer interdiffuse, but do not react to any appreciable degree.

3.6.2 The Transient Case

The simplest time dependent case is the unstrained mixing layer. Two streams, one consisting of fuel and the other of oxidizer, flow in same direction with equal velocities u. For $x < 0$ they are separated by a splitter plate. At $x = 0$ the plate ends with a sharp edge and for $x > 0$ the two streams diffuse into one another and react. Using the boundary layer approximation, allowing diffusion in y only, and noting that u is constant, results is a transformation from a two dimensional problem in x and y to a transient one dimensional problem in t and y, if one sets $t = \frac{x}{u}$.

If the activation energy were unimportant, equations 3.23a and 3.23b could be used, with the result (since $\bar{\tau} = t$ in this case) that the fuel consumption would increase as $\sqrt{x}$ at first, until $x = ut_{ch}$, and then decrease as $\frac{1}{\sqrt{x}}$. If the activation energy is important, the problem is much harder.

For large activation energies, the case of interest is the upper branch of the steady solutions. For the transient case, one is likewise interested in strongly burning solutions. The problem is, how do they become established? For this unstrained flame, the Damköhler number is proportional to the distance from the edge of the splitter plate. (Carrier *et al.* (1975) and Liñan (1963)) If the strongly burning solution is valid only above a certain critical Damköhler number, then clearly the flame cannot extend all the way upstream to the edge of the splitter plate since the Damköhler number goes to zero there.

Liñan and Crespo's (1976) solution to the transient ignition problem, discussed earlier, consisits of three regions. First, immediately downstream of the trailing edge, the fuel and oxidizer diffuse into one another. The reaction proceeds slowly. The temperature slowly rises, until a runaway occurs. The area where fuel and oxidizer have mixed is swept by a premixed flame. Downstream, the flame is hot and is described by the Burke-Schumann solution. As discussed before, this solution relies on the reaction of fuel and oxidizer at T_∞, and in addition the flow velocity u must be large compared to the premixed laminar flame speed to avoid violating the boundary layer assumptions.

Liñan and Crespo's solution suggests another possibility consisting of an upstream region of diffusion with no reaction and a downstream region of vigorous reaction corresponding to the Burke-Schumann solution. If the flow velocity u is less than the premixed laminar flame speed, then the transition between the two regions consists of a premixed flame propagating upstream. The overlap between the fuel and oxidizer profiles, created by diffusion, serves as a layer of flammable mixture which grows thinner as the flame approaches the splitter plate. Thus the speed of the premixed flame will decrease as its curvature is increased, and it will reach a steady position downstream of the trailing edge.

This ignition mechanism has been noticed experimentally. Melvin *et al.* (1971) have observed that hydrogen-oxygen diffusion flames "lift off" the edge of the splitter plate under some conditions. In particular, the mechanism has been explored in some detail by Phillips (1964).

No theoretical discussion of this problem can be found. The problem is complicated by the fact that propagation of the premixed flame is governed by heat conduction and concentration diffusion in the upstream direction. Since these were ignored in the boundary layer approximation, it is of no use in describing the transition region. In addition, such an ignition mechanism would be difficult to incorporate into this analysis, since it rests on treating each piece of a complicated, distorted flame surface as a one dimensional transient strained flame. For this analysis to be valid, conduction and diffusion normal to the flame surface must dominate that parallel to the flame surface. Large gradients parallel to the flame surface would violate this fundamental assumption. Thus, another mechanism to ignite the flame is required.

One solution to the ignition problem which is consistent with this method of analysis is provided by Clarke (1969). Instead of a sharp edged splitter plate, Clarke formulated the mixing layer problem for a parabolic splitter plate. He found that the requirement of a sufficiently large Damköhler number to sustain the vigorously burning solution translated into a requirement that the radius of curvature of the trailing edge be sufficiently large.

Therefore, instead of solving the problem of how a flame with an initial Damköhler number of zero ever becomes lit, instead assume a flame with a nonzero Damköhler number as an initial condition. This is equivalent to saying that the flame has been in existence for a time t_0 when the vortex is imposed at $t = 0$.

3.6.3 How Large Does the Activation Energy Have To Be?

The behavior of a laminar diffusion flame depends on whether the reaction rate changes significantly when evaluated at the supply temperature and at the adiabatic flame temperature. Unfortunately, one cannot say exactly what is meant by "significantly", only that for hydrocarbon fuels the difference apparently is significant enough. This may not always be the case. Numerical computations by Liu and Libby (1970) for an air jet impinging on a wall through which hydrogen is blown do not show any multivalued solutions. Liu and Libby used a system of eight reversible reactions, and took the hydrogen supply temperature to be 1000 K and the air supply temperature to be 2000 K and 2500 K. The results indicate a continuous transition from frozen flow to equilibrium flow as the strain rate is changed. This is probably due to the high initial temperatures of the reactants.

3.7 Summary

For reaction systems in which the rate change due to temperature rise is not important, calculate the fuel consumption rate per unit flame area using equations 3.24. When the change is important, an already established flame will be assumed, and equation 3.24b will be used to calculate the fuel consumption, provided the Damköhler number does not fall below the critical value for extinction.

4. NUMERICAL RESULTS FOR THE HYDROGEN-FLUORINE FLAME

4.1 Introduction

In chapter two, the strain rate ε for a vortex flame was found as a function of r, Γ, and t. Since Γ is a property of the vortex, and r is a constant for a given piece of the flame, then equation 2.13 defines the strain rate as a function of time. Therefore, one would like to use the results of chapter three (specifically, equations 3.24) to find the time dependent fuel consumption rate, for the known time dependent strain rate.

The assumptions of chapter three are rather restrictive. Few actual chemical reactions are single step, although sometimes a single step may control the overall reaction rate. In addition, real chemical reaction rates are temperature dependent, and this has been overlooked in equations 3.24. Most importantly, equations 3.24 are strictly valid only if $\frac{t}{t_{ch}}$ is very large or very small. One would like to know how accurate they are for values of $\frac{t}{t_{ch}}$ near one.

The purpose of this chapter is to determine how accurately the approximate equations 3.24 describe the behavior of a realistic kinetic system. Of specific interest is the case where $\varepsilon(t)$ is given by equation 2.13, for different values of the parameter $\frac{\Gamma}{\pi r^2}$.

4.2 The Hydrogen-Fluorine Reaction System

Equations 3.24 will be useful only for reaction systems which do not exhibit the ignition-extinction behavior typical of "large activation energy" systems. This requirement excludes hydrocarbon fuels, at least near room temperatures. As the result of previous experience (Marble *et al.* (1979)) the reaction $H_2 + F \rightarrow HF + H$ was chosen. The kinetic data are readily available, for a recent compilation see Cohen (1977). Cummings *et al.* (1977) have reported

that the chosen kinetic scheme agrees well with experimental results. The system is of practical interest for its potential use in chemical lasers, see Emanuel *et al.* (1973).

Hydrogen and fluorine react vigorously when combined, thus one does not have to specify some ignition mechanism to start the reaction. Although the reaction rates are temperature dependent, intuitively, the temperature dependence should not be strong enough to produce a bifurcated solution.

For the solutions to be presented, both reactants were at 300 K and at 5 *torr*. The fuel was composed of 2.67×10^{-8} *gram moles/cm*^{3} of hydrogen diluted with 2.47×10^{-7} *gram moles/cm*^{3} of helium. The oxidizer was 2.67×10^{-8} *gram moles/cm*^{3} of monatomic fluorine, again diluted with 2.47×10^{-7} *gram moles/cm*^{3} of helium.

The viscosities and specific heats were allowed to differ for the different species and were allowed to be functions of temperature as well. For convenience, the thermal conductivities and diffusivities for each species were calculated assuming constant Prandtl and Lewis numbers of unity.

The reaction scheme for the hydrogen-fluorine system consists of over one hundred reactions. For the given conditions of temperature and concentration, it was decided that the eighteen reactions given in table 4.1 adequately describe the problem. The first three reactions describe the "pumping" reactions $H_2 + F \rightarrow HF(j) + H$; where j is the vibrational quantum number. By collisions with H, H_2, F and HF itself (the symbol M represents HF in any state), the excited states are deactivated (reactions four through eighteen). The coefficients F_0, F_1 and F_2 describe the temperature dependent forward reaction rate

$$k_f = F_0 T^{F_2} e^{\frac{-1000\,F_1}{T}} \qquad 4.1$$

and the coefficients G_0, G_1 and G_2 describe the backward reaction rate

$$k_b = G_0 T^{G_2} e^{\frac{-1000\,G_1}{T}} \qquad 4.2$$

of each reaction. The units of these coefficients are such that if temperatures are measured in degrees Kelvin, and concentrations in gram moles per cubic centimeter, then the resulting reaction rate has units of gram moles per cubic centimeter per second.

Thus, the system involves many separate individual reactions, with temperature dependent reaction rates. Specific heats and viscosities (and thus thermal conductivities and diffusion coefficients, calculated from the Prandtl and Lewis numbers) are different for the different species, and are functions of temperature as well. Thus, the reaction system described has many complications not included in the derivation of equations 3.24.

4.3 The Numerical Solution

To numerically solve the concentration and energy equations describing the $H_2 + F$ reaction, the BLOTTNER boundary layer computer code was used. Originally written to solve chemically reacting boundary layer problems which arise in reentry situations (the program is described in Blottner (1970) and Blottner *et al.* (1971)), the program has been modified by the TRW Space and Defense Systems Group to solve the laminar mixing layer problem instead. To start the solution, initial velocity, concentration, and temperature profiles are specified at an initial station $x = 0$. Downstream (for $x > 0$), edge conditions (velocity, concentration, and temperature at $y = +\infty$ and at $y = -\infty$) are input as functions of x. The BLOTTNER program then solves the boundary layer equations for velocity, concentration, and temperature by the finite difference

method; marching downstream from the initial profile. The y as well as the x coordinates are broken into discrete intervals; in these calculations the y mesh consists of 49 points. The value of y at the n^{th} node will be denoted y_n.

In a numerical calculation of this type, one cannot actually apply boundary conditions at $y = +\infty$ and $y = -\infty$. The y mesh of 49 points extends only over a finite domain, the width of this domain is $y_{49} - y_1$. So, the program equates the velocity, concentration, and temperature at y_{49} and at y_1 to the boundary values specified by the user. The width of the domain is controllable by the user, so the objective is to specify a domain thick enough that the flame is not influenced by the boundaries. Effectively, one wants to place y_1 and y_{49} far enough from the flame that the boundary conditions applied at these points are effectively boundary conditions at infinity. When this is done, the solutions for a finite domain are applicable to the infinite domain of interest.

BLOTTNER solves the boundary layer equations for a laminar mixing layer; the problem of interest is a one dimensional flame which is strained as a function of time. This problem may be solved using BLOTTNER in the following manner: Consider the degenerate mixing layer wherein the velocities of the upper and lower streams are equal. If the initial velocity profile is uniform, and the specified boundary or edge velocities are equal to each other (the upper stream velocity equal to the lower) and constant (the velocities of both streams are constant as one moves downstream, in the x direction), then the problem of solving for the velocity is trivial, with the solution that $u(x,y) = U_0$. Since the boundary layer equations allow diffusion and heat conduction in the y direction only, the equations solved by BLOTTNER for concentration and temperature as functions of x and y are the same as the equations for a one dimensional transient flame as functions of t and y, with the substitution $t = \frac{x}{U_0}$. Thus the

boundary layer program BLOTTNER can be used to solve the problem of a transient, unstrained, one-dimensional diffusion flame.

Similarly, for a transiently strained flame, with a time dependent strain rate $\varepsilon(t)$, then let the initial velocity profile be uniform, and specify that the upper and lower streams have equal velocities (*i.e.*, $u_1(x) = u_{49}(x) = U(x)$). Note that the upper and lower streams have equal velocities at a given value of x, but that the velocity of each stream is a function of x. This increase in the edge velocities as a function of x produces the straining. If the desired strain history $\varepsilon(t)$ is given, then $\frac{dU}{dx} = \varepsilon(t)$ and $\frac{dx}{dt} = U$. Solving these two equations yields the edge conditions $U(x)$ which must be input into BLOTTNER to produce the desired strain rate together with a relation between x and t which relates the downstream distance of a piece of the flame to the time it has existed since being born at $x = 0$.

This use of the BLOTTNER program, relating distance downstream in the boundary layer problem to elapsed time in the transient problem, requires that the velocity profile be uniform as one traverses the mixing layer. However, the velocities at the edges are being increased as the flame travels downstream. One must somehow ensure that the velocities in the middle of the layer do not lag behind the acceleration of the edges. A pressure gradient may be used to accelerate the middle of the mixing layer so it keeps up with the edges, but this approach suffers two disadvantages. First, the density is not constant across the layer, so a given pressure gradient will accelerate the flow unevenly. Second, for the one dimensional transient flame the pressure should be constant in time, but this will not be true if the pressure in the analogous mixing layer flow decreases in the downstream direction.

To guarantee velocity profiles which are uniform in the y direction, note

that the viscosity does not enter into the equations for the concentrations or temperature (ignoring viscous dissipation). The viscosity matters only in the momentum equation for finding the velocity u. Therefore, specify an artificially large value for the viscosity to ensure that the fluid in the middle of the layer is dragged along with the edges with essentially no slip.

The artifice just described relies on the fact that the boundary conditions are really applied at y_1 and at y_{49}, and not at $-\infty$ and $+\infty$. For a Prandtl number of 10^4, $y_{49} - y_1$ may be chosen so that the mixing layer is thin as far as the momentum equation is concerned, thus even the middle of the layer responds rapidly to increasing edge velocities, yet be thick as far as the species and energy equations are concerned, thus preserving the effective concentration and temperature conditions at infinity.

In this way the BLOTTNER program, originally written for chemically reacting boundary layers, can be used to solve the problem of a one dimensional flame which is strained according to an arbitrary strain history $\varepsilon(t)$. In this section the initial temperature profile was assumed to be uniform, $T = 300\ K$ across the layer. For initial concentration profiles, for all $y < 0$ the mixture was taken to consist of F and He in the proportions given previously. Similiarly, for $y > 0$ the mixture was specified to be H_2 plus He.

4.4 Previous Results

In previous work (Marble, Broadwell, Norton and Subbaiah (1979)), it was found that for the $H_2 + F$ system the time dependent unstrained flame and the steady state strained flame yield approximately the same results for fuel consumption rate and for surface density of HF in the different vibrational states if $t = \frac{1}{2\varepsilon}$. This was true for strain rates of $10^3\ sec^{-1}$, $10^4\ sec^{-1}$, and $10^5\ sec^{-1}$.

The previous results are graphed in figures 4.1 and 4.2. In figure 4.1, the rate of consumption of fuel per unit area of flame, which was denoted by $\dot{m}$ in chapter three, is shown as a function of time for the transient unstrained flame as a solid line. For a flame subjected to constant straining, the fuel consumption rate $\dot{m}$ approaches a constant value as $t \to \infty$. For these numerical computations, the program was allowed to run for a finite time and the results were extrapolated to $t = \infty$ for the constant strain rate flames. The resulting values of $\dot{m}$ are also plotted in figure 4.1, with $t = \frac{1}{2\varepsilon}$. In figure 4.2, the surface density (mass of product per unit per unit area of flame) is plotted for each vibrational state of *HF*.

These results show, first, that the $H_2 + F$ flame obeys the general form of equations 3.24, consisting of a region $\frac{t}{t_{ch}} << 1$ where $\dot{m}$ is proportional to $\sqrt{t}$, and a region $\frac{t}{t_{ch}} >> 1$ where $\dot{m}$ is proportional to $\frac{1}{\sqrt{t}}$. For intermediate values of $\frac{t}{t_{ch}}$, a smooth transition is found from one region to the other. One may interpret the result as consisting of a reaction limited regime for small $\frac{t}{t_{ch}}$, and a diffusion limited regime for large $\frac{t}{t_{ch}}$. For values of $\frac{t}{t_{ch}}$ of approximately one, both limitations are apparently effective, thus the fuel consumption rate is less than predicted by either equation 3.24a or equation 3.24b.

Another result is the correspondence between $\dot{m}(t)$ for the unstrained flame and $\dot{m}(1/2\varepsilon)$ for steadily strained flames at large times. This result is consistent with the analysis of chapter three. For a transient unstrained flame, $\bar{\tau} = t$, and for the steadily strained flame, $\bar{\tau} \to \frac{1}{2\varepsilon}$ as $t \to \infty$. Thus, if the fuel consumption rate were a function only of $\bar{\tau}$, one would expect $\dot{m}$ for transient unstrained flames to be equal to $\dot{m}$ for steadily strained flames at large times,

when t for the unstrained flame equals $\frac{1}{2\varepsilon}$ for the steady strained flame.

In either limit, for small or large $\frac{\bar{\tau}}{t_{ch}}$, this correspondence is expected, since equations 3.24a and 3.24b are valid in these limits, and these equations show that $\dot{m}$ will be a function of only of $\bar{\tau}$. However, the numerical evidence indicates that this correspondence may be approximately valid even if $\frac{\bar{\tau}}{t_{ch}}$ is of order one.

4.5 Curvefitting

The system that has been numerically analyzed does not fit the requirements of the simple model treated theoretically in chapter three. Nevertheless, the existence of a region where $\dot{m} \sim \sqrt{\bar{\tau}}$ for small $\bar{\tau}$ and a region where $\dot{m} \sim \frac{1}{\sqrt{\bar{\tau}}}$ for large values of $\bar{\tau}$ suggests that equations 3.24 usefully approximate the behavior of the system, provided that suitable values of ρ_0, D_0, and t_{ch} can be found. Consider these values as empirical constants, to be determined so that equations 3.24 approximate the BLOTTNER numerical results as closely as possible.

Examine the numerical results for the unstrained transient flame, with the resulting fuel consumption rate graphed as a solid line in figure 4.1. Turning first to the region where $\frac{t}{t_{ch}}$ is small, $\dot{m}$ is proportional to $\sqrt{t}$. Such a relation will appear as a straight line in log-log coordinates, as shown by the dashed line in figure 4.1. The equation of this dashed line is

$$\dot{m} \approx 7.08\times10^{-2}\ gram\ moles/cm^2 sec^{3/2}\ t^{\frac{1}{2}} \qquad 4.3$$

Likewise the fuel consumption rate for large times is proportional to $\frac{1}{\sqrt{t}}$, and the numerical results in this case are approximated by

$$\dot{m} \approx 2.11\times10^{-7}\ gram\ moles/cm^2 sec^{1/2}\ t^{-\frac{1}{2}} \qquad 4.4$$

which is also plotted as a dashed line in figure 4.1.

Since the concentration of each reactant at infinity is equal to $2.67\times10^{-8} gram\ moles/cm^3$, it seems appropriate to choose this value for ρ_0. The values of D_0 and t_{ch} which, when substituted into equations 3.24a and 3.24b, produce equations 4.3 and 4.4 are

$$D_0 \approx 196 \frac{cm^2}{sec} \qquad 4.5$$

and

$$t_{ch} \approx 2.98\times10^{-6} sec \qquad 4.6$$

Thus, with these values of ρ_0, D_0, and t_{ch}, equations 3.24 are represented by the dashed lines in figure 4.1, which approximate the true fuel consumption rate, shown as the solid line.

Even though equation 3.24a is strictly valid only asymptotically for small times, and equation 3.24b for large times, the agreement is reasonable even for $t \approx t_{ch}$. If equation 3.24a were used for all times less than t_{ch}, and equation 3.24b for all times larger than t_{ch}, the maximum error would occur for times near t_{ch}. As seen in figure 4.1, this formulation would be have a slope discontinuity at $t = t_{ch}$, and it would overestimate the fuel consumption rate by less than a factor of two.

4.6 Time Varying Strain Rate

The ultimate aim is to determine whether equations 3.24 may be used to find the fuel consumption rate as a function of time for a flame which is strained as a function of time. The results so far are encouraging, but the previous discussion was based on numerical results for unstrained transient

flames and the steady flames found at large times with a constant strain rate. For the problem of a diffusion flame wound up by a vortex, the straining will be a function of time, which was given by equation 2.13.

$$\varepsilon = \frac{1}{t} \frac{\left[\frac{\Gamma t}{\pi r^2}\right]^2}{1+\left[\frac{\Gamma t}{\pi r^2}\right]^2} \qquad 2.13$$

If a piece of the flame is followed as it is convected by the vortex, the parameter $\frac{\Gamma}{\pi r^2}$ will be a constant. Thus, equation 2.13 may be considered as specifying the strain rate as a function of time for a given piece of the flame.

Therefore, choose a value for $\frac{\Gamma}{\pi r^2}$, compute a time varying strain rate from equation 2.13, and use the BLOTTNER program to solve for the fuel consumption rate as a function of time for this flame. To encompass the flames lying at different radii from the center of the vortex, this process should be repeated for several values of $\frac{\Gamma}{\pi r^2}$. The BLOTTNER computer program was run for $\frac{\Gamma}{\pi r^2}$ values of $10^4\ sec^{-1}$, $10^5\ sec^{-1}$, $10^6\ sec^{-1}$, and $10^7\ sec^{-1}$. These values were chosen to span the range from $\frac{\Gamma}{\pi r^2} << \frac{1}{t_{ch}}$ to $\frac{\Gamma}{\pi r^2} >> \frac{1}{t_{ch}}$. As before, the reactant consumption rate and the surface densities of the different vibrational states of *HF* are graphed as functions of time in figures 4.3 through 4.10.

Consider the fuel consumption rate as a function of time for $\frac{\Gamma}{\pi r^2} = 10^7\ sec^{-1}$. The graph (figure 4.3) closely resembles the graph in figure 4.1 (for the unstrained case) except for an inflection near $t = 10^{-7}\ sec$. Suggestively, the inflection occurs as $\frac{\Gamma t}{\pi r^2}$ passes through the value of one.

This inflection may be explained in terms of the proposed model. To do so, one first needs an expression for $\bar{\tau}$ for this transiently strained flame. Since

equation 2.13 gives the strain rate as a function of time, the parameter $\bar{\tau}$ may be found as a function of time from equations 3.8 and 3.12, together with the initial condition that $\bar{\tau} = 0$ at $t = 0$. The result is

$$\frac{\Gamma\bar{\tau}}{\pi r^2} = \frac{\left[\frac{\Gamma t}{\pi r^2}\right] + \frac{1}{3}\left[\frac{\Gamma t}{\pi r^2}\right]^3}{1 + \left[\frac{\Gamma t}{\pi r^2}\right]^2} \qquad 4.7$$

Equation 4.7 may be analysed in the separate limits of $\frac{\Gamma t}{\pi r^2} << 1$ and $\frac{\Gamma t}{\pi r^2} >> 1$, with the results

$$\bar{\tau} \sim t \quad \text{for} \quad \frac{\Gamma t}{\pi r^2} << 1 \qquad 4.8a$$

$$\bar{\tau} \sim \frac{t}{3} \quad \text{for} \quad \frac{\Gamma t}{\pi r^2} >> 1 \qquad 4.8b$$

First, one understands why all our plots of fuel consumption versus time for these strained flames resemble the unstrained case so much. For the unstrained case, $\bar{\tau} = t$, and for the strainings found in spiral flames, equations 4.8 show that $\bar{\tau}$ is still closely related to the time. The inflection occurs when $\frac{\Gamma t}{\pi r^2} \approx 1$, so one should explore the transition from equation 4.8a and equation 4.8b. The inflection occurs at a time much less than the chemical time, thus, from equations 4.8 $\bar{\tau}$ will be small compared to t_{ch} in the neighborhood of the inflection. The proposed model states that the fuel consumption rate is given by equation 3.24a when $\bar{\tau} << t_{ch}$, so substituting equations 4.8 for $\bar{\tau}$ into equation 3.24a results in

$$\dot{m} \sim \frac{\rho_0}{t_{ch}}\left[\frac{D_0 t}{\pi}\right]^{\frac{1}{2}} \quad \text{for} \quad \frac{\Gamma t}{\pi r^2} << 1 \qquad 4.9a$$

$$\dot{m} \sim \frac{\rho_0}{t_{ch}}\left[\frac{D_0 t}{3\pi}\right]^{\frac{1}{2}} \quad \text{for} \quad \frac{\Gamma t}{\pi r^2} >> 1$$

4.9b

Figure 4.3 shows the fuel consumption rate $\dot{m}$ plotted as a function of the time t in *log –log* coordinates. Since both equations 4.9a and 4.9b show the fuel consumption rate to be proportional to $\sqrt{t}$, if they were plotted in *log –log* coordinates each equation would result in a straight line with a slope of one half. However, equations 4.9 differ by a factor of $\sqrt{3}$, which means that their graphs in *log –log* coordinates would be parallel lines, of the same slope but with intercepts which differ by a factor of $log(\sqrt{3})$.

Thus, the inflection in figure 4.3 may be explained. It is found where $\frac{\Gamma t}{\pi r^2} \approx 1$, where the transition from equation 4.9a to equation 4.9b will occur. As the time passes through this value, the graph of $\dot{m}$ in log-log coordinates will move from one straight line down to another parallel line. Examination of the inflection in figure 4.3 indicates that the BLOTTNER result is consistent with the theoretical explanation.

Figure 4.9, for a value of $\frac{\Gamma}{\pi r^2}$ of $10^4\, sec^{-1}$, shows an inflection which is apparently a shift upwards to a parallel line with a greater intercept. This result is consistent with the theory, since this inflection occurs in a region where equation 3.24b should be valid. Using equation 3.24b, and repeating the previous argument yields a result which is consistent with the numerical results. In this case, $\dot{m}$ is proportional to $\frac{1}{\sqrt{\tau}}$, so decreasing τ by a factor of three will cause $\dot{m}$ to increase by a factor of $\sqrt{3}$. Thus, the upward shift occurs when $\frac{\Gamma t}{\pi r^2} \approx 1$.

Figures 4.5 and 4.7 show the fuel consumption rate when $\frac{\Gamma}{\pi r^2}$ is equal to $10^6\, sec^{-1}$ and $10^5\, sec^{-1}$. Since these values are nearly the reciprocal of the

chemical time of the system, neither equation 3.24a or 3.24b is accurate when the transition inflection occurs.

The final test is to plot the fuel consumption rate $\dot{m}$ as a function of $\bar{\tau}$ rather than of time. As shown in figures 4.11 through 4.14, the inflections are removed. One sees that the fuel consumption rate may be expressed as a function only of $\bar{\tau}$ with accuracy when $\bar{\tau}$ is large or small compared to the chemical time, and approximately even if $\bar{\tau} \approx t_{ch}$. In addition, equations 3.24a and 3.24b are shown as dashed lines, with the values of D_0 and t_{ch} determined empirically from the transient unstrained flame. (equations 4.5 and 4.6)

4.7 Summary

The theoretical predictions of chapter three have been verified for a genuine chemical reaction system of practical interest. The example chosen does not necessarily represent all practical reaction systems; indeed, the $H_2 + F$ reaction was selected because the reactants ignite spontaneously when allowed to mix, and no special initial conditions need be introduced to ensure a vigorously burning solution. This same characteristic avoids the question of extinction at too large strain rates, found in systems characterised by high activation energies.

On the basis of numerical calculations for transiently strained $H_2 + F$ flames, the asymptotic equations 3.24 may be used for this more complicated system if one considers D_0 and t_{ch} to be empirical constants. For the $H_2 + F$ reaction described in this section, the appropriate values are $D_0 \approx 196 \frac{cm^2}{sec}$ and $t_{ch} \approx 2.98 \times 10^{-6} sec$.

If equations 3.24 are used to predict $\dot{m}$ even if $\frac{\bar{\tau}}{t_{ch}}$ is of order one, the fuel consumption rate will be overestimated by approximately a factor of two. In

addition, the slope discontinuity built into this flame model at $t = t_{ch}$, where equations 3.24a and 3.24b patch together, will introduce a slope discontinuity into later results.

5. THE CALCULATION OF SPIRAL FLAME PROPERTIES

5.1 Introduction

The aim of this chapter is to compute the increase in fuel consumption due to the presence of a vortex. In chapter two, the increase in flame area and the flame straining due to the vortex were calculated. Chapter three described the approximations which allow the prediction of fuel consumption rate per unit of flame area, given an arbitrary strain rate as a function of time. For systems where the reaction rate is essentially constant, these results are summarized by equations 3.24, which incorporate the effect of an unsteady strain rate into the parameter $\bar{\tau}$. Chapter four compared these approximate formulae to results of numerical calculations for the $H_2 + F$ reaction system, strained as it would be in a spiral flame. Now the various pieces of the model are assembled to calculate the properties of a spiral flame. For simplicity, initially consider the case where a, the distance from the flame to the vortex, is equal to zero.

5.2 The Burned Out Core

As shown in the second chapter, at any given radius the flame density increases indefinitely and thus the spacing between adjacent flames becomes smaller and smaller. This is important for two reasons. First, if the radial diffusion of reactants and products is ignored, the amount of each reactant present at a given radius is finite. Eventually, the flame must consume all of the available fuel or oxidizer. The reaction must cease, and the further increase of flame surface at that radius cannot result in the consumption of additional fuel or oxidizer.

Secondly, the theoretical analysis of chapter three and the numerical analysis of chapter four assumed a one dimensional flame located on the x axis. The upper half plane contained fuel and the lower half plane contained oxidizer.

Thus the flame had infinite reservoirs of fuel and oxidizer to draw on and could grow in thickness indefinitely. In the tightly wrapped center of a spiral flame, the flame surfaces are nearly circles, and if one started at one flame surface and travelled normal to that surface, one would soon encounter another flame.

Thus, rather than a single flame located on the x axis, a more appropriate local analysis would consist of alternate layers of fuel and oxidizer, with many flame surfaces parallel to the x axis. Clearly, each flame may be considered as independent of its neighbors only as long as the spacing between flames is greater than the thickness of an individual flame. When the flame thickness is comparable to the spacing between flames, the results of chapters three and four are not accurate. The interaction of adjacent flames must eventually cause the fuel consumption rate to go to zero.

5.2.1 Approximation

More complicated models describing the interaction of adjacent flame surfaces will be developed in chapter six; a simpler model used by Marble (1982) will be employed here. Pick a fixed radius r, and consider the circular annulus $(r, r+dr)$. In chapter two (see equation 2.12), an expression for the increasing flame area within this annulus was derived. In addition, using equations 3.24, the rate of fuel consumption per unit flame area is known. Forming the product, one then knows the rate at which fuel (and also oxidizer) within this annulus is being consumed. This result is valid only as long as there is are available fuel and oxidizer to be burned, or until each piece of flame feels the influence of its neighbors.

As an approximation, suppose that the fuel consumption rate in the annulus is given accurately by the product of the flame area and the result of equations 3.24 until all the available fuel is consumed, and at that point the

consumption of fuel abruptly stops. Thus, one can define a burnout time t^*, and find $\dot{m}$ from equations 3.24 if $t < t^*$, and set $\dot{m} = 0$ if $t > t^*$.

To find the burnout time t^*, note that the annulus $(r, r+dr)$ initially contains a finite supply of both fuel and oxidizer. (In the current problem, the initial concentrations of fuel and oxidizer are equal, and the stoichiometry of the reaction consumes them in 1:1 proportions. Thus, exhaustion of fuel and oxidizer will occur simultaneously. For brevity, burnout will be referred to as due to exhaustion of fuel.) The velocity field of the vortex is purely tangential, so no radial convection will occur. If radial diffusion is neglected, (this assumption will be examined in chapter six), then the quantity of fuel within the annulus at any time is equal to the amount initially present minus the amount consumed since $t = 0$. Thus, the burnout time t^* may be found as the time required for the flames within the annulus to consume all the fuel originally present.

5.2.2 Calculations

Chapter two gives the flame surface within an annulus $(r, r+dr)$ as $2\left[1+\left[\frac{\Gamma t}{\pi r^2}\right]^2\right]^{\frac{1}{2}} dr$. The mass of fuel originally within that annulus is easily found to be $\rho_0 \pi r\, dr$. Approximate the fuel consumption rate per unit flame area by equations 3.24

$$\dot{m} \sim \frac{\rho_0}{t_{ch}}\left[\frac{D_0 \bar{\tau}}{\pi}\right]^{\frac{1}{2}} \quad \text{for} \quad \bar{\tau} < t_{ch} \qquad 3.24a$$

$$\dot{m} \sim \rho_0\left[\frac{D_0}{\pi \bar{\tau}}\right]^{\frac{1}{2}} \quad \text{for} \quad \bar{\tau} > t_{ch} \qquad 3.24b$$

In keeping with the proposed flame model, equation 3.24a has been written so it applies for all $\bar{\tau}$ less than t_{ch}, and equation 3.24b will be used for all $\bar{\tau}$ greater than t_{ch}.

The parameter $\bar{\tau}$ was found in chapter four,

$$\frac{\Gamma\bar{\tau}}{\pi r^2} = \frac{\left[\frac{\Gamma t}{\pi r^2}\right] + \frac{1}{3}\left[\frac{\Gamma t}{\pi r^2}\right]^3}{1 + \left[\frac{\Gamma t}{\pi r^2}\right]^2} \qquad 4.7$$

The calculation will be complicated by the fact that different expressions are used for $\dot{m}$ depending on the value of $\bar{\tau}$. Equation 4.7 indicates that $\bar{\tau}$ is a monotonically increasing function of t, so denote the time at which $\bar{\tau} = t_{ch}$ by the symbol t'. Thus,

$$\frac{\Gamma t_{ch}}{\pi r^2} = \frac{\frac{\Gamma t'}{\pi r^2} + \frac{1}{3}\left[\frac{\Gamma t'}{\pi r^2}\right]^3}{1 + \left[\frac{\Gamma t'}{\pi r^2}\right]^2} \qquad 5.1$$

Therefore, if $t < t'$ then $\bar{\tau} < t_{ch}$ and $\dot{m}$ is found from equation 3.24a; if $t > t'$ then $\bar{\tau} > t_{ch}$ and $\dot{m}$ is found from equation 3.24b.

So, if the burnout time t^* is less than t', then equation 3.24a is valid from $t = 0$ until burnout, and the burnout time t^* is found by setting the fuel consumed from $t = 0$ until $t = t^*$ equal to the fuel originally present.

$$\int_0^{t^*} \frac{\rho_0}{t_{ch}} \left[\frac{D_0\bar{\tau}}{\pi}\right]^{\frac{1}{2}} 2\left[1+\left[\frac{\Gamma t}{\pi r^2}\right]^2\right]^{\frac{1}{2}} dt = \rho_0 \pi r \qquad 5.2$$

Making the variable of integration $p \equiv \frac{\Gamma t}{\pi r^2}$ and calling $\frac{\Gamma t^*}{\pi r^2} \equiv p^*$, and substituting for $\bar{\tau}$ from equation 4.7, equation 5.2 becomes,

$$\frac{t^*}{t_{ch}} \frac{1}{p^*} \int_0^{p^*} \left[p + \frac{1}{3}p^3\right]^{\frac{1}{2}} dp = \frac{\pi}{2}\left[\frac{\Gamma}{D_0}\right]^{\frac{1}{2}} \qquad 5.3$$

If t^* is greater than t', then first integrate from $t = 0$ to $t = t'$ using equation 3.24a, and then integrate from $t = t'$ to $t = t^*$ using equation 3.24b. Calling $\frac{\Gamma t'}{\pi r^2} \equiv p'$, the result is

$$\frac{t^*}{t_{ch}}\frac{1}{p^*}\int_0^{p'}\left[p+\frac{1}{3}p^3\right]^{\frac{1}{2}}dp+\int_{p'}^{p^*}\frac{1+p^2}{\left[p+\frac{1}{3}p^3\right]^{\frac{1}{2}}}dp=\frac{\pi}{2}\left[\frac{\Gamma}{D_0}\right]^{\frac{1}{2}} \qquad 5.4$$

To put the problem entirely in terms of the new variable p, equation 5.1 for t' may be rewritten as

$$p_{ch}\equiv\frac{\Gamma t_{ch}}{\pi r^2}=\frac{p'+\frac{1}{3}p'^3}{1+p'^2} \qquad 5.5$$

Equations 5.3, 5.4, and 5.5 determine the dimensionless burnout time $\frac{\Gamma t^*}{\pi r^2}$ as a function of $\frac{\Gamma t_{ch}}{\pi r^2}$ and the ratio of the vortex circulation to the diffusivity, $\frac{\Gamma}{D_0}$. The equations 5.3, 5.4 and 5.5 could be solved numerically, but closed form solutions can be found by examining the limit $\frac{\Gamma}{D_0}\to\infty$.

The limit is most easily taken by first rescaling the variables. Marble (1982) found that the radius of his burned out core was proportional to $\Gamma^{\frac{1}{3}}D^{\frac{1}{6}}t^{\frac{1}{2}}$ in the large *Re* limit. This suggests a scaled variable of the form

$$q\equiv\frac{\Gamma^{\frac{2}{3}}D_0^{\frac{1}{3}}t}{\pi r^2}=\left[\frac{D_0}{\Gamma}\right]^{\frac{1}{3}}p \qquad 5.6$$

Similiarly, define

$$q'\equiv\left[\frac{D_0}{\Gamma}\right]^{\frac{1}{3}}p' \qquad 5.7$$

$$q^*\equiv\left[\frac{D_0}{\Gamma}\right]^{\frac{1}{3}}p^* \qquad 5.8$$

$$q_{ch}\equiv\left[\frac{D_0}{\Gamma}\right]^{\frac{1}{3}}p_{ch} \qquad 5.9$$

Substituting the new variables, equations 5.5, 5.3 and 5.4 become

$$q_{ch} = \frac{\frac{1}{3} q'^3 + \left[\frac{D_0}{\Gamma}\right]^{\frac{2}{3}} q'}{q'^2 + \left[\frac{D_0}{\Gamma}\right]^{\frac{2}{3}}} \qquad 5.10$$

and

$$\frac{1}{q_{ch}} \int_0^{q^*} \left[\frac{1}{3} q^3 + \left[\frac{D_0}{\Gamma}\right]^{\frac{2}{3}} q\right]^{\frac{1}{2}} dq = \frac{\pi}{2} \quad \text{for} \quad q^* < q' \qquad 5.11$$

and for $q^* > q'$,

$$\frac{1}{q_{ch}} \int_0^{q'} \left[\frac{1}{3} q^3 + \left[\frac{D_0}{\Gamma}\right]^{\frac{2}{3}} q\right]^{\frac{1}{2}} dq \qquad 5.12$$

$$+ \int_0^{q^*} \left[q^2 + \left[\frac{D_0}{\Gamma}\right]^{\frac{2}{3}}\right] \left[\frac{1}{3} q^3 + \left[\frac{D_0}{\Gamma}\right]^{\frac{2}{3}} q\right]^{-\frac{1}{2}} dq = \frac{\pi}{2}$$

The second integral in equation 5.12 can be evaluated in closed form, but the integral in equation 5.11 and the first integral in equation 5.12 cannot. In addition, equation 5.10 must be inverted to find q' as a function of q_{ch}.

The solution for $\frac{\Gamma}{D_0} \to \infty$ is easily found by setting $\frac{D_0}{\Gamma}$ equal to zero in equations 5.10, 5.11 and 5.12 and assuming that q^*, q', and q_{ch} are all of order one. Equation 5.10 becomes,

$$q' \sim 3q_{ch} \quad \text{or} \quad t' \sim 3t_{ch} \qquad 5.13$$

Thus for $t^* < 3t_{ch}$,

$$q^* \sim \left[\frac{5\pi\sqrt{3}}{4} \frac{t_{ch}}{t}\right]^{\frac{2}{3}} \qquad 5.14$$

and for $t^* > 3t_{ch}$,

$$q^* \sim \left[\frac{\pi}{4}\right]^{\frac{2}{3}} \left[\frac{1}{\sqrt{3}} - \frac{6}{5}\left[\frac{t_{ch}}{t}\right]^{\frac{3}{2}}\right]^{\frac{2}{3}} \qquad 5.15$$

These results may be interpreted in another way. Rather than fixing r and finding the time t^* required to exhaust the fuel, one may define r^* as the radius of the burned out core and rearrange equations 5.14 and 5.15 to find r^* as a function of t. Denoting the scaled core radius η^*, defined as $\eta^* \equiv \frac{\pi^{\frac{1}{2}} r}{\Gamma^{\frac{1}{3}} D_0^{\frac{1}{6}} t^{\frac{1}{2}}}$, the result is

$$\eta^* \sim \left[\frac{4}{5\pi\sqrt{3}} \frac{t}{t_{ch}}\right]^{\frac{1}{3}} \quad \text{for} \quad \frac{t}{t_{ch}} < 3 \qquad 5.16a$$

$$\eta^* \sim \left[\frac{2}{\pi}\left[\frac{2}{\sqrt{3}} - \frac{12}{5}\left[\frac{t_{ch}}{t}\right]^{\frac{3}{2}}\right]\right]^{\frac{1}{3}} \qquad 5.16b$$

Assuming infinitely fast chemistry, Marble (1982) found that η^* was a constant; taking the finite chemistry into account, equations 5.16 indicate that it is a function of $\frac{t}{t_{ch}}$. (If the limit $\frac{\Gamma}{D_0} \to \infty$ had not been taken, η^* would be a function of $\frac{\Gamma}{D_0}$ as well.) The function is graphed in figure 5.1. As one might expect, for times large compared to the chemical time, the core radius, scaled by $\Gamma^{\frac{1}{3}} D_0^{\frac{1}{6}} t^{\frac{1}{2}}$, approaches a constant value.

5.2.3 The Rate of Growth of the Core

The structure of a spiral flame consists of a dead, burned out core, where all fuel has been consumed, surrounded by the two spiral flame arms. For this problem a 1:1 stoichiometry and equal concentrations of fuel and oxidizer have been assumed; thus the core is composed solely of combustion products. Were this not the case, the core would consist of a mixture of combustion products

and whichever reactant was present in excess.

The radius of the core is r^*, and the volume of the core is proportional to πr^{*2}. Denoting the core volume by C (really the core area in two dimensions), the rate of increase of the product contained in the core is $\dot{C} = \frac{d}{dt}(\pi r^{*2})$. From equations 5.16,

$$\frac{\dot{C}}{\Gamma^{\frac{2}{3}} D_0^{\frac{1}{3}}} \sim \frac{5}{3}\left[\frac{4}{5\pi\sqrt{3}}\frac{t}{t_{ch}}\right]^{\frac{2}{3}} \quad \text{for} \quad \frac{t}{t_{ch}} < 3 \qquad 5.17a$$

$$\frac{\dot{C}}{\Gamma^{\frac{2}{3}} D_0^{\frac{1}{3}}} \sim \left[\frac{2}{\sqrt{3}} - \frac{12}{5}\left[\frac{t}{t_{ch}}\right]^{-\frac{3}{2}}\right]^{\frac{2}{3}} \qquad 5.17b$$

$$\times \left[1 + \frac{\frac{12}{5}\left[\frac{t}{t_{ch}}\right]^{-\frac{3}{2}}}{\frac{2}{\sqrt{3}} - \frac{12}{5}\left[\frac{t}{t_{ch}}\right]^{-\frac{3}{2}}}\right] \quad \text{for} \quad \frac{t}{t_{ch}} > 3$$

This function is graphed in figure 5.3. Compare these results and those of Marble (1982) and Karagozian (1982), who assumed infinitely fast chemical reactions. Marble and Karagozian found the rate of accumulation of products in the core is constant and proportional to $\Gamma^{\frac{2}{3}} D_0^{\frac{1}{3}}$. In this case, taking a finite chemical reaction rate into account, the core radius, scaled by $\Gamma^{\frac{2}{3}} D_0^{\frac{1}{3}}$, rather than being a constant, is a function of $\frac{t}{t_{ch}}$ which approaches a constant value for times large compared to the chemical time.

5.3 The Flame Surface Area

The total surface area of the spiral flame is unbounded, since the original flame was infinite in extent. However, the increase in flame surface area due to

the vortex can be evaluated. A piece of flame at radius r of original length dr is extended by the vortex velocity field to a length of $\left[1+\left[\frac{\Gamma t}{\pi r^2}\right]^2\right]^{\frac{1}{2}} dr$ at time t. Therefore, the increase in length of this differential flame element is $\left[\left[1+\left[\frac{\Gamma t}{\pi r^2}\right]^2\right]^{\frac{1}{2}} - 1\right] dr$. Since flame elements at radii less than r^* are no longer active, due to exhaustion of fuel, the above quantity should be integrated from r^* to ∞ to find the increase in flame surface area due to the vortex.

Letting σ stand for the augmented surface area of the flame, or the increase in flame area due to the presence of the vortex, and including both flame arms yields

$$\sigma = 2\int_{r^*}^{\infty} \left[\left[1 + \left[\frac{\Gamma t}{\pi r^2}\right]^2\right]^{\frac{1}{2}} - 1\right] dr \qquad 5.18$$

Transforming the variable of integration in equation 5.18 to η, defined as $\eta \equiv \frac{\pi^{\frac{1}{2}} r}{\Gamma^{\frac{1}{3}} D_0^{\frac{1}{6}} t^{\frac{1}{2}}}$ results in

$$\sigma = \frac{2}{\sqrt{\pi}}\left[\frac{\Gamma}{D_0}\right]^{\frac{1}{3}} \Gamma^{\frac{1}{3}} D_0^{\frac{1}{6}} t^{\frac{1}{2}} \int_{\eta^*}^{\infty} \left[\left[\frac{1}{\eta^4} + \left[\frac{D_0}{\Gamma}\right]^{\frac{2}{3}}\right]^{\frac{1}{2}} - \left[\frac{D_0}{\Gamma}\right]^{\frac{1}{3}}\right] d\eta \qquad 5.19$$

The reason for evaluating σ is to explore the method of taking the limit $\frac{\Gamma}{D_0} \to \infty$. The flame area itself is not of much interest, what is of interest is the increase in the rate of fuel consumption along the flame arms due to the presence of the vortex. To calculate the fuel consumption rate, multiply together the fuel consumption rate per unit flame area and the flame area per unit radius, and integrate this quantity from the edge of the core to infinity in r. The resulting integral will be the same as the integral for σ but with an

additional factor accounting for the fuel consumption per unit flame surface.

To take the limit as $\frac{\Gamma}{D_0} \to \infty$ of equation 5.19, the obvious approach would be to set $\frac{D_0}{\Gamma}$ equal to zero. However, proceed more carefully by writing

$$\sigma = \frac{2}{\sqrt{\pi}} \left[\frac{\Gamma}{D_0} \right]^{\frac{1}{3}} \Gamma^{\frac{1}{3}} D_0^{\frac{1}{6}} t^{\frac{1}{2}} \left[\int_{\eta^*}^{\infty} \frac{1}{\eta^2} d\eta + R \right] \qquad 5.20$$

where the remainder term R is given by

$$R = \int_{\eta^*}^{\infty} \left[\left[\frac{1}{\eta^4} + \left[\frac{D_0}{\Gamma} \right]^{\frac{2}{3}} \right]^{\frac{1}{2}} - \frac{1}{\eta^2} + \left[\frac{D_0}{\Gamma} \right]^{\frac{1}{3}} \right] d\eta \qquad 5.21$$

Introduction of a stretched variable η, defined by $\eta \equiv \left[\frac{D_0}{\Gamma} \right]^{\frac{1}{6}} \eta$ enables equation 5.21 for the remainder to be rewritten as

$$R = \left[\frac{D_0}{\Gamma} \right]^{\frac{1}{6}} \int_{\left[\frac{D_0}{\Gamma} \right]^{\frac{1}{2}} \eta^*}^{\infty} \left[\left[\frac{1}{\eta^4} + 1 \right]^{\frac{1}{2}} - \left[\frac{1}{\eta^2} + 1 \right] \right] d\eta \qquad 5.22$$

The remainder is of order $\left[\frac{D_0}{\Gamma} \right]^{\frac{1}{6}}$; if the integral in equation 5.22 is bounded. Note that the integrand of equation 5.22 is always negative, so write

$$|R| \leq \left[\frac{D_0}{\Gamma} \right]^{\frac{1}{6}} \int_0^{\infty} \left[\frac{1}{\eta^2} + 1 - \left[\frac{1}{\eta^4} + 1 \right]^{\frac{1}{2}} \right] d\eta \qquad 5.23$$

In spite of appearances, the integrand in equation 5.23 approaches one as η approaches zero and goes like $\frac{1}{\eta^2}$ for large η. Thus, the integral is finite (actually, the solution may be found in terms of elliptic functions, but the actual value is unimportant), and the remainder term has been shown to be of order $\left[\frac{D_0}{\Gamma} \right]^{\frac{1}{6}}$. The increase in surface area of the flame due to the vortex is

found to lowest order by neglecting the remainder term in equation 5.20. Therefore,

$$\sigma \sim \frac{2}{\sqrt{\pi}}\left[\frac{\Gamma}{D_0}\right]^{\frac{1}{3}}\Gamma^{\frac{1}{3}}D_0^{\frac{1}{6}}t^{\frac{1}{2}}\int_{\eta^*}^{\infty}\frac{1}{\eta^2}\,d\eta = \frac{2}{\sqrt{\pi}}\left[\frac{\Gamma}{D_0}\right]^{\frac{1}{3}}\Gamma^{\frac{1}{3}}D_0^{\frac{1}{6}}t^{\frac{1}{2}}\,\frac{1}{\eta^{*3}} \qquad 5.24$$

where η^* is the scaled core radius and is given by equations 5.16. Note that for large times, η^* is constant, and thus σ goes like $\left[\frac{\Gamma}{D_0}\right]^{\frac{1}{3}}\Gamma^{\frac{1}{3}}D_0^{\frac{1}{6}}t^{\frac{1}{2}}$. Thus the flame surface area increases like $\sqrt{t}$, but it depends on the vortex strength to the $\frac{2}{3}$ power and the diffusivity to the $-\frac{1}{6}$ power.

The principal result is the conclusion that the asymptotic results for large $\frac{\Gamma}{D_0}$ could have been obtained with much less effort. For example, setting $\frac{D_0}{\Gamma}$ equal to zero in equation 5.19 would have directly resulted in equation 5.24. However, if one had directly expanded equation 5.19 in powers of $\frac{D_0}{\Gamma}$, the lowest order term would yield equation 5.24, but the expansion would be in powers of $\left[\frac{D_0}{\Gamma}\right]^{\frac{1}{3}}$, rather than in powers of $\left[\frac{D_0}{\Gamma}\right]^{\frac{1}{6}}$, and, had the processes of integration and limit-taking been interchanged, one would find that the supposedly higher order terms involve integrals which do not converge.

However, this approach would correctly yield the lowest order result. Thus, starting from the beginning, one could have noted that the flame surface per unit radius is $2\left[1+\left[\frac{\Gamma t}{\pi r^2}\right]^2\right]^{\frac{1}{2}}$. This may be rewritten as $2\left[1+\left[\frac{\Gamma}{D_0}\right]^{\frac{2}{3}}\left[\frac{\Gamma^{\frac{2}{3}}D_0^{\frac{1}{3}}t}{\pi r^2}\right]^2\right]^{\frac{1}{2}}$. If $\frac{\Gamma}{D_0}$ is large but $\frac{\Gamma^{\frac{2}{3}}D_0^{\frac{1}{3}}t}{\pi r^2}$ is of order one, the flame area per unit radius becomes, to lowest order, $2\left[\frac{\Gamma}{D_0}\right]^{\frac{1}{3}}\frac{\Gamma^{\frac{2}{3}}D_0^{\frac{1}{3}}t}{\pi r^2}$. The surface

area of the flame is found by integrating this term from r^* to infinity in r, which results in equation 5.24. Previously, equation 5.24 was proven to be the correct answer, to lowest order as $\frac{\Gamma}{D_0} \to \infty$.

As a result, one sees that as $\frac{\Gamma}{D_0} \to \infty$, the flame surface for which $\frac{\Gamma^{\frac{2}{3}} D_0^{\frac{1}{3}} t}{\pi r^2}$ is of order one composes "all" of the flame, and the contributions from other parts of the flame to the total flame area are negligible. Thus, the region where $\frac{\Gamma^{\frac{2}{3}} D_0^{\frac{1}{3}} t}{\pi r^2}$ is of order one has been established as the region of primary interest in the analysis.

What is the flame structure like in this region? Note that $\frac{\Gamma t}{\pi r^2}$ is equal to $\left[\frac{\Gamma}{D_0}\right]^{\frac{1}{3}} \frac{\Gamma^{\frac{2}{3}} D_0^{\frac{1}{3}} t}{\pi r^2}$, therefore, $\frac{\Gamma t}{\pi r^2}$ will be large in the region of interest. Chapter two discussed the structure of the spiral flame in the region where $\frac{\Gamma t}{\pi r^2}$ is large, so one is referred to these previous results.

5.4 The Fuel Consumption Rate

The calculation of the instantaneous fuel consumption rate of the spiral flame is similar to the preceding calculation of the flame area. First, since the flame is assumed to be put out once all available fuel has been exhausted, only the flame outside the core radius r^* is included. Fuel consumption per unit flame area is multiplied by the flame surface area per unit radius, and the result is integrated in r from r^* to infinity.

Examination of equation 4.7 reveals that at any time t the value of $\bar{\tau}$ lies in the range $\frac{t}{3} \leq \bar{\tau} \leq t$. Referring to equations 3.24, it is apparent that the fuel

consumption rate per unit flame area will vary by at most a factor of $\sqrt{3}$ over the entire flame at a given time. Therefore, the region where $\frac{\Gamma^{\frac{2}{3}} D_0^{\frac{1}{3}} t}{\pi r^2}$ is of order one will dominate the total fuel consumption as $\frac{\Gamma}{D_0} \to \infty$.

Finally, one realizes that just the increase in fuel consumption due to the vortex should be computed. Just as in the flame surface area calculation, this requirement is necessary to get a finite answer.

The various ingredients for calculating the fuel consumption rate are already in hand, so approximate them in the limit as $\frac{\Gamma}{D_0} \to \infty$, assuming that $\frac{\Gamma^{\frac{2}{3}} D_0^{\frac{1}{3}} t}{\pi r^2}$ is of order one. As discussed in the previous section, the flame surface area per unit radius becomes

$$2\left[1 + \left[\frac{\Gamma t}{\pi r^2}\right]^2\right]^{\frac{1}{2}} \sim 2\left[\frac{\Gamma}{D_0}\right]^{\frac{1}{3}} \frac{\Gamma^{\frac{2}{3}} D_0^{\frac{1}{3}} t}{\pi r^2} \qquad 5.25$$

Equation 4.7 for $\bar{\tau}$ becomes

$$\bar{\tau} = t \frac{1 + \frac{1}{3}\left[\frac{\Gamma}{D_0}\right]^{\frac{2}{3}}\left[\frac{\Gamma^{\frac{2}{3}} D_0^{\frac{1}{3}} t}{\pi r^2}\right]^2}{1 + \left[\frac{\Gamma}{D_0}\right]^{\frac{2}{3}}\left[\frac{\Gamma^{\frac{2}{3}} D_0^{\frac{1}{3}} t}{\pi r^2}\right]^2} \sim \frac{t}{3} \qquad 5.26$$

Thus the fuel consumption rate per unit flame area becomes, substituting equation 5.26 into equations 3.24,

$$\dot{m} \sim \frac{\rho_0}{t_{ch}}\left[\frac{D_0 t}{3\pi}\right]^{\frac{1}{2}} \quad \text{for} \quad \frac{t}{t_{ch}} \lesssim 3 \qquad 5.27a$$

$$\dot{m} \sim \rho_0 \left[\frac{3D_0}{\pi t}\right]^{\frac{1}{2}} \quad \text{for} \quad \frac{t}{t_{ch}} \gtrsim 3 \qquad 5.27b$$

Using the results from equations 5.25, 5.26 and 5.27, and using the symbol $\dot{M}$ to denote the augmented fuel consumption rate due to the vortex, then as $\frac{\Gamma}{D_0} \to \infty$,

$$\dot{M} \sim \int_{r^*}^{\infty} \frac{\rho_0}{t_{ch}} \left[\frac{D_0 t}{3\pi}\right]^{\frac{1}{2}} 2\left[\frac{\Gamma}{D_0}\right]\frac{1}{3}\frac{\Gamma^{\frac{2}{3}} D_0^{\frac{1}{3}} t}{\pi r^2}\, dr \quad \text{for} \quad t < 3t_{ch} \qquad 5.28a$$

$$\dot{M} \sim \int_{r^*}^{\infty} \rho_0 \left[\frac{3D_0}{\pi t}\right]^{\frac{1}{2}} 2\left[\frac{\Gamma}{D_0}\right]\frac{1}{3}\frac{\Gamma^{\frac{2}{3}} D_0^{\frac{1}{3}} t}{\pi r^2}\, dr \quad \text{for} \quad t > 3t_{ch} \qquad 3.28b$$

Transforming from r to η as the variable of integration, the equations may be written

$$\dot{M} \sim \rho_0 \Gamma^{\frac{2}{3}} D_0^{\frac{1}{3}} \frac{1}{\pi\sqrt{3}} \frac{t}{t_{ch}} \int_{\eta^*}^{\infty} \frac{1}{\eta^2}\, d\eta \quad \text{for} \quad \frac{t}{t_{ch}} < 3 \qquad 5.29a$$

$$\dot{M} \sim \rho_0 \Gamma^{\frac{2}{3}} D_0^{\frac{1}{3}} \frac{\sqrt{3}}{\pi} \int_{\eta^*}^{\infty} \frac{1}{\eta^2}\, d\eta \quad \text{for} \quad \frac{t}{t_{ch}} > 3 \qquad 5.29b$$

Equations 5.29 suggest certain natural dimensionless groups. First, the augmented fuel consumption rate $\dot{M}$ is proportional to $\rho_0 \Gamma^{\frac{2}{3}} D_0^{\frac{1}{3}}$. Secondly, time appears only as a ratio of the time to the chemical time of the system. Performing the indicated integrations, and substituting for η^* from equations 5.16, results in

$$\frac{\dot{M}}{\rho_0 \Gamma^{\frac{2}{3}} D_0^{\frac{1}{3}}} \sim \frac{2}{\pi\sqrt{3}} \left[\frac{5\pi\sqrt{3}}{4}\right]^{\frac{1}{3}} \left[\frac{t}{t_{ch}}\right]^{\frac{2}{3}} \quad \text{for} \quad \frac{t}{t_{ch}} < 3 \qquad 5.30a$$

and

$$\frac{\dot{M}}{\rho_0 \Gamma^{\frac{2}{3}} D_0^{\frac{1}{3}}} \sim \frac{2\sqrt{3}}{\pi}\left[\frac{4}{\pi}\left[\frac{1}{\sqrt{3}} - \frac{6}{5}\left[\frac{t}{t_{ch}}\right]^{-\frac{3}{2}}\right]\right]^{-\frac{1}{3}} \quad \text{for} \quad \frac{t}{t_{ch}} > 3 \qquad 5.30b$$

Of course, had the limit $\frac{\Gamma}{D_0} \to \infty$ not been taken, then $\frac{\dot{M}}{\rho_0 \Gamma^{\frac{2}{3}} D_0^{\frac{1}{3}}}$ would depend on the dimensionless ratio $\frac{\Gamma}{D_0}$ as well as on $\frac{t}{t_{ch}}$. However, this result shows that for large $\frac{\Gamma}{D_0}$ the fuel consumption rate of the spiral flame does not depend on the vortex strength Γ or on the diffusivity D_0 separately, but is proportional to the combined transport coefficient $\Gamma^{\frac{2}{3}} D_0^{\frac{1}{3}}$. Plotting equations 5.30, as shown in figure 5.4, reveals that a finite chemical reaction rate affects the fuel consumption rate of the spiral flame only for times which are smaller than and of the same order as the chemical time. For large $\frac{t}{t_{ch}}$, the fuel consumption rate approaches a constant.

5.5 The Case of a Vortex a Distance Away from the Flame

The previous calculations were done for the special case of the offset distance a (distance from the flame to the vortex) equal to zero. Even for a vortex a distance away from the flame, the velocity field will still increase the flame surface area and cause local straining of the flame. Recalling the necessary formulae from chapter two, from equation 2.10 one finds the flame surface area dl at time t in terms of its original area at $t = 0$ as

$$dl = \left[\left[\frac{\lambda}{r}\right]^2 \left[\left[\frac{\Gamma t}{\pi r^2}\right]\frac{\lambda}{r} - \frac{a}{r}\right]^2\right]^{\frac{1}{2}} d\lambda \qquad 5.31$$

and the strain rate is given by equation 2.11 as

$$\varepsilon = \frac{1}{t}\frac{\left[\left[\left[\frac{\Gamma t}{\pi r^2}\right]\frac{\lambda}{r} - \frac{a}{r}\right]\left[\left[\frac{\Gamma t}{\pi r^2}\right]\frac{\lambda}{r}\right]\right]}{\left[\frac{\lambda}{r}\right]^2 + \left[\left[\frac{\Gamma t}{\pi r^2}\right]\frac{\lambda}{r} - \frac{a}{r}\right]^2} \qquad 2.11$$

For a given piece of flame, λ, a and r are constants, so equation 2.11 gives the strain rate as a function of time. Thus equations 3.8 and 3.12 may be used with equation 2.11 to find the parameter $\bar{\tau}$, with the result

$$\bar{\tau} = \frac{t\left[1 - \frac{a}{r}\frac{\lambda}{r}\left[\frac{\Gamma t}{\pi r^2}\right] + \frac{1}{3}\frac{\lambda^2}{r^2}\left[\frac{\Gamma t}{\pi r^2}\right]^2\right]}{1 - 2\frac{a}{r}\frac{\lambda}{r}\left[\frac{\Gamma t}{\pi r^2}\right] + \frac{\lambda^2}{r^2}\left[\frac{\Gamma t}{\pi r^2}\right]^2} \qquad 5.32$$

As before, it will be the instantaneous value of $\bar{\tau}$ which determines the instantaneous fuel consumption per unit area of each infinitesimal piece of the flame.

5.5.1 The Case of Infinitely Fast Chemistry

In the interest of simplicity, temporarily ignore the effects of finite chemical reaction rates and assume that the rate of fuel consumption per unit flame area is given by the solution for infinitely fast chemistry,

$$\dot{m} = \rho_0\left[\frac{D_0}{\pi\bar{\tau}}\right]^{\frac{1}{2}} \qquad 3.24b$$

Next, let $\frac{\Gamma}{D_0} \to \infty$ as before, again assuming that $\frac{\Gamma^{\frac{2}{3}} D_0^{\frac{1}{3}} t}{\pi r^2}$ is of order one. In addition, some assumptions must be made about the magnitudes of the dimensionless ratios $\frac{a}{r}$ and $\frac{\lambda}{r}$. The purpose of this calculation is to discover the effect of the offset distance a, so a reasonable assumption is that $\frac{a}{r}$ and $\frac{\lambda}{r}$ are both of order one. (Recall that $a^2 + \lambda^2 = r^2$.) With these assumptions, as $\frac{\Gamma}{D_0} \to \infty$ equation 5.31 becomes

$$dl \sim \left[\frac{\Gamma}{D_0}\right]^{\frac{1}{3}} \frac{\Gamma^{\frac{2}{3}} D_0^{\frac{1}{3}} t}{\pi r^2} \frac{\lambda}{r} d\lambda \qquad 5.33$$

and equation 5.32 becomes

$$\bar{\tau} \sim \frac{t}{3} \qquad 5.34$$

The notion of the burned out core is applicable to this case as well, the only difference being that the annulus $(r, r+dr)$ no longer contains equal amounts of fuel and oxidizer. (See figure 5.5.) If one still assumes that the initial concentrations of fuel and oxidizer are equal, and that they react in 1:1 proportions, then whichever reactant lies on the same side of the flame as the vortex will be present in excess, and the burnout time will depend on the available supply of the other reactant. As is evident from the figure, the annulus $(r, r+dr)$ initially contains the quantity $2\rho_0 \arctan\left[\frac{\lambda}{a}\right] r\, dr$ of the deficient reactant, and setting the total consumption of that reactant from $t = 0$ to $t = t^*$ equal to the amount originally present results in the following expression for the burnout time:

$$\frac{\Gamma^{\frac{2}{3}} D_0^{\frac{1}{3}} t^*}{\pi r^2} \sim \left[\frac{\sqrt{3}}{2} \arctan\left[\frac{\lambda}{a}\right]\right]^{\frac{2}{3}} \qquad 5.35$$

This equation gives the burnout time t^* as a function of radius. (Keep in mind that a is constant and that $\lambda = \sqrt{r^2 - a^2}$.) From examination of figure 5.4, one realizes that equation 5.35 is applicable only to radii such that $r > a$.

The relationship may be presented another way, by considering a burnout radius r^* to be a function of the time t, just as for the case $a \equiv 0$. After a little algebra, once again calling $\eta^* \equiv \frac{\pi^{\frac{1}{2}} r^*}{\Gamma^{\frac{1}{3}} D_0^{\frac{1}{6}} t^{\frac{1}{2}}}$, equation 5.35 becomes,

$$\eta^* \sim \left[\frac{\sqrt{3}}{2} \arctan \left[\frac{t}{\hat{t}} \eta^{*2} - 1 \right]^{\frac{1}{2}} \right] \qquad 5.36$$

which implicitly defines the dimensionless burnout radius η^* as a function of the dimensionless time $\frac{t}{\hat{t}}$, where the time scale $\hat{t}$ is defined

$$\hat{t} \equiv \frac{\pi a^2}{\Gamma^{\frac{2}{3}} D_0^{\frac{1}{3}}} \qquad 5.37$$

The augmented fuel consumption rate due to the vortex may be calculated as before, with the result that as $\frac{\Gamma}{D_0} \to \infty$,

$$\frac{\dot{M}}{\rho_0 \Gamma^{\frac{2}{3}} D_0^{\frac{1}{3}}} \sim \frac{2\sqrt{3}}{\pi} \frac{1}{\eta^*} \qquad 5.38$$

Equation 5.36 was solved numerically to find η^* for certain values of $\frac{t}{\hat{t}}$, which was in turn used to find $\frac{\dot{M}}{\rho_0 \Gamma^{\frac{2}{3}} D_0^{\frac{1}{3}}}$. The results are plotted in figures 5.5 and 5.6.

These calculations for a finite offset distance a proceeded in much the same way as did earlier calculations with $a = 0$. The parameter $\bar{\tau}$, which one uses to approximate the fuel consumption per unit flame area, was equal to $\frac{t}{3}$ in the large $\frac{\Gamma}{D_0}$ limit, just as it was for $a = 0$. (Equations 5.34 and 5.26 are identical.) Likewise, if one notes that $\frac{\lambda}{r} d\lambda = dr$, and that r extends from 0 to ∞ whereas λ goes from $-\infty$ to $+\infty$, then equation 5.33 for the flame surface area is the same as the right hand side of equation 5.25. Thus, after taking the limit $\frac{\Gamma}{D_0} \to \infty$, one is left with the same expressions for fuel consumption rate per unit flame area and for the surface area of flame per unit radius as for the previous case $a = 0$.

The annulus $(r, r+dr)$ contains less of one reactant than the other; the burnout time is determined by the availability of the reactant in shortest supply. This is the only reason the burnout time for the case of nonzero offset difference differs from the burnout time for the case $a = 0$. The augmented fuel consumption rate depends on the offset distance a only because the lower limit of integration is the burnout radius r^*.

5.5.2 The Finite Chemistry Solution

In this section, the solution in the limit $\frac{\Gamma}{D_0} \to \infty$ for a vortex flame including the effects of both an offset distance a and a finite chemical time t_{ch} is given. The same methods are used as were used previously, so details of the algebra are not given here. As one might expect, the burned out core radius is once again proportional to $\Gamma^{\frac{1}{3}} D_0^{\frac{1}{6}} t^{\frac{1}{2}}$, so the dimensionless variable η^* appears again. Also, the increased fuel consumption rate due to the vortex is proportional to $\rho_0 \Gamma^{\frac{2}{3}} D_0^{\frac{1}{3}}$, so the dimensionless variable $\frac{\dot{M}}{\rho_0 \Gamma^{\frac{2}{3}} D_0^{\frac{1}{3}}}$ reappears. Since a finite offset distance and a finite chemical time are included in the analysis, both time scales $\hat{t}$ and t_{ch} appear in the results. The dimensionless core radius is found to be

$$\eta^* \sim \left[\frac{2}{5\sqrt{3}} \frac{\frac{t}{t_{ch}}}{\arctan\left[\frac{t}{\hat{t}}\eta^{*2} - 1\right]^{\frac{1}{2}}} \right]^{\frac{1}{3}} \quad \text{for} \quad \frac{t}{t_{ch}} < 3 \qquad 5.39a$$

$$\eta^* \sim \left[\frac{\frac{2}{\sqrt{3}} - \frac{12}{5}\left[\frac{t}{t_{ch}}\right]^{-\frac{3}{2}}}{\arctan\left[\frac{t}{\hat{t}}\eta^{*2} - 1\right]^{\frac{1}{2}}} \right]^{\frac{1}{3}} \quad \text{for} \quad \frac{t}{t_{ch}} > 3$$

5.39b

Thus, if values of $\frac{t}{\bar{t}}$ and $\frac{t}{t_{ch}}$ are specified, equations 5.39 can be solved to find η^*.

The equations for the fuel consumption rate are found in terms of η^* from equations 5.39

$$\frac{\dot{M}}{\rho_0 \Gamma^{\frac{2}{3}} D_0^{\frac{1}{3}}} \sim \frac{2}{\pi\sqrt{3}} \frac{t}{t_{ch}} \frac{1}{\eta^*} \quad \text{for} \quad \frac{t}{t_{ch}} < 3 \qquad 5.40a$$

$$\frac{\dot{M}}{\rho_0 \Gamma^{\frac{2}{3}} D_0^{\frac{1}{3}}} \sim 2\frac{\sqrt{3}}{\pi} \frac{1}{\eta^*} \quad \text{for} \quad \frac{t}{t_{ch}} > 3 \qquad 5.40b$$

As before, there is a cylindrical core of radius r^*, which grows as a function of time. In the very center of the core, for $r < a$, only one reactant is present. At larger radii but still within the core, $r^* > r > a$, a mixture of combustion products and the excess reactant is found. At $r = r^*$, on the edge of the core, the flame is consuming all of one reactant and going out; the radius of the core is increasing with time. Previously, for the case $a = 0$, the rate of growth of the core is calculated. The quantity of combustion products in the core was proportional to to $C = \pi r^{*2}$, so $\frac{d}{dt}(\pi r^{*2})$ was proportional to the rate of incorporation of combustion products into the core.

Examine figure 5.6. Although the rate of growth of the core volume is proportional to $\frac{d}{dt}(\pi r^{*2})$ as before, the core is not composed exclusively of combustion products. The amount of product inside the core when it has radius r^* is proportional to the amount of the scarcer reactant initially within a circle of radius r^* at $t = 0$ (the area of the shaded region in figure 5.6). Denoting this

area by the symbol C,

$$C = (\theta^* r^{*2} - a\lambda^*) \tag{5.41}$$

where $\lambda^* \equiv \sqrt{r^{*2} - a^2}$ and $\theta^* \equiv arctan\left[\frac{r^{*2}}{a^2} - 1\right]^{\frac{1}{2}}$. So the rate of growth of the volume of product within the core is $\dot{C} \equiv \frac{dC}{dt}$. After some algebra, $\dot{C}$ is found from equations 5.41 and 5.39 to be

$$\frac{\dot{C}}{\Gamma^{\frac{2}{3}} D_0^{\frac{1}{3}}} \sim \frac{2}{\pi\sqrt{3}} \frac{t}{t_{ch}} \frac{1}{\eta^*} \frac{\left[\frac{t}{\hat{t}}\eta^{*2} - 1\right]^{\frac{1}{2}} arctan\left[\frac{t}{\hat{t}}\eta^{*2} - 1\right]^{\frac{1}{2}}}{3\left[\frac{t}{\hat{t}}\eta^{*2} - 1\right]^{\frac{1}{2}} arctan\left[\frac{t}{\hat{t}}\eta^{*2} - 1\right]^{\frac{1}{2}} + 1} \tag{5.42a}$$

$$\text{for} \quad \frac{t}{t_{ch}} < 3$$

and

$$\frac{\dot{C}}{\Gamma^{\frac{2}{3}} D_0^{\frac{1}{3}}} \sim \frac{2\sqrt{3}}{\eta^*} \frac{\left[\frac{t}{\hat{t}}\eta^{*2} - 1\right]^{\frac{1}{2}} arctan\left[\frac{t}{\hat{t}}\eta^{*2} - 1\right]^{\frac{1}{2}}}{3\left[\frac{t}{\hat{t}}\eta^{*2} - 1\right]^{\frac{1}{2}} arctan\left[\frac{t}{\hat{t}}\eta^{*2} - 1\right]^{\frac{1}{2}} + 1} \tag{5.42b}$$

$$\text{for} \quad \frac{t}{t_{ch}} > 3$$

The two time variables $\frac{t}{t_{ch}}$ and $\frac{t}{\hat{t}}$ are useful for understanding the results, but for describing core growth and fuel consumption as functions of time only one time variable is permissible. For a given vortex, the ratio of $\frac{t_{ch}}{\hat{t}}$ is a constant, and either t_{ch} or $\hat{t}$ may be used to nondimensionalize the time. Define the constant β

$$\beta \equiv \frac{t_{ch}}{\hat{t}} = \frac{\Gamma^{\frac{2}{3}} D_0^{\frac{1}{3}} t_{ch}}{\pi a^2} \qquad 5.43$$

Thus η^*, $\frac{\dot{M}}{\rho_0 \Gamma^{\frac{2}{3}} D_0^{\frac{1}{3}}}$, and $\frac{\dot{C}}{\Gamma^{\frac{2}{3}} D_0^{\frac{1}{3}}}$ may be expressed as functions of $\frac{t}{t_{ch}}$ and the parameter β. These functions are graphed in figures 5.7, 5.8, and 5.9 for an assortment of values of β.

The results indicate that if β is less than one, then $\hat{t}$ is the most important time scale, rather than t_{ch}. Figure 5.10 contains the same information as figure 5.9, but the dimensionless augmented fuel consumption rate is shown as a function of $\frac{t}{\hat{t}}$ rather than of $\frac{t}{t_{ch}}$. The ratio of the two time scales, β, is again a parameter.

5.6 Summary

The spiral flame was analysed including the effects of both a finite chemical reaction time and a vortex displaced from the original flame position, and solutions were given for large $\frac{\Gamma}{D_0}$. Just as in Marble's results for a large Reynolds number, the burned out core radius was scaled by $\Gamma^{\frac{1}{3}} D_0^{\frac{1}{6}} t^{\frac{1}{2}}$, and the increase in total fuel consumption was proportional to $\rho_0 \Gamma^{\frac{2}{3}} D_0^{\frac{1}{3}}$. In Marble's analysis the scaled core radius and the increase in fuel consumption were constants, but here they are functions of time. Two time scales were found, t_{ch} and $\hat{t}$. For times that are large compared to both time scales, the solutions approach constant values. The approach to the large t solution is governed by both time scales, the slowest one being the most important.

The time scale t_{ch} could have easily been anticipated. The time $\hat{t}$ is more interesting. Recall that $\hat{t} \equiv \frac{\pi a^2}{\Gamma^{\frac{2}{3}} D_0^{\frac{1}{3}}}$. For a zero offset distance, the core radius

grows like $\Gamma^{\frac{1}{3}} D_0^{\frac{1}{6}} t^{\frac{1}{2}}$. Thus, the time required for the core to grow to a radius a would be proportional to $\frac{a^2}{\Gamma^{\frac{2}{3}} D_0^{\frac{1}{3}}}$, which is proportional to $\hat{t}$. Therefore, the time scale $\hat{t}$ may be interpreted as the time required for the influence of the vortex to reach the flame sheet.

One of the interesting features of the results of Marble (1982) and Karagozian (1982) was that in the limit of a large Reynolds number, the core radius and fuel consumption rate depended on the combined transport coefficient $\Gamma^{\frac{2}{3}} D_0^{\frac{1}{3}}$. The same result was found here; neither the diffusivity nor the vortex circulation are individually important; only the combination $\Gamma^{\frac{2}{3}} D_0^{\frac{1}{3}}$ appears in the results.

6. THE EXAMINATION OF ASSUMPTIONS AND FURTHER REFINEMENTS

6.1 Introduction

The results of chapter five were derived after making many simplifying assumptions. Some of these will be examined in this chapter and in some cases new results will be calculated and compared to the previous results from chapter five. Equations 3.24 will be replaced with a formulation which more closely describes the numerical results of chapter four. The validity of assuming that each piece of the flame is locally one dimensional will be examined. The burned out core radius was calculated assuming that no fuel or oxidizer diffused into or out of a given circular annulus. This assumption will be verified. The effects of viscosity will be discussed.

Finally, chapters three and four assumed a single flame with infinite reservoirs of fuel and oxidizer to draw upon. In a spiral flame, alternate bands of fuel and oxidizer are separated by essentially parallel flames. Thus, each individual piece of flame has finite fuel and oxidizer available. As each flame grows thicker, consuming the available reactants, it will gradually go out. In chapter five, this effect was approximated by the burnout time, assuming that each flame was independent of its neighbors until all available fuel or oxidizer was consumed, then suddenly the fuel consumption rate was set equal to zero. The gradual decrease in fuel consumption rate due to the interaction of a flame with its neighbors, will be modelled, and the properties of a spiral flame will be recalculated using the new formulae in place of the burned out core idea.

For simplicity, all calculations done in this chapter will be done for an offset distance α of zero.

6.2 Equations 3.24

Of the assumptions made in the previous analysis, one of the key ones was that the fuel consumption rate per unit area of flame surface was given by equations 3.24,

$$\dot{m} \sim \frac{\rho_0}{t_{ch}} \left[\frac{D_0 \bar{\tau}}{\pi}\right]^{\frac{1}{2}} = \rho_0 \left[\frac{D_0}{\pi \bar{\tau}}\right]^{\frac{1}{2}} \left[\frac{\bar{\tau}}{t_{ch}}\right] \quad \text{for} \quad \bar{\tau} << t_{ch} \qquad 3.24a$$

$$\dot{m} \sim \rho_0 \left[\frac{D_0}{\pi \bar{\tau}}\right]^{\frac{1}{2}} \quad \text{for} \quad \bar{\tau} >> t_{ch} \qquad 3.24b$$

Although the equations were derived for the limiting cases of small $\frac{\bar{\tau}}{t_{ch}}$ for equation 3.24a and large $\frac{\bar{\tau}}{t_{ch}}$ for equation 3.24b, in chapter five equation 3.24a was used for all $\frac{\bar{\tau}}{t_{ch}}$ less than one and equation 3.24b was used if $\frac{\bar{\tau}}{t_{ch}}$ were greater than one. This approximation was compared to the behavior of a real flame in chapter four, with the unsurprising result that equations 3.24 were accurate for both small and large times, but overestimated the fuel consumption rates for times approximately equal to the chemical time.

The results of chapter five for the fuel consumption rate of a spiral flame (equations 5.30 and figure 5.3) exhibit a slope discontinuity at $\frac{t}{t_{ch}} = 3$. This discontinuity is the direct result of the slope discontinuity in equations 3.24 at $\frac{\bar{\tau}}{t_{ch}} = 1$, since $\bar{\tau} \sim \frac{t}{3}$ in the limit $\frac{\Gamma}{D_0} \to \infty$. Here possible improvements on equations 3.24 will be investigated which provide better estimates of $\dot{m}$ in the region $\frac{\bar{\tau}}{t_{ch}} \approx 1$, and which have no discontinuities.

One method, suggested by equations 3.24 as well as by the numerical results of chapter four, is to consider $\dot{m}$ to be a function of the parameter $\bar{\tau}$.

This supposition is not strictly true; the dependence of a transiently strained flame on the time varying strain rate cannot be reduced to a simple function of the parameter $\bar{\tau}$ except to lowest order in the limits $\frac{\bar{\tau}}{t_{ch}} \to 0$ and $\frac{\bar{\tau}}{t_{ch}} \to \infty$. Nevertheless, in figure 6.1 the instantaneous fuel consumption rate $\dot{m}$ is plotted versus $\bar{\tau}$ for a transient unstrained flame, several steady strained flames, and several transiently strained flames, strained as they would be in a vortex. (These data were previously presented in chapter four, here they are simply plotted together on the same sheet.) At least for the types of straining considered here, the instantaneous value of $\dot{m}$ may be approximated as a function of the instantaneous value of $\bar{\tau}$.

Therefore, one seeks a function $\dot{m}(\bar{\tau})$. One obvious requirement is that it should have equations 3.24 as asymptotes in the limits $\frac{\bar{\tau}}{t_{ch}} << 1$ and $\frac{\bar{\tau}}{t_{ch}} >> 1$. A second requirement is that the function make a smooth transition from one asymptote to the other; that the function should have no discontinuities. Finally, the function should fit the data presented in chapter four and graphed in figure 6.1.

One simple function which fits these requirements is

$$\dot{m}(\bar{\tau}) = \rho_0 \left[\frac{D_0}{\pi \bar{\tau}}\right]^{\frac{1}{2}} \frac{\frac{\bar{\tau}}{t_{ch}}}{1 + \frac{\bar{\tau}}{t_{ch}}} \qquad 6.1$$

This relationship, essentially the same used by Marble *et al.* (1979), has no physical basis other than having the correct asymptotes (*i.e.*, equations 3.24) in the limits $\frac{\bar{\tau}}{t_{ch}} \to 0$ and $\frac{\bar{\tau}}{t_{ch}} \to \infty$. Equation 6.1 provides a better approximation to the data of chapter four than equations 3.24.

If the calculations of chapter five leading up to equations 5.16 for the core radius, 5.17 for the rate of core growth, and 5.30 for the fuel consumption rate (for $a = 0$) are redone using equation 6.1 in place of equations 3.24 for the local fuel consumption rate per unit flame area, the result for the core radius is

$$\eta^* \sim \left[\frac{4}{\pi\sqrt{3}} - \frac{12\sqrt{3}}{\pi} \frac{t_{ch}}{t} + \frac{36}{\pi} \left[\frac{t}{t_{ch}} \right]^{-\frac{3}{2}} \arctan \left[\frac{1}{3} \frac{t}{t_{ch}} \right]^{\frac{1}{2}} \right]^{\frac{1}{3}} \qquad 6.2$$

The rate of core growth is found in terms of the previous result for η^* as

$$\frac{\dot{C}}{\Gamma^{\frac{2}{3}} D_0^{\frac{1}{3}}} \sim \eta^{*2} + \frac{2}{3\eta^*} \left[\frac{12\sqrt{3}}{\pi} \frac{t_{ch}}{t} - \frac{54}{\pi} \left[\frac{t}{t_{ch}} \right]^{-\frac{3}{2}} \arctan \left[\frac{1}{3} \frac{t}{t_{ch}} \right]^{\frac{1}{2}} \right. \qquad 6.3$$

$$\left. + \frac{18}{\pi\sqrt{3}} \frac{\frac{t_{ch}}{t}}{\left[1 + \frac{1}{3} \frac{t}{t_{ch}} \right]} \right]$$

and the fuel consumption rate of the vortex is found in terms of η^* as

$$\frac{\dot{M}}{\rho^0 \Gamma^{\frac{2}{3}} D_0^{\frac{1}{3}}} \sim \frac{2}{\pi\sqrt{3}} \frac{\frac{t}{t_{ch}}}{1 + \frac{1}{3} \frac{t}{t_{ch}}} \frac{1}{\eta^*} \qquad 6.4$$

Thus, η^* can be found from equation 6.2, then the core growth rate and fuel consumption rate can be found from equations 6.3 and 6.4. All these results were found in the limit $\frac{\Gamma}{D_0} \to \infty$, as before.

The solution is fundamentally unchanged. (See figures 6.2, 6.3, and 6.4.) The core radius is still scaled by $\Gamma^{\frac{1}{3}} D_0^{\frac{1}{6}} t^{\frac{1}{2}}$, and the fuel consumption is still proportional to $\rho_0 \Gamma^{\frac{2}{3}} D_0^{\frac{1}{3}}$. Both the scaled core radius and the fuel consumption rate are functions of $\frac{t}{t_{ch}}$. As is evident from the figures 6.3 and 6.4, the slope

discontinuity at $\frac{t}{t_{ch}} = 3$ is now gone. The fuel consumption rate approaches the steady solution for large t from below, rather than overshooting as before.

6.3 Flame One-Dimensionality

The first aspect of one-dimensionality to be considered is the assumption that the curvature of the flame surface can be neglected. More strictly, one wants to show that the radius of curvature of a piece of flame is large compared to the thickness of that piece. In chapter two, it was shown that the radius of curvature of the flame approaches the radius r as the flame is wound into a spiral. In chapter three, the thickness of an assumed one-dimensional flame element was found to be proportional to $\sqrt{D_0 \bar{\tau}}$. Again, as the flame is wound into a spiral, $\bar{\tau}$ is asymptotic to $\frac{t}{3}$. Therefore, one wants to determine the conditions under which $\frac{\sqrt{D_0 t}}{r}$ is small.

Clearly, this will not be true for small radii, but recall the burned out core. For radii less than the core radius r^*, the flame is no longer burning; therefore, the calculated flame curvature in this region is meaningless. What one really wants to show is that $\frac{\sqrt{D_0 t}}{r^*}$ is small.

For large times, r^* is proportional to $\Gamma^{\frac{1}{3}} D_0^{\frac{1}{6}} t^{\frac{1}{2}}$. Substitution shows that the ratio of flame thickness to flame curvature is proportional to $\left[\frac{D_0}{\Gamma}\right]^{\frac{1}{3}}$. Thus, for spiral flames where $\frac{D_0}{\Gamma}$ is small, the flame curvature can be safely neglected, at least for large times.

For smaller times, equation 5.16a shows that the burned out core radius is proportional to $\Gamma^{\frac{1}{3}} D_0^{\frac{1}{6}} t^{\frac{1}{2}} \left[\frac{t}{t_{ch}}\right]^{\frac{1}{3}}$. Substitution of this expression reveals that in

the limit $\frac{\Gamma}{D_0} \rightarrow \infty$, the curvature of any flame lying outside the core is small compared to its thickness except at very small times, where $\frac{t}{t_{ch}}$ is of order $\frac{D_0}{\Gamma}$.

Another aspect of flame one-dimensionality to be explored is the assumption that concentration and temperature gradients normal to the flame surface (in the y direction) are large compared to those parallel to the flame surface (in the x direction). Clearly, gradients in the normal direction are proportional to $\frac{1}{\delta}$, since δ is the flame thickness. Therefore, if one lets l be a measure of flame length, then one wants $\frac{d\delta}{dl}$ to be small. If it is, then the flame is approximately one-dimensional.

Now, $\frac{d\delta}{dl}$ is equal to $\frac{1}{\frac{dl}{dr}} \frac{d\delta}{dr}$. From equation 2.12, $\frac{dl}{dr} = \left[1 + \left[\frac{\Gamma t}{\pi r^2}\right]^2\right]^{\frac{1}{2}}$. (The factor of two has been omitted, since only one flame arm is being considered.) Previously, δ was found to be equal to $\sqrt{D_0 \bar{\tau}}$, and $\bar{\tau}$ is given by equation 4.7. Substituting, after some algebra one finds

$$\frac{d\delta}{dl} = \frac{4}{3} \frac{\left[\frac{\Gamma t}{\pi r^2}\right]^2}{\left[1 + \frac{1}{3}\left[\frac{\Gamma t}{\pi r^2}\right]^2\right]^{\frac{1}{2}} \left[1 + \left[\frac{\Gamma t}{\pi r^2}\right]^2\right]^2} \frac{\sqrt{D_0 t}}{r} \qquad 6.5$$

Realizing again that radii which lie within the core are of no concern, then for large times, $\frac{\Gamma^{\frac{2}{3}} D_0^{\frac{1}{3}} t}{\pi r^2}$ will be of order one in the limit as $\frac{\Gamma}{D_0} \rightarrow \infty$. In this limit, from equation 6.5 one finds that $\frac{d\delta}{dl}$ goes like $\left[\frac{D_0}{\Gamma}\right]^{\frac{7}{3}}$. Thus, the effect of variation of flame thickness with flame length is of considerably less importance in the limit than the effect of flame curvature, and will not be considered

further.

6.4 Flame Thinness

This topic is treated by Karagozian (1982). Here, note that the velocity field in the neighborhood of the flame was approximated by the first terms in a local expansion. (The normal velocity was taken to be $v = -\varepsilon y$ in chapter two. Thus, higher order terms, such as the y^2 term were ignored. See equations 2.1.) This assumption is valid only as the flame is thin with respect to the scale of velocity nonuniformity.

Examination of the velocity field for a potential vortex (equations 2.3), reveals that the only possible characteristic length scale is the radius r. Thus, the degree of nonuniformity in the velocity field is proportional to the distance one is from the origin. As in the previous discussion on the flame curvature, the flame thickness is proportional to $\sqrt{D_0 t}$, so the local analysis of the velocity field about the flame is valid only where $r >> \sqrt{D_0 t}$. Once again, radii which lie within the core are of no concern, so one seeks to show that $r^* >> \sqrt{D_0 t}$. This requirement is the same as found previously, in the discussion of the effects of flame curvature. The rest of this discussion follows the previous one, and will not be repeated. However, one should again note that large $\frac{\Gamma}{D_0}$ seems to be a necessity rather than a convenience.

6.5 Viscosity

Marble (1982) included viscosity in his analysis and found that it had no effect on the large Reynolds number limit. Viscosity has been ignored in this formulation; one hopes that for large $\frac{\Gamma}{D_0}$ this will have no effect on the results. This is indeed the case, as one may see by noting that a viscous vortex consists of a core of radius $\sqrt{\nu t}$, where viscosity is important, surrounded by an outer

region, where the velocity field is described by the inviscid equations used in this analysis (equations 2.3). Thus, viscosity should not be important, and this analysis is valid, at radii large compared to $\sqrt{\nu t}$.

Once again, once a flame is within the burned out core it is no longer of interest. For times larger than the chemical time, the burned out core radius is proportional to $\Gamma^{\frac{1}{3}} D_0^{\frac{1}{6}} t^{\frac{1}{2}}$. Thus, the radius of the viscous core of the vortex is smaller than the radius of the burned out core by the ratio $\left[\frac{D_0}{\Gamma}\right]^{\frac{1}{3}} \left[\frac{\nu}{D_0}\right]^{\frac{1}{6}}$. Only for small times, *i.e.*, $\frac{t}{t_{ch}} \sim \frac{D_0}{\Gamma}\left[\frac{\nu}{D_0}\right]^{\frac{1}{2}}$ is the viscosity important. The dimensionless ratio $\frac{\nu}{D_0}$ is the Schmidt number, which is roughly one for gases but is 600 for water. Thus, one can safely neglect the viscosity provided that the ratio $\frac{\Gamma}{D_0}$ is large enough.

6.6 Neglect of Radial Diffusion

In calculating the formation of the burned out core, it was assumed that the amount of each reactant present in a given annulus is equal to the amount of fuel originally present minus the amount consumed by the flame surface in that annulus. This formulation ignores the effects of diffusion. Within the core, at least one reactant is entirely absent. Outside the core, that reactant is present. As order of magnitude estimates,

concentration difference between core and area outside core $\sim \rho_0$

length scale for calculating concentration gradient $\sim r^*$

diffusion coefficient $\sim D_0$

surface area available for diffusion $\sim 2\pi r^*$

Therefore, the diffusive flux of fuel and oxidizer into the core and the flux of products out of the core is approximately $D_0 \frac{\rho_0}{r^*} 2\pi r^*$. As an order of magnitude estimate, this quantity goes like $\rho_0 D_0$.

To estimate the importance of this term, consider that the rate of incorporation of products into the core is proportional to $\rho_0 \Gamma^{\frac{2}{3}} D_0^{\frac{1}{3}}$ (for large $\frac{t}{t_{ch}}$). As a result, the relative importance of radial diffusion goes like $\left[\frac{D_0}{\Gamma}\right]^{\frac{2}{3}}$. Once again, the the radial diffusion is not negligible for small times, $\frac{t}{t_{ch}} \sim \frac{D_0}{\Gamma}$.

6.7 Interaction of Adjacent Flames

One expects that the equations of chapter three and the numerical analysis of chapter four provide an accurate description of flame behavior only as long as the thickness of each individual flame is less than the spacing between flames. From chapter two, the spacing between flames is given by equation 2.15, which in the tightly wrapped spiral region of interest is approximated by equation 2.20

$$\Delta \sim \frac{\pi^2 r^3}{\Gamma t} \qquad 2.20$$

The thickness of an individual flame δ is proportional to $\sqrt{D_0 \bar{\tau}}$. Within the tightly wrapped inner spiral, $\bar{\tau}$ is asymptotic to $\frac{t}{3}$, so as an order of magnitude estimate, $\delta \sim \sqrt{D_0 t}$.

Solving for the point at which the flame thickness and the flame spacing are roughly equal, one finds that this occurs when

$$\frac{\delta}{\Delta} \sim \frac{\sqrt{D_0 t}\ \Gamma t}{r^3} \sim 1 \qquad 6.6$$

Thus one concludes that each flame is essentially independent of its neighbors for radii large compared to $\Gamma^{\frac{1}{3}} D_0^{\frac{1}{6}} t^{\frac{1}{2}}$, and that the interaction of adjacent flames

cannot be ignored for radii which are small compared to $\Gamma^{\frac{1}{3}} D_0^{\frac{1}{6}} t^{\frac{1}{2}}$.

A critical radius has been found, proportional to $\Gamma^{\frac{1}{3}} D_0^{\frac{1}{6}} t^{\frac{1}{2}}$, where the interaction of adjacent flames becomes important. From chapter five, for large $\frac{t}{t_{ch}}$ the burned out core radius was proportional to $\Gamma^{\frac{1}{3}} D_0^{\frac{1}{6}} t^{\frac{1}{2}}$. These two criteria: for the interaction of neighboring flames and for the exhaustion of available fuel, are the same. At least for times large compared to the chemical time, the exhaustion of fuel and the interaction of adjacent flames are really the same phenomenon, (see Marble (1982)) viewed in two different ways. Thus, the idea of a burned out core is an approximate way to handle the interaction of adjacent flames.

For times less than the chemical time, adjacent flames will grow and begin to interact with each other before all available fuel has been consumed. In this case, interaction of neighboring flames and the exhaustion of fuel are two different occurrences, which need to be dealt with separately.

In this section, a more refined method of describing the interaction between two adjacent flames is sought. In the approximation previously used, a burnout time was artificially introduced, and each piece of the flame was assumed to burn independently of the others until the burnout time t^* was reached. Subsequently, the fuel consumption rate was set equal to zero, and the flame was said to have burned out. One expects, for large $\frac{t}{t_{ch}}$, that the flame will slowly go out as the available fuel and oxidizer are consumed, rather than suddenly as before. This gradual attenuation of the fuel consumption rate will produce a core with blurred edges, rather than the sharply defined structure previously found.

6.7.1 Problem Formulation

In the region of interest, where $\frac{\pi^{\frac{1}{2}} r}{\Gamma^{\frac{1}{3}} D_0^{\frac{1}{6}} t^{\frac{1}{2}}}$ is of order one, the two flame arms are tightly wrapped around the vortex. A radial line drawn outward from the center will intersect the flame sheets many times, passing through alternating layers of fuel and oxidizer. In the spiral flame, each flame sheet is curved, nearly a circle about the origin, and the radial spacing of successive flames grows tighter near the origin. It has been shown that the curvature is negligible, so the problem can be replaced by a one dimensional one. In addition, one expects that the greatest influence on an individual flame will be from its nearest neighbors, so the nonuniformity of spacing will be neglected. Therefore, consider the following problem:

The problem is one dimensional; concentrations and temperatures vary with y and not with x. A strain field is imposed, constant in x and y but allowed to vary arbitrarily with t. The straining is along the x axis, with velocity component $u = \varepsilon(t)\, x$. So far, the problem is the same one discussed in chapter three.

The difference is in the initial conditions. Rather than semi-infinite regions of fuel and oxidizer separated by a single flame, separate the fuel and oxidizer into alternating strips, each strip of width d. (See figure 6.5) These strips lie parallel to the x axis, so the system includes an infinite number of flames, each one parallel to the x axis. Each flame is initially separated from its nearest neighbor by a distance d. A positive value of the strain ε will stretch the flames in the x direction, and cause them to move closer to one another in the y direction. If the fluid is considered to be incompressible, then a straining along the x axis with velocity $u = \varepsilon(t)\, x$ causes a flow along the y axis $v = -\varepsilon(t)\, y$. If

each flame is considered to move with the local fluid velocity, then denoting the distance between adjacent flames by the variable $\Delta(t)$ yields the following equation

$$\frac{d\Delta}{dt} = -\varepsilon(t)\,\Delta \qquad 6.7$$

Since the initial flame spacing is d, the appropriate initial condition is $\Delta(0) = d$, so the solution to 6.7 is

$$\Delta(t) = d\; e^{-\int_0^t \varepsilon(t'')\,dt''} \qquad 6.8$$

The equations of species conservation and energy conservation will be the same as before, in chapter three. This problem differs from those discussed previously only in the initial and boundary conditions.

6.7.2 Infinite Reaction Rate Solution

As discussed in chapter three, if the reaction is assumed to be fast, the two reactants coexist only within an extremely thin reaction zone. Outside of this zone, one finds one reactant or the other, but not both.

In the infinite reaction rate solution, the region where the reaction takes place is approximated as a surface of zero thickness. On one side of the sheet, fuel and products but no oxidizer are found. On the other side, oxidizer and products exist but no fuel is found. At the flame surface, the concentration of fuel and oxidizer both vanish, and the diffusion of fuel from one side and oxidizer from the other occur in stoichiometric proportions and determine the rate of consumption of fuel and oxidizer.

In chapter three, only one flame was considered, so the equations for fuel and oxidizer concentrations were solved directly. Here the geometry is more complex, so what is known as the "Schvab-Zeldovitch" formulation will be used. (See Williams (1965).)

Consider the variable $\varphi = Y_f - Y_o$. Both concentration profiles can be recovered from φ. In regions where fuel is found, the oxidizer concentration is zero, so $Y_f = \varphi$. Likewise, where there is oxidizer there can be no fuel, so $Y_o = -\varphi$. The reaction zone is found where $\varphi = 0$. An equation for φ can be derived by subtracting the conservation equation for oxidizer from the equation for conservation of fuel, with the result that the chemical reaction terms cancel and leave

$$\frac{\partial \varphi}{\partial t} - \varepsilon(t)\, \xi \frac{\partial \varphi}{\partial \xi} = D_0 \frac{\partial^2 \varphi}{\partial \xi^2} \qquad 6.9$$

The stoichiometry condition at the reaction is automatically satisfied, since $\frac{\partial \varphi}{\partial \xi}$ will be continuous across the surface. The rate of consumption of fuel or oxidizer is then

$$\dot{m} = \rho_0 D_0 \left. \frac{\partial \varphi}{\partial \xi} \right]_{\varphi=0} \qquad 6.10$$

where the derivative is evaluated at the reaction surface, where $\varphi = 0$.

Before, separate equations for fuel and oxidizer concentrations on either side of the reaction zone were solved. These concentrations had discontinuous gradients across the reaction zone, and the flux of fuel from one side had to be equal to the flux of oxidizer from the other. With the Schvab-Zeldovitch formulation, there is only one equation for a variable φ, which has no discontinuities in slope. The flame is located where φ is equal to zero, and the gradient of φ at that point determines the fuel consumption rate.

For the problem under consideration, at $t = 0$ the initial condition for φ is a square wave oscillating from -1 to $+1$ with a period of $2d$. (The mass fraction of fuel is initially one in the strips which contain fuel, and the same is true for oxidizer.) Transforming the equation 6.9 from (t,ξ) coordinates to (τ,ζ)

coordinates by means of equations 3.7 and 3.8 results in the diffusion equation

$$\frac{\partial \varphi}{\partial \tau} = D_0 \frac{\partial^2 \varphi}{\partial \zeta^2} \qquad 6.11$$

The periodic initial condition in ξ becomes a periodic initial condition in ζ, since $\zeta = \xi$ at $t = 0$. Equation 6.11 is easily solved by separation of variables to yield a periodic solution in ζ times an exponential solution in τ. Incorporating the initial conditions by expressing the square wave initial condition in terms of its Fourier components A_n yields

$$\varphi = \sum_{n=1}^{\infty} A_n \sin\left[\frac{n\pi\zeta}{d}\right] e^{\frac{-n^2\pi^2 D_0 \tau}{d^2}} \qquad 6.12$$

Fortuitous initial conditions have been chosen. The flames will remain at their initial positions in the ζ coordinate, so the task of finding the zeroes of 6.12 is much easier than it otherwise would be. The flames are found at $\zeta = 0$, $\zeta = \pm d$, $\zeta = \pm 2d$, *etc.*

The equation for the reactant consumption rate 6.10, when transformed according to 3.7 and 3.8, becomes

$$\dot{m} = \rho_0 D_0 e^{\int_0^t \varepsilon(t'')\, dt''} \left.\frac{\partial \varphi}{\partial \zeta}\right|_{\varphi=0} \qquad 6.13$$

Choosing the flame at $\zeta = 0$, the fuel consumption rate is found by differentiating equation 6.12 with respect to ζ, evaluating it at $\zeta = 0$, and substituting into equation 6.13.

The result of interest is the reduction in fuel consumption due to the effect of the nearby flames. If the flame at $\zeta = 0$ were the only one present and it had infinite reservoirs of fuel and oxygen to draw on, the fuel consumption rate would be given by equation 3.24b from chapter three

$$\dot{m}_0 = \rho_0 \left[\frac{D_0}{\pi\bar{\tau}}\right]^{\frac{1}{2}} \qquad 3.24b$$

Here the subscript zero on $\dot{m}$ indicates what the fuel consumption rate would be predicted from equation 3.24b, neglecting the interaction of neighboring flames. Thus, the degree to which neighboring flames affect the fuel consumption rate may be expressed in terms of the ratio $\frac{\dot{m}}{\dot{m}_0}$, which is found from equations 3.24b, 6.12, and 6.13 as

$$\frac{\dot{m}}{\dot{m}_0} = \sum_{n=1}^{\infty} A_n \frac{n\pi^{\frac{3}{2}}\sqrt{D_0\tau}}{d} e^{-n^2\pi^2\left[\frac{D_0\tau}{d^2}\right]} \qquad 6.14$$

The ratio $\frac{\dot{m}}{\dot{m}_0}$ is a function of the dimensionless group $\frac{\sqrt{D_0\tau}}{d}$. The answer has been found, but what does it mean?

Recall that the flame thickness was defined to be $\sqrt{D_0\bar{\tau}}$. Equation 6.8 gave the spacing between flames as $d\, e^{-\int_0^t \varepsilon(t'')\, dt''}$. Thus, the dimensionless group $\frac{\sqrt{D_0\tau}}{d}$ may be rewritten as

$$\frac{\sqrt{D_0\tau}}{d} = \frac{\sqrt{D_0\tau}\, e^{-\int_0^t \varepsilon(t'')\, dt''}}{d\, e^{-\int_0^t \varepsilon(t'')\, dt''}} = \frac{\sqrt{D_0\bar{\tau}}}{\Delta} = \frac{\delta}{\Delta} \qquad 6.15$$

The result is intuitively appealing. The ratio of the actual fuel consumption rate of a flame (including interactions with its neighbors) to the fuel consumption rate calculated as if the other flames were not present is a function of the ratio of the flame thickness $\delta = \sqrt{D_0\bar{\tau}}$ to the distance between flames Δ. For the particular case taken here, equal concentrations of fuel and oxidizer and a one to one stoichiometric ratio, the function is found by substituting for δ, Δ and the Fourier coefficients A_n in equation 6.14 with the result

$$\frac{\dot{m}}{\dot{m}_0} = 4\sqrt{\pi}\left[\frac{\delta}{\Delta}\right]\sum_{n=1,3,5,\ldots}^{\infty} e^{-n^2\pi^2\left[\frac{\delta}{\Delta}\right]^2} \qquad 6.16$$

Numerical summation of the series in equation 6.16 results in the values which are graphed in figure 6.6. (The series does not converge at $\frac{\delta}{\Delta} = 0$, but $\frac{\dot{m}}{\dot{m}_0}$ must approach one for small values of $\frac{\delta}{\Delta}$.)

6.7.3 Application to the Spiral Flame

The analysis of the previous section assumed an infinite chemical reaction rate, thus it is applicable to the spiral flame for times which are large compared to the chemical time. First use the result to see how sharp the boundary of the burned out core really is.

For radii where $\frac{\pi^{\frac{1}{2}} r}{\Gamma^{\frac{1}{3}} D_0^{\frac{1}{6}} t^{\frac{1}{2}}}$ is of order one as the limit $\frac{\Gamma}{D_0} \to \infty$ is taken, the flame thickness δ is asymptotic to $\left[\frac{D_0 t}{3}\right]^{\frac{1}{2}}$ and the distance between flames Δ is asymptotic to $\frac{\pi^2 r^3}{\Gamma t}$. Therefore,

$$\frac{\delta}{\Delta} \sim \frac{1}{\sqrt{3\pi}}\left[\frac{\Gamma^{\frac{2}{3}} D_0^{\frac{1}{3}} t}{\pi r^2}\right]^{\frac{3}{2}} \qquad 6.17$$

A burned out core radius r^* was calculated previously, and it was assumed that $\frac{\dot{m}}{\dot{m}_0}$ is equal to zero for $r < r^*$ and is equal to unity for $r > r^*$. Now, calculate $\frac{\dot{m}}{\dot{m}_0}$ as a function of $\frac{r}{r^*}$, and see how sharp the transition really is.

For times large compared to the chemical time, equation 5.16b shows that $\eta^* \sim \left[\frac{4}{\pi\sqrt{3}}\right]^{\frac{1}{3}}$. Therefore, equation 6.17 may be put in terms of the ratio $\frac{r}{r^*}$ to

yield

$$\frac{\delta}{\Delta} \sim \frac{\sqrt{\pi}}{4}\left[\frac{r}{r^*}\right]^{-3} \qquad 6.18$$

From equation 6.16, $\frac{\dot{m}}{\dot{m}_0}$ as a function of $\frac{\delta}{\Delta}$ is already known. One may now find $\frac{\dot{m}}{\dot{m}_0}$ as a function of $\frac{r}{r^*}$ from equations 6.16 and 6.18. This function is graphed in figure 6.7.

From figure 6.7, the concept of the burned out core seems valid. At radii only fifteen percent greater than the core radius calculated in chapter five, the fuel consumption is still ninety percent of the full value. At radii ten percent less than the core radius, the fuel consumption rate has dropped to only ten percent of what it otherwise would have been. The transition from a fully burning flame, unattenuated by the lack of fuel, to one which is almost completely put out occurs rapidly. Therefore, the idea of letting a flame consume fuel without any attenuation at all until all fuel has been consumed, and then setting the fuel consumption rate to zero is well justified.

If one redoes the calculation of the fuel consumption rate of the spiral flame, including the attenuation function of equation 6.16, integrating in r from zero to infinity rather than from r^* to infinity as before, numerical integration provides the result

$$\frac{\dot{M}}{\rho_0 \Gamma^{\frac{2}{3}} D_0^{\frac{1}{3}}} \approx 1.210 \qquad 6.19$$

The previous result, equations 5.30, approach

$$\frac{\dot{M}}{\rho_0 \Gamma^{\frac{2}{3}} D_0^{\frac{1}{3}}} \approx 1.222 \qquad 6.20$$

in the limit as $\frac{t}{t_{ch}}$ is large. The difference is less than one percent.

Thus, at least for $t >> t_{ch}$ where the infinite reaction rate solutions are valid, assuming a burned out core is an accurate (and far simpler) method of accounting for the interference due to neighboring flames. In reality, the transition from a strongly burning flame to one which has been put out due to lack of fuel is continuous, and not a sudden jump, yet assuming an abrupt cutoff provides an accurate description of the flame structure and predicts the fuel consumption rate to within one percent.

6.7.4 The Weak Reaction Limit

Previously, in chapter five, the behavior of the spiral flame for $t < 3t_{ch}$ was due to the behavior of a strained laminar diffusion flame for $\bar{\tau} < t_{ch}$. The recipe used for the fuel consumption rate per unit flame area in this case was given by equation 3.24a

$$\dot{m} \sim \frac{\rho_0}{t_{ch}} \left[\frac{D_0 \bar{\tau}}{\pi} \right]^{\frac{1}{2}} = \rho_0 \left[\frac{D_0}{\pi \bar{\tau}} \right]^{\frac{1}{2}} \left[\frac{\bar{\tau}}{t_{ch}} \right] \quad \text{for} \quad \bar{\tau} << t_{ch} \qquad 3.24a$$

which was calculated (see chapter three) by neglecting the chemical reaction terms, allowing the fuel and oxidizer to diffuse and convect into one another, and calculating the consumption of fuel and oxidizer by the reaction as a perturbation.

Equation 3.24b has been modified in the previous section to account for the effects of neighboring flames. Here, the analysis which produced equation 3.24a is extended to account for neighboring flames, which will result in a new picture of spiral flames for times small compared to the chemical time.

Equation 3.24a may be interpreted as saying that the fuel consumption rate is proportional to the flame thickness, $\delta = \sqrt{D_0 \bar{\tau}}$. One realizes that, if instead of just one flame, one had a series of parallel flames, it would be unreasonable to expect further increases in the fuel consumption rate after δ has exceeded the

flame spacing Δ. Once δ is equal to Δ, the fuel and oxidizer are homogenously mixed, and further diffusion will not increase the fuel consumption rate any more.

In this section, the initial condition of alternate strips of fuel and oxidizer is solved according to the method which led to equation 3.24a. To lowest order, neglect the chemical reaction, and calculate fuel and oxidizer concentration profiles resulting from convection and diffusion. As a result, fuel and oxidizer profiles are found to be

$$Y_o = \frac{1}{2}\left[1 + \sum_{n=1}^{\infty} A_n \sin\left[\frac{n\pi\zeta\sqrt{D_0}}{d}\right] e^{-\frac{n^2\pi^2 D_0 \tau}{d^2}}\right] \qquad 6.21a$$

$$Y_f = \frac{1}{2}\left[1 - \sum_{n=1}^{\infty} A_n \sin\left[\frac{n\pi\zeta\sqrt{D_0}}{d}\right] e^{-\frac{n^2\pi^2 D_0 \tau}{d^2}}\right] \qquad 6.21b$$

Where the Fourier coefficients A_n are the same as before. The objective is to calculate the fuel consumption rate per unit of flame surface, which is equal to $\rho_0 k(T_\infty) Y_o Y_f$ integrated over one flame. (Recall that equations 6.21 describe many flames, spaced at intervals of Δ along the y axis.) Choosing the flame centered at $y = 0$, integrate from $-\frac{\Delta}{2}$ to $+\frac{\Delta}{2}$ in y. (Δ is given by equation 6.8.) Making a change of variables to ψ, where $\psi \equiv \frac{\pi\xi}{d} e^{-\int_0^t \varepsilon(t'')\,dt''}$, dividing by the fuel consumption rate if only one flame were present, now given by equation 3.24a, and substituting for δ and Δ results in

$$\frac{\dot{m}}{\dot{m}_0} = \frac{\sqrt{2\pi}}{8\pi}\left[\frac{\Delta}{\delta}\right]\int_{-\frac{\pi}{2}}^{+\frac{\pi}{2}}\left[1 + \sum_{n=1}^{\infty} A_n \sin(n\psi)\, e^{-n^2\pi^2\frac{\delta^2}{\Delta^2}}\right] \qquad 6.22$$

$$\times\left[1 - \sum_{n=1}^{\infty} A_n \sin(n\psi)\, e^{-n^2\pi^2\frac{\delta^2}{\Delta^2}}\right] d\psi$$

Already, one sees that $\frac{\dot{m}}{\dot{m}_0}$ will be a function of $\frac{\delta}{\Delta}$, as before. Interchanging the summation and integration, performing the integration, and substituting for the Fourier coefficients results in

$$\frac{\dot{m}}{\dot{m}_0} = \frac{\sqrt{2\pi}}{8}\frac{\Delta}{\delta}\left[1 - \frac{8}{\pi^2}\sum_{n=1,3,5,\ldots}^{\infty}\frac{1}{n^2}e^{-2n^2\pi^2\frac{\delta^2}{\Delta^2}}\right] \qquad 6.23$$

Once again the series does not converge at $\frac{\delta}{\Delta} = 0$, but again one expects that $\frac{\dot{m}}{\dot{m}_0}$ will be equal to one for small values of $\frac{\delta}{\Delta}$. Numerical summation of the series in equation 6.23 allows the evaluation $\frac{\dot{m}}{\dot{m}_0}$ as a function of $\frac{\delta}{\Delta}$. The function is graphed in figure 6.8.

Inspection of figure 6.8 reveals the existence of two distinct regions, where equation 6.23 may be approximated as

$$\frac{\dot{m}}{\dot{m}_0} \approx 1 \quad \text{for} \quad \frac{\delta}{\Delta} < \frac{1}{4}\left[\frac{\pi}{2}\right]^{\frac{1}{2}} \qquad 6.24a$$

and

$$\frac{\dot{m}}{\dot{m}_0} \approx \frac{1}{4}\left[\frac{\pi}{2}\right]^{\frac{1}{2}}\frac{\Delta}{\delta} \quad \text{for} \quad \frac{\delta}{\Delta} > \frac{1}{4}\left[\frac{\pi}{2}\right]^{\frac{1}{2}} \qquad 6.24b$$

Recalling that $\dot{m}_0$ is proportional to δ, equations 6.24 may be interpreted as meaning that $\dot{m}$ is proportional to δ for small values of $\frac{\delta}{\Delta}$, and is proportional to Δ for large values of $\frac{\delta}{\Delta}$. In fact, substituting for $\dot{m}_0$ from equation 3.24a into equation 6.24b yields

$$\dot{m} \approx \frac{\rho_0 \Delta}{4 t_{ch}\sqrt{2}} \qquad 6.25$$

Replacing t_{ch} by $\frac{1}{\sqrt{2}\,k(T_\infty)}$ allows equation 6.25 to be written as

$$\dot{m} \approx \frac{\rho_0 k(T_\infty) \Delta}{4} \qquad 6.26$$

The fuel consumption rate per unit volume is equal to the product of the fuel consumption rate per unit flame area times the flame area per unit volume, or $\dot{m}\,\Sigma$. Recall that Σ is equal to $\frac{1}{\Delta}$. Thus, equation 6.26 means that the fuel consumption rate per unit volume is constant, equal to $\frac{\rho_0 k(T_\infty)}{4}$. This is exactly the same as one would find for a homogenous mix of half fuel and half oxidizer.

To summarize the findings, for values of $\frac{\delta}{\Delta}$ less than $\frac{1}{4}\left[\frac{\pi}{2}\right]^{\frac{1}{2}}$, the flames are independent of each other, and equation 3.24a should be used to find the fuel consumption rate per unit flame area. For values of $\frac{\delta}{\Delta}$ greater than $\frac{1}{4}\left[\frac{\pi}{2}\right]^{\frac{1}{2}}$, the separate regions of fuel and oxidizer have disappeared, replaced by a homogenous mixture of equal volumes of fuel and oxidizer. In this case, one may either use equation 6.25, wherein the fuel consumption rate per unit flame area is proportional to Δ rather than δ, or else calculate the fuel consumption rate on the basis of fuel consumption per unit volume rather than per unit flame area.

One consequence of this result not yet explored is the issue of fuel exhaustion. The weak reaction limit ignores (at least to lowest order) the fuel and oxidizer which have been converted into product. The result is a constant fuel consumption rate per unit volume, which will continue forever unless the theory is modified. The correct way would be to consider a homogenously mixed region containing fuel and oxidizer, write conservation equations for the fuel and oxidizer concentrations as functions of time, and solve for the diminishing

fuel consumption rate as the concentrations of fuel and oxidizer go to zero. For this analysis, a simpler method will be used: the burnout time t^* will be introduced again.

Thus, for times small compared to the chemical time, use the following prescription to calculate the fuel consumption rate: Initially, $\frac{\delta}{\Delta}$ will be small, so use equation 3.24a. As time passes, δ will grow and Δ will decrease, so eventually $\frac{\delta}{\Delta}$ will equal $\frac{1}{4}\left[\frac{\pi}{2}\right]^{\frac{1}{2}}$. Call the time when this occurs $\tilde{t}$. For times greater than $\tilde{t}$, $\frac{\delta}{\Delta}$ exceeds $\frac{1}{4}\left[\frac{\pi}{2}\right]^{\frac{1}{2}}$, so use equation 6.25, until all the fuel (or oxidizer) has been consumed (this occurs at $t = t^*$). Thereafter, the fuel consumption rate is zero.

Now, use this prescription to recalculate the behavior of a spiral flame for times smaller than the characteristic chemical time. Repeating the analysis of chapter five; taking the limit as $\frac{\Gamma}{D_0} \to \infty$ results in:

for $\tilde{t}$,

$$\frac{\Gamma^{\frac{2}{3}} D_0^{\frac{1}{3}} \tilde{t}}{\pi r^2} \sim \left[\frac{\pi}{4}\sqrt{\frac{3}{2}}\right]^{\frac{2}{3}} \qquad 6.27$$

Thus the time $\tilde{t}$ required for the flames at a given radius r to merge into a homogenous reacting mixture of fuel and oxidizer is given by equation 6.27. One may reinterpret 6.27 as representing the radius $\tilde{r}$ of the homogenously mixed region as a function of the time t. Thus one may also write,

$$\tilde{\eta} \equiv \frac{\pi^{\frac{1}{2}} \tilde{r}}{\Gamma^{\frac{1}{3}} D_0^{\frac{1}{6}} t^{\frac{1}{2}}} \sim \left[\frac{\pi}{4}\sqrt{\frac{3}{2}}\right]^{-\frac{1}{3}} \qquad 6.28$$

Thus, there is a region of homogenously mixed fuel and oxidizer whose radius is

growing as $\sqrt{t}$.

Solving for the burnout time as before gives

$$\frac{\Gamma^{\frac{2}{3}} D_0^{\frac{1}{3}} t^*}{\pi r^2} \sim 2\sqrt{2}\, \frac{\Gamma^{\frac{2}{3}} D_0^{\frac{1}{3}} t_{ch}}{\pi r^2} + \frac{3}{5}\left[\frac{\pi}{4}\sqrt{\frac{3}{2}}\right]^{\frac{2}{3}} \qquad 6.29$$

Here one sees a difference between 6.29 and the earlier result 5.16a. In the present case, there is no burned out core at all for values of $\frac{t}{t_{ch}}$ less than $2\sqrt{2}$. Solving for the burned out core radius r^* as a function of t gives

$$\eta^* \equiv \frac{\pi^{\frac{1}{2}} r^*}{\Gamma^{\frac{1}{3}} D_0^{\frac{1}{6}} t^{\frac{1}{2}}} \sim \sqrt{\frac{5}{3}}\left[\frac{\pi}{4}\sqrt{\frac{3}{2}}\right]^{-\frac{1}{3}}\left[1 - 2\sqrt{2}\,\frac{t_{ch}}{t}\right]^{\frac{1}{2}} \qquad 6.30$$

Finally, integrating to find the augmented fuel consumption rate for the spiral flame,

$$\frac{\dot{M}}{\rho_0 \Gamma^{\frac{2}{3}} D_0^{\frac{1}{3}}} \sim \frac{\sqrt{3}}{\pi}\left[\frac{\pi}{4}\sqrt{\frac{3}{2}}\right]^{\frac{1}{3}} \frac{t}{t_{ch}} \quad \text{for} \quad \frac{t}{t_{ch}} < 2\sqrt{2} \qquad 6.31a$$

$$\frac{\dot{M}}{\rho_0 \Gamma^{\frac{2}{3}} D_0^{\frac{1}{3}}} \sim \frac{\sqrt{3}}{\pi}\left[\frac{\pi}{4}\sqrt{\frac{3}{2}}\right]^{\frac{1}{3}} \frac{t}{t_{ch}} - \frac{5}{3\pi\sqrt{3}}\left[\frac{\pi}{4}\sqrt{\frac{3}{2}}\right]^{\frac{1}{3}}\left[1 - 2\sqrt{2}\,\frac{t_{ch}}{t}\right] \qquad 6.31b$$

$$\text{for} \quad \frac{t}{t_{ch}} > 2\sqrt{2}$$

In contrast to the results for $t >> t_{ch}$, one is left with a different picture of the spiral flame than in chapter five. The center of the spiral consists of homogenously mixed reactants, and the radius of this center is increasing like $\sqrt{t}$. There is no burned out core at all if $\frac{t}{t_{ch}}$ is less than $2\sqrt{2}$.

Some aspects of the results are reassuringly the same as before. The vortex circulation Γ and the molecular diffusivity D_0 appear only in the

combination $\Gamma^{\frac{2}{3}} D_0^{\frac{1}{3}}$. The radius of the homogenously mixed core $\tilde{r}$ and the radius of the burned out core r^*, both nondimensionalized by $\Gamma^{\frac{1}{3}} D_0^{\frac{1}{6}} t^{\frac{1}{2}}$, are both functions of $\frac{t}{t_{ch}}$. Once again, the fuel consumption rate for the entire spiral $\dot{M}$ is proportional to $\rho_0 \Gamma^{\frac{2}{3}} D_0^{\frac{1}{3}}$ and is again a function of $\frac{t}{t_{ch}}$.

Examine figure 6.9, a plot of $\frac{\dot{M}}{\rho_0 \Gamma^{\frac{2}{3}} D_0^{\frac{1}{3}}}$ as a function of $\frac{t}{t_{ch}}$. Both the new solution, equations 6.31, and the previous solution, equation 5.30a, are shown. The figure shows surprisingly little change. The primary difference is that now $\frac{\dot{M}}{\rho_0 \Gamma^{\frac{2}{3}} D_0^{\frac{1}{3}}}$ is proportional to $\frac{t}{t_{ch}}$ near $t = 0$, whereas before it was proportional to $\left[\frac{t}{t_{ch}}\right]^{\frac{2}{3}}$.

The changes are understandable. No matter how efficiently the vortex and diffusion mix the reactants, a finite time proportional to t_{ch} is required for them to completely react. Therefore, one should not expect a burned out core to appear until some multiple of the chemical time has passed. The radius of the homogenous core is proportional to $\sqrt{t}$, therefore its volume (including an arbitrary span in the third dimension) will be proportional to t. The fuel consumption rate per unit volume is constant in the core, so the total fuel consumption rate will be proportional to the core volume, or t.

One more aspect of this new solution requires mention. The previous solution for the total fuel consumption rate (equations 5.28a and 5.28b) was continuous (the slope was discontinuous, but the value of $\dot{M}$ was continuous) across the transition at $t = 3t_{ch}$ because equations 3.24a and 3.24b were forced to give the same value for $\dot{m}$ at the changeover point $\bar{r} = t_{ch}$. In treating the

interaction of one flame with neighboring flames, the cases $\bar{\tau} << t_{ch}$ and $\bar{\tau} >> t_{ch}$ were analyzed separately, resulting in equations 6.24 and 6.16, which are analogous to to equations 3.24a and 3.24b. Indeed, one may consider 3.24a and 3.24b to be special cases of 6.24 and 6.16 for $\frac{\delta}{\Delta} = 0$.

The current solution for $\dot{M}$ is not continuous at $t = 3t_{ch}$; equations 6.31 and 6.19 differ by roughly twenty percent at the changeover point. The jump is not physically real, of course. It is a result of equations 6.16 and 6.24 not yielding the same value for $\dot{m}$ at the crossover $\bar{\tau} = t_{ch}$ except for the special case $\frac{\delta}{\Delta} = 0$. This point will not be pursued further. The discontinuity is not large in numerical terms, and solving for the fuel consumption rate $\dot{m}$ of a strained laminar flame for arbitrary $\frac{\bar{\tau}}{t_{ch}}$ and $\frac{\delta}{\Delta}$ would seem to be a quite difficult problem.

6.8 Summary

The validity of several assumptions of this analysis have been examined. Equations 3.24a and 3.24b were replaced by a more accurate (according to the numerical analysis of chapter four) formula for $\dot{m}$ which had no slope discontinuity at $\bar{\tau} = t_{ch}$. As a result, the slope discontinuity in the total fuel consumption rate $\dot{M}$ which was present at $t = 3t_{ch}$ was removed, but the improvement accomplished little else.

Several assumptions regarding the neglect of local flame curvature, variation of flame thickness along the length of the flame, and diffusion of reactants into the core were examined. The validity of the local approximation to the velocity field about the flame was examined, and the effect of viscosity was considered. The results showed that these factors were indeed negligible, provided that $\frac{\Gamma}{D_0}$ was large. This limit was taken in chapter five so that closed

form solutions could be found, rather than resorting to numerical integration. The current results show that $\frac{\Gamma}{D_0}$ must be large anyhow, to ensure the validity of assumptions made from the start.

Finally, reduction in the fuel consumption rate of a flame due to its neighbors was evaluated. For times large compared to the chemical time, where the Burke-Schumann approximation is applicable, the idea of a burned out core was found to be valid. The more complicated model made less than a one percent difference in the total fuel consumption rate of the spiral. A larger effect was found when the slow reaction rate approximation is applicable. For small values of $\frac{t}{t_{ch}}$, the center of the vortex contains a region where fuel and oxidizer are completely mixed before burning. Fortunately, the dimensional scalings were unchanged, and the total fuel consumption rate of the spiral was roughly the same as before.

7. ACOUSTIC EMISSION BY A SPIRAL FLAME

7.1 Introduction

One technological application of these results is to screeching instabilities in ramjet combustors; in particular to the instability mechanism found by Rogers and Marble (1956) (also see Rogers (1954) and Barker (1958)) in their experiments. A diagram of the experiment is shown in figure 7.1. The setup was two dimensional, and the flow passed from left to right in the figure. Premixed fuel and oxidizer were burned by a premixed flame, which originated from the sharp edge of the flameholder.

As the equivalence ratio was increased, the steady flow of figure 7.1 would become unstable, and high frequency (roughly 3800 Hz) oscillations would ensue. The unstable oscillations were transverse, from top to bottom in the figure, and coincided with the lowest frequency transverse mode of the combustor. As shown in figure 7.2, the screeching was accompanied by rows of vortices shed by the edges of the flameholder. The vortices were shed at the flame attachment point, and distorted the flame sheet as they were swept downstream.

Rogers and Marble concluded that an acoustic wave passing a sharp edge would generate a vortex, which would distort the flame sheet into a spiral. This increase in flame surface area would, after a delay time characteristic of the fuel oxidizer mixture, cause an increase in the burning rate. Since combustion products typically occupy a larger volume than the original reactants, the unsteady combustion would be a source of a pressure pulse.

Thus, the Rayleigh criterion for instability could be met provided the ignition delay were suitably related to the other parameters of the system. According to the theory proposed by Rogers and Marble, this delay is a

characteristic of the particular chemical reaction system. Later experiments by Barker (1958) reinforced this idea. Barker was able to change the equivalence ratio at the onset of screech by using different fuel mixtures and different mixture temperatures. Barker compared his results to ignition delay times deduced from flame blowoff measurements. He concluded that, at the onset of screech, the ignition delay was approximately constant, and equal to one period of oscillation.

Later work by Jarosin'ski and Wo'jcicki (1976) found a similar instability mechanism. Vortices shed from the flameholder resulted in a delayed pressure pulse, which, if the delay were right, would reinforce the original acoustic pulse. In this way, self excited oscillations could arise. In this case, the oscillations were longitudinal, and corresponded to the organ pipe frequency of the pipe upstream of the flameholder.

The present analysis differs from these experiments in one important respect; the experiments were done for premixed fuel and oxidizer and the theoretical results were derived for a diffusion flame. Nevertheless, when a vortex distorts a flame, an increase in burning rate after a delay characteristic of the chemistry has been predicted, so the acoustic pressure pulse emitted by a vortex created on a flame sheet will be calculated.

Although not strictly applicable, the results will bear an obvious similarity to the instability mechanism of Marble and Rogers and Jarosin'ski and Wo'jcicki. Furthermore, the results will provide a mechanism for explaining the generation of acoustic noise by diffusion flames and a mechanism for generating instabilities in diffusion flames.

7.2 Relationship between Burning Rate and Acoustic Pulse

For an acoustic pulse to be generated, the products must occupy a different

(usually larger) volume than the original reactants. This is usually true because the heat of the reaction creates products which are much hotter than the reactants, thus occupying a larger volume when combustion occurs under constant pressure. Therefore, assume a compact source; the vortex flame occupies a small (compared to a wavelength) region of space, and take a control volume which includes the vortex. The conversion of fuel and oxidizer into products occupying a greater volume will cause the outflow of fluid from our control volume.

The rate of fuel consumption of a vortex flame, $\dot{M}$, has been previously found. This is actually the fuel consumption per unit length of vortex, due to the two dimensional nature of our problem. If a small piece of the vortex flame of length dz in the third dimension is considered, then fuel is being converted into product at a rate $\dot{M}\,dz$, and so is oxidizer. Since the fuel and oxidizer were originally of density ρ_0, and letting the density of the products be ρ_1, then the rate of volume outflow from the compact source is $Q(t)$, given by

$$Q(t) = \frac{2(\alpha - 1)\dot{M}\,dz}{\rho_0} \qquad 7.1$$

where the parameter α is the expansion ratio (ratio of volume of products to reactants, or $\frac{\rho_0}{\rho_1}$). The factor of two is present because $\dot{M}$ is the rate of consumption of fuel, and oxidizer will be consumed at an equal rate.

Thus, the vortex flame, considered as a compact region, acts as a monopole source of sound provided that $\alpha \neq 1$. According to standard texts on acoustics (*e.g.* Lighthill (1978)), if a compact region of three dimensional space contains a volume source of strength $Q(t)$, that is, fluid is pouring out of the volume at a rate Q, then the resulting pressure perturbation seen by an observer at a distance r in a fluid of density ρ_0 and sound speed c is given by

$$P - P_0 = \rho_0 \frac{\dot{Q}(t - r/c)}{4\pi r} \qquad 7.2$$

Note that equation 7.2 contains $\dot{Q}$, the derivative of $Q(t)$. Thus steady combustion corresponding to a constant value of Q will not cause an acoustic pulse. Therefore, the vortex will not create any noise for times large compared to t_{ch}, because the fuel consumption rate $\dot{M}$ approaches a constant value for large times.

Previous results showed a fuel consumption rate proportional to $\rho_0 \Gamma^{\frac{2}{3}} D_0^{\frac{1}{3}}$ which rose from zero to its steady value for large times on a time scale proportional to t_{ch}. Already one can see that a small piece of vortex flame will act as a monopole source for times on the order of the chemical time whose strength will be proportional to $(\alpha - 1)\frac{\rho_0 \Gamma^{\frac{2}{3}} D_0^{\frac{1}{3}}}{t_{ch}}$. Thus, as the chemical time is decreased, the source strength becomes greater, although lasting for a shorter time.

7.3 Assumed Fuel Consumption Rate

The numerical values calculated will depend on the form chosen for the fuel consumption rate $\dot{M}(t)$. Equation 7.2 shows that the derivative of $\dot{M}$ is the quantity of importance. The result of chapter five, equation 5.30a for the fuel consumption rate for $\frac{t}{t_{ch}} < 3$, shows that $\dot{M}$ is proportional to $\left[\frac{t}{t_{ch}}\right]^{\frac{2}{3}}$, thus having an infinite derivative at $t = 0$. Such an infinite value for $\dot{Q}$ would predict an infinite pressure pulse, thus the result of chapter six, equation 6.31a, is especially welcome. The predicted time dependence proportional to $\frac{t}{t_{ch}}$ causes no problems.

The one problem is patching equations 6.31 to the results for large times,

since any artificial jumps in $\dot{M}$ will play havoc with its derivative. For this chapter choose

$$\frac{\dot{M}}{\rho_0 \Gamma^{\frac{2}{3}} D_0^{\frac{1}{3}}} = 0 \quad \text{for} \quad \frac{t}{t_{ch}} < 0 \tag{7.3a}$$

$$\frac{\dot{M}}{\rho_0 \Gamma^{\frac{2}{3}} D_0^{\frac{1}{3}}} = \frac{\sqrt{3}}{\pi}\left[\frac{\pi}{4}\sqrt{\frac{3}{2}}\right]^{\frac{1}{3}} \frac{t}{t_{ch}} \quad \text{for} \quad 0 < \frac{t}{t_{ch}} < 2^{\frac{7}{6}} \tag{7.3b}$$

$$\frac{\dot{M}}{\rho_0 \Gamma^{\frac{2}{3}} D_0^{\frac{1}{3}}} = \frac{2\sqrt{3}}{\pi}\left[\frac{\pi}{4}\sqrt{\frac{3}{2}}\right]^{\frac{1}{3}} \quad \text{for} \quad \frac{t}{t_{ch}} > 2^{\frac{7}{6}} \tag{7.3c}$$

Equation 7.3a was chosen so that the fuel consumption rate would be zero for times less than zero. Equation 7.3b expresses the result of equation 6.31a, and 7.3c shows the constant fuel consumption rate appropriate for large times from equation 5.30b. The crossover point $\frac{t}{t_{ch}} = 2^{\frac{7}{6}}$ was selected to ensure continuity between equations 7.3b and 7.3c.

Taking $\dot{M}$ from equations 7.3, and substituting into equation 7.1 yields

$$\dot{Q}(t) = 0 \quad \text{for} \quad \frac{t}{t_{ch}} < 0 \tag{7.4a}$$

$$\dot{Q}(t) = 2(\alpha - 1)\frac{\Gamma^{\frac{2}{3}} D_0^{\frac{1}{3}}}{t_{ch}} \frac{\sqrt{3}}{\pi}\left[\frac{\pi}{4}\sqrt{\frac{3}{2}}\right]^{\frac{1}{3}} dz \quad \text{for} \quad 0 < \frac{t}{t_{ch}} < 2^{\frac{7}{6}} \tag{7.4b}$$

$$\dot{Q}(t) = 0 \quad \text{for} \quad \frac{t}{t_{ch}} > 2^{\frac{7}{6}} \tag{7.4c}$$

Thus, assuming that equations 7.3 are approximately accurate, a piece of a spiral flame of length dz will act as a monopole source beginning at $t = 0$ and lasting for $2^{\frac{7}{6}} t_{ch}$. The strength of the source will be $2(\alpha - 1)\frac{\Gamma^{\frac{2}{3}} D_0^{\frac{1}{3}}}{t_{ch}} \frac{\sqrt{3}}{\pi}\left[\frac{\pi}{4}\sqrt{\frac{3}{2}}\right]^{\frac{1}{3}} dz$.

7.4 Calculation of Two Dimensional Pressure Pulse

One could now substitute equations 7.4 for $\dot{q}(t)$ into equation 7.2 to find the pressure signal seen a distance r from a small piece of vortex flame of length dz. However, the problem was originally stated in two dimensions, and the experiment of Marble and Rogers was done for a two dimensional test section. Additionally, a vortex line cannot end except at a boundary, so one should find the pressure signal treating the spiral flame as a two dimensional source.

The acoustic field for a two dimensional source can be found from the acoustic field for a three dimensional source by placing a continuous distribution of two dimensional sources along the z axis. The linearity of the equations of acoustics enables one to superimpose solutions, thus the solution for a two dimensional source can be obtained by integrating along the z axis (see Lighthill)

$$P - P_0 = \frac{\rho_0}{4\pi}\int_{-\infty}^{+\infty} \frac{\dot{Q}(t - r/c)}{r}\, dz \qquad 7.5$$

The geometry is shown in figure 7.3. Since x is the distance of the observer from the two dimensional source, then $r^2 = z^2 + x^2$. The integrand is an even function, so equation 7.5 may be written as

$$P - P_0 = \frac{\rho_0}{2\pi}\int_{x}^{+\infty} \frac{\dot{Q}(t - r/c)}{\left[r^2 - x^2\right]^{\frac{1}{2}}}\, dr \qquad 7.6$$

Substituting equations 7.4 for $\dot{Q}$ into equation 7.6 and performing the integration results in an expression for the pressure pulse seen by an observer a distance x away from a infinitely long vortex. The solution is

$$P - P_0 = 0 \quad \text{for} \quad t - \frac{x}{c} < 0 \qquad 7.7a$$

$$P - P_0 = (\alpha - 1)\frac{\rho_0 \Gamma^{\frac{2}{3}} D_0^{\frac{1}{3}}}{t_{ch}} \frac{\sqrt{3}}{\pi^2}\left[\frac{\pi}{4}\sqrt{\frac{3}{2}}\right]^{\frac{1}{3}} \tag{7.7b}$$

$$\times \log\left[\frac{ct + \sqrt{c^2t^2 - x^2}}{x}\right] \quad \text{for} \quad 0 < t - \frac{x}{c} < 2^{\frac{7}{6}} t_{ch}$$

$$P - P_0 = (\alpha - 1)\frac{\rho_0 \Gamma^{\frac{2}{3}} D_0^{\frac{1}{3}}}{t_{ch}} \frac{\sqrt{3}}{\pi^2}\left[\frac{\pi}{4}\sqrt{\frac{3}{2}}\right]^{\frac{1}{3}} \tag{7.7c}$$

$$\times \log\left[\frac{ct + \sqrt{c^2t^2 - x^2}}{c(t - 2^{\frac{7}{6}} t_{ch}) + \sqrt{c^2(t - 2^{\frac{7}{6}} t_{ch})^2 - x^2}}\right] \quad \text{for} \quad t - \frac{x}{c} > 2^{\frac{7}{6}} t_{ch}$$

Simpler forms may be found by noting that one is interested in the "far field" radiation. Usually, for periodic sources of frequency ω, the far field is found for large values of x, such that $x >> \frac{c}{\omega}$. In this case, equation 7.4 shows that the radiation from a given piece of the vortex lasts for a time proportional to t_{ch}, so the far field will consist of distances such that $x >> ct_{ch}$. Therefore, simplify equations 7.7, assuming that $\frac{x}{ct_{ch}}$ is large. (Take the limit $\frac{x}{ct_{ch}} \to \infty$, but keep in mind that $\frac{t}{t_{ch}} - \frac{x}{ct_{ch}}$ is of order one.) The result is,

$$P - P_0 = 0 \quad \text{for} \quad \frac{t - x/c}{t_{ch}} < 0 \tag{7.8a}$$

$$P - P_0 \approx (\alpha - 1)\rho_0 \Gamma^{\frac{2}{3}} D_0^{\frac{1}{3}} \sqrt{\frac{c}{xt_{ch}}} \frac{\sqrt{6}}{\pi^2} \tag{7.8b}$$

$$\times \left[\frac{\pi}{4}\sqrt{\frac{3}{2}}\right]^{\frac{1}{3}} \left[\frac{t - x/c}{t_{ch}}\right]^{\frac{1}{2}} \quad \text{for} \quad 0 < \frac{t - x/c}{t_{ch}} < 2^{\frac{7}{6}}$$

$$P - P_0 \approx (\alpha - 1)\rho_0 \Gamma^{\frac{2}{3}} D_0^{\frac{1}{3}} \sqrt{\frac{c}{xt_{ch}}} \frac{\sqrt{6}}{\pi^2} \tag{7.8c}$$

$$\times \left[\frac{\pi}{4}\sqrt{\frac{3}{2}}\right]^{\frac{1}{3}} \left[\left[\frac{t - x/c}{t_{ch}}\right]^{\frac{1}{2}} - \left[\frac{t - x/c}{t_{ch}} - 2^{\frac{7}{6}}\right]^{\frac{1}{2}} \right] \quad \text{for} \quad \frac{t - x/c}{t_{ch}} > 2^{\frac{7}{6}}$$

Equation 7.8a shows that no pressure pulse is received until a time $\frac{x}{c}$ has elapsed. The maximum pressure occurs at $t = \frac{x}{c} + 2^{\frac{7}{6}} t_{ch}$, where equations 7.8b and 7.8c join. The maximum pressure is given by

$$\left[P - P_0\right]_{max} \approx (\alpha - 1)\rho_0 \Gamma^{\frac{2}{3}} D_0^{\frac{1}{3}} \sqrt{\frac{c}{x t_{ch}}} \qquad 7.9$$

$$\times \frac{\sqrt{6}}{\pi^2}\left[\frac{\pi}{4}\sqrt{\frac{3}{2}}\right]^{\frac{1}{3}} 2^{\frac{7}{12}} \quad at \quad t = \frac{x}{c} + 2^{\frac{7}{6}} t_{ch}$$

Equation 7.8c shows the "tail" which is characteristic of acoustics in two dimensions. A typical plot of pressure versus time is given in figure 7.4, showing the shape of the pressure pulse.

7.5 Effects of Heat Release on the Fuel Consumption Rate

The release of heat by the combustion process will cause the products of the reaction to occupy a greater volume than the original fuel and oxidizer. This effect was responsible for the generation of an acoustic pulse as a vortex wraps up a laminar diffusion flame.

However, the analysis which resulted in the equations 5.30b and 6.31a, which were used to derive these results, only partially included the effects of the heat release. The analysis of chapter three of a one dimensional strained flame included the density change caused by heat release by using the Howarth transformation. Likewise, the numerical calculations of chapter four allowed the density to vary across the flame. But, in chapter two, when following a piece of flame as it is convected by the fluid, and calculating the flame density per

unit volume and the transient strain rate, the fluid was assumed to be of a constant density. If the density change were included in an honest manner, the creation of volume near the center of the spiral, due to the conversion of fuel and oxidizer into products, would displace the outlying flames outward to larger radii. Thus, the expressions for strain rate and flame surface density would involve the fuel consumption rate.

This problem will not be solved here. Instead, refer to the results of Karagozian (1982) for infinite reaction rate spiral flames, where the growth of the core was allowed to displace the surrounding spiral flame arms outwards. The results of the calculations show a surprisingly small effect of the density change. Even for products which occupy six times the volume of the original reactants, the total fuel consumption rate of the spiral is changed by a factor of two. The effect is hardly negligible, but not as large as one might expect. In any case, the present results seem to be good order of magnitude estimates of the noise generation, and the dimensional form of the results is itself quite interesting.

7.6 Summary

If the products occupy a greater volume than the reactants, a spiral flame will serve as a monopole source of volume outflow. Acoustic theory provides that a source of efflux will act as a monopole acoustic source, with the strength of the pressure pulse proportional to the time derivative of the rate of volume outflow. Therefore, a steady fuel consumption rate produces no acoustic emission. The effect is due to the transient behavior of spiral flames at times comparable to the chemical time, where the fuel consumption rate is increasing. In keeping with the two dimensional nature of the analysis so far, the two dimensional acoustic field was found for a vortex lying along the z axis. For an observer a distance x from the vortex, no pressure pulse is seen until a time $\frac{x}{c}$

has elapsed. In the far field where $\frac{x}{ct_{ch}}$ is large, the peak pressure pulse occurs at $t = \frac{x}{c} + 2^{\frac{7}{6}} t_{ch}$, and its strength is proportional to $\rho_0 \Gamma^{\frac{2}{3}} D_0^{\frac{1}{3}} (\alpha - 1) \sqrt{\frac{c}{xt_{ch}}}$. Thus, the amplitude of the pressure pulse varies as $\frac{1}{\sqrt{x}}$, and is proportional to $\frac{1}{\sqrt{t_{ch}}}$. Again, note that the dependence of the acoustic source strength depends on the combined transport coefficient $\Gamma^{\frac{2}{3}} D_0^{\frac{1}{3}}$.

When applied to the instability mechanism of Rogers and Marble, these results are interesting for two principle reasons. First, the peak pressure pulse occurs after a delay proportional to the characteristic chemical time of the system. This would explain the dependence of screeching on the fuel type and the equivalence ratio. Secondly, the strength of the pulse is proportional to the circulation of the vortex raised to the two-thirds power. If the gas velocity past the edge of the flameholder were U, then a length L of the resulting shear layer would have a net circulation of UL. Therefore, if t_{osc} is the period of the oscillations, then the vorticity of shear layer would be lumped into vortices, each vortex containing the vorticity from a length $L = Ut_{osc}$ of the shear layer, thus each vortex would have a net circulation of $\Gamma = U^2 t_{osc}$. As a result, the strength of the acoustic source would go like $U^{\frac{4}{3}}$.

8. LARGE ACTIVATION ENERGY FLAMES

8.1 Introduction

The results derived thus far have been applicable only to reaction systems described as "low activation energy". The distinction between low activation energy systems and high activation energy systems was discussed in chapter three. In short, low activation energy systems exhibit a smooth transition from the small Damköhler number to the large Damköhler number regimes, but high activation energy systems may have more than one possible solution at a single Damköhler number, and may undergo sudden jumps as the Damköhler number is slowly varied. The large activation energy case is of great practical interest; the combustion of many hydrocarbon fuels in air (initially at room temperature) fall into this category.

8.2 The Transient Extinction Problem

As discussed in chapter three, most work on one dimensional diffusion flames with a large activation energy has concentrated on steady flames. These solutions, independent of time, are found when the strain rate ε is constant. Whether the flame is burning according to the Burke-Schumann solution or is extinct depends on the Damköhler number, the ratio of the flow time of the system to a chemical time. For the constant strain case, the characteristic flow time is usually taken to be $\frac{1}{\varepsilon}$, and the chemical time is customarily taken to be $\frac{1}{k_0}$, where k_0 is the preexponential constant in the reaction rate equation 3.25. Thus the Damköhler number is defined as $\frac{k_0}{\varepsilon}$.

One may argue that the parameter $\bar{\tau}$ divided by a characteristic chemical time is the transient analogue of the steady state Damköhler number. First, the flame thickness δ is proportional to $\sqrt{D_0\bar{\tau}}$, thus the characteristic time required

to diffuse a distance δ is $\frac{\delta^2}{D_0}$, which is equal to $\bar{\tau}$. Secondly, the approximate analyses by Zeldovitch (1951), Spalding (1954), and Liñan (1963) of the inner reaction zone suggest that the reaction zone has a limited capacity, and one may construct an intuitive picture of the extinction process whereby extinction occurs when the outer diffusion zone transports too much fuel and oxidizer into the inner reaction zone. In chapter three (see equation 3.24b), it was demonstrated that the fuel consumption rate for a transiently strained Burke-Schumann flame depends on the parameter $\bar{\tau}$, with $\dot{m}$ increasing as $\bar{\tau}$ is decreased. Thus, an extinction criterion which specifies a maximum fuel consumption rate also sets a lower limit on $\bar{\tau}$. Extinction would occur if $\bar{\tau}$ were too small.

This suggests that in the transient case, the ratio $\frac{\bar{\tau}}{t_{ch}}$ corresponds to the steady state Damköhler number. Indeed, if one sets ε constant, and calculates $\bar{\tau}$ from equations 3.8 and 3.12, for large times $\bar{\tau}$ approaches a constant value of $\frac{1}{2\varepsilon}$. Thus, (except for a factor of two) the ratio $\frac{\bar{\tau}}{t_{ch}}$ reduces to the usual Damköhler number for the special case of a constant strain rate. Perhaps the parameter $\bar{\tau}$ is useful for predicting extinction for transiently strained flames.

8.3 Theory

Choose the single step, second order reaction

$$A + B \rightarrow 2C$$

The factor of two is necessary; all species are to have identical properties.

The mass fraction Y of each species will vary from zero to one. For a Lewis number of one, the temperature T will range from T_∞ to T_f, where $T_f = T_\infty + \frac{\Delta H}{2c_p}$. A dimensionless temperature Θ may be introduced, defined by

$$\Theta \equiv \frac{(T-T_\infty)}{(T_f-T_\infty)} \qquad 8.1$$

so that Θ=0 corresponds to $T = T_\infty$ and $\Theta = 1$ corresponds to $T = T_f$. Starting with equation 3.2, substitute for $\frac{w}{\rho}$ from equations 3.3 and 3.25. Let $\mu_T = 1$ for convenience, especially since the strong variation of w with temperature is due mostly to the exponential term. The results are

$$\frac{\partial Y_A}{\partial t} - \varepsilon\xi \frac{\partial Y_A}{\partial \xi} = D_0 \frac{\partial^2 Y_A}{\partial \xi^2} - k_0 Y_A Y_B e^{\frac{-T_a}{\Theta(T_f-T_\infty)+T_\infty}} \qquad 8.2a$$

$$\frac{\partial Y_B}{\partial t} - \varepsilon\xi \frac{\partial Y_B}{\partial \xi} = D_0 \frac{\partial^2 Y_B}{\partial \xi^2} - k_0 Y_A Y_B e^{\frac{-T_a}{\Theta(T_f-T_\infty)+T_\infty}} \qquad 8.2b$$

$$\frac{\partial Y_C}{\partial t} - \varepsilon\xi \frac{\partial Y_C}{\partial \xi} = D_0 \frac{\partial^2 Y_C}{\partial \xi^2} + 2k_0 Y_A Y_B e^{\frac{-T_a}{\Theta(T_f-T_\infty)+T_\infty}} \qquad 8.2c$$

$$\frac{\partial \Theta}{\partial t} - \varepsilon\xi \frac{\partial \Theta}{\partial \xi} = D_0 \frac{\partial^2 \Theta}{\partial \xi^2} + 2k_0 Y_A Y_B e^{\frac{-T_a}{\Theta(T_f-T_\infty)+T_\infty}} \qquad 8.2d$$

The temperature dependence of the reaction rate may be incorporated into two dimensionless ratios, such as $\frac{T_f}{T_\infty}$ and $\frac{T_a}{T_f}$.

Note that if equation 8.2b is subtracted from equation 8.2a, the resulting equation will contain no chemical reaction term. Thus one may simplify the system by introducing Schvab-Zeldovitch variables.

$$\varphi_1 = Y_A - Y_B \qquad 8.3a$$

$$\varphi_2 = Y_A + Y_B + Y_C \qquad 8.3b$$

$$\varphi_3 = Y_C - \Theta \qquad 8.3c$$

$$\varphi_4 = Y_C \qquad 8.3d$$

The system still has four independent variables, but now equations 8.2 can be written in the simpler form

$$\frac{\partial \varphi_1}{\partial t} - \varepsilon\xi \frac{\partial \varphi_1}{\partial \xi} = D_0 \frac{\partial^2 \varphi_1}{\partial \xi^2} \tag{8.4a}$$

$$\frac{\partial \varphi_2}{\partial t} - \varepsilon\xi \frac{\partial \varphi_2}{\partial \xi} = D_0 \frac{\partial^2 \varphi_2}{\partial \xi^2} \tag{8.4b}$$

$$\frac{\partial \varphi_3}{\partial t} - \varepsilon\xi \frac{\partial \varphi_3}{\partial \xi} = D_0 \frac{\partial^2 \varphi_3}{\partial \xi^2} \tag{8.4c}$$

$$\frac{\partial \varphi_1}{\partial t} - \varepsilon\xi \frac{\partial \varphi_1}{\partial \xi} = D_0 \frac{\partial^2 \varphi_1}{\partial \xi^2} + 2k_0 Y_A Y_B e^{\frac{-T_a}{\theta(T_f - T_\infty)+T_\infty}} \tag{8.4d}$$

Note that the chemical reaction term has been eliminated from all equations but one. One could express Y_A and Y_B in terms of the φ's in equation 8.4d, but this will be done later.

Now one may define a characteristic chemical time $t_{ch} \equiv \frac{1}{k_0}$ and define a system of dimensionless coordinates

$$_*t = \frac{t}{t_{ch}} \tag{8.5a}$$

$$_*\xi = \frac{\xi}{\sqrt{D_0 t_{ch}}} \tag{8.5b}$$

$$_*\varepsilon = \varepsilon t_{ch} \tag{8.5c}$$

Equations 8.4 may be written in these new coordinates, with the result

$$\frac{\partial \varphi_1}{\partial_* t} - {}_*\varepsilon\, {}_*\xi \frac{\partial \varphi_1}{\partial_* \xi} = \frac{\partial^2 \varphi_1}{\partial_* \xi^2} \tag{8.6a}$$

$$\frac{\partial \varphi_2}{\partial_* t} - {}_*\varepsilon\, {}_*\xi \frac{\partial \varphi_2}{\partial_* \xi} = \frac{\partial^2 \varphi_2}{\partial_* \xi^2} \tag{8.6b}$$

$$\frac{\partial \varphi_3}{\partial_* t} - {}_*\varepsilon\, {}_*\xi \frac{\partial \varphi_3}{\partial_* \xi} = \frac{\partial^2 \varphi_3}{\partial_* \xi^2} \tag{8.6c}$$

$$\frac{\partial \varphi_4}{\partial_* t} - {}_*\varepsilon\, {}_*\xi \frac{\partial \varphi_4}{\partial_* \xi} = \frac{\partial^2 \varphi_4}{\partial_* \xi^2} + 2 Y_A Y_B e^{\frac{-T_a}{\theta(T_f - T_\infty)+T_\infty}} \tag{8.6d}$$

Equations 8.6 are dimensionless.

Before proceeding further, initial conditions are needed. The initial conditions used in chapter three, when transformed into the Schvab-Zeldovitch variables, become

$$at \quad {}_*t = 0 \quad \text{for} \quad {}_*\xi < 0 \qquad 8.7a$$

$$\varphi_1 = -1$$

$$\varphi_2 = +1$$

$$\varphi_3 = 0$$

$$\varphi_4 = 0$$

$$at \quad {}_*t = 0 \quad \text{for} \quad {}_*\xi > 0 \qquad 8.7b$$

$$\varphi_1 = +1$$

$$\varphi_2 = +1$$

$$\varphi_3 = 0$$

$$\varphi_4 = 0$$

Two trivial solutions are apparent. First, $\varphi_2 = 1$ everywhere. This should have been obvious at the beginning, since only three species are present and the sum of the mass fractions must always equal one. Thus, $\varphi_2 = Y_A + Y_B + Y_C = 1$. Secondly, $\varphi_3 = 0$ everywhere, thus $\Theta = Y_C$. This should have been obvious too, since the production of heat is proportional to the production of product C. With the Lewis number equal to one then the temperature rise and the product

will diffuse at the same rate. Since the dimensionless temperature Θ has been scaled so that it varies from zero to one, and with the initial conditions that $\Theta = Y_C = 0$ for all ${}_*\xi$, then $\Theta = Y_C$ for all ${}_*\xi$ and ${}_*t$.

One is left with equations for φ_1 and φ_4, and equation 8.6a for φ_1 does not involve the chemistry at all. Thus, first solve for φ_1. This equation was solved in chapter three, so use the same method of solution. Previously, the convection term was eliminated by the coordinate transformation (given by equations 3.7 and 3.8) from (ξ,t) to (ζ,τ) coordinates. Define an analogous transformation to go from $({}_*\xi,{}_*t)$ to $({}_*\zeta,{}_*\tau)$ coordinates. One realizes that the previous (ξ,t) coordinates of chapter three were not dimensionless, so the resulting (ζ,τ) coordinates were not dimensionless either. In the present case, the original $({}_*\xi,{}_*t)$ coordinates are dimensionless, so the final $({}_*\zeta,{}_*\tau)$ coordinates will be dimensionless as well.

Equation 8.6a becomes

$$\frac{\partial \varphi_1}{\partial {}_*\tau} = \frac{\partial^2 \varphi_1}{\partial {}_*\zeta^2} \tag{8.8}$$

The initial conditions given by equations 8.7 transform as

$$at \quad {}_*\tau = 0 \quad for \quad {}_*\zeta < 0 \quad \varphi_1 = -1 \tag{8.9a}$$

$$at \quad {}_*\tau = 0 \quad for \quad {}_*\zeta > 0 \quad \varphi_1 = +1 \tag{8.9b}$$

The solution to equation 8.8 with initial conditions given by equations 8.9 is

$$\varphi_1 = erf\left[\frac{{}_*\zeta}{2\sqrt{{}_*\tau}}\right] \tag{8.10}$$

$$= erf\left[\frac{\xi}{2\sqrt{D_0\bar{\tau}}}\right]$$

In chapter three, the flame thickness δ was identified as $\sqrt{D_0\bar{\tau}}$. This was done on

the basis of asymptotic solutions for weak and strong chemical reactions. Equation 8.10 shows that if the flame thickness in ξ coordinates is defined in terms of the difference in fuel concentration and oxidizer concentration, $Y_A - Y_B$, then the flame thickness is always proportional to $\sqrt{D_0 \bar{\tau}}$ regardless of how the strain rate varies with time.

Although the remaining equation for φ_4 cannot be solved exactly, it is useful to transform this equation as well. In the $({}_*\zeta, {}_*\tau)$ coordinate system, equation 8.6d becomes

$$\frac{\partial \varphi_4}{\partial {}_*\tau} - \frac{\partial^2 \varphi_4}{\partial {}_*\zeta^2} = e^{-2\int_0^t \varepsilon(t'')\,dt''} \, Y_A Y_B \, e^{\frac{-T_a}{\Theta(T_f - T_\infty) + T_\infty}} \tag{8.11}$$

Since φ_1, φ_2, and φ_3 are known, Y_A, Y_B, and Θ can be written in terms of φ_4. Previously, it was shown that $\varphi_4 = Y_C = \Theta$, so use Θ as the dependent variable rather than φ_4. The result of these substitutions is

$$\frac{\partial \Theta}{\partial {}_*\tau} - \frac{\partial^2 \Theta}{\partial {}_*\zeta^2} = e^{-2\int_0^t \varepsilon(t'')\,dt''} \left[1 + erf\, \frac{{}_*\zeta}{2\sqrt{{}_*\tau}} - \Theta\right] \tag{8.12}$$

$$\times \left[1 - erf\, \frac{{}_*\zeta}{2\sqrt{{}_*\tau}} - \Theta\right] e^{\frac{-T_a}{\Theta(T_f - T_\infty) + T_\infty}}$$

Yet another transformation, from the $({}_*\tau, {}_*\zeta)$ coordinates to the "similarity" coordinates $({}_*\tau, {}_*\gamma)$, where ${}_*\gamma \equiv \frac{{}_*\zeta}{\sqrt{{}_*\tau}}$, yields

$$2\,{}_*\tau \frac{\partial \Theta}{\partial {}_*\tau} - \left[\frac{\partial^2 \Theta}{\partial {}_*\gamma^2} + {}_*\gamma \frac{\partial \Theta}{\partial {}_*\gamma}\right] = 2\,{}_*\bar{\tau} \left[1 + erf\, \frac{{}_*\gamma}{2} - \Theta\right] \tag{8.13}$$

$$\times \left[1 - erf\, \frac{{}_*\gamma}{2} - \Theta\right] e^{\frac{-T_a}{\Theta(T_f - T_\infty) + T_\infty}}$$

In equation 8.13, ${}_*\bar{\tau}$ has been defined as $\frac{\bar{\tau}}{t_{ch}}$, therefore ${}_*\bar{\tau} = {}_*\tau \, e^{-2\int_0^t \varepsilon(t'')\,dt''}$.

As an aside, several properties of equation 8.13 deserve mention. First, rather than speaking of the strain rate as a function of time one could just as well specify $\bar{\tau}$ as a function of the time t, or of the transformed time τ. Secondly, in the completely dimensionless coordinates used here, the magnitude of the chemical reaction term relative to the other terms of the equation is determined by the value of ${}_*\bar{\tau}$. Thus, one is justified in calling ${}_*\bar{\tau}$ the Damköhler number, and the limits considered in chapter three of weak chemistry and strong chemistry may be found by letting ${}_*\bar{\tau}$ approach zero and infinity, respectively.

Looking back to chapter three, the lowest order solution for weak chemistry was found by neglecting the reaction term. For strong chemistry, the reaction was confined to a small region, thus outside this region the reaction term could again be neglected. Examining the results, one finds that the concentration profiles (equations 3.16 for slow chemistry and equations 3.10 for fast chemistry) can be written as functions of only the similarity variable ${}_*\gamma$, and are independent of ${}_*\tau$ and ${}_*\bar{\tau}$. Thus, in the two limiting cases, the variable ${}_*\gamma$ is a true similarity variable. This is not true for intermediate values of ${}_*\bar{\tau}$, but the natural appearance of the similarity variable ${}_*\gamma$ in the weak and strong chemistry limits, as well as in the solution for $Y_A - Y_B$ suggests that the $({}_*\tau, {}_*\gamma)$ coordinates are the most convenient system. The transformation of the equations of interest into $({}_*\tau, {}_*\gamma)$ coordinates has resulted in equation 8.13, where the parameter ${}_*\bar{\tau}$ has spontaneously appeared.

If the strain rate were constant, then steady solutions could be found by dropping the time derivative terms and solving the resulting equation

$$\frac{\partial^2 \Theta}{\partial {}_*\gamma^2} + {}_*\gamma \frac{\partial \Theta}{\partial {}_*\gamma} = -2 {}_*\bar{\tau} \left[1 + erf \frac{{}_*\gamma}{2} - \Theta \right] \qquad 8.14$$

$$\times \left[1 - erf\,\frac{{}_*\gamma}{2} - \Theta\right] e^{\frac{-T_a}{\Theta(T_f - T_\infty)+T_\infty}}$$

The ratios $\frac{T_f}{T_\infty}$ and $\frac{T_a}{T_f}$ are constants, therefore the solution to equation 8.14 is a function of the variable ${}_*\gamma$ and the parameter ${}_*\bar{\tau}$. For this special case of constant strain steady solutions, ${}_*\bar{\tau} = \frac{k_0}{2\varepsilon}$, thus the behavior of equation 8.14 with respect to different values of the parameter ${}_*\bar{\tau}$ has been discussed in chapter three. The most important characteristic of this behavior is extinction if ${}_*\bar{\tau}$ should drop below a critical value, which depends on the ratios $\frac{T_f}{T_\infty}$ and $\frac{T_a}{T_f}$.

Returning to the general case of equation 8.13, the dependence of the strain rate on time will cause ${}_*\bar{\tau}$ to be a function of time. Since the solutions to equation 8.14 depend on ${}_*\bar{\tau}$, the time dependence of ${}_*\bar{\tau}$ will cause Θ to be a function of time as well as ${}_*\gamma$. Thus, the time derivative term in equation 8.13 cannot be set equal to zero.

If ${}_*\bar{\tau}$ were a slowly varying function of time, one could properly claim that the time derivative terms are negligible. Thus, to find the solution of equation 8.13 at a given time, one could take the solution of equation 8.14 for the same value of the parameter ${}_*\bar{\tau}$.

This approach suffers from two flaws. First, for a spiral flame the parameter ${}_*\bar{\tau}$ is not slowly varying. Additionally, no matter how slowly one varies ${}_*\bar{\tau}$, in the neighborhood of the extinction and ignition points an infinitesimal change in ${}_*\bar{\tau}$ will produce a large change in the solution Θ, so the time derivative term cannot be ignored.

In summary, one can interpret the instantaneous value of ${}_*\bar{\tau}$, or $\frac{\bar{\tau}}{t_{ch}}$, as the Damköhler number. If one attempts to relate extinction of a transient flame to

the instantaneous value of $\bar{\tau}$, one cannot do so rigorously. The best that can be accomplished is a pseudo-steady approximation, whereby if $\bar{\tau}$ is below the critical value one can assert that the flame is in the process of going out, but cannot say how fast. The correlation between extinction and the instantaneous value of $\bar{\tau}$ should be excellent if $\bar{\tau}$ is slowly changing, and poor if it is changing rapidly. Therefore, one must return to BLOTTNER numerical computations to see how well the proposed criterion performs.

8.4 Numerical Solution

To find a method of predicting extinction, numerical solutions are used for comparison. Using the BLOTTNER program, described in chapter four, flames were transiently strained as they would be in a spiral vortex. The rate of strain ε as a function of time was found in chapter two, and is given by equation 2.13.

$$\varepsilon = \frac{1}{t} \frac{\left[\frac{\Gamma t}{\pi r^2}\right]^2}{1+\left[\frac{\Gamma t}{\pi r^2}\right]^2} \qquad 2.13$$

The chosen reaction system consists of two reactants, which react irreversibly to form product according to the single step second order reaction

$$A + B \rightarrow 2C$$

The mass fractions of A and B at $-\infty$ and $+\infty$ are unity. All species have identical physical properties; constant specific heats, Prandtl and Lewis numbers of unity, and viscosities which are proportional to temperature. (BLOTTNER assumes ideal gases, so density is inversely proportional to temperature. Assuming μ proportional to T makes $\rho\mu$ a constant. Since Prandtl and Lewis numbers are constant, $\rho^2 D$ and the product of the density and the thermal conductivity will be constant. This temperature dependence of the

transport properties was assumed in deriving equation 8.1, and one would like the conditions of the numerical solution to correspond to the theoretical treatment as much as possible.)

The ambient temperature, heat release of the reaction, and activation energy (in the Arrhenius expression for temperature dependence of the reaction rate) were chosen such that $\frac{T_a}{T_f} = 10$ and $\frac{T_f}{T_\infty} = 4.5$.

8.4.1 Initial Conditions

A diffusion flame is initiated when a partition, separating two reactants, is removed. At the instant of creation, the flame is of zero thickness, and an unstrained flame grows in thickness as $\sqrt{D_0 t}$. The problem solved in the previous eight chapters was that of a diffusion flame whose birth occurs simultaneously with the establishment of a vortex. The initial conditions of concentration and temperature for such a problem were introduced in chapter three. Briefly, they consist of one reactant in one half plane, the other reactant in the other half plane, no product present at all, and a uniform initial temperature profile ($T = T_\infty$ for all y). This approach is appropriate for low activation energy reaction systems; it causes difficulties when applied to high activation energy systems.

For high activation energy systems the reaction rate is much slower at T_∞ than at T_f. (For the numerical values chosen here, the reaction rates differ by a factor of e^{35}.) As a consequence, if the same initial conditions are used for a high activation energy system, the reactants simply diffuse into one another with negligible reaction. Thus, the attempted numerical solution encounters a problem: even without any straining a source of ignition must be provided. Possible ignition mechanisms were discussed in the third chapter. The ignition problem was not resolved in that chapter, and will not be resolved here either.

Instead, initial conditions were specified (such as a region of elevated temperatures) to ensure that the flame is established on the vigorously burning branch of solutions.

The ultimate purpose of these calculations is to verify an extinction criterion based on $\bar{\tau}$. If the pseudo-steady approximation were exact, at any time the instantaneous value of $\bar{\tau}$ would determine the profiles of concentration and temperature. Thus, one does not have complete freedom in specifying initial conditions; if the pseudo-steady approximation is to work at all, the initial concentration and temperature profiles must belong to the family of profiles parameterized by an initial choice of $\bar{\tau}$.

The initial profile selected should establish a flame which is vigorously burning. The vigorously burning solutions are described by the Burke-Schumann approximation. The concentration profiles were given in chapter three, (equations 3.10) the temperature profile may be found similiarly (see Marble (1979)) and the results are

$$Y_A = erf\left[\frac{\xi}{2\sqrt{D_0\bar{\tau}}}\right] \qquad Y_B = 0 \qquad \text{8.15a}$$

$$\Theta = erf\left[\frac{\xi}{2\sqrt{D_0\bar{\tau}}}\right] \qquad \text{for} \qquad \xi > 0$$

$$Y_A = 0 \qquad Y_B = -erf\left[\frac{\xi}{2\sqrt{D_0\bar{\tau}}}\right] \qquad \text{8.15b}$$

$$\Theta = -erf\left[\frac{\xi}{2\sqrt{D_0\bar{\tau}}}\right] \qquad \text{for} \qquad \xi < 0$$

So, if one chooses an initial value of $\bar{\tau}$, equations 8.15 will specify an initial condition to use for input to BLOTTNER. The value of $\bar{\tau}$ chosen will affect the later solution, so denote it by the symbol t_0. The resulting solution may be

envisioned as corresponding to a diffusion flame which was ignited by an unknown cause, allowed to develop without straining for a time t_0, and then strained according to equation 2.13. In other words, the flame has existed for a time t_0 before the vortex is imposed at $t = 0$.

With these initial conditions, formula 4.7 for $\bar{\tau}$ is no longer correct. Equations 3.8 and 3.12 are still valid, but the initial condition $\bar{\tau} = 0$ at $t = 0$ is incorrect. If the instantaneous value of $\bar{\tau}$ is to characterize the solution, then $\bar{\tau} = t_0$ at $t = 0$. With this new initial condition, the solution to equations 3.8 and 3.12 is

$$\frac{\Gamma\bar{\tau}}{\pi r^2} = \frac{t_0 + \left[\frac{\Gamma t}{\pi r^2}\right] + \frac{1}{3}\left[\frac{\Gamma t}{\pi r^2}\right]^3}{1 + \left[\frac{\Gamma t}{\pi r^2}\right]^2} \qquad 8.16$$

Equation 8.16 will be used in place of equation 4.7 for the rest of this chapter.

8.4.2 Numerical Results

The results of the numerical calculations are given in dimensionless form. For convenience, the characteristic chemical time has been taken as $\frac{1}{\sqrt{2}\,k(T_f)}$ rather than as $\frac{1}{k_0}$. The choice was appropriate, since one is interested in the strongly burning solution where $T_{max} \approx T_f$.

With initial conditions given by equation 8.15, the spectrum of possible initial conditions is determined by different choices of t_0. Likewise, for a transient strain rate given by equation 2.13, the parameter $\frac{\Gamma}{\pi r^2}$ determines the transient strain history of the flame. In dimensionless form, each transient flame history one computes may be characterized by the ratios $\frac{t_0}{t_{ch}}$ and $\frac{\Gamma t_{ch}}{\pi r^2}$.

As functions of the dimensionless time $\frac{t}{t_{ch}}$, the quantities of interest are the dimensionless maximum flame temperature (at any time, the maximum temperature found by traversing the flame in the y direction), $\Theta_{max} = \frac{T_{max}}{T_\infty}$ (which will lie between 1 and 4.5), the dimensionless fuel consumption rate, $\frac{\dot{m}}{\rho_0}\left[\frac{t_{ch}}{D_0}\right]^{\frac{1}{2}}$, the instantaneous strain rate, εt_{ch}, and the instantaneous value of $\frac{\bar{\tau}}{t_{ch}}$.

For the first run, $\frac{t_0}{t_{ch}} = 10{,}000$ and $\frac{\Gamma t_{ch}}{\pi r^2} = 1$. (Actually, equations 8.15 do not include an inner reaction zone. Consequently, if one numerically evaluates equations 8.15 and uses them as initial conditions for BLOTTNER, the reactant consumption rate is zero at first. As a result, initial conditions were computed from equations 8.15 for $\frac{t_0}{t_{ch}} = 9{,}000$, and the vortex straining according to equation 2.13 was not begun until an additional 1,000 chemical times had elapsed. Thus, an inner reaction zone was allowed to develop, and the fuel consumption rate predicted from equation 3.24b matched the BLOTTNER results at the onset on straining. The results are corrected such that $t = 0$ still corresponds to the onset of the straining.)

The results, graphed in figures 8.1, 8.2, 8.3, and 8.4, show a flame which almost immediately goes out. The extinction is characterized by a drop in the fuel consumption rate accompanied by a drop in the maximum flame temperature. The predicted Burke-Schumann fuel consumption rate, found from equation 3.24b, is shown as a dashed line in figure 8.1. Note that the actual fuel consumption rate decreases, rather than increases as the straining is begun.

One would like to find a flame which remains lit. Of the two parameters at ones disposal, decreasing $\frac{\Gamma t_{ch}}{\pi r^2}$ will provide a gentler strain history for the flame, and increasing $\frac{t_0}{t_{ch}}$ will increase the initial Damköhler number, and perhaps make the flame more resistant to being strained out. In the present work, $\frac{\Gamma t_{ch}}{\pi r^2}$ was decreased.

Using $\frac{\Gamma t_{ch}}{\pi r^2}$ values of 0.1 and 0.01 produces flames which take longer to go out, but still go out. (These results are also graphed in figures 8.1, 8.2, 8.3, and 8.4.) The results for $\frac{\Gamma t_{ch}}{\pi r^2} = 0.01$ are especially striking. After the straining begins; the flame burns for hundreds of chemical times. The fuel consumption rate is well approximated by equation 3.24b (compare the solid and dashed lines in figure 8.1). The maximum flame temperature is nearly the adiabatic flame temperature, but is decreasing slowly with time. After a long time (so long that one is never quite sure how long to let the program run), the maximum flame temperature drops suddenly, and the reactant consumption rate no longer follows equation 3.24b, but instead decreases by many orders of magnitude. With little warning, the flame has suddenly gone out. Extinction has occurred again.

Can extinction be explained in terms of the instantaneous value of the strain rate? Can one say that extinction occurs if and when the strain rate exceeds a critical value? The instantaneous value of the strain rate is graphed in figure 8.3 as a function of time. Examination of these data (especially for $\frac{\Gamma t_{ch}}{\pi r^2} = 0.01$) shows that the strain rate has reached a maximum and begun to decrease when extinction occurs. Indeed, the maximum strain rate occurs at $\frac{t}{t_{ch}} = 100$, whereas extinction does not occur until much later, at approximately

$\frac{t}{t_{ch}} = 500$. (There is some uncertainty in defining exactly when extinction takes place.)

One concludes that the instantaneous strain rate is not useful in predicting extinction of these transiently strained flames. On the other hand, the instantaneous value of $\bar{\tau}$, graphed in figure 8.4, does a better job of predicting extinction. For all three cases, extinction occurs before $\bar{\tau}$ reaches a minimum, in the region where $\bar{\tau}$ is decreasing. As one sees from the case $\frac{\Gamma t_{ch}}{\pi r^2} = 0.01$, extinction occurs as $\bar{\tau}$ decreases below a critical value, approximately equal to $1000 t_{ch}$.

The data for $\frac{\Gamma t_{ch}}{\pi r^2} = 0.1$ and $\frac{\Gamma t_{ch}}{\pi r^2} = 1$ support this view, but with some qualification. The precise moment of extinction cannot be precisely determined. Even when the criterion for extinction is satisfied, the theory of the previous section says nothing about how long the process will take. Finally, the accuracy of $\bar{\tau}$ as an extinction criterion is expected to suffer as $\bar{\tau}$ changes more rapidly with time. These effects can all be seen by examining figures 8.1, 8.2, and 8.4.

To find a flame which does not go out, $\frac{\Gamma t_{ch}}{\pi r^2}$ was decreased again to a value of 0.001. The results for this case are also graphed in figures 8.1, 8.2, 8.3, and 8.4. One sees that the maximum flame temperature slowly decreases for a long while, but finally begins to increase again. One suspects that this flame will never go out. Indeed, the parameter $\bar{\tau}$ has reached a minimum and begun to grow. (One may verify from equation 8.15 that $\bar{\tau}$ will continue to increase as $t \to \infty$.) If extinction occurs when $\bar{\tau}$ drops below a critical value, $\bar{\tau}_{ext}$ (where $\bar{\tau}_{ext} \approx 1000 t_{ch}$), then this flame will never go out, since the minimum value of $\bar{\tau}$ is greater than the estimated $\bar{\tau}_{ext}$.

Another interesting feature of the solution for $\frac{\Gamma t_{ch}}{\pi r^2} = 0.001$ is the accuracy of equation 3.24b. The solid line and the dashed line are barely distinguishable in figure 8.1, indicating that the reactant consumption rate is almost exactly predicted by the Burke-Schumann approximation.

Before using $\bar{\tau}$ as a criterion for extinction, one should compare the $\bar{\tau}_{ext}$ observed in our numerical computations with the extinction strain rate for steady flames with a constant strain rate. Not only would the strain rate required for extinction be easier to measure in a steady flame, but the use of $\bar{\tau}$ is the result of an analogy between transiently strained flames and steadily strained flames. Thus, if the approximation is correct (recall that for a steady strained flame, $\bar{\tau} = \frac{1}{2\varepsilon}$), then the value of $\bar{\tau}_{ext}$ found from transiently strained flames should be approximately equal to $\frac{1}{2\varepsilon_{ext}}$, where ε_{ext} is the constant strain rate where extinction occurs for steadily strained flames.

Liñán has derived an equation which gives the extinction strain rate for steady strained flames, which was discussed in chapter three. Converting from the current notation into Liñán's,

$$\left[\frac{\bar{\tau}}{t_{ch}}\right]_{ext} = \frac{1}{2\varepsilon}\sqrt{2}k_0 e^{-\frac{T_a}{T_f}} = \frac{e^{-\frac{T_a}{T_f}}}{\sqrt{2}}\left[\frac{k_0}{\varepsilon}\right]_{ext} \qquad 8.17$$

Liñán has defined his Damköhler number as $\frac{k_0}{\varepsilon}$, so equation 3.27 can be used for the extinction Damköhler number to find $\left[\frac{\bar{\tau}}{t_{ch}}\right]_{ext}$. In Liñán's system of dimensionless temperature, the values chosen for this numerical example are $\hat{\Theta}_\infty = \frac{1}{7}$, $\hat{\Theta}_f = \frac{4.5}{7}$, and $\hat{\Theta}_a = \frac{45}{7}$. Substituting these values into equation 3.27 gives

$$\left[\frac{k_0}{\varepsilon}\right]_{ext} = 1.12\times10^{7} \qquad 8.18$$

and substituting this result into equation 8.17 yields

$$\left[\frac{\bar{\tau}}{t_{ch}}\right]_{ext} = 360 \qquad 8.19$$

This value is at least within an order of magnitude of the value of $\bar{\tau}_{ext} \approx 1000 t_{ch}$ found from the transiently strained flames.

8.4.3 Summary of Numerical Results

As a result of numerical BLOTTNER calculations, the instantaneous value of $\bar{\tau}$ is proposed as an approximate extinction criterion. It was necessary to assume that the flame had been ignited and allowed to develop for a time t_0 before the onset of straining. When the straining began at $t = 0$, the parameter $\bar{\tau}$ is equal to t_0. Thereafter, the parameter $\bar{\tau}$ is given by equation 8.16, which shows that $\bar{\tau}$ will decrease to a minimum and thereafter increase. If the minimum value reached by $\bar{\tau}$ is greater than the critical extinction value $\bar{\tau}_{ext}$, no extinction will occur, and the fuel consumption rate follows equation 3.24b for all time. On the other hand, if the transient value of $\bar{\tau}$ drops below $\bar{\tau}_{ext}$, extinction will occur.

For a fixed value of t_0, a range of different values of $\frac{\Gamma t_{ch}}{\pi r^2}$ were tried. If $\frac{\Gamma t_{ch}}{\pi r^2}$ were sufficiently small, the flame never went out, and equation 3.24b accurately predicted the fuel consumption rate. At a larger value of $\frac{\Gamma t_{ch}}{\pi r^2}$ (for a flame closer to the center of the vortex), the flame went out. For progressively larger values of $\frac{\Gamma t_{ch}}{\pi r^2}$, extinction occurred at earlier and earlier times, and the accuracy of the extinction criterion and prediction of the fuel consumption rate became worse.

These inaccuracies are not serious, because if one is interested in prediction of the extinct core radius, it is found from the value of $\frac{\Gamma t_{ch}}{\pi r^2}$ which separates the extinction from the nonextinction cases. Since the extinction criterion worked fairly well for the value of $\frac{\Gamma t_{ch}}{\pi r^2}$ which came closest to not going out, one should be able to predict the maximum extinct core radius fairly well. The worst performance of the approximation came at larger values of $\frac{\Gamma t_{ch}}{\pi r^2}$ where extinction occurred quickly, and as long as one is not interested in predicting the time delay until extinction, this defect is not important.

Thus, use the following model to describe flame behavior: Calculate $\bar{\tau}$ from equation 8.16. Thus, $\bar{\tau}$ will be a function of time which decreases to a minimum and then increases. For flames where the minimum value of $\bar{\tau}$ is greater than $\bar{\tau}_{ext}$, the flame does not go out and the fuel consumption rate $\dot{m}$ is found from equation 3.24b for all times. If the value of $\bar{\tau}$ drops below $\bar{\tau}_{ext}$, then the flame will go out, leaving unburned fuel and oxidizer. If the time at which $\bar{\tau} = \bar{\tau}_{ext}$ is denoted as t_{ext}, then the flame will be out for all $t > t_{ext}$. As an approximation to the fuel consumption rate, find $\dot{m}$ from equation 3.24b for $t < t_{ext}$, and set $\dot{m} = 0$ for $t > t_{ext}$. Note that reignition is not allowed; if $\bar{\tau}$ should fall below $\bar{\tau}_{ext}$ and then later rise to a value greater than $\bar{\tau}_{ext}$ the fuel consumption rate remains zero. (This is in deference to the S shaped curve discussed in chapter three.)

8.5 Application of Model to a Spiral Flame

Now, apply the model of large activation energy, strained, laminar diffusion flames to calculate the properties of a flame which is being strained by a vortex. The first property to be computed is the extinct core radius.

8.5.1 The Extinct Core and its Maximum Radius

According to the model, extinction occurs when the instantaneous value of $\bar{\tau}$ falls below $\bar{\tau}_{ext}$. By examining equation 8.16 for $\bar{\tau}$, one sees that, since t_0 and Γ are constants for a given problem, then for a fixed radius r, $\bar{\tau}$ is a function of time. As seen from the graphs of $\bar{\tau}$ versus time in figure 8.4, the function reaches a minimum value and then increases. For larger radii, the minimum value of $\bar{\tau}$ becomes larger, until eventually the minimum value of $\bar{\tau}$ is greater than the value required for extinction, $\bar{\tau}_{ext}$. Thus, a maximum radius for extinction may be calculated.

To simplify the calculations, and to allow analytical results, again take the large $\frac{\Gamma}{D_0}$ limit. This limit is taken in the same way as before; assuming that $\frac{\Gamma^{\frac{2}{3}} D_0^{\frac{1}{3}} t}{\pi r^2}$ is of order one. Additionally, the magnitude of t_0 is unknown, therefore do not exclude any terms containing t_0. Equation 8.16 for $\bar{\tau}$ becomes

$$\bar{\tau} \sim \frac{t_0 + \frac{1}{3}\left[\frac{\Gamma}{D_0}\right]\left[\frac{\Gamma^{\frac{2}{3}} D_0^{\frac{1}{3}} t}{\pi r^2}\right]^3}{\left[\frac{\Gamma}{D_0}\right]^{\frac{2}{3}}\left[\frac{\Gamma^{\frac{2}{3}} D_0^{\frac{1}{3}} t}{\pi r^2}\right]^2} \qquad 8.20$$

From equation 8.20, the time where $\bar{\tau}$ reaches its minimum value is

$$\frac{\Gamma t_{min}}{\pi r^2} \sim \left[6\frac{\Gamma t_0}{\pi r^2}\right]^3 \qquad 8.21$$

and the value of tau bar at this time is

$$\frac{\Gamma \bar{\tau}_{min}}{\pi r^2} \sim \frac{1}{2}\left[6\frac{\Gamma t_0}{\pi r^2}\right]^3 \qquad 8.22$$

According to the model, no extinction will occur if $\bar{\tau}_{min} > \bar{\tau}_{ext}$. Thus, no extinction will occur for radii larger than a critical radius, which one may call

$r_{ext\ max}$. The value of $r_{ext\ max}$ is found by substituting equation 8.22 for $\bar{\tau}_{min}$ into the inequality $\bar{\tau}_{min} > \bar{\tau}_{ext}$. The result is

$$\frac{\pi r_{ext\ max}^2}{\Gamma^{\frac{2}{3}} D_0^{\frac{1}{3}} t_0} \sim \sqrt{\frac{3}{4}} \left[\frac{\bar{\tau}_{ext}}{t_0} \right]^{\frac{3}{2}} \qquad 8.23$$

Thus, the extinction criterion will never be satisfied for large radii, such that $r > r_{ext\ max}$. On the other hand, for smaller radii, such that $r < r_{ext\ max}$, $\bar{\tau}$ will decrease to a minimum value which is less than $\bar{\tau}_{ext}$, so the extinction criterion will eventually be satisfied (at a time yet to be determined). Seemingly, there will always be an extinguished core, for all possible choices of Γ, D_0, t_0, and $\bar{\tau}_{ext}$. One sees that $r_{ext\ max}$ represents the maximum radius of the extinguished core.

8.5.2 The Extinct Core Radius as a Function of Time

For radii less than $r_{ext\ max}$, eventually $\bar{\tau}$ will drop below the critical extinction value $\bar{\tau}_{ext}$. The next objective is to calculate the time which elapses from the initiation of the vortex until extinction.

Find t_{ext} as the time when $\bar{\tau}$ equals $\bar{\tau}_{ext}$. If equation 8.20 were used for $\bar{\tau}$, one would find a cubic equation to solve for t_{ext}; one which would have two positive roots; one root where $\bar{\tau}$ decreases below the critical extinction value $\bar{\tau}_{ext}$, and another larger root where $\bar{\tau}$ increases above $\bar{\tau}_{ext}$. (This is true, of course, only for $r < r_{ext\ max}$. Larger radii never experience extinction, because if we set $\bar{\tau}$ equal to $\bar{\tau}_{ext}$, the resulting equation would have no real positive roots.)

Cubic equations can be solved in closed form, but instead, examine equation 8.20 and note that the numerator consists of two terms. As $\bar{\tau}$ descends to its minimum value, the first term dominates the second, thus

$$\bar{\tau} \approx \frac{t_0}{\left[\frac{\Gamma}{D_0}\right]^{\frac{2}{3}}\left[\frac{\Gamma^{\frac{2}{3}} D_0^{\frac{1}{3}} t}{\pi r^2}\right]^2} = \frac{t_0}{\left[\frac{\Gamma t}{\pi r^2}\right]^2} \qquad 8.24$$

Note that equation 8.24 approximates equation 8.20 only during the time when $\bar{\tau}$ is decreasing. From equation 8.20, $\bar{\tau}$ reaches a minimum and then increases; from equation 8.24, $\bar{\tau}$ decreases indefinitely. Thus, if one uses equation 8.24, one will find an extinction time for all radii. For radii greater than $r_{ext\ max}$, the result is meaningless and should be ignored.

Setting $\bar{\tau}$ from equation 8.24 equal to $\bar{\tau}_{ext}$ yields the following formula for the extinction time:

$$t_{ext} \approx \frac{t_0}{\bar{\tau}_{ext}} \frac{\pi r^2}{\Gamma} \qquad 8.25$$

Just as with the burned out core, equation 8.25 (which gives the time required for extinction as a function of radius) may be rewritten to yield an extinct core radius as a function of time.

$$r_{ext}^2 \approx \frac{\Gamma t}{\pi} \frac{\bar{\tau}_{ext}}{t_0} \qquad 8.26$$

The result will be valid only for radii less that $r_{ext\ max}$.

If $r_{ext\ max}$ is substituted into equation 8.25, the time required for the maximum radius extinct core to form will be found. It is

$$t_{ext\ max} \approx \sqrt{\frac{3}{4}} \sqrt{t_0 \bar{\tau}_{ext}} \qquad 8.27$$

Thus, one may view extinction either as sitting at a fixed radius which is less than $r_{ext\ max}$ and waiting for extinction, which occurs at t_{ext} (given by equation 8.25), or as an extinct core of unburned fuel and oxidizer, whose radius r_{ext} grows as the square root of time (given by equation 8.26) for times less than $t_{ext\ max}$. When the time is equal to $t_{ext\ max}$, the extinct core radius is

equal to $r_{ext\ max}$. This is the maximum radius of the extinct core, and it grows no larger.

8.5.3 The Burned Out Core

The proposed model for large activation energy, strained, laminar diffusion flames provides that the fuel consumption rate $\dot{m}$ is calculated from equation 3.24b until extinction occurs at t_{ext}. Recall the results of chapter four, where the flame at a fixed radius would consume all available fuel and go out at a time t^*.

No work has been done assessing the mutual interaction of exhaustion of fuel and extinction. For this reason, the phenomena will be considered independently. The previously found t_{ext} is valid only if the flame does not exhaust its fuel supply first. Shortly, t^* will be calculated, assuming that $\dot{m}$ is given by equation 3.24b until the fuel is exhausted. This result will not be valid if extinction occurs first, since equation 3.24b will no longer hold.

Thus, at a given radius, one will not observe both extinction and burnout, but whichever one occurs first. If $t_{ext} < t^*$, no burned out core will be seen, since the flame will be extinguished by high strain rates before the fuel is exhausted. If $t_{ext} > t^*$, the fuel will be exhausted before the flame is strained out.

The calculation of t^* has been discussed previously and will not be discussed in detail. The present calculation differs from that of chapter four in three respects: equation 3.24b is used exclusively rather than equations 3.24a and 3.24b; the value of $\bar{\tau}$ is found from equation 8.16 rather than from equation 4.7, and the flame has consumed some fuel during the time t_0 it burned with no straining. Repeating the previous calculation with these changes results in the following equation for t^*, valid in the limit as $\frac{\Gamma}{D_0} \rightarrow \infty$.

$$\frac{\Gamma^{\frac{2}{3}} D_0^{\frac{1}{3}} t^*}{\pi r^2} \sim \left[3 \left[\frac{\pi^2}{16} - \left[\frac{D_0}{\Gamma} \right]^{\frac{2}{3}} \frac{\Gamma^{\frac{2}{3}} D_0^{\frac{1}{3}} t_0}{\pi r^2} \right] \right]^{\frac{1}{3}} \qquad 8.28$$

Equation 8.28 does not yield a real positive value for t^* for certain radii. If equation 8.28 were interpreted as specifying a burned out core radius r^* as a function of time, one sees that r^* does not go to zero at $t = 0$, but is equal to $\frac{4}{\pi}\sqrt{t_0 \frac{D_0}{\pi}}$. This is the effect allowing the flame to burn for a time t_0 before starting the vortex, and explains why equation 8.28 does not yield a burnout time for lesser radii.

8.5.4 Burnout or Extinction?

Compare t_{ext} from equation 8.25 and t^* from equation 8.28. Find the smaller of the two. Rewrite equation 8.25 as

$$\frac{\Gamma^{\frac{2}{3}} D_0^{\frac{1}{3}} t_{ext}}{\pi r^2} \sim \frac{t_0}{\bar{\tau}_{ext}} \left[\frac{\Gamma}{D_0} \right]^{\frac{1}{3}} \qquad 8.29$$

From equation 8.28, one sees that

$$\frac{\Gamma^{\frac{2}{3}} D_0^{\frac{1}{3}} t^*}{\pi r^2} > \left[\frac{3\pi^2}{16} \right]^{\frac{1}{3}} \qquad 8.30$$

From equations 8.29 and 8.30, one can guarantee that $t^* > t_{ext}$ at all radii, provided that

$$\left[\frac{3\pi^2}{16} \right]^{\frac{1}{3}} > \frac{t_0}{\bar{\tau}_{ext}} \left[\frac{D_0}{\Gamma} \right]^{\frac{1}{3}} \qquad 8.31$$

Therefore, if the condition expressed by equation 8.31 is met, extinction will never be observed at any radius (even those less than $r_{ext\ max}$) because exhaustion of fuel will occur before extinction does.

When this inequality is not satisfied, then t^* occurs before t_{ext} for small

radii, and t_{ext} occurs before t^* for larger radii. The limiting radius may be found by setting t^* from equation 8.28 equal to t_{ext} from equation 8.29. The result is that for radii such that

$$\frac{\pi r^2}{\Gamma^{\frac{2}{3}} D_0^{\frac{1}{3}} t_0} < \frac{\left[\frac{D_0}{\Gamma}\right]^{\frac{2}{3}}}{\frac{\pi^2}{16} - \frac{1}{3}\frac{D_0}{\Gamma}\left[\frac{t_0}{\bar{\tau}_{ext}}\right]^3} \qquad 8.32$$

burnout from exhaustion of fuel will occur before extinction. For large radii which do not satisfy inequality 8.32, extinction will occur before burnout. (This is true only for radii less than $r_{ext\ max}$.)

Thus, just as equation 8.23 for $r_{ext\ max}$ specifies a maximum radius for the burned out core, equation 8.32 specifies a minimum radius. The result will be an annular region in which the flame has been strained out. The inner core is an artifact of the initial period t_0, when the flame burned with no straining. Indeed, equation 8.32 shows that the radius of this inner region will be of order $\left[\frac{D_0}{\Gamma}\right]^{\frac{2}{3}}$. If one thinks to secure a more stringent limitation than equation 8.31 for the occurrence of extinction by requiring that the outer extinction radius from equation 8.23 be larger than the inner radius from equation 8.32, one finds that for the outer radius to be less than the inner radius, either the assumption that $\frac{\Gamma}{D_0}$ is large must be violated, or else the denominator of the right side of equation 8.32 must be nearly zero. Since these formulae have been derived assuming large $\frac{\Gamma}{D_0}$, one cannot use these formulae otherwise. If the denominator of the right side of equation 8.32 is set to zero, one recovers equation 8.31. Thus, the inner radius will be smaller than the outer radius.

8.6 Summary

The calculation will be discontinued at this point, for reasons to be explained. To summarize the results so far, a model of large activation energy, strained, laminar diffusion flames has been proposed. According to the model, until extinction the fuel consumption rate is calculated from the Burke-Schumann solution, equation 3.24b. The onset of extinction is predicted by the transient Damköhler number, which is the parameter $\bar{\tau}$ divided by a characteristic chemical time.

To verify the proposed model, numerical calculations were performed using BLOTTNER. One important result was the necessity for appropriate initial conditions. If one tries to solve the problem of a vortex initiated at the same time as the reactants are brought together, then the initial conditions would be those used in chapter four, a semi-infinite region of fuel in contact with a semi-infinite region of oxidizer, with no product present or any region of elevated temperature. For large activation energy reactions, both numerical computation and practical experience show that the reactants simply diffuse into one another with negligible reaction. (For a contrary view, see the paper by Lina'n and Crespo (1976), and the discussion in chapter three.) Diffusion flames are possible with hydrocarbon fuels and air, therefore there must be some mechanism for establishing the flame on the strongly burning solution branch.

Various possibilities were discussed in chapter three. One suggestion was the formation of a region of premixed fuel and oxidizer as the two diffused into one another, which would then be burned by a premixed flame propagating along the flame sheet from a region where ignition had already occurred. This possiblity is attractive, but would violate the assumption that flames behave as if they were one-dimensional. In addition, to explain some observed phenomena (discussed in chapter three), such as the lifting of a diffusion flame from a

splitter plate, would require knowledge of how rapidly premixed flames propagate in thin fuel-oxidzer layers.

Another possibility lies in the conditions at the trailing edge of the splitter plate. If the diffusion flame does not have a zero thickness as it leaves the trailing edge, but instead has a thickness δ_0, then the initial Damköhler number would be $\frac{\delta_0^2}{D_0 t_{ch}}$. Thus, the flame would be established on the strongly burning branch of solutions. It is this situation which comes closest to the initial condition actually used here for numerical calculations. Initial concentration and velocity profiles were specified which correspond to a flame which was already ignited and allowed to develop for a time t_0. Thus, when the vortex straining was imposed, the flame had an initial Damköhler number of $\frac{t_0}{t_{ch}}$. Unfortunately, the results were dependent on the value of t_0 chosen; a flame with a larger initial value of t_0 would more resistant to straining out.

The first result was the maximum extinct core radius $r_{ext\ max}$, given by equation 8.23. This result showed that for every choice of the parameters t_0, $\bar{\tau}_{ext}$, and Γ, extinction would be observed. For radii less than $r_{ext\ max}$, the transient Damköhler number $\bar{\tau}$ would eventually fall below the critical extinction value $\bar{\tau}_{ext}$.

An approximate formula, equation 8.25, was derived which predicted the time required for extinction to occur. Interpreting the result as an extinct core, growing in time, one sees that the radius of the extinct core would grow as the square root of time, until the maximum radius $r_{ext\ max}$ is reached.

Calculation of the burned out core radius, as in chapter four, modifies the earlier conclusion that extinction would always be observed. If the time required for extinction is compared to the time required for burnout, no

extinction will be seen unless it occurs before burnout. Thus the more stringent requirement, expressed by equation 8.31, that extinction will never be observed at any radius as long as $\frac{t_0}{\bar{\tau}_{ext}}\left[\frac{D_0}{\Gamma}\right]^{\frac{1}{3}}$ is less than $\left[\frac{3\pi^2}{16}\right]^{\frac{1}{3}}$. When this requirement is not met, extinction will be seen in an annulus whose outer radius is $r_{ext\ max}$, and whose inner radius is given by equation 8.32. (Note that the inner core of combustion products is an artifact of the time t_0 the flame burned with no straining, and in any case the radius of this inner core is small, of order $\left[\frac{D_0}{\Gamma}\right]^{\frac{2}{3}}$ compared to the outer radius.) The time required for this structure to form is $t_{ext\ max}$, and is given by equation 8.27.

Once the annulus of strained out flames has formed, the calculation cannot be continued. Ignorance of the ignition process was circumvented by assuming an initial flame which was already lit, but the question of the eventual reignition of strained out flames cannot be avoided. The transient Damköhler number $\bar{\tau}$ decreases to a minimum and then increases, behaving like $\frac{t}{3}$ for large times. Thus, flames which were strained out could become relit by contact with adjacent flames which were not extinguished.

In addition, consider two adjacent flames. If they were strongly burning, burnout due to exhaustion of fuel is equivalent to saying that the thickness of an individual flame, δ, is comparable to the interflame distance Δ. If the flames are extinct due to excessive strain rates, δ will still eventually exceed Δ. In this case, unburned fuel and oxidizer will still be present, and they will merge to form a homogenous combustible mixture. So, not only would one have to deal with the possible reignition of diffusion flames, but premixed flames are also a possibility.

The inclusion of either of these effects is beyond the present analysis. Current knowledge of diffusion flames does not adequately describe the ignition process. In addition, this analysis is based on treating each piece of the flame independently as a one dimensional strained flame. Allowing one piece of flame to be ignited by its neighbors, or for adjacent flames to merge, forming a mixture capable of supporting premixed flames, would undermine the basic assumptions of the analysis. Even if the physical processes could be adequately modeled, they would be difficult to incorporate into the analysis.

9. REFERENCES

Barker, C. L., (1958), Experiments Concerning the Occurrence and Mechanism of High-Frequency Combustion Instability, *Ph.D. Thesis*, California Institute of Technology.

Blottner, F. G., (1970), Finite-Difference Methods of Solution of the Boundary-Layer Equations, *AIAA Journal*, **8**, 193-205.

Blottner, F.G., M. Johnson, and M. Ellis, (1971), Chemically Reacting Viscous Flow Program for Multi-Component Gas Mixtures, *Sandia Laboratories Report SC-RR-70-754.*

Burke, S. P. and T. E. W. Schumann, (1928), Diffusion Flames, *Industrial and Engineeering Chemistry*, **120**, 998-1004.

Bush, W. B., P. S. Feldman, and F. E. Fendell, (1976), On Diffusion Flames in Turbulent Shear Flows: Modeling Reactant Consumption in a Mixing Layer, *Combustion Science and Technology*, **13**, 27-54.

Bush, W. B. and F. E. Fendell, (1974), On Diffusion Flames in Turbulent Shear Flows, *Acta Astronautica*, 1, 645-666.

Carrier, G. F., F. E. Fendell, and F. E. Marble, (1975), The Effect of Strain Rate on Diffusion Flames, *SIAM Journal of Applied Mathematics*, **28**, 463-500.

Chung, P. M. and V. D. Blankenship, (1966), Equilibrium Structure of Thin Diffusion Flame Zone, *The Physics of Fluids*, **9**, 1569-1577.

Chung, P. M., F. E. Fendell, and J. F. Holt, (1966), Nonequilibrium Anomalies in the Development of Diffusion Flames, *AIAA Journal*, **4**, 1020-1026.

Clarke, J. F., (1967), The laminar diffusion flame behind a blunt body- A constant-pressure Oseen-flow model, *Journal of the Institute of Mathematics and its Applications*, **3**, 347-361.

Clarke, J. F., (1968), On the structure of a hydrogen-oxygen diffusion flame, *Proceedings of the Royal Society A*, **307**, 283-302.

Clarke, J. F., (1969), Reaction broadening in a hydrogen-oxygen diffusion flame, *Proceedings of the Royal Society A*, **312**, 65-83.

Clarke, J. F. and J. B. Moss, (1969), The effect of the large hydrogen dissociation activation energy on an equilibrium-broadened hydrogen-oxygen diffusion flame, *Proceedings of the Royal Society A*, **313**, 433-443.

Cohen. N., (1977), A Review of Rate Coefficients in the $H_2 - F_2$ Chemical Laser System - Supplement (1977), *Aerospace report SAMSO-TR-78-41.*

Cummings, J. C., J. E. Broadwell, W. L. Shackleford, A. B. Witte, J. E. Trost, and G. Emanuel, (1977), $H_2 - F_2$ Chain Reaction Rate Investigation, *Journal of Quantitative Spectroscopic Radiative Transfer*, **17**, 97-116.

Damköhler, G., (1939), Effect of Turbulence on Flame Velocity in Gas Mixtures, *Report of the Hermann Goering Aeronautical Research Institute*, **II**, 3-21, (English Translation: G. A. Awater, *National Research Council of Canada Technical Translation*, TT-10, (1948)).

Damköhler, G., (1940), The Effect of Turbulence on the Flame Velocity in Gas Mixtures, *Zeitschrift für Elektrochemie und angewandte Physikalische Chemie*, **46**, (English Translation: J. Vanier, *NACA TM-1112*, (1947)).

Emanuel, G., N. Cohen, and T. A. Jacobs, (1973), Theoretical Performance of an HF Chemical CW Laser, *Journal of Quantitative Spectroscopy and Radiative Transfer*, **13**, pp. 1365-1393.

Fendell, F. E., (1965), Ignition and Extinction in Combustion of Initially Unmixed Reactants, *Journal of Fluid Mechanics*, **21**, 281-303.

Fendell, F. E., (1967), Combustion in Initially Unmixed Reactants for One-Step Reversible Chemical Kinetics, *Astronautica Acta*, **13**, 183-191.

Friedlander, S. K. and K. H. Keller, (1963), The Structure of the Zone of Diffusion Controlled Reaction, *Chemical Enginering Science*, **18**, 305-375.

Feng, C. C. and J. S. T'ien, (1978), Transient Extinction History of a Solid Fuel Diffusion Flame, *Combustion Science and Technology*, **18**, 119-126.

Hahn, W. A. and J. O. L. Wendt, (1981a), NO_x Formation in Flat, Laminar, Opposed Jet Methane Diffusion Flames, *Eighteenth Symposium (International) on Combustion*, 121-131.

Hahn, W. A. and J. O. L. Wendt, (1981b), The Flat Laminar Opposed Jet Diffusion Flame: A Novel Tool for Kinetic Studies of Trace Species Formation, *Chemical Engineering Communications*, **9**, 121-136.

Hahn, W. A., (1979), Pollutant Formation in Flat Laminar Opposed Jet Diffusion Flames, *Ph.D. Thesis*, University of Arizona.

Jain, V. K. and H. S. Mukunda, (1968), On the Ignition and Extinction Problems in Forced Convection Systems, *International Journal of Heat and Mass Transfer*, 11, 491-508.

Jain, V. K. and H. S. Mukunda, (1969), The Extinction Problem in an Opposed Jet Diffusion Flame with Competitive Reactions, *Combustion Science and Technology*, 1, 105-117.

Jarosin'ski, J. and S. Wo'jcicki, (1976), The Mechanism of Interaction between a Combustion Region and Acoustic Resonator, *Acta Astronautica*, **3**, 567-572.

Karagozian, A. R., (1982), An Analytical Study of Diffusion Flames in Vortex Structures, *Ph.D. Thesis*, California Institute of Technology.

Karlovitz, B., D. W. Denniston Jr., and F. E. Wells, (1951), Investigation of Turbulent Flames, *Journal of Chemical Physics*, **19**, 541-547.

Kent, J. H. and F. A. Williams, (1974), Extinction of Laminar Diffusion Flames for Liquid Fuels, *Fifteenth Symposium (International) on Combustion*, 315-325.

Kirkby, L. L. and R. A. Schmitz, (1966), An Analytical Study of the Stability of a Laminar Diffusion Flame, *Combustion and Flame*, **10**, 205-220.

Krishnamurthy, L., (1975), Diffusion-Flame Extinction in the Stagnation-Point Boundary Layer of PMMA in O_2/N_2 Mixtures, *Combustion Science and Technology*, **10**, 21-25.

Krishnamurty, L., F. A. Williams, and K. Seshadri, (1976), Asymptotic Theory of Diffusion-Flame Extinction in the Stagnation-Point Boundary Layer, *Combustion and Flame*, **26**, 363-377.

Lighthill, M. J., (1978), *Waves in Fluids*, Cambridge University Press, Cambridge, 17-23.

Liñ a'n, A., (1963), On the Structure of Laminar Diffusion Flames, *Engineer's Thesis*, California Institute of Technology.

Liñan, A., (1974), The Asymptotic Structure of Counterflow Diffusion Flames for Large Activation Energies, *Acta Astronautica*, **1**, 1007-1039.

Liñan, A. and A. Crespo, (1976), An Asymptotic Analysis of Unsteady Diffusion Flames for Large Activation Energies, *Combustion Science and Technology*, **14**, 95-117.

Liu, T. M. and P. A. Libby, (1970), Boundary Layer at a Stagnation Point with Hydrogen Injection, *Combustion Science and Technology*, **2**, 131-144.

Marathe, A. G. and V. K. Jain, (1972), Some Studies on Opposed-Jet Diffusion Flame Considering General Lewis Numbers, *Combustion Science and Technology*, **6**, 151-157.

Marathe, A. G., H. S. Mukunda, and V. K. Jain, (1977), Some Studies on Hydrogen-Oxygen Diffusion Flame, *Combustion Science and Technology*, **15**, 49-64.

Marble, F. E., J. E. Broadwell, O. P. Norton, and M. V. Subbaiah, (1979), The Turbulent Chemical Reaction of a Hydrogen Jet Discharged into Fluorine, (Appears in: H. W. Liepmann, G. L. Brown, P. E. Dimotakis, F. E. Marble, A. Roshko, and P. G. Saffman, Chemical Reactions in Turbulent Mixing, *GALCIT report 151, AFOSR Contract No. F44620-76-C-0046*, (1979)).

Marble, F. E. and J. E. Broadwell, (1977), The Coherent Flame Model for Turbulent Chemical Reactions, *Project SQUID Technical Report*, TRW-9-PU.

Marble, F. E., (1979), Dynamics of Reacting Gases, *unpublished lecture notes*.

Marble, F. E., (1982), Growth of a Diffusion Flame in the Field of a Vortex, to appear in *Luigi Crocco Anniversary Volume*.

Melvin, A., J. B. Moss, and J. F. Clarke, (1971), The Structure of a Reaction-Broadened Diffusion Flame, *Combustion Science and Technology*, **4**, 17-30.

Phillips, H., (1964), Flame in a Buoyant Methane Layer, *Tenth Symposium (International) on Combustion*, 1277-1283.

Potter, A. E., S. Heimel, and J. N. Butler, (1960), Apparent Flame Strength, A Measure of Maximum Reaction Rate in Diffusion Flames, *Eighth Symposium (International) on Combustion*, 1027-1034.

Rogers, D. E., (1954), An Experimental Investigation of High-Frequency Combustion Instability in a Fuel-Air Combustor, *Engineer's Thesis*, California Institute of Technology.

Rogers, D. E. and F. E. Marble, (1956), A Mechanism for High Frequency Oscillation in Ramjet Combustors and Afterburners, *Jet Propulsion*, **26**, 456-462.

Schmitz, R. A., (1967), A Further Study of Diffusion Flame Stability, *Combustion and Flame*, **11**, 49-62.

Scurlock, A. C. and J. H. Grover, (1952), Propagation of Turbulent Flames, *Fourth Symposium (International) on Combustion*, 645-658.

Seshadri, K., (1978), Structure and Extinction of Laminar Diffusion Flames Above Condensed Fuels with Water and Nitrogen, *Combustion and Flame*, **33**, 197-215.

Shelkin, K. I., (1943), On Combustion in a Turbulent Flow, *Zhurnal Tekhnicheskoi Fiziki*, **13**, 520-530, (English Translation: S. Reiss, *NACA TM-1110*, (1947)).

Spalding, D. B., (1954), A Theory of the Extinction of Diffusion Flames, *Fuel*, **33**, 255-273.

T'ien, J. S., S. N. Singhal, D. P. Harrold, and J. M. Prahl, (1978), Combustion and Extinction in the Stagnation-Point Boundary Layer, *Combustion and Flame*, **33**, 55-68.

Tsuji, H. and I. Yamaoka, (1968), The Structure of Counterflow Diffusion Flames in the Forward Stagnation Region of a Porous Cylinder, *Twelfth Symposium (International) on Combustion*, 997-1005.

Williams, F. A., (1965), *Combustion Theory, The Fundamental Theory of Chemically Reacting Flow Systems*, Addison-Wesley, Reading, Massachusetts.

Williams, F. A., (1971), Theory of Combustion in Laminar Flows, *Annual Review of Fluid Mechanics*, M. Van Dyke, W. G. Vincenti, and J. V. Wehausen editors, **3**, 171-188.

Zeldovitch, Y. B., (1949), On the Theory of Combustion of Initially Unmixed Gases, *Zhurnal Tekhnicheskoi Fiziki*, **19**, 1199-1210, (English Translation: S. Reiss, *NACA TM 1296*, (1951)).

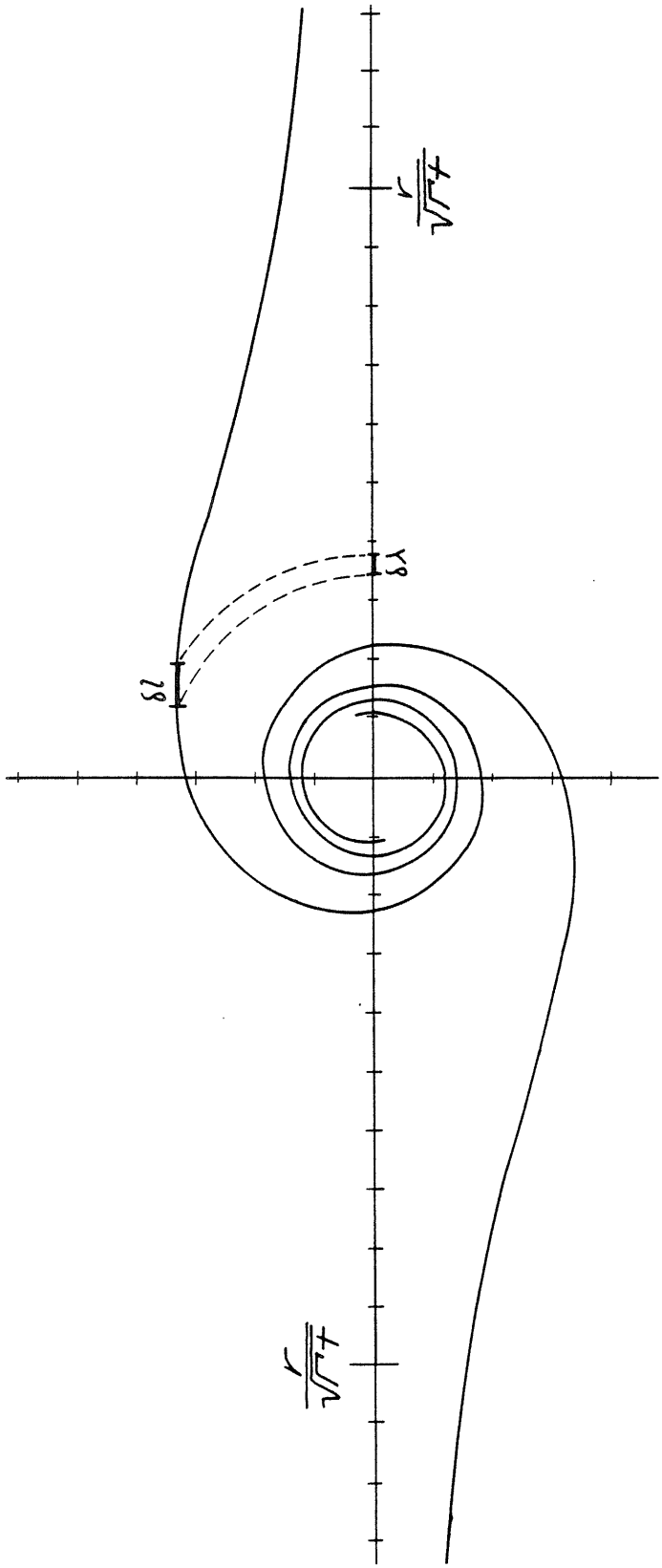

Figure 2.1 An initially flat flame has been wound into a spiral by a vortex; in this case the vortex is located on the flame sheet. Locally, a piece of the flame initially of length $\delta\lambda$ has been elongated to length δl. Note the similarity present in the vortex structure, the vortex grows with time as $\sqrt{\nu t}$.

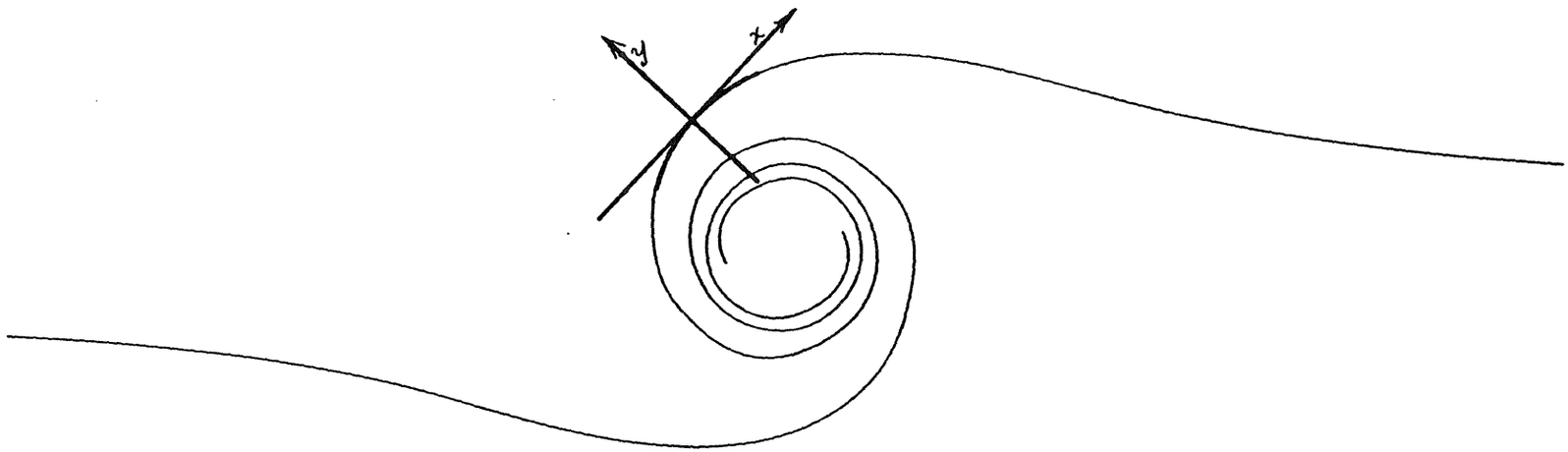

Figure 2.2 At each point on the flame, a local (x,y) coordinate system is constructed. The origin is translated with the local fluid velocity, and rotated so the x axis remains tangent to the flame. In this coordinate system, the flame will be treated as a one-dimensional, flat, transiently strained laminar diffusion flame.

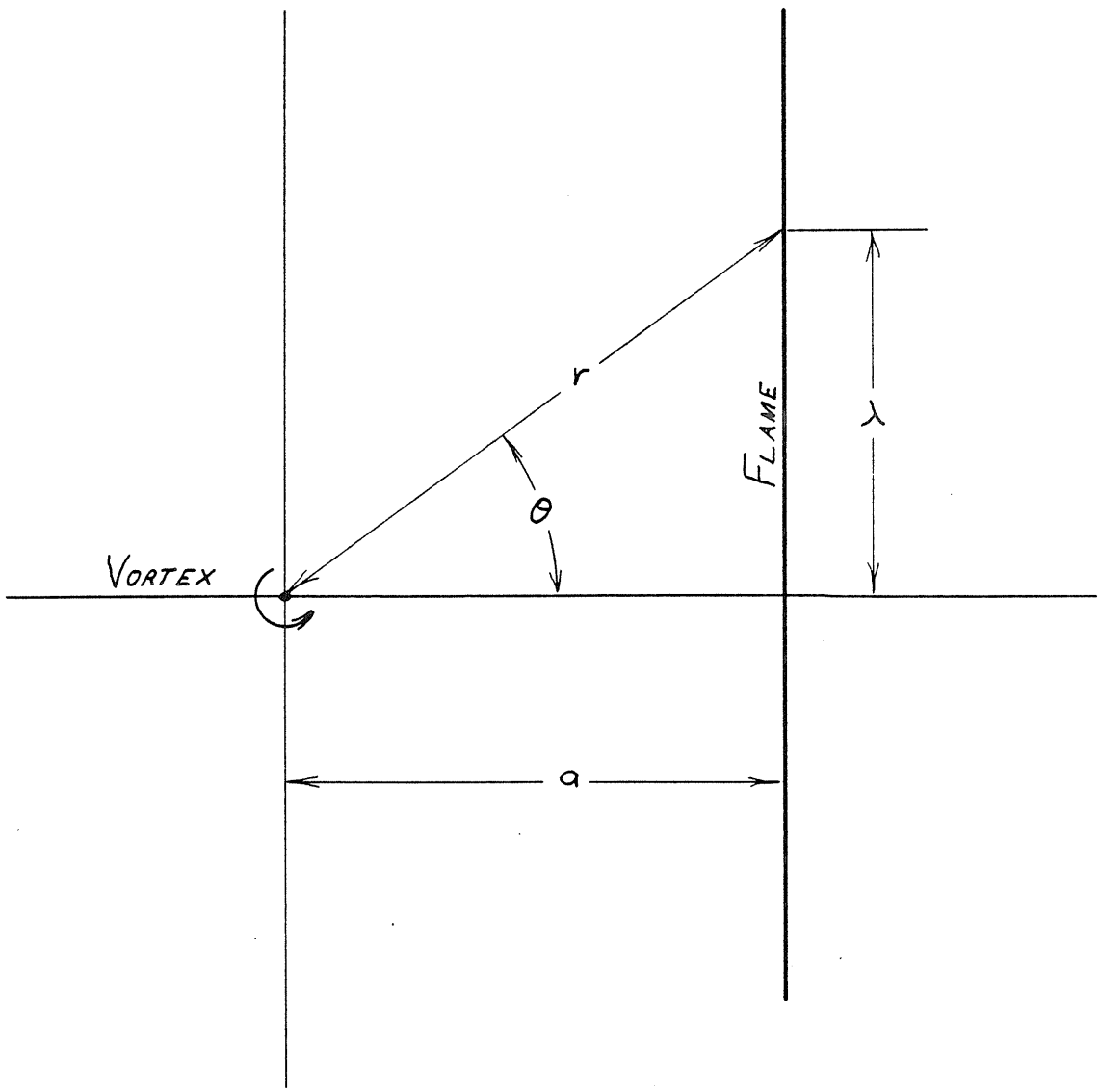

Figure 2.3 The vortex is located at the origin. An initially flat flame is displaced a distance a from the vortex. A given piece of the flame is identified by specifying a value of λ.

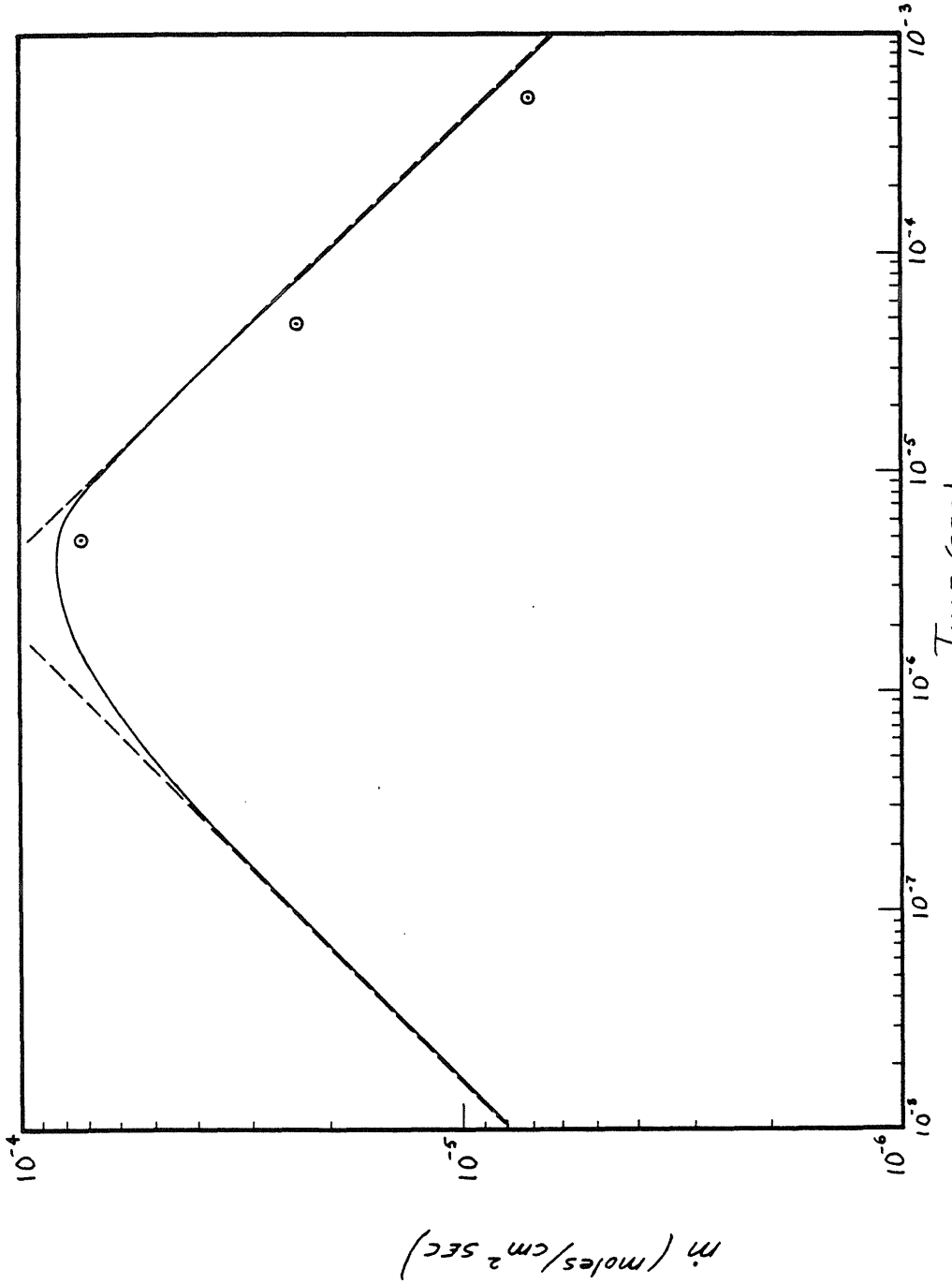

Figure 4.1 Specific fuel consumption rate $\dot{m}$ for an unstrained $H_2 + F$ flame as a function of time (solid line), and steady, constant strain flames (discrete points, with $t = 1/2\varepsilon$).

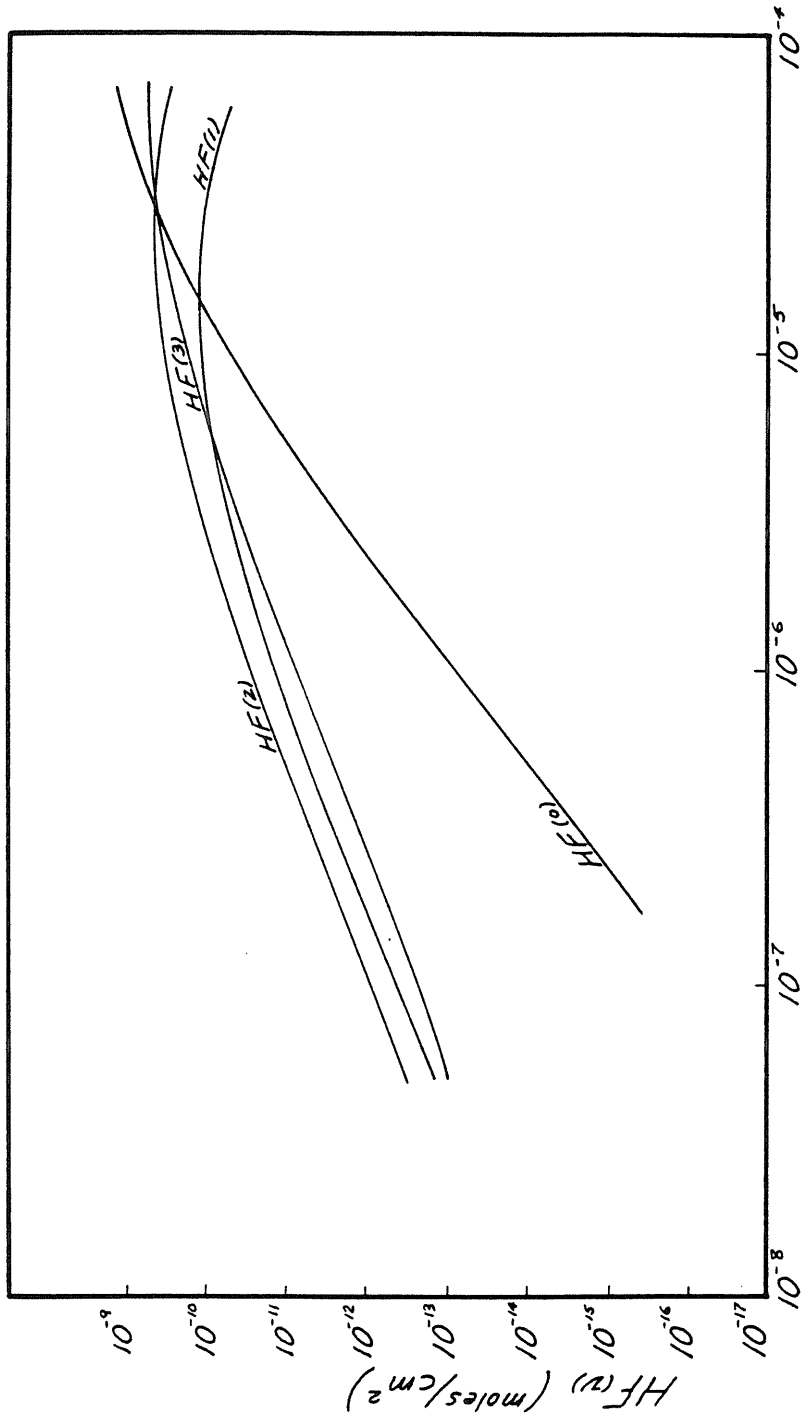

Figure 4.2 Surface density of the different excited states, $HF(j)$, as a function of time for the unstrained $H_2 + F$ flame.

	F_o	F_1	F_2	G_o	G_1	G_2
$F + H_2 \rightarrow HF^1 + H$	2.70×10^{13}	0.8051	0.0	9.78×10^{12}	10.97	0.152
$F + H_2 \rightarrow HF^2 + H$	8.85×10^{13}	0.8051	0.0	3.22×10^{13}	5.535	0.152
$F + H_2 \rightarrow HF^3 + H$	4.30×10^{13}	0.8051	0.0	1.55×10^{13}	0.3044	0.152
$HF^3 + M \rightarrow HF^2 + M$	3.00×10^{14}	0.0	-0.800	3.00×10^{14}	5.211	-0.800
$HF^2 + M \rightarrow HF^1 + M$	2.00×10^{14}	0.0	-0.800	2.00×10^{14}	5.452	-0.800
$HF^1 + M \rightarrow HF^0 + M$	1.00×10^{14}	0.0	-0.800	1.00×10^{14}	5.700	-0.800
$HF^1 + H \rightarrow HF^0 + H$	9.10×10^{13}	0.5898	-0.275	9.10×10^{13}	6.290	-0.275
$HF^2 + H \rightarrow HF^1 + H$	4.36×10^{12}	0.3633	0.201	4.36×10^{12}	5.816	0.201
$HF^2 + H \rightarrow HF^0 + H$	4.26×10^{13}	0.4509	-0.084	4.26×10^{13}	11.60	-0.084
$HF^3 + H \rightarrow HF^2 + H$	3.71×10^{13}	0.4474	-0.090	3.71×10^{13}	5.695	-0.090
$HF^3 + H \rightarrow HF^1 + H$	2.82×10^{13}	0.3397	-0.078	2.82×10^{13}	11.00	-0.078
$HF^3 + H \rightarrow HF^0 + H$	3.88×10^{13}	0.3829	-0.063	3.88×10^{13}	16.75	-0.063
$HF^3 + H_2 \rightarrow HF^2 + H_2$	2.90×10^{8}	0.7714	1.500	1.45×10^{7}	0.000	1.500
$HF^2 + H_2 \rightarrow HF^1 + H_2$	2.00×10^{8}	0.5304	1.500	1.00×10^{7}	0.000	1.500
$HF^1 + H_2 \rightarrow HF^0 + H_2$	1.50×10^{8}	0.2828	1.500	7.50×10^{6}	0.000	1.500
$HF^3 + F \rightarrow HF^2 + F$	1.50×10^{10}	0.5535	1.000	1.50×10^{10}	5.765	1.000
$HF^2 + F \rightarrow HF^1 + F$	1.50×10^{10}	0.5535	1.000	1.50×10^{10}	6.006	1.000
$HF^1 + F \rightarrow HF^0 + F$	1.50×10^{10}	0.5535	1.000	1.50×10^{10}	6.253	1.000

M Includes HF^0, HF^1, HF^2, and HF^3

Table 4.1 The $H_2 + F$ reaction system.

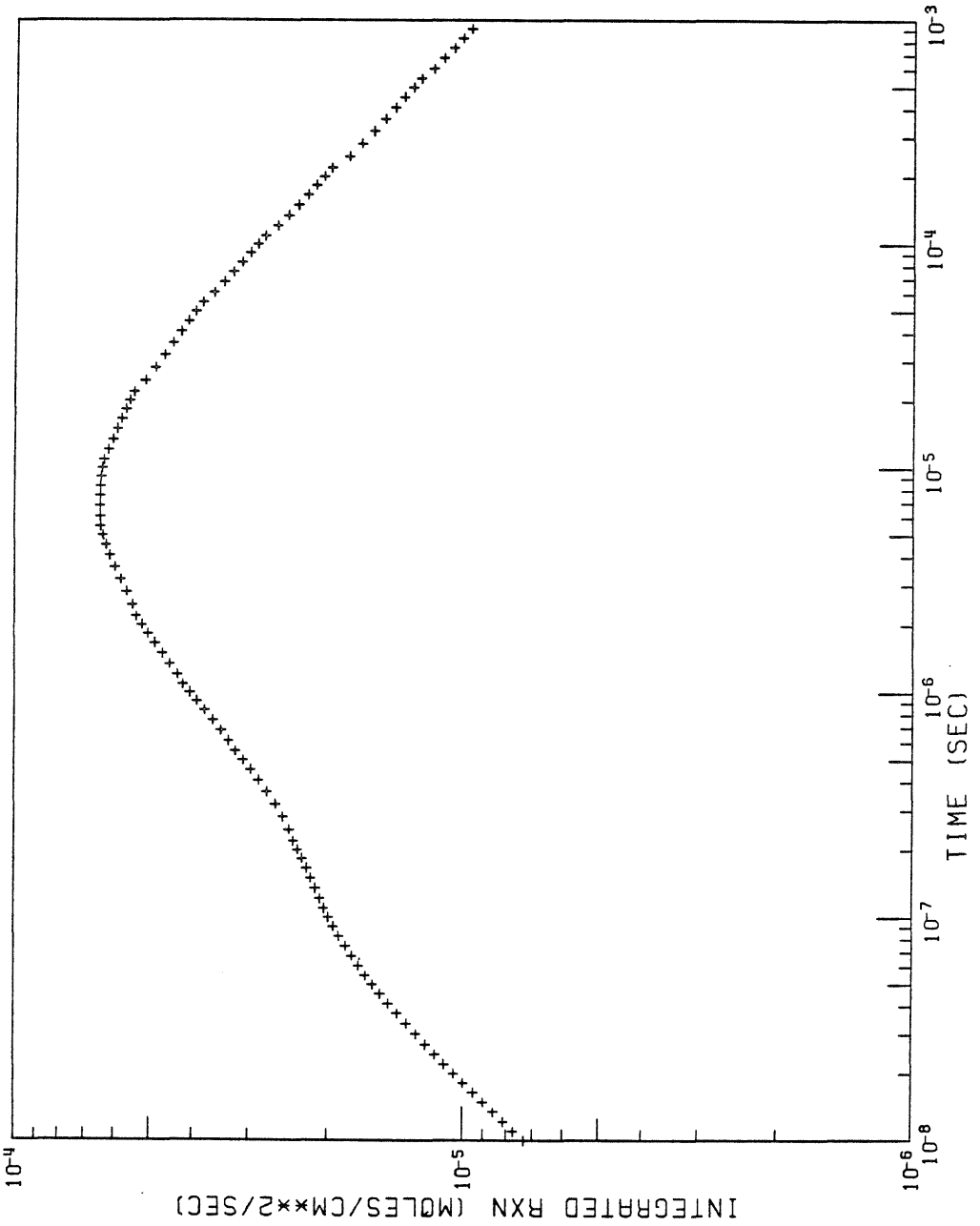

Figure 4.3 Specific fuel consumption rate $\dot{m}$ for a transiently strained $H_2 + F$ flame as a function of time. The transient strain rate is given by equation 2.13. Here, the parameter $\Gamma/\pi r^2 = 10^7\ sec^{-1}$.

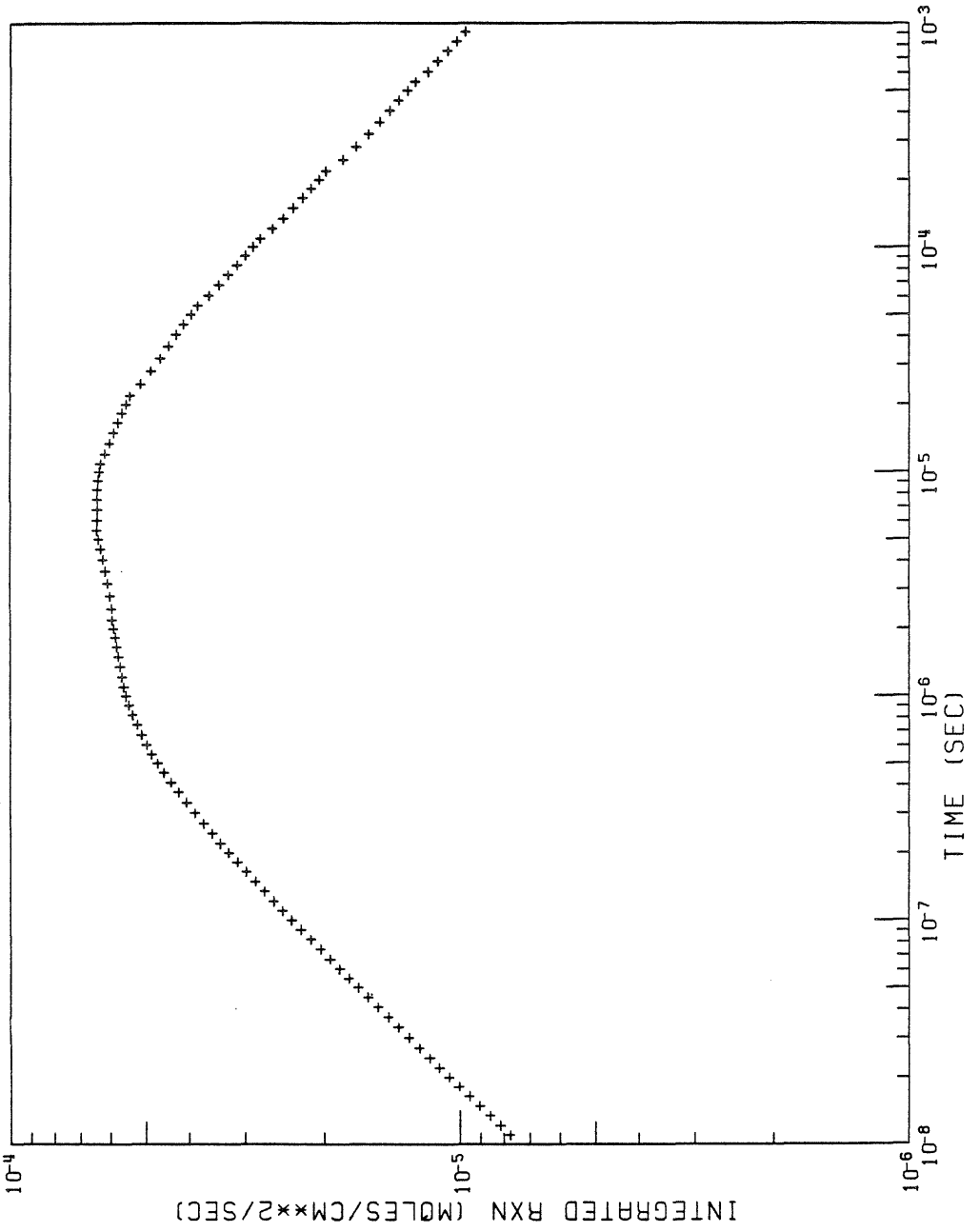

Figure 4.4 Specific fuel consumption rate $\dot{m}$ for a transiently strained $H_2 + F$ flame as a function of time. The transient strain rate is given by equation 2.13. Here, the parameter $\Gamma/\pi r^2 = 10^6\ sec^{-1}$.

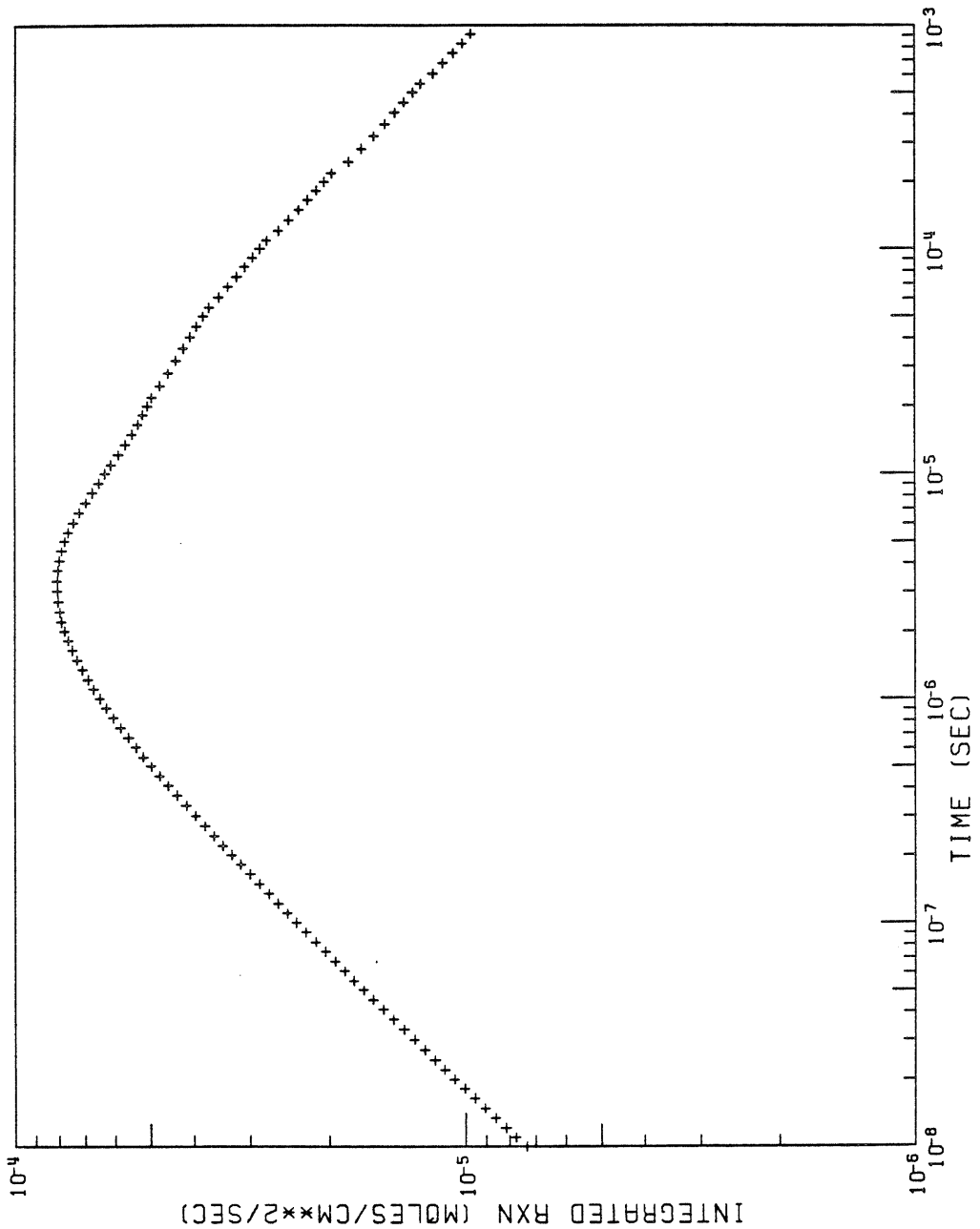

Figure 4.5 Specific fuel consumption rate $\dot{m}$ for a transiently strained $H_2 + F$ flame as a function of time. The transient strain rate is given by equation 2.13. Here, the parameter $\Gamma/\pi r^2 = 10^5\ sec^{-1}$.

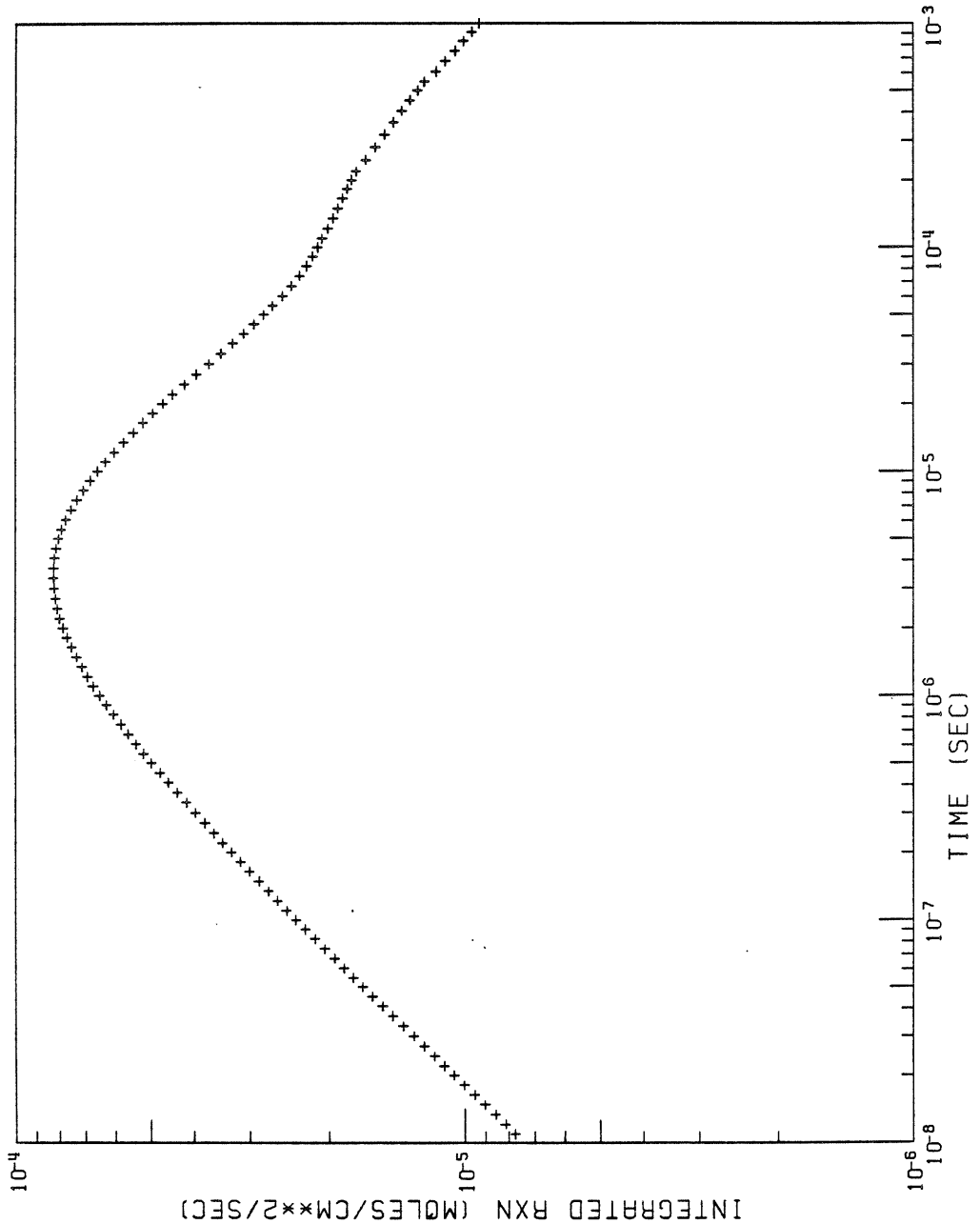

Figure 4.6 Specific fuel consumption rate $\dot{m}$ for a transiently strained $H_2 + F$ flame as a function of time. The transient strain rate is given by equation 2.13. Here, the parameter $\Gamma/\pi r^2 = 10^4\ sec^{-1}$.

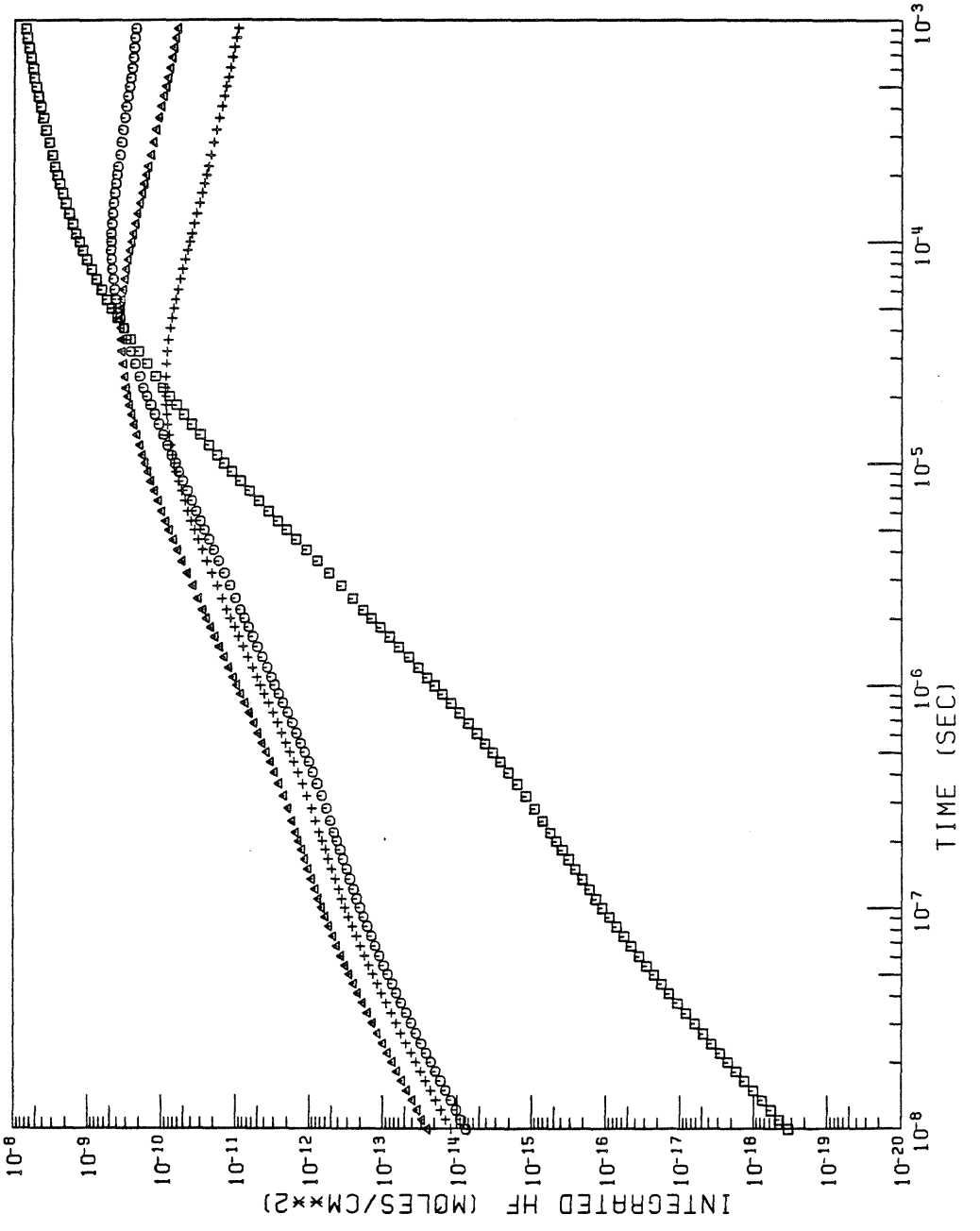

Figure 4.7 Surface density of the different excited states, $HF(j)$, as a function of time for a transiently strained $H_2 + F$ flame. The transient strain rate is given by equation 2.13. Here, the parameter $\Gamma/\pi r^2 = 10^7\ sec^{-1}$.

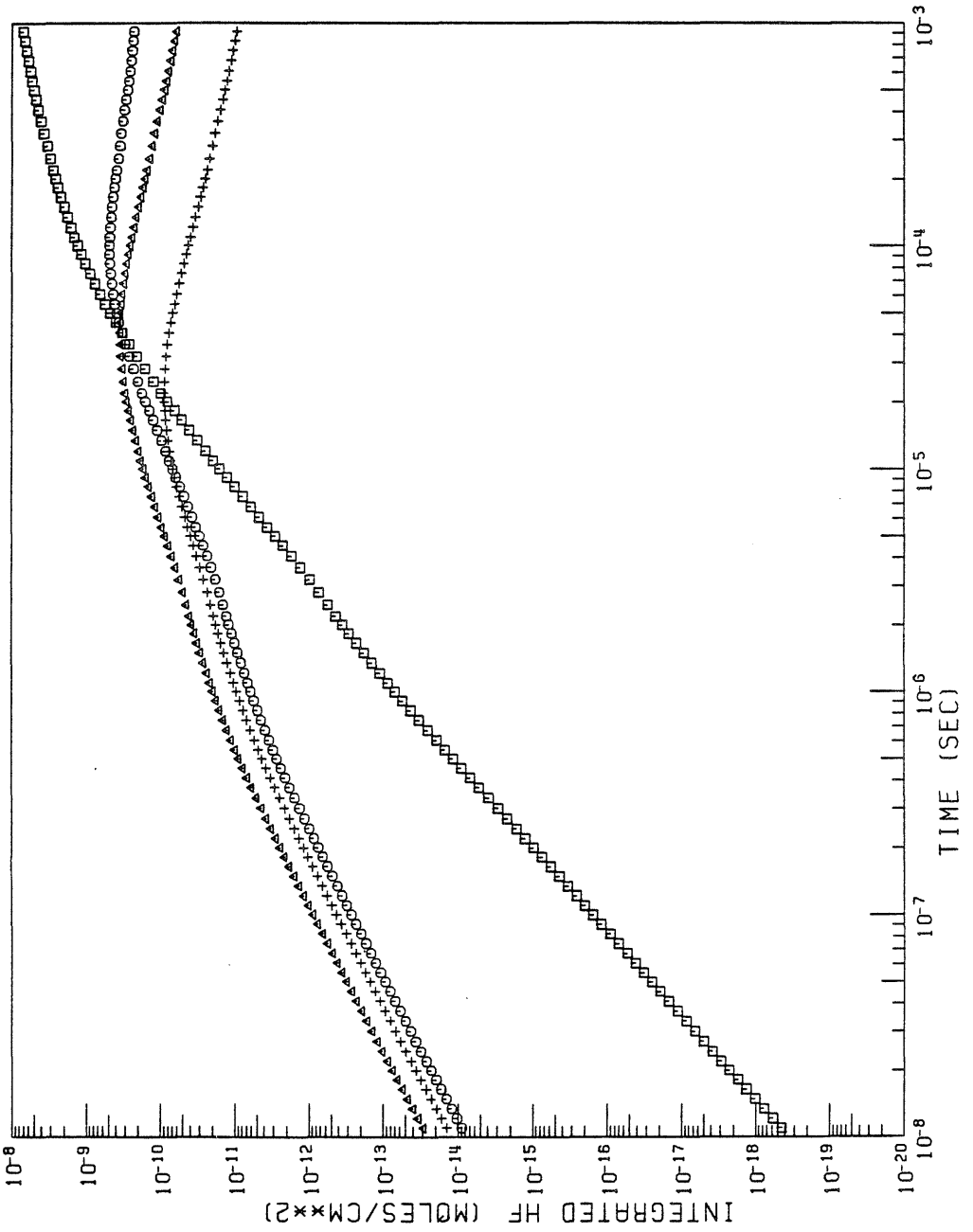

Figure 4.8 Surface density of the different excited states, $HF(j)$, as a function of time for a transiently strained $H_2 + F$ flame. The transient strain rate is given by equation 2.13. Here, the parameter $\Gamma/\pi r^2 = 10^6\ sec^{-1}$.

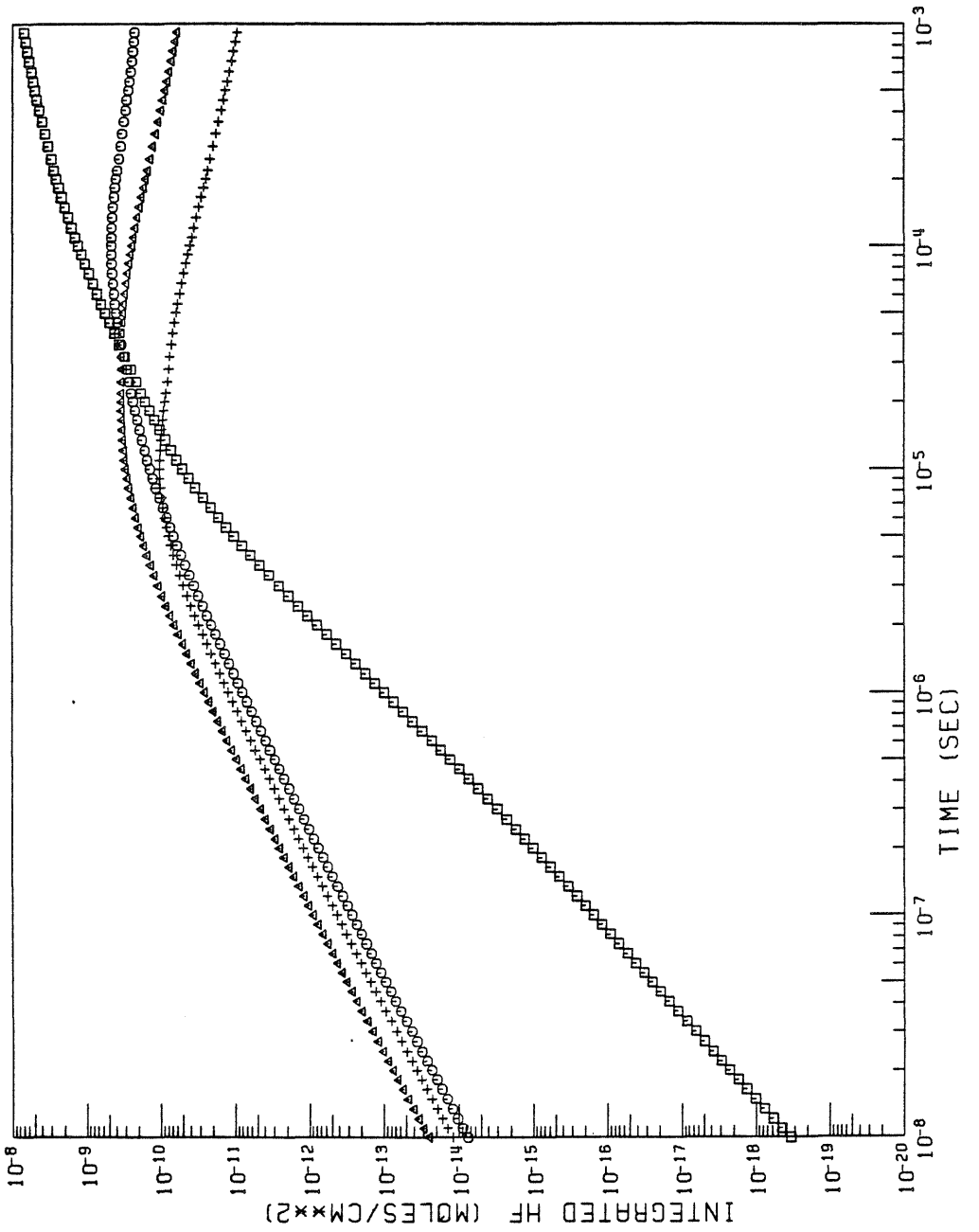

Figure 4.9 Surface density of the different excited states, $HF(j)$, as a function of time for a transiently strained $H_2 + F$ flame. The transient strain rate is given by equation 2.13. Here, the parameter $\Gamma/\pi r^2 = 10^5\ sec^{-1}$.

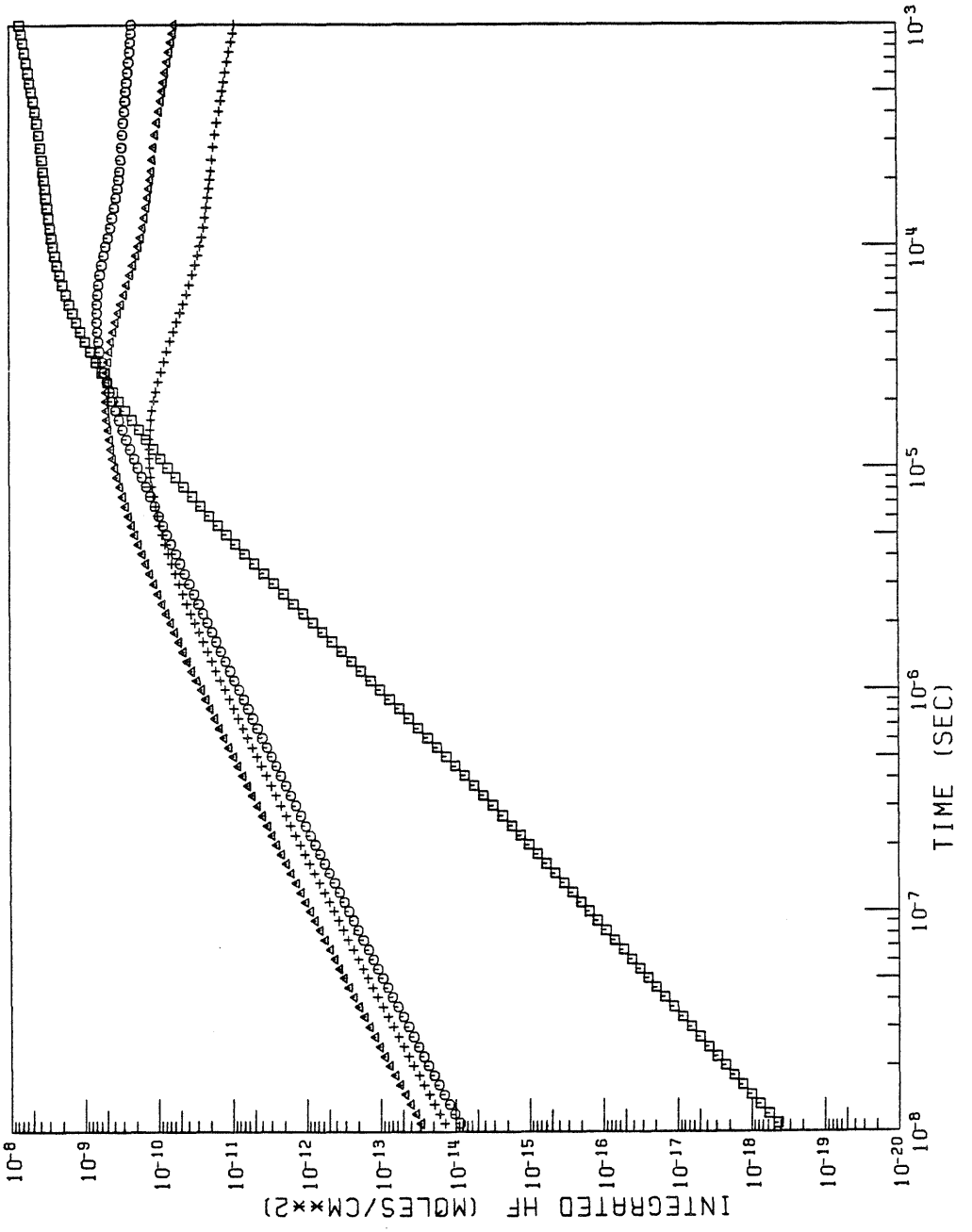

Figure 4.10 Surface density of the different excited states, $HF(j)$, as a function of time for a transiently strained $H_2 + F$ flame. The transient strain rate is given by equation 2.13. Here, the parameter $\Gamma/\pi r^2 = 10^4\ sec^{-1}$.

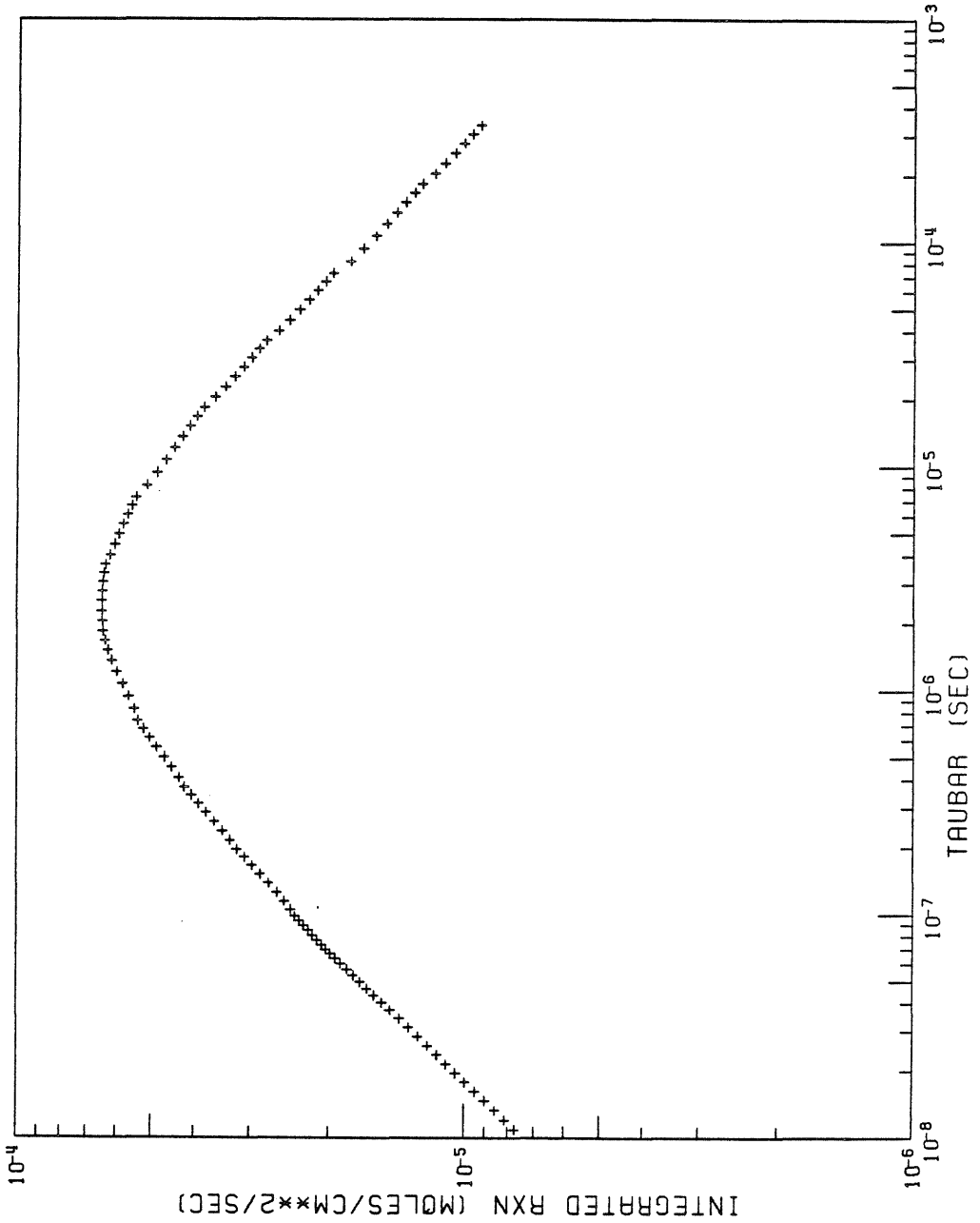

Figure 4.11 Specific fuel consumption rate $\dot{m}$ for a transiently strained $H_2 + F$ flame as a function of $\bar{\tau}$. The transient strain rate is given by equation 2.13. Here, the parameter $\Gamma/\pi r^2 = 10^7\ sec^{-1}$. The variable $\bar{\tau}$ is found as a function of time from equation 4.7.

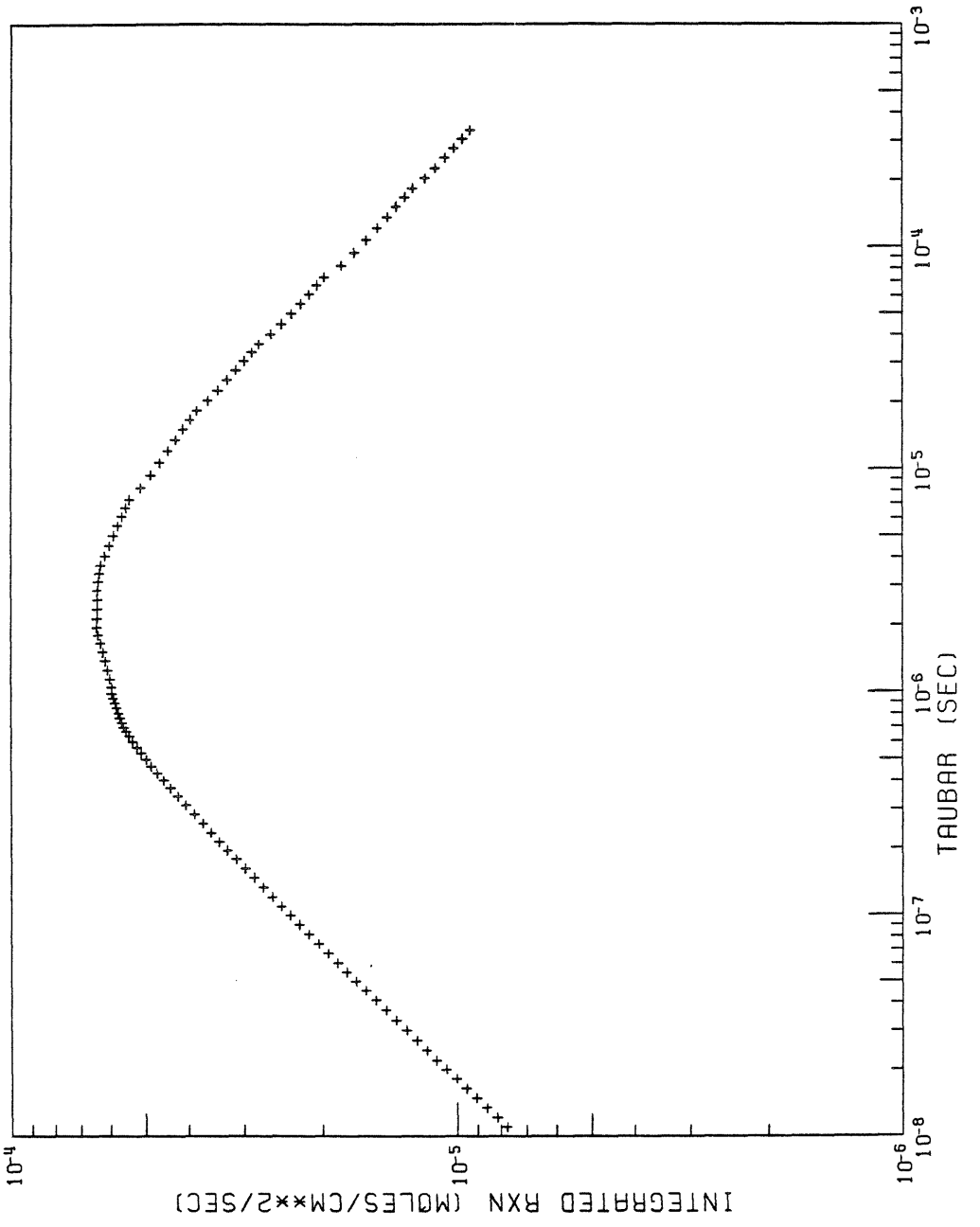

Figure 4.12 Specific fuel consumption rate $\dot{m}$ for a transiently strained $H_2 + F$ flame as a function of $\bar{\tau}$. The transient strain rate is given by equation 2.13. Here, the parameter $\Gamma/\pi r^2 = 10^6\ sec^{-1}$. The variable $\bar{\tau}$ is found as a function of time from equation 4.7.

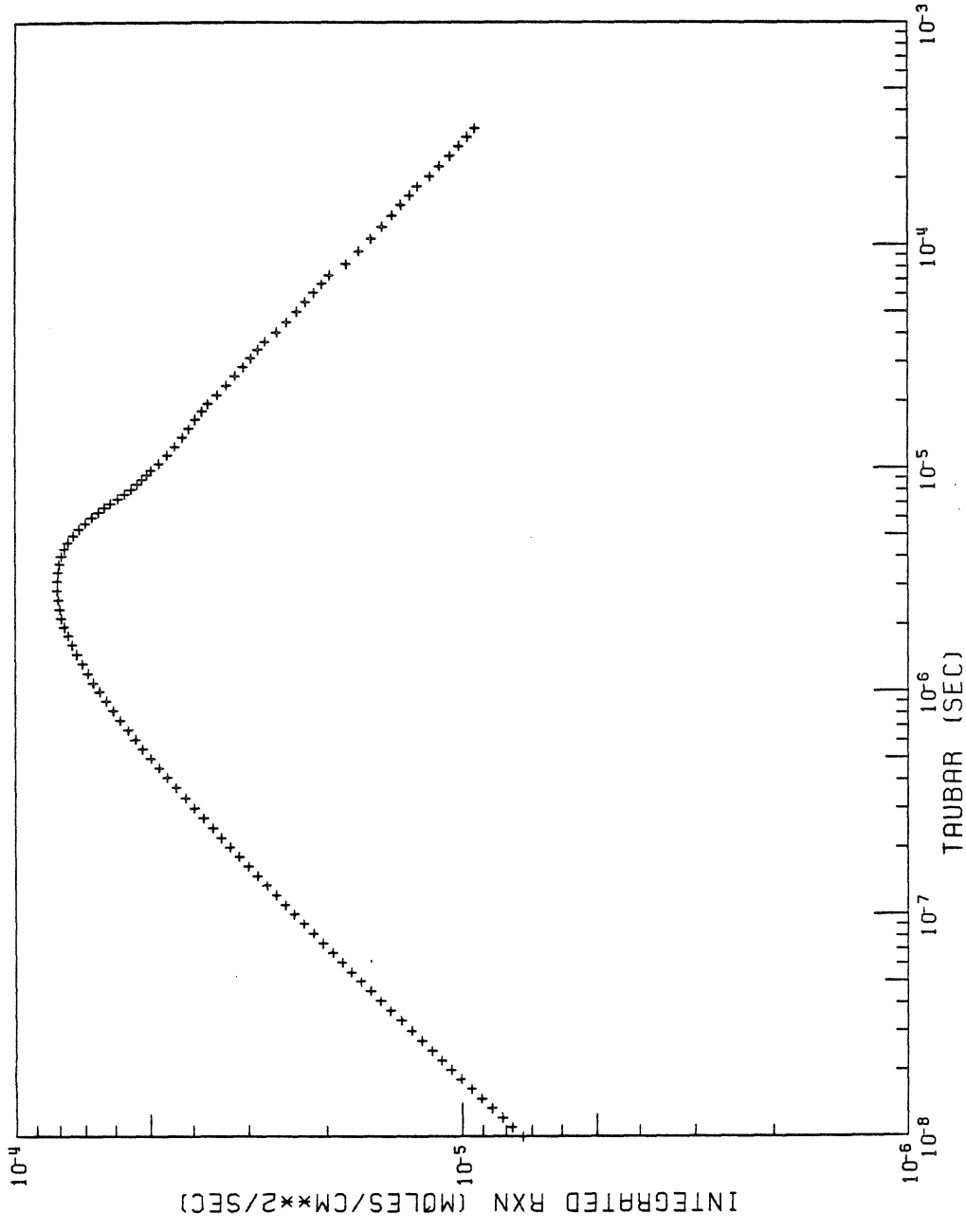

Figure 4.13 Specific fuel consumption rate $\dot{m}$ for a transiently strained $H_2 + F$ flame as a function of $\bar{\tau}$. The transient strain rate is given by equation 2.13. Here, the parameter $\Gamma/\pi r^2 = 10^5\ sec^{-1}$. The variable $\bar{\tau}$ is found as a function of time from equation 4.7.

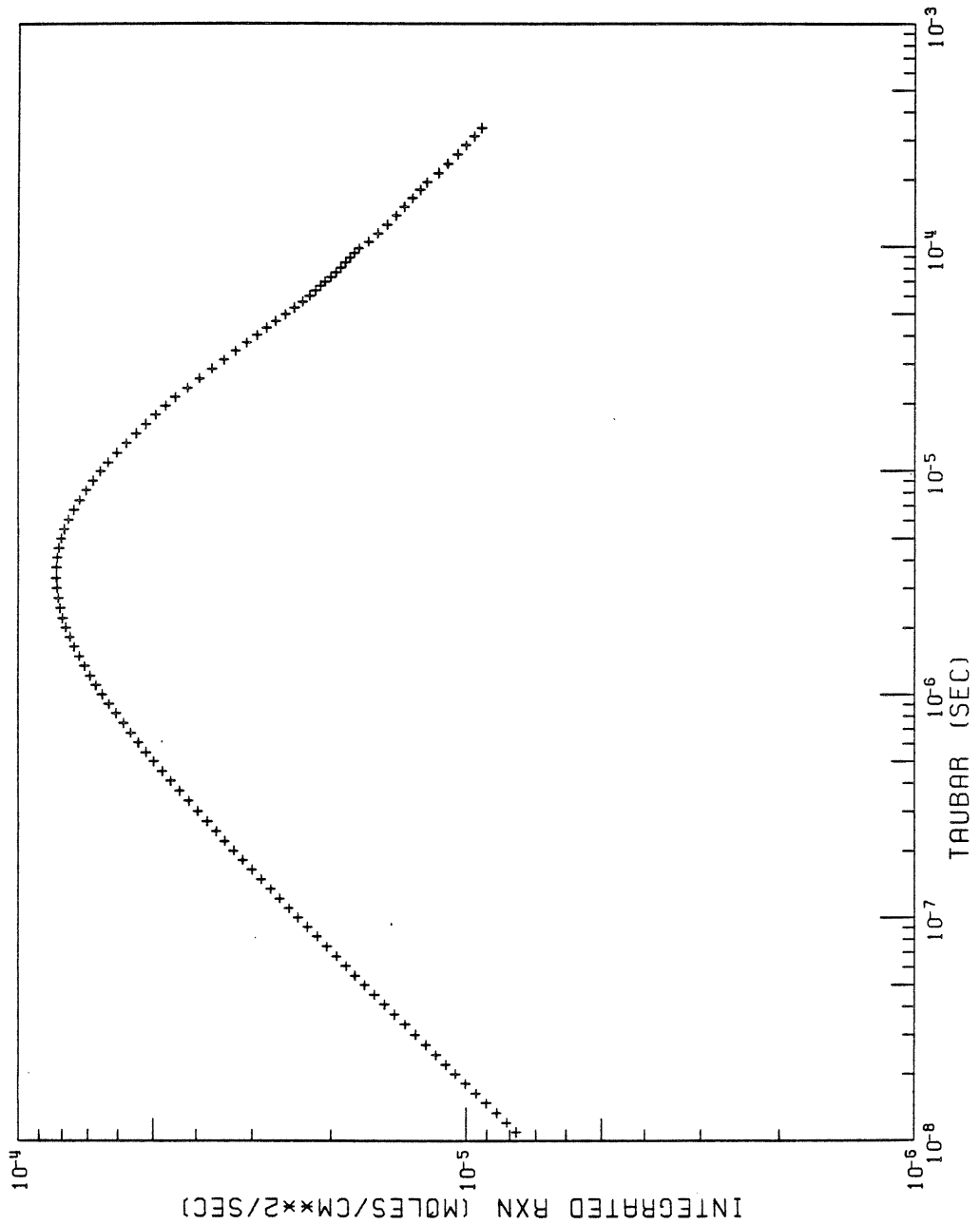

Figure 4.14 Specific fuel consumption rate $\dot{m}$ for a transiently strained $H_2 + F$ flame as a function of $\bar{\tau}$. The transient strain rate is given by equation 2.13. Here, the parameter $\Gamma/\pi r^2 = 10^4\ sec^{-1}$. The variable $\bar{\tau}$ is found as a function of time from equation 4.7.

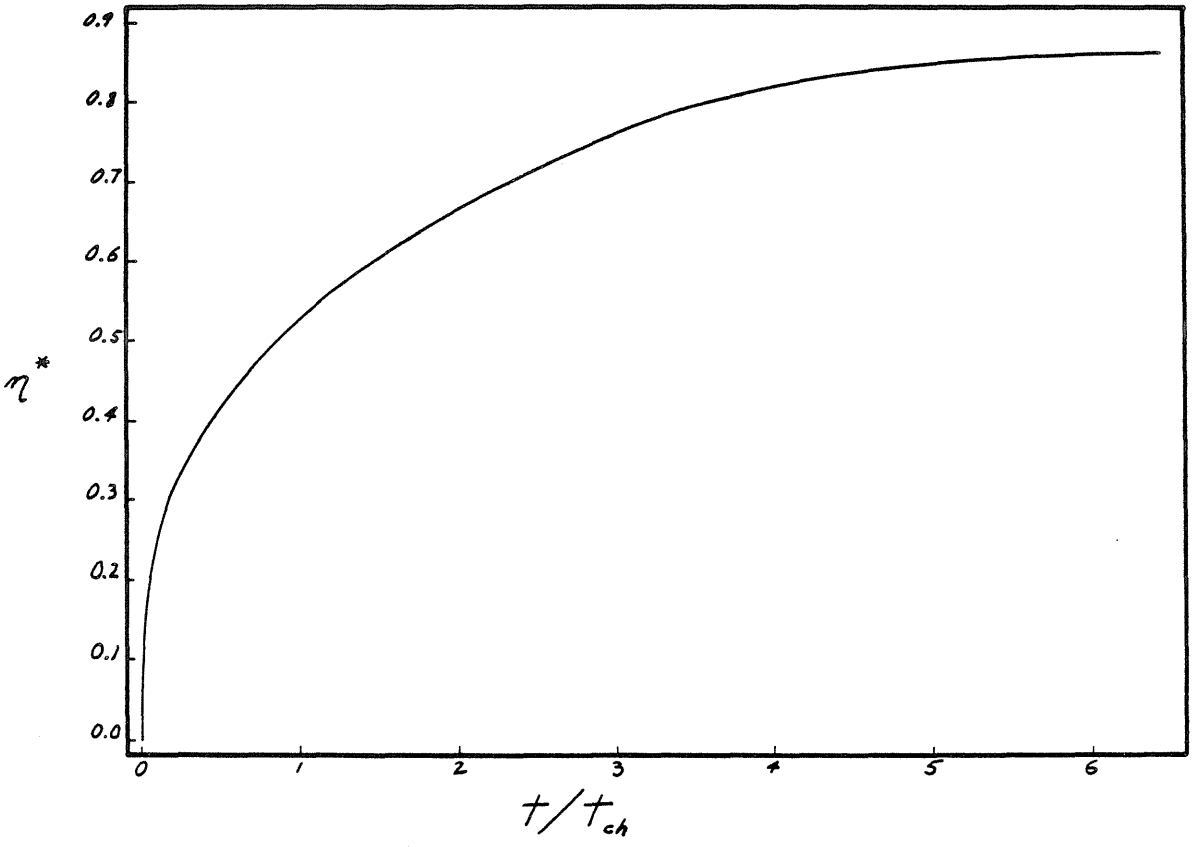

Figure 5.1 The dimensionless core radius η^* is shown as a function of t/t_{ch}. The results were obtained from equation 5.16.

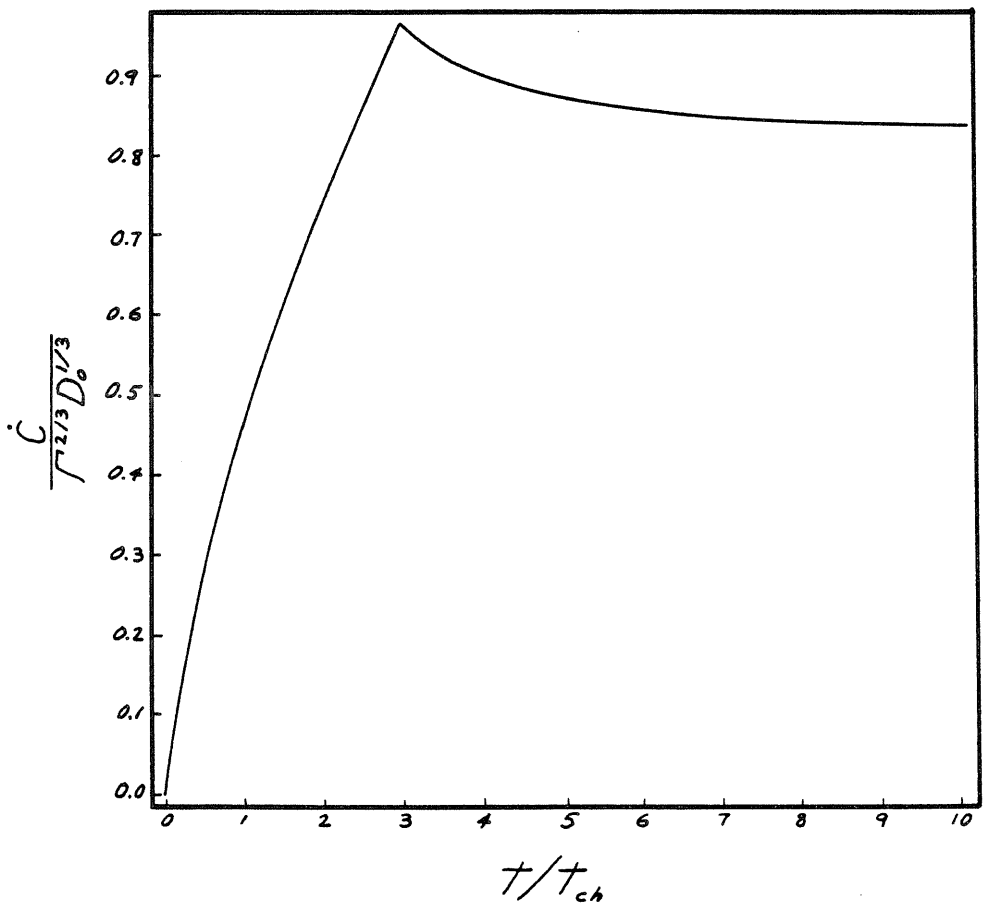

Figure 5.2 The rate of growth of the core volume, $\dot{C}$, is made dimensionless by $\Gamma^{2/3}D_0^{1/3}$ and shown as a function of t/t_{ch}. The results are from equation 5.17.

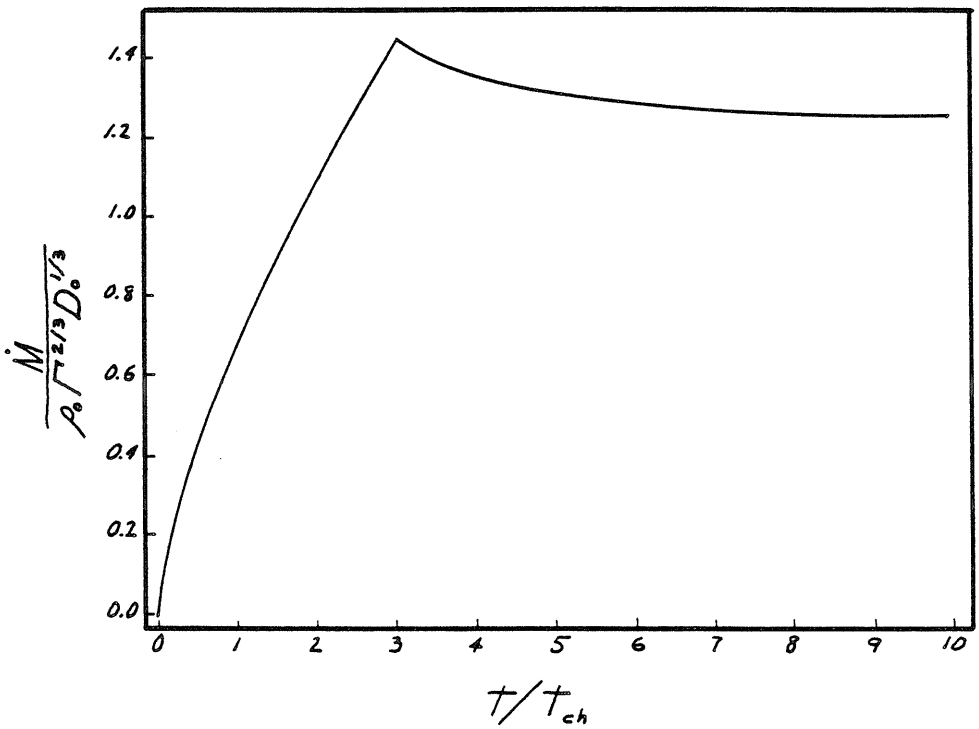

Figure 5.3 Here $\dot{M}$, the augmented fuel consumption rate of the flame due to the presence of the vortex, is made dimensionless by $\rho_0 \Gamma^{2/3} D_0^{1/3}$ and shown as a function of t/t_{ch}.

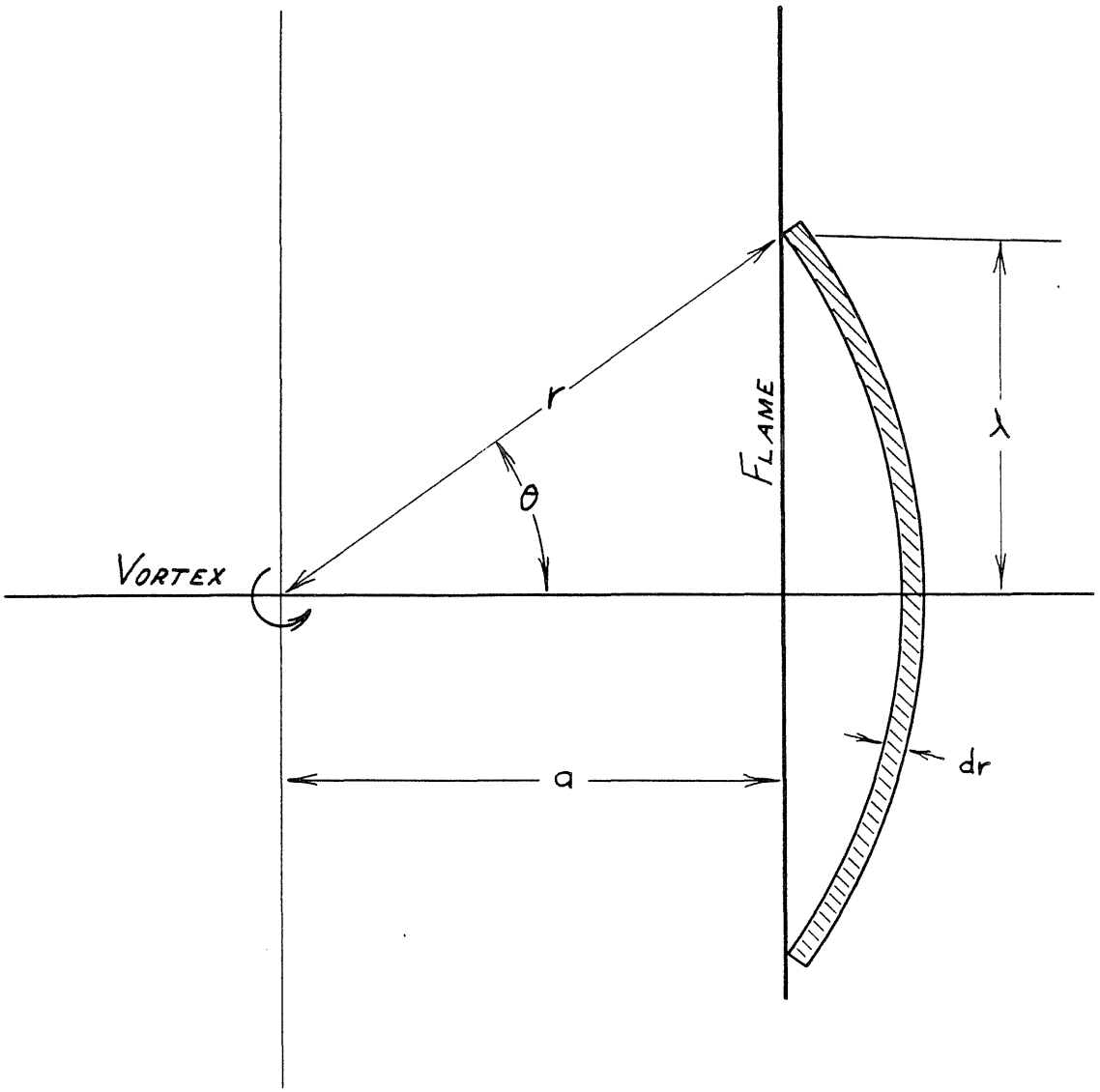

Figure 5.4 When the offset distance a is not zero, a circular annulus about the center of the vortex will contain less of one reactant than the other. Here, the vortex lies to the left of the flame, so the supply of the reactant on the right will control the burnout time, and thus the radius of the burned out core. The supply of this reactant available at a given radius r is proportional to the area of the shaded region.

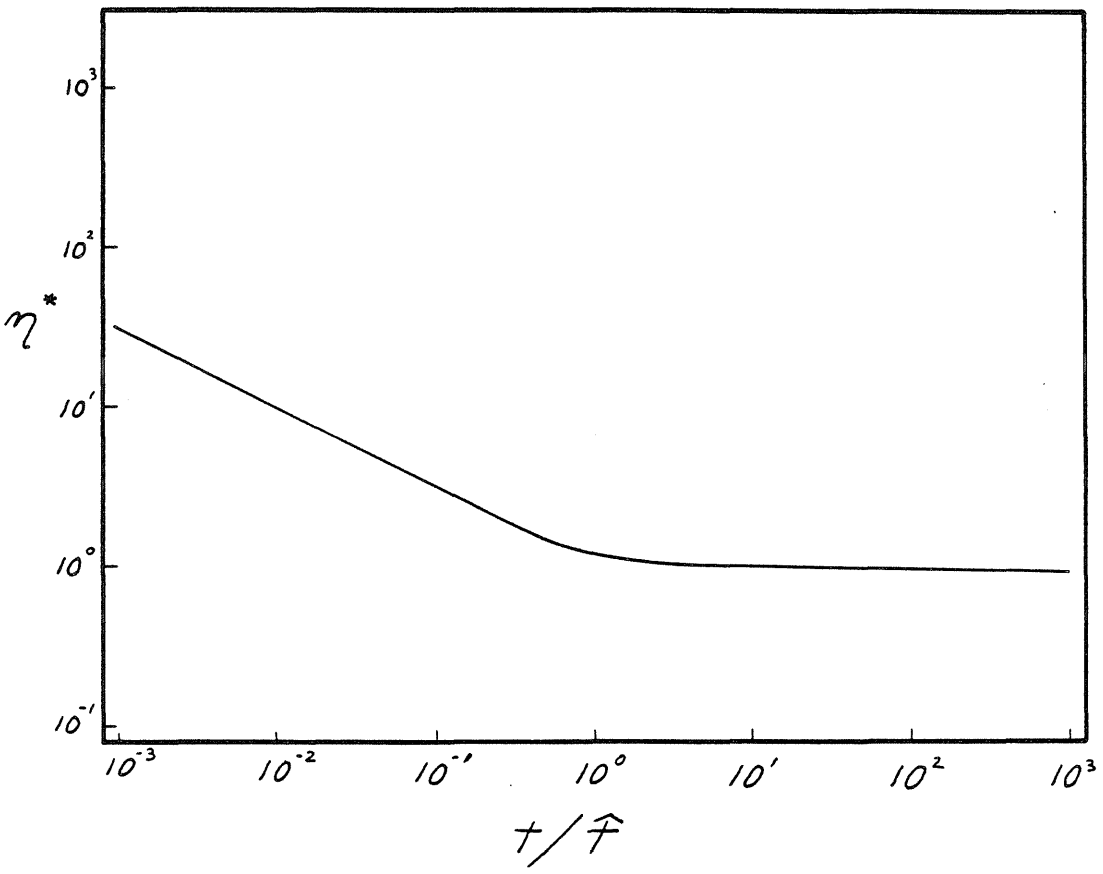

Figure 5.5 Temporarily ignoring the effects of finite chemical reaction rates, the dimensionless burned out core radius η^* is found as a function of $t/\hat{t}$ in equation 5.36. The apparent growth in the core radius as $t \to 0$ is illusory, because the dimensionless core radius η^* contains a factor of $1/\sqrt{t}$. Since the core radius can never be less than a, and indeed $r^* \to a$ as $t \to 0$, η^* behaves like $a/\sqrt{t}$ for small t.

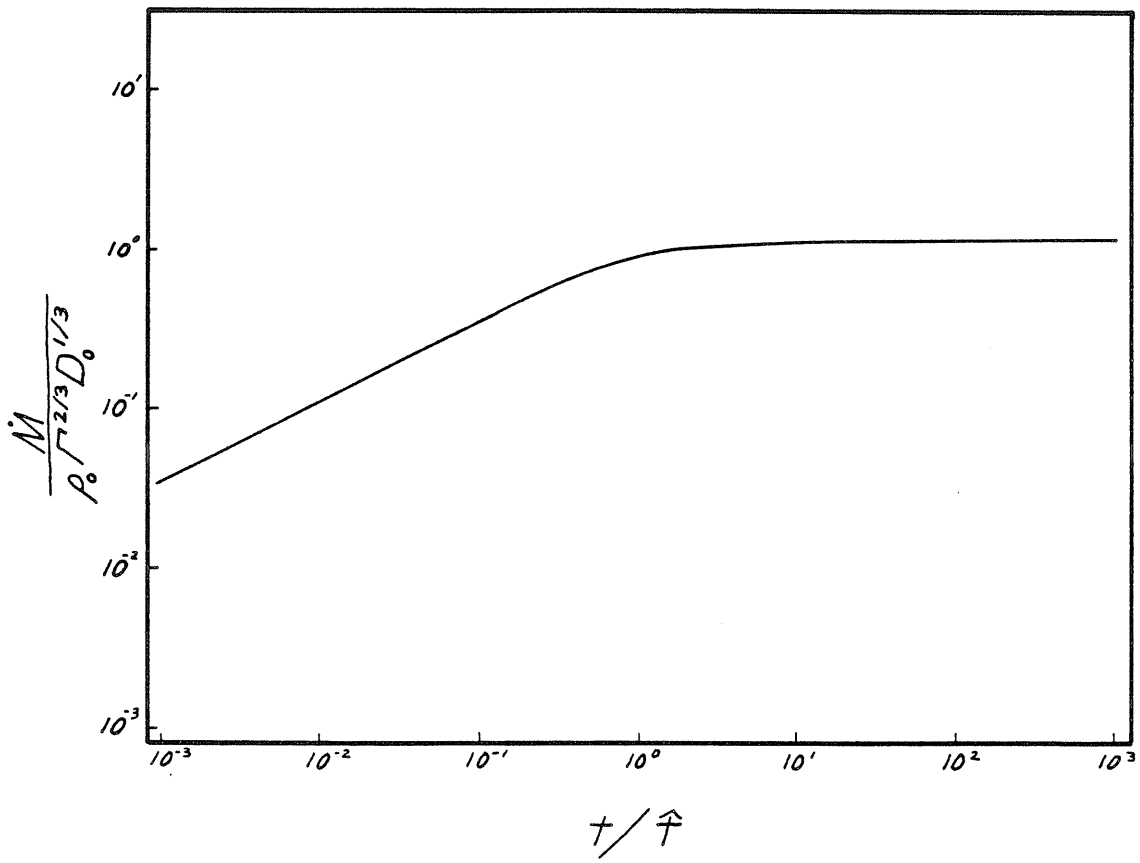

Figure 5.6 When the chemical reaction is assumed to be infinitely fast, a nonzero offset distance a produces a time scale $\hat{t}$, which governs the evolution of the spiral flame. Here, the results of equation 5.38 are plotted. The dimensionless augmented fuel consumption rate, $\dot{M}$, made dimensionless by $\rho_0 \Gamma^{2/3} D_0^{1/3}$, is shown as a function of $t/\hat{t}$.

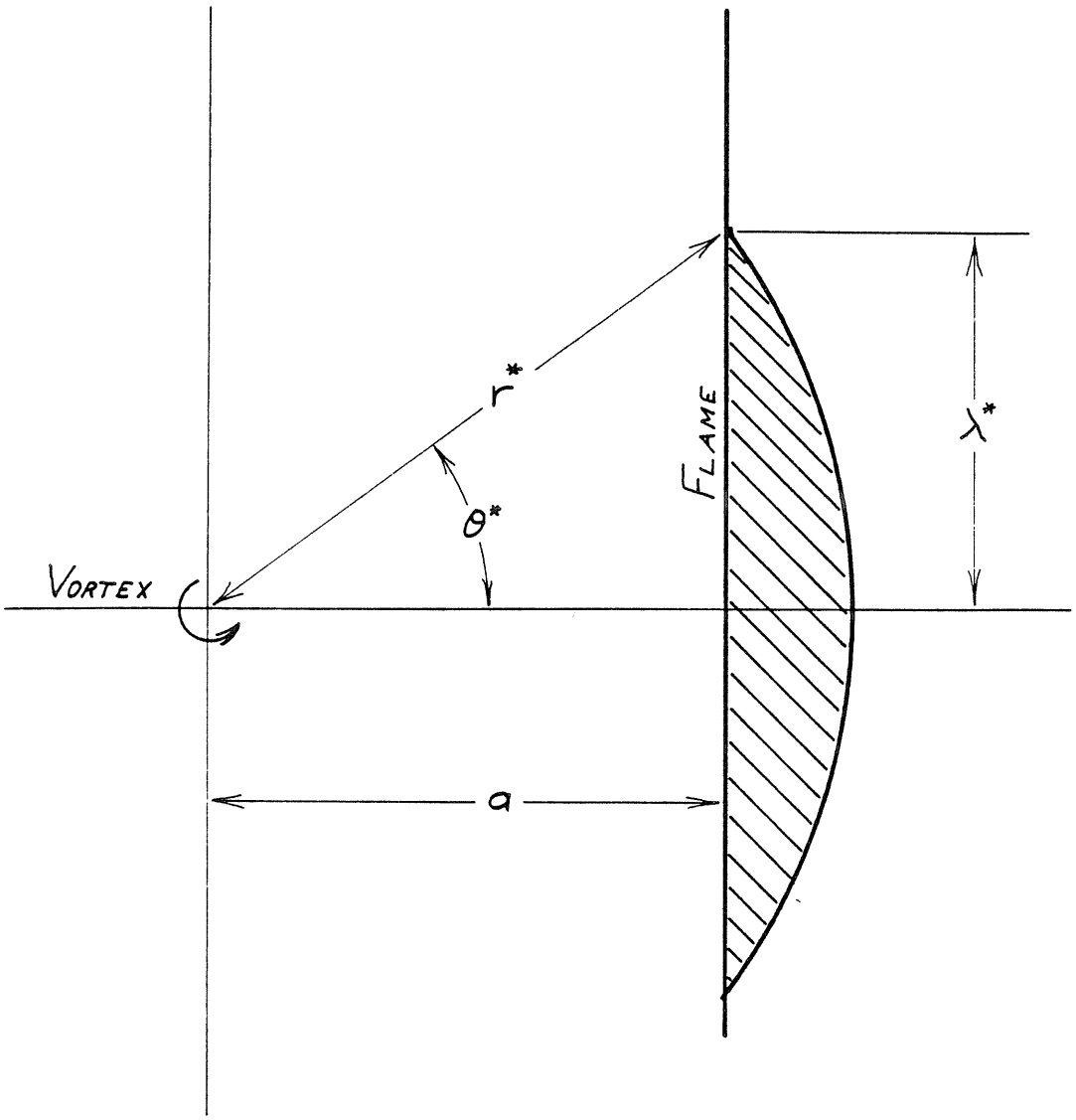

Figure 5.7 When the burned out core has a radius of r^*, the combustion product in the core is proportional to the volume of fuel originally contained within a circle of radius r^* about the vortex, or to the area of the shaded region in the figure. Since a is known, the extent of the core may be given as r^*, λ^*, or θ^*.

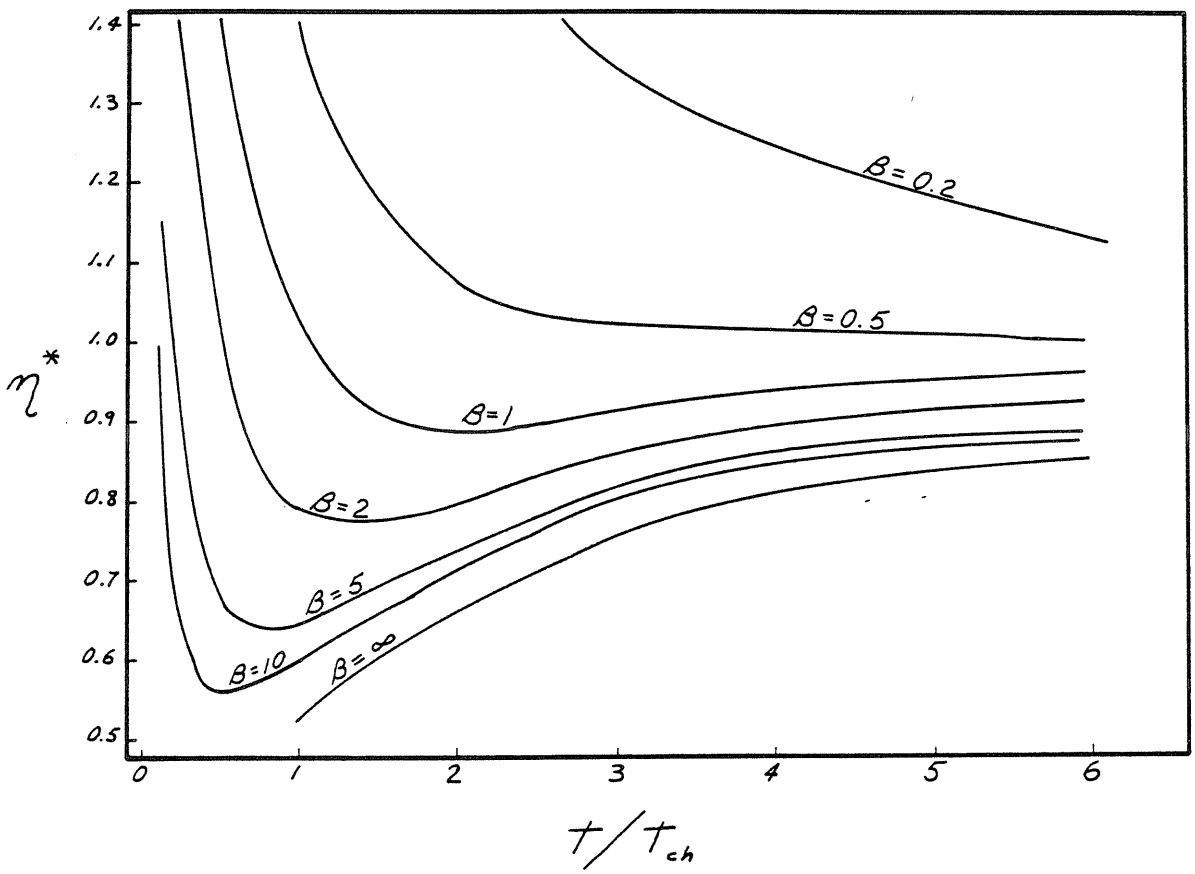

Figure 5.8 Here the effects of both finite chemistry and a nonzero offset distance a have been considered. Equation 5.39 has been graphed, showing the dimensionless core radius η^* as a function of t/t_{ch}. The parameter $\beta \equiv t/t_{ch}$ represents the ratio of the two characteristic time scales. The apparent growth in the core radius as $t \to 0$ is illusory, because the dimensionless core radius η^* contains a factor of $1/\sqrt{t}$. Since the core radius can never be less than a, and indeed $r^* \to a$ as $t \to 0$, η^* behaves like $a/\sqrt{t}$ for small t.

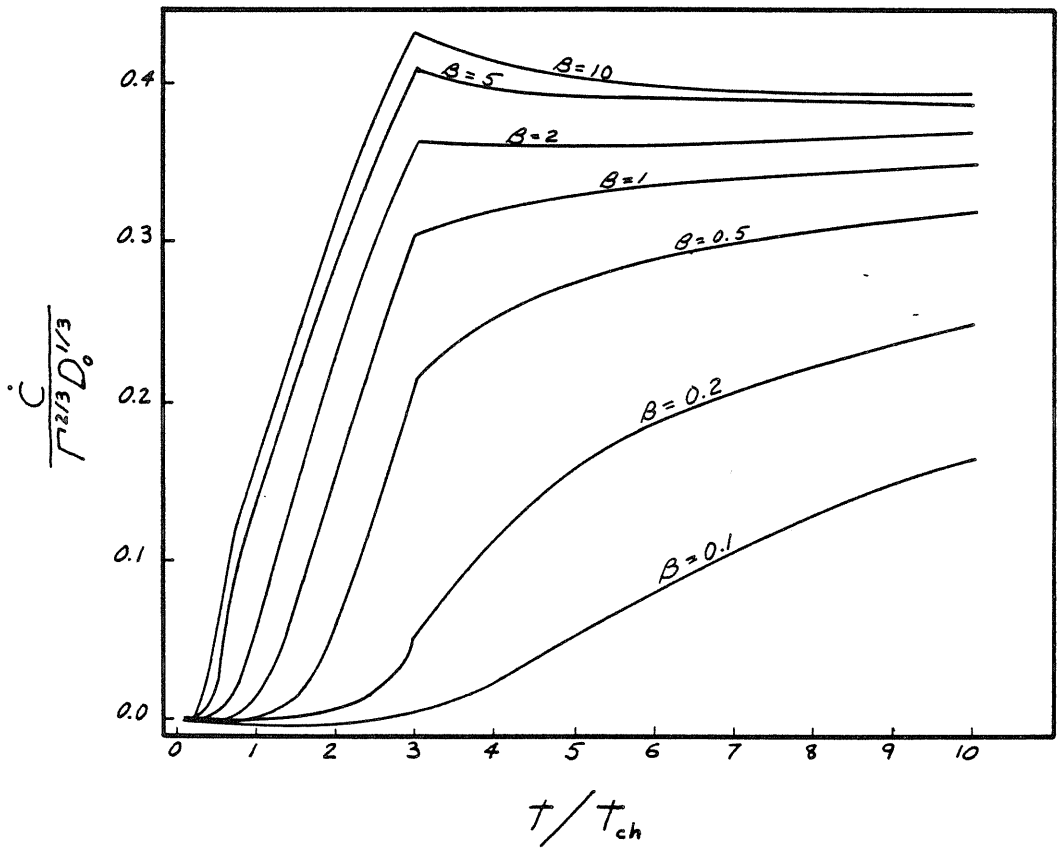

Figure 5.9 The rate of increase of combustion products in the core, $\dot{C}$, made dimensionless by $\Gamma^{2/3}D_0^{1/3}$, is evaluated from equations 5.42 and plotted against t/t_{ch} for several values of the parameter β.

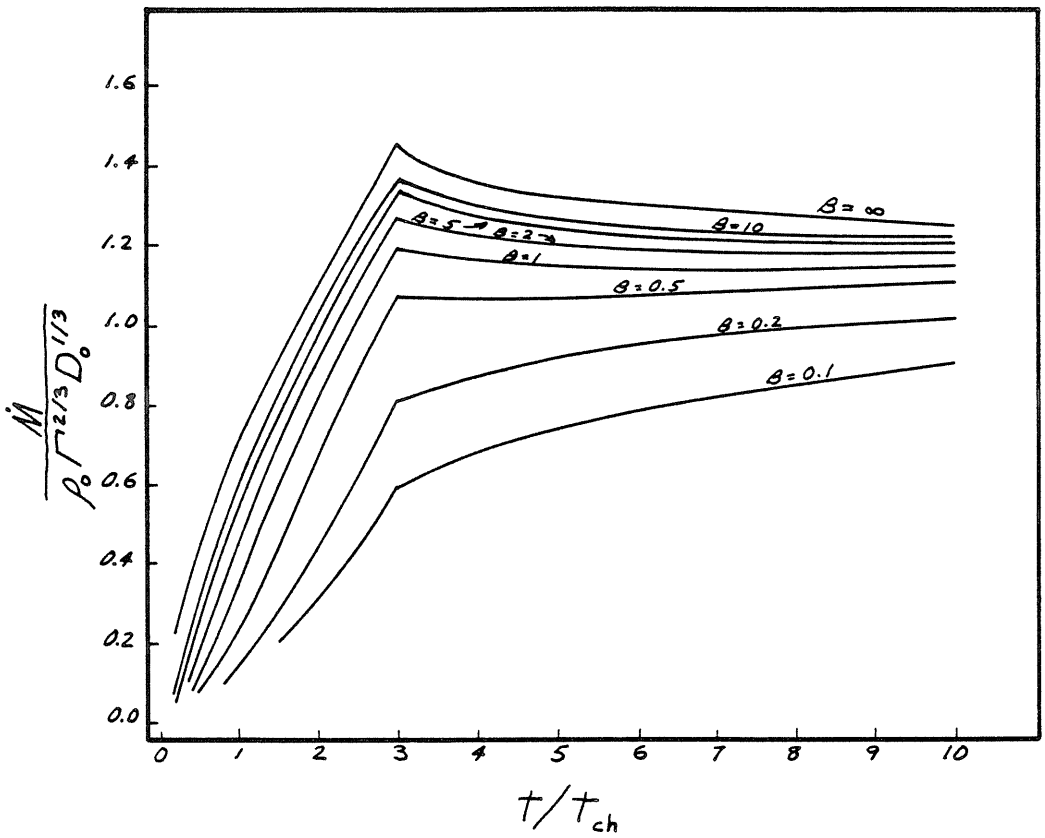

Figure 5.10 The augmented fuel consumption rate due to the vortex, $\dot{M}$, has been made dimensionless by $\rho_0 \Gamma^{2/3} D_0^{1/3}$ and plotted as a function of t/t_{ch} for several values of the parameter β. The data were obtained by evaluating equations 5.40.

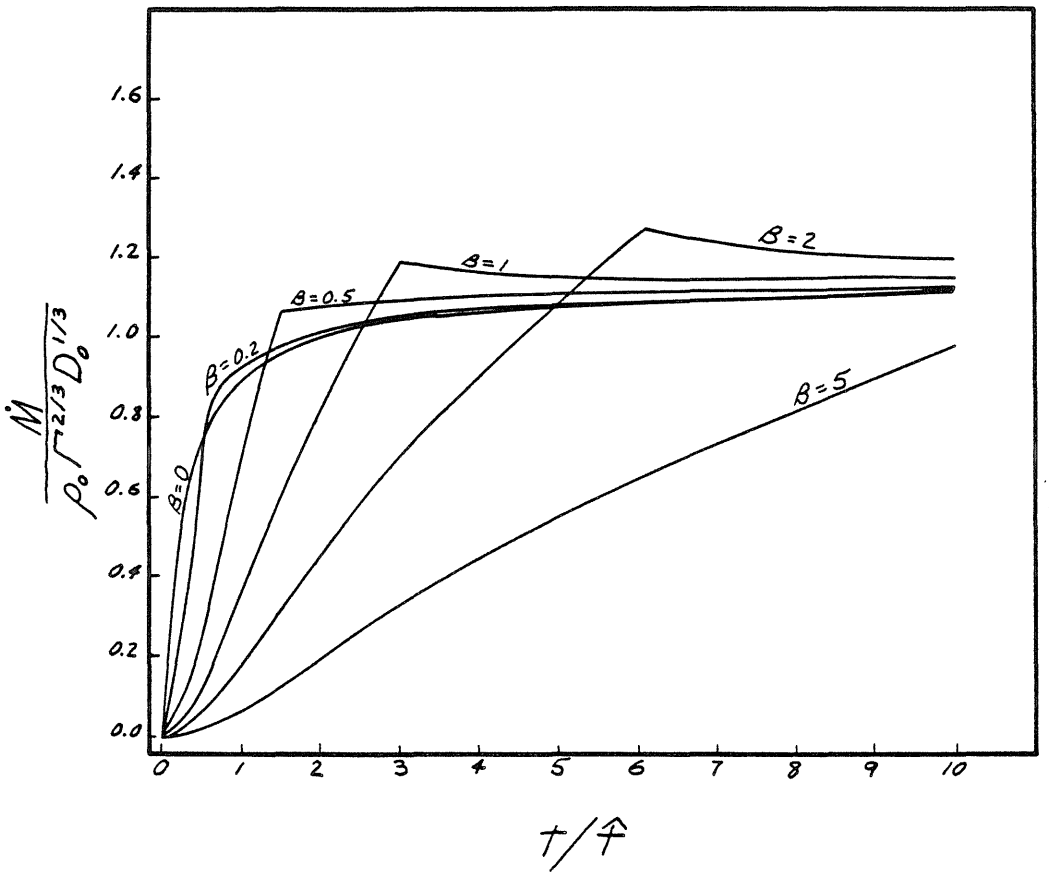

Figure 5.11 The data of the previous figure have been replotted, with $t/\hat{t}$ as the time variable rather than t/t_{ch}. One sees that for large values of β, t_{ch} is the controlling time scale, whereas for small values of β, $\hat{t}$ governs the increase of the fuel consumption rate to its constant steady state value.

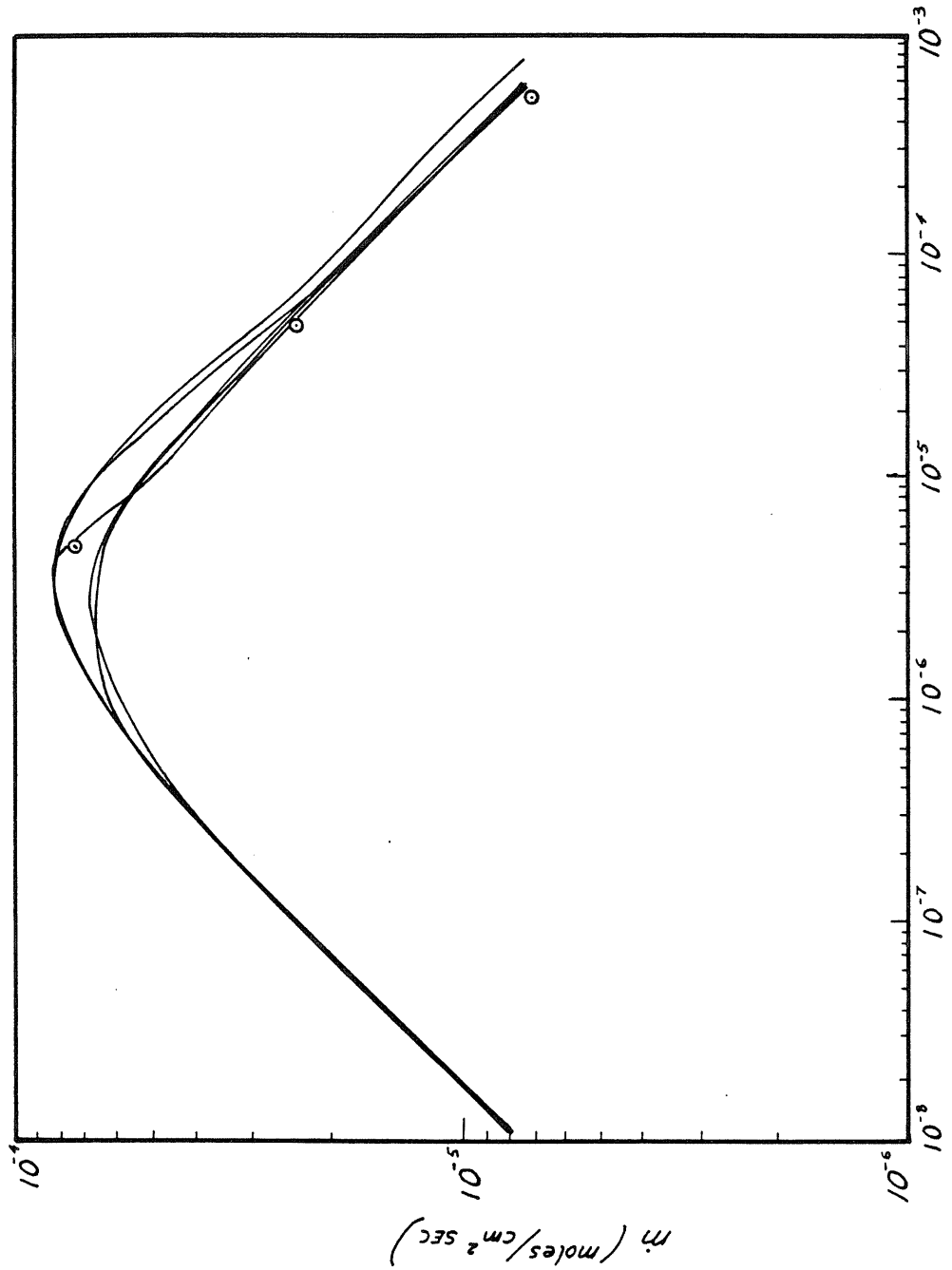

Figure 6.1 Can one consider $\dot{m}$ as a function only of $\bar{r}$? Here, figures 4.1, 4.11, 4.12, 4.13, and 4.14 have been traced on the same sheet. Equation 6.1 is plotted as a dashed line.

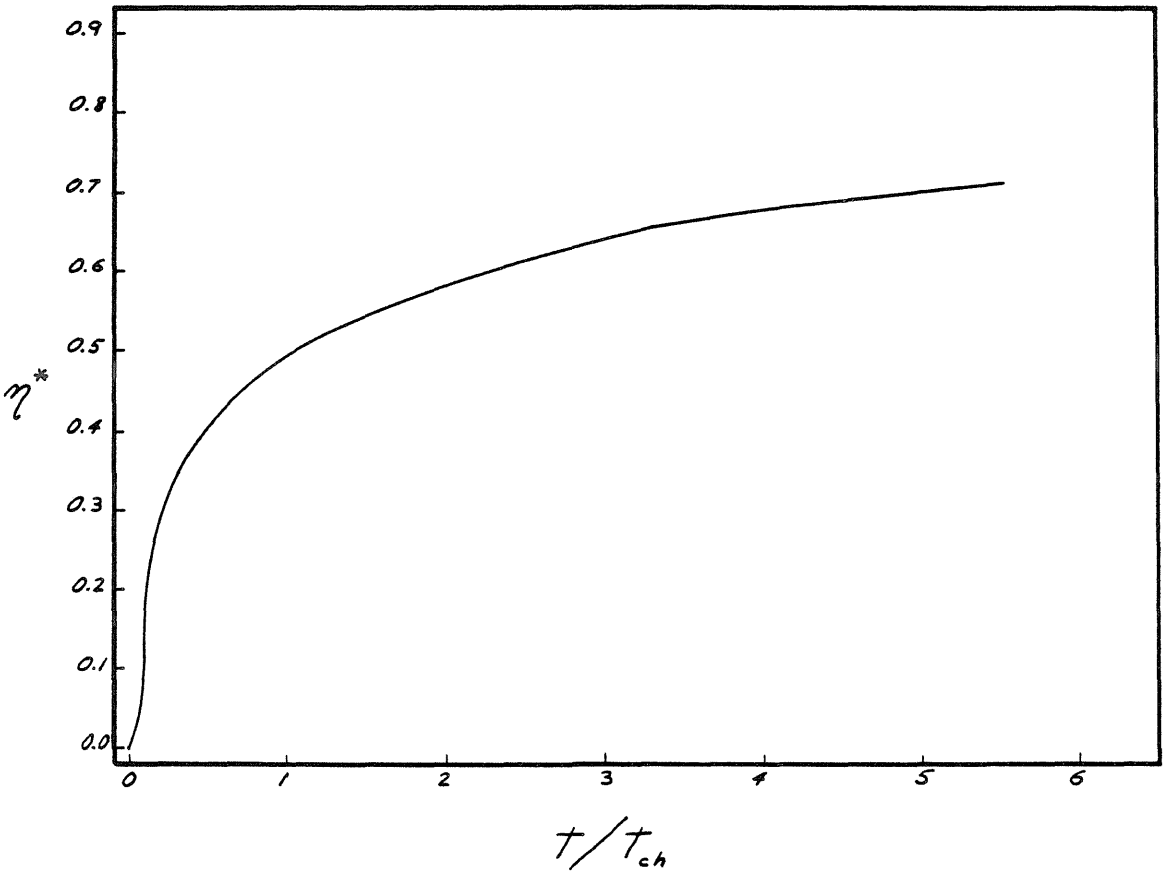

Figure 6.2 The dimensionless core radius η^* is plotted as a function of t/t_{ch}. The data are from equation 6.2, which was derived using equation 6.1 for $\dot{m}$ rather than equations 3.24.

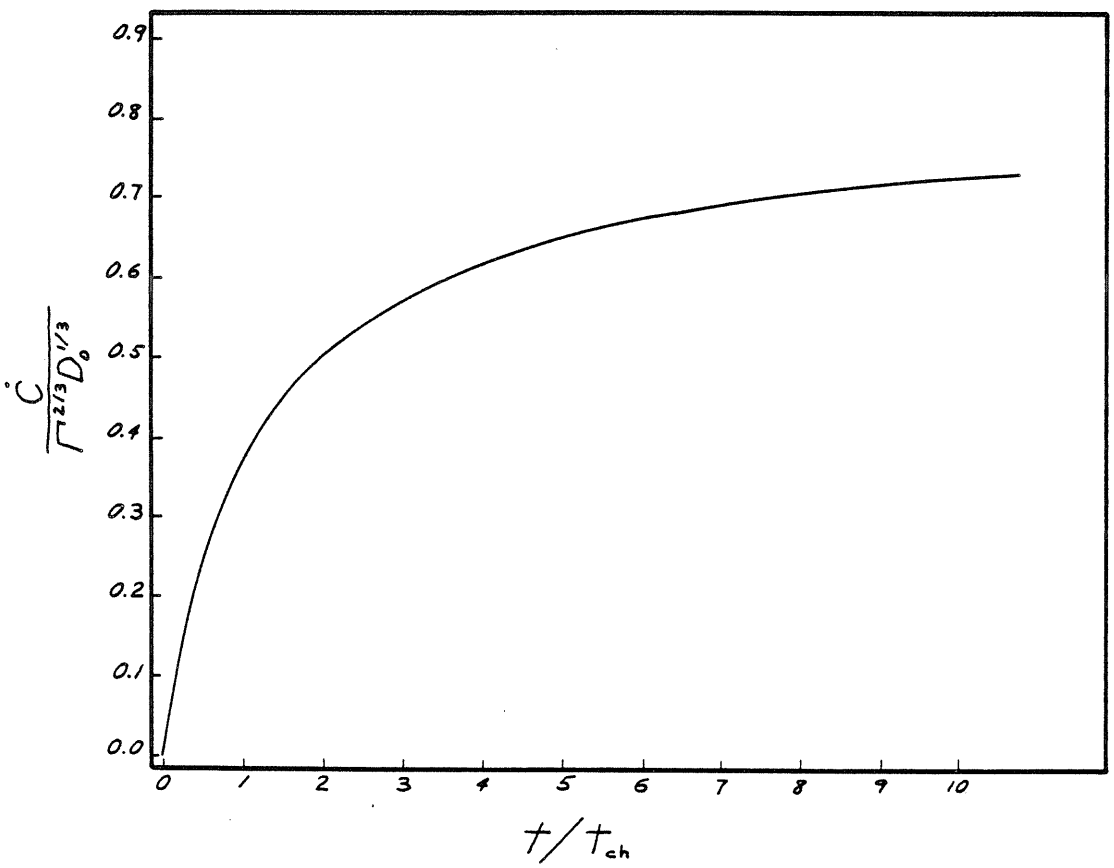

Figure 6.3 The core growth rate, $\dot{C}$, made dimensionless by $\Gamma^{2/3} D_0^{1/3}$, is found from equation 6.3 and plotted as a function of t/t_{ch}.

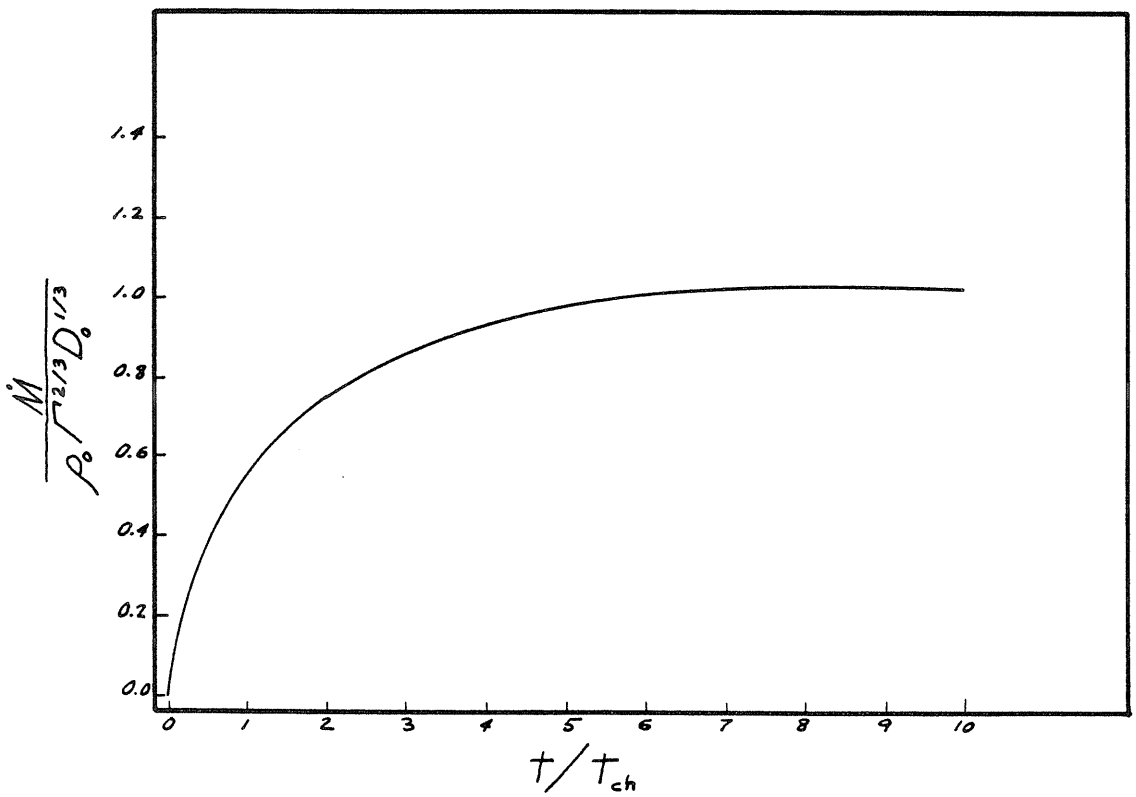

Figure 6.4 The augmented fuel consumption rate, $\dot{M}$, made dimensionless by $\rho_0 \Gamma^{2/3} D_0^{1/3}$, is found from equation 6.4 and plotted as a function of t/t_{ch}.

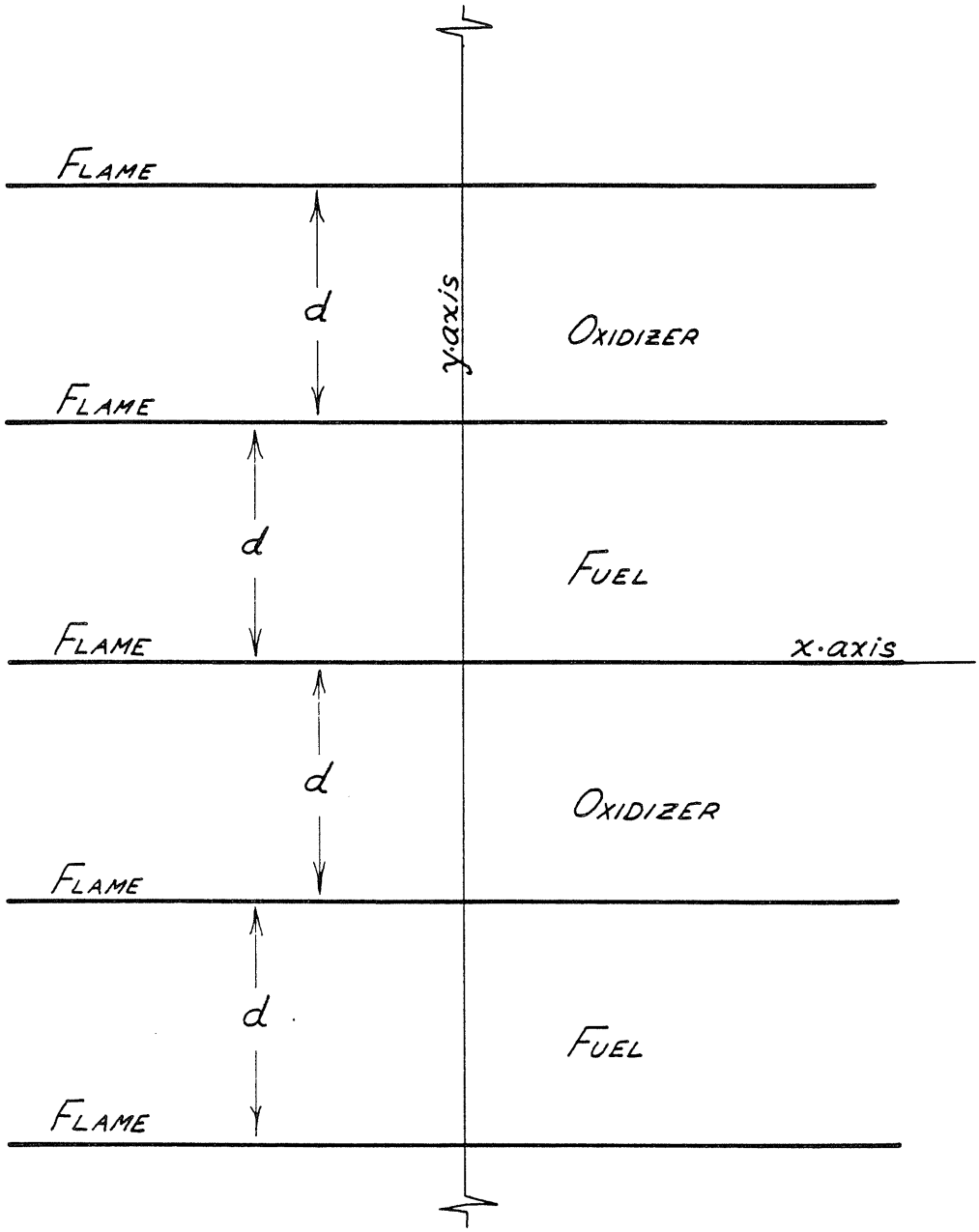

Figure 6.5 Initial conditions for the problem of section 6.7. Fuel and oxidizer are separated into strips of initial width d, creating an infinite number of flames, parallel to the x axis and initially a distance d apart. Straining along the x axis creates an inflow in the y direction, convecting the flames closer together. This decrease in the spacing between adjacent flames, coupled with the increasing thickness of each individual flame, causes the flames to interact and eventually go out.

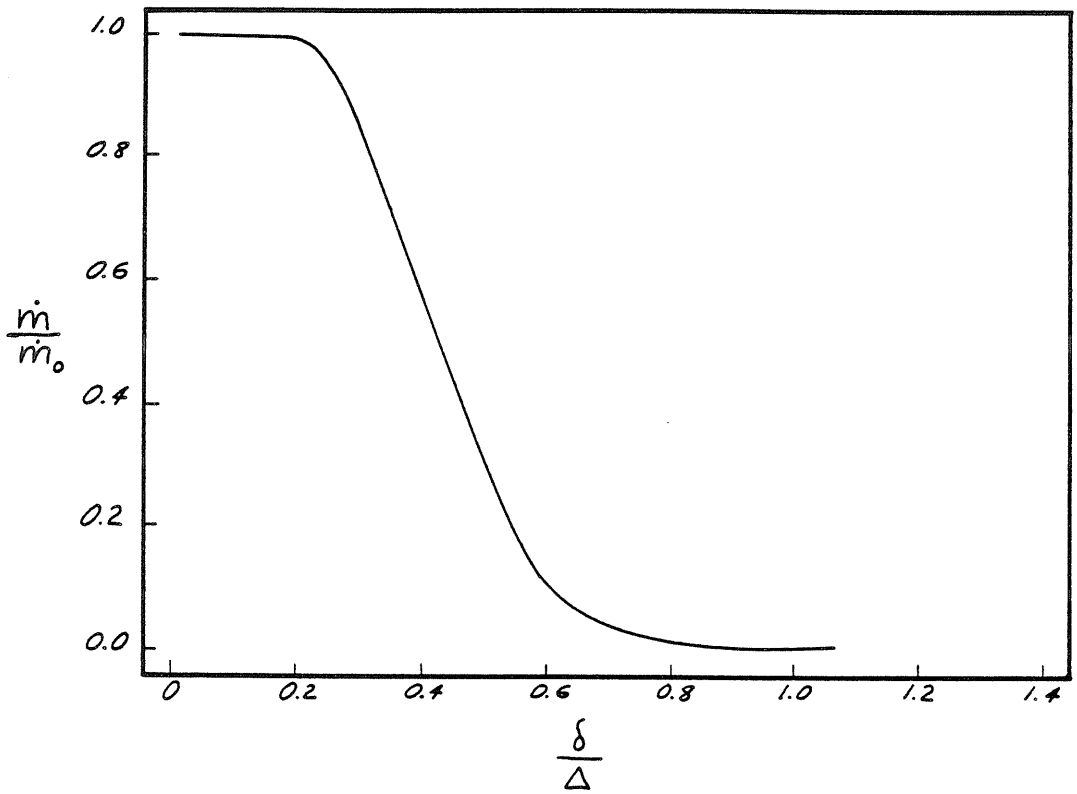

Figure 6.6 If infinitely fast chemical reactions are assumed, one obtains the solution to the flame interaction problem as equation 6.16. One may express the result in the form of an attenuation ratio, the ratio of the actual fuel consumption rate of an individual flame to the fuel consumption rate as if its neighbors were not present, $\dot{m}/\dot{m}_0$. The attenuation ratio is a function of the ratio of the thickness of an individual flame to the spacing between flames, δ/Δ.

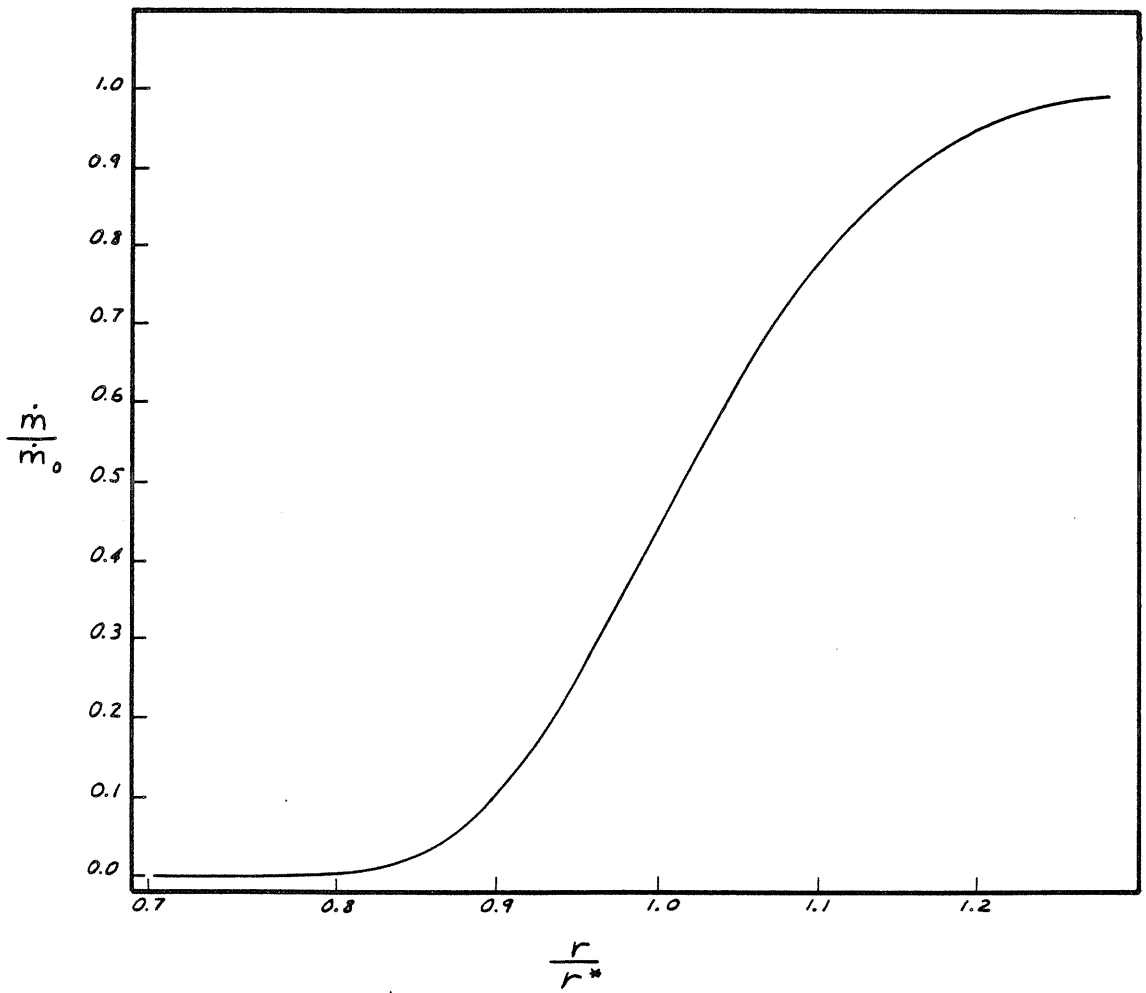

Figure 6.7 Applied to the spiral flame problem, the analysis allows one to see how sharp the edges of the burned out core really are. Here the attenuation ratio is plotted as a function of r/r^*. The data are from equations 6.16 and 6.18.

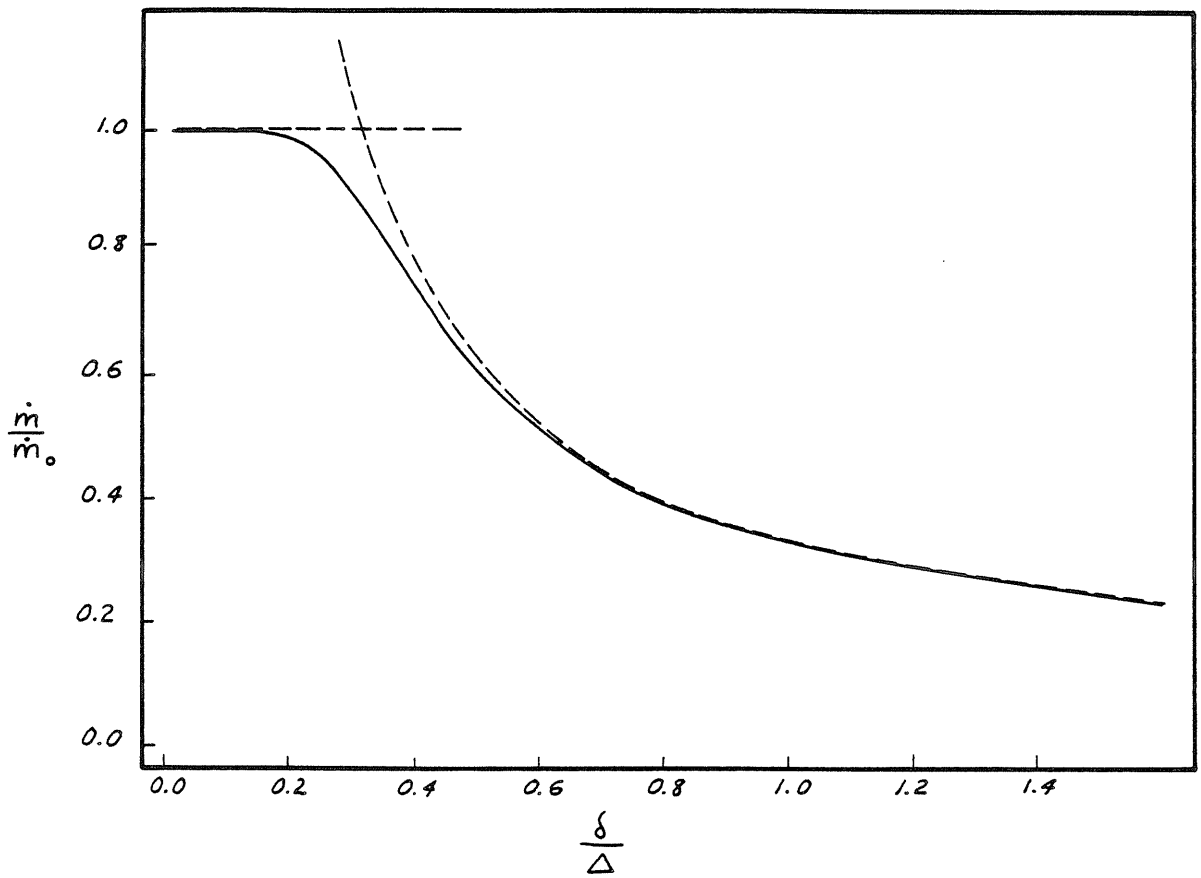

Figure 6.8 Just as in the infinite reaction rate limit, one also obtains an attenuation ratio $\dot{m}/\dot{m}_0$ as a function of δ/Δ in the weak reaction limit. Here the solid line is obtained by evaluation of equation 6.23, and the dashed lines are the asymptotes of equations 6.24.

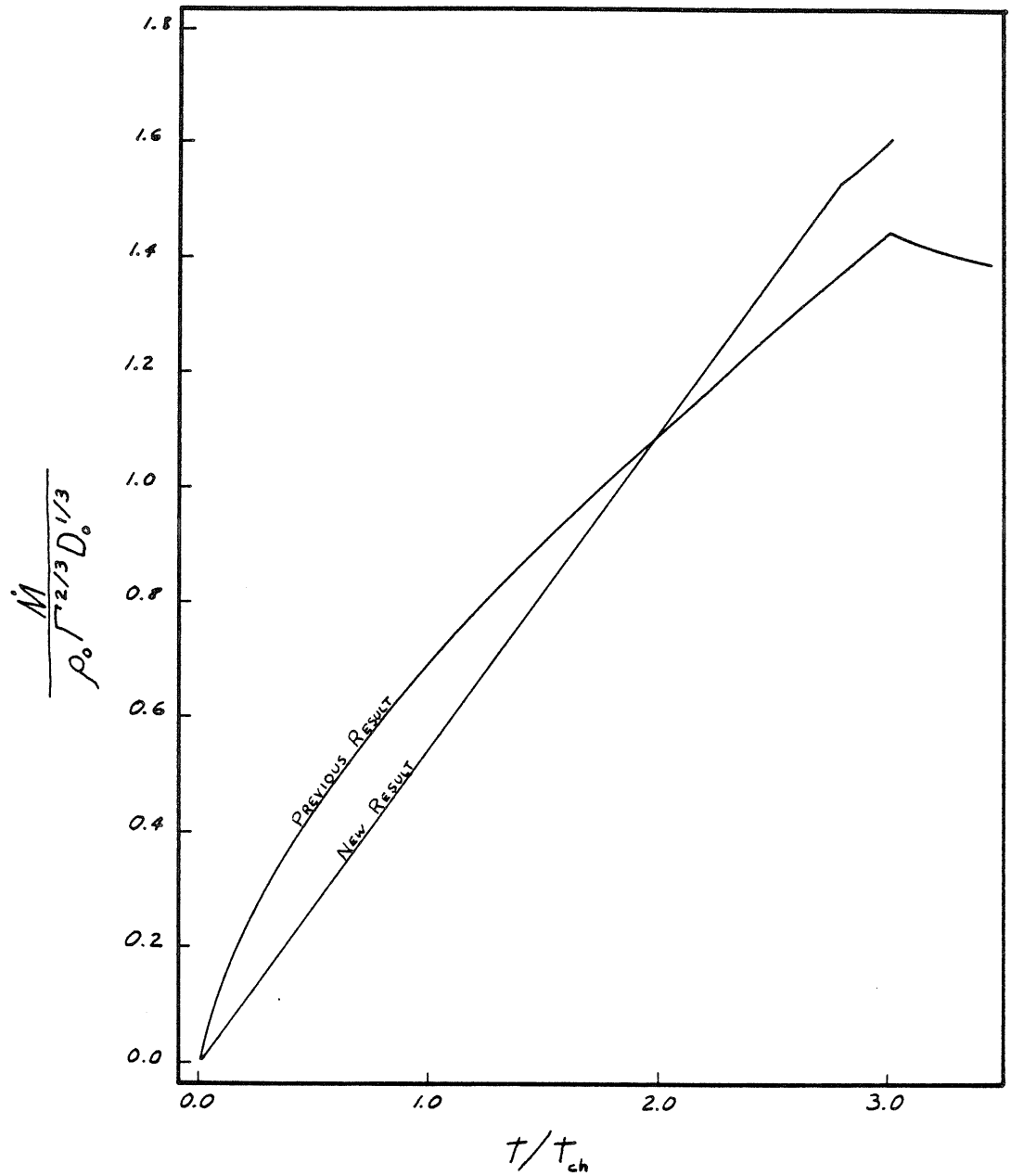

Figure 6.9 Recalculating the augmented fuel consumption rate, $\dot{M}$, for times small compared to the chemical time, and incorporating the new description of the interaction of adjacent flames results in equations 6.31. The result is plotted here, along with the previous result from equation 5.30a. Once again, $\dot{M}$, is made dimensionless by $\rho_0 \Gamma^{2/3} D_0^{1/3}$ and is a function of t/t_{ch}. The principal difference is the behavior near the origin; the new solution goes like (t/t_{ch}), whereas the old goes like $(t/t_{ch})^{2/3}$.

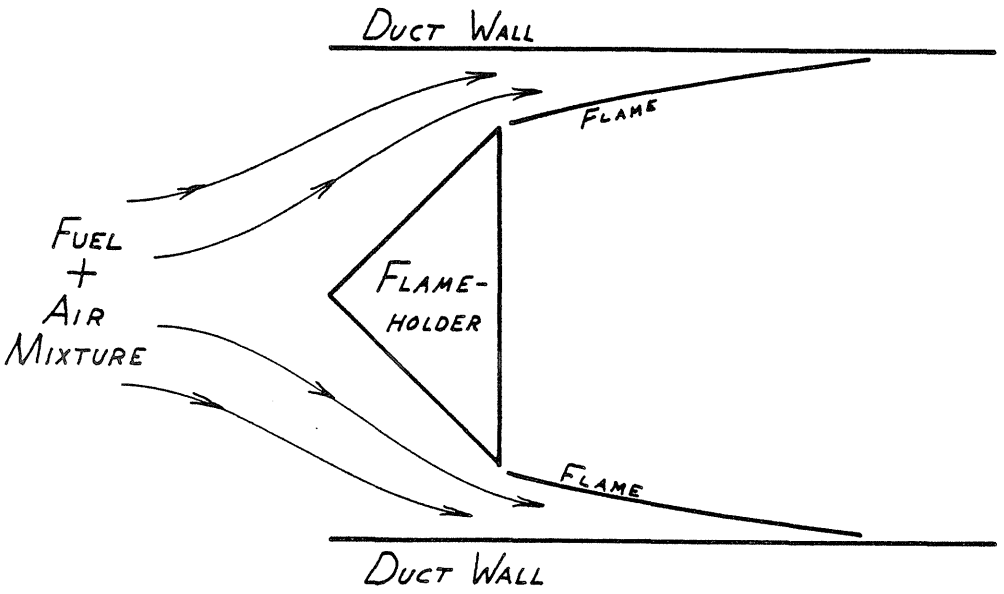

Figure 7.1 An idealized representation of the experimental setup of Rogers and Marble (1956). A condition of steady burning is shown here.

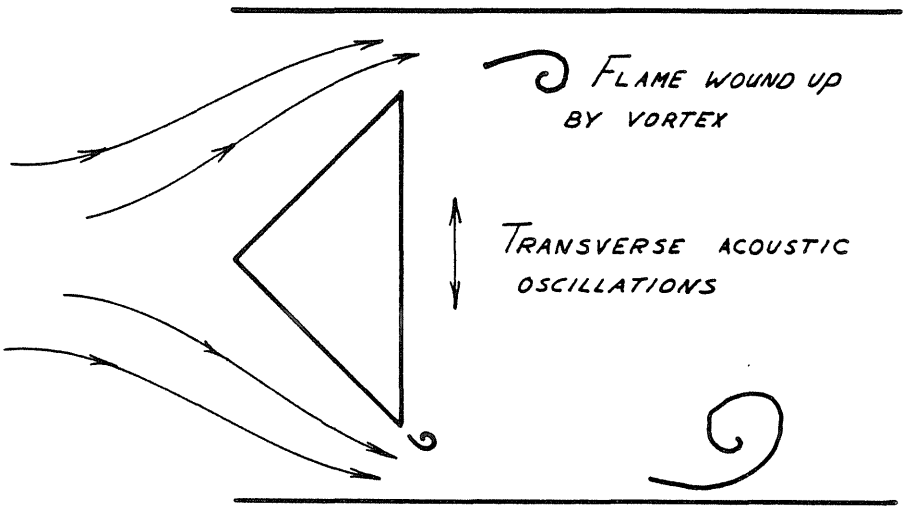

Figure 7.2 The same configuration as the previous figure, only under screeching conditions. The unstable oscillations corresponded to the transverse mode of the combustion chamber, thus the acoustic oscillations are from top to bottom in this figure. The flame sheets are wound up by vortices alternately shed from the top and bottom of the flameholder.

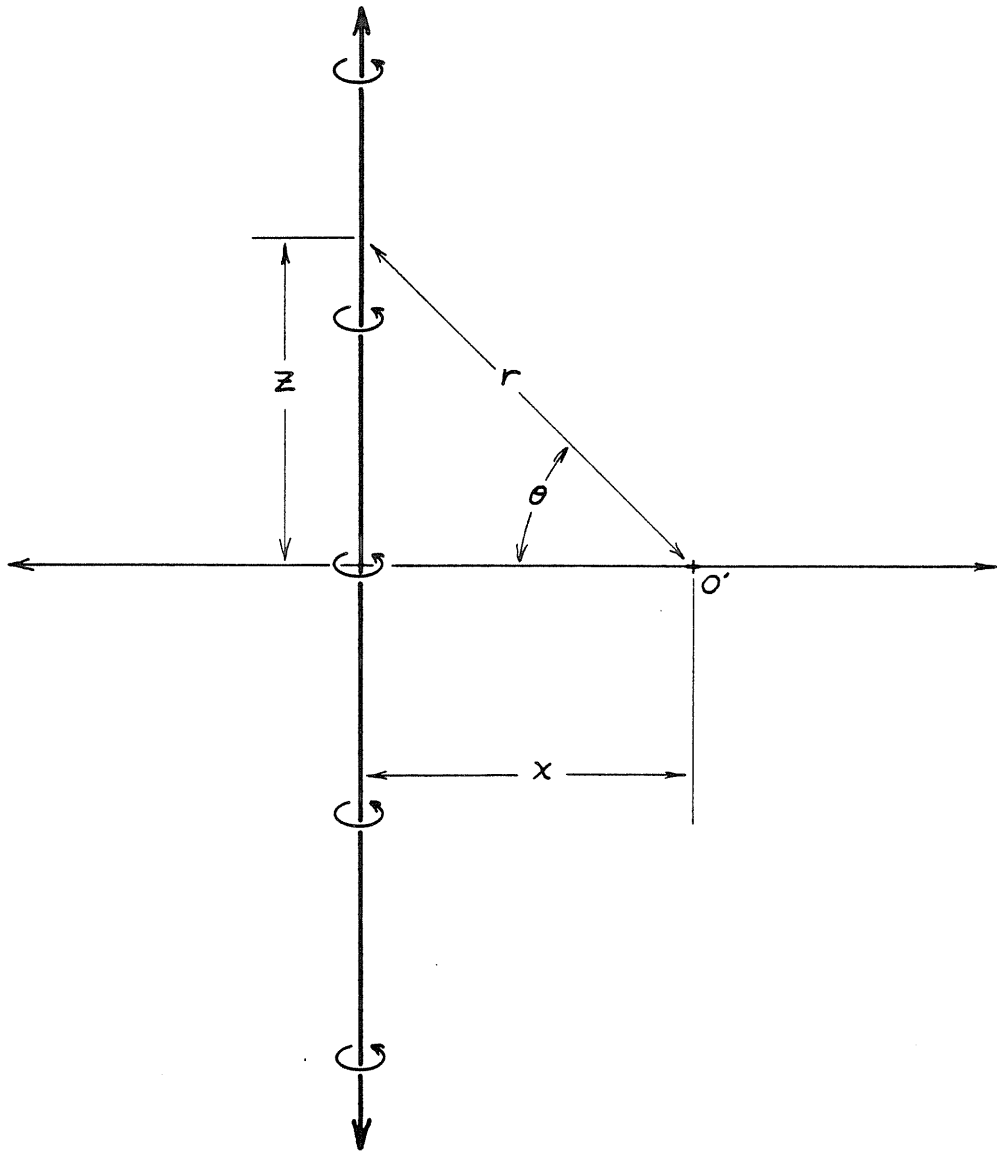

Figure 7.3 To calculate the two-dimensional acoustic field caused by the spiral flame, one imagines the spiral flame occupying the z axis in a three-dimensional region, and an observer at O', a distance x from the spiral flame. The pressure pulse at O' can be obtained by superimposing the pressure pulses from a line of three- dimensional sources distributed along the z axis.

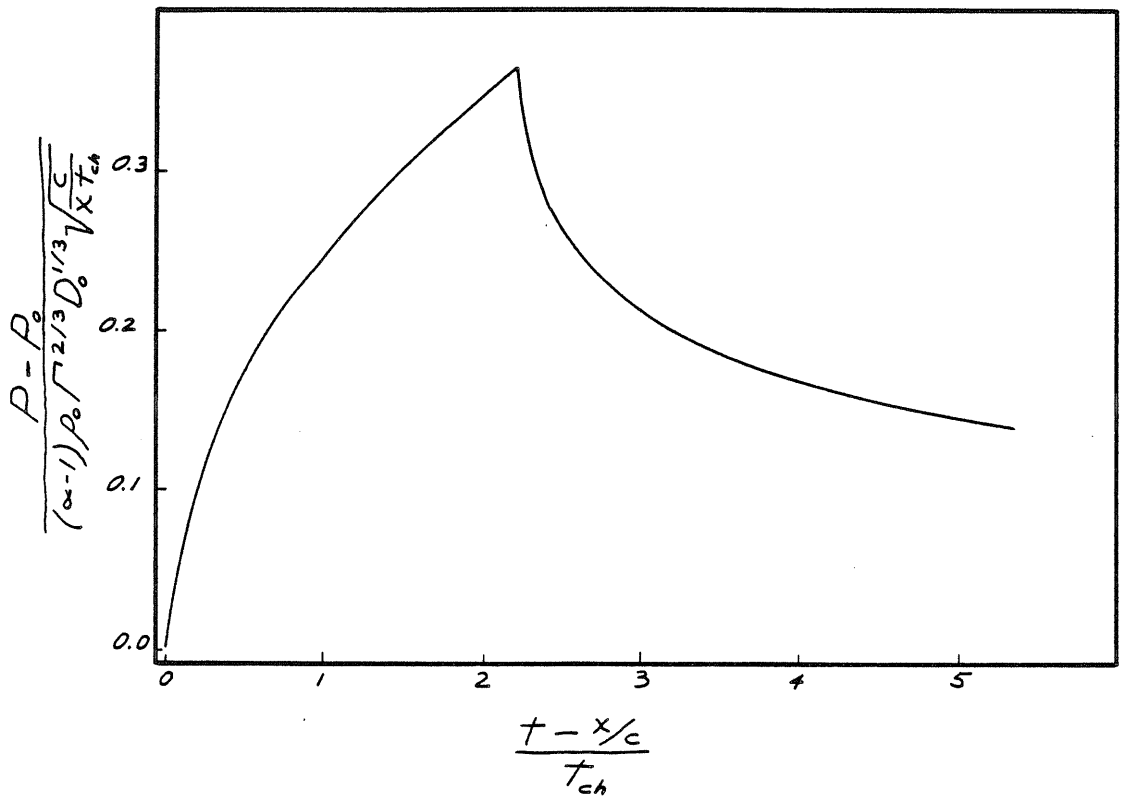

Figure 7.4 The pressure pulse seen at a distance x from the vortex, when x is large enough to lie in the far field, is given by equations 7.8. Here the pressure rise, $P - P_0$, made dimensionless by $(\alpha - 1)\,\rho_0\Gamma^{2/3}D_0^{1/3}\,\sqrt{c/(xt_{ch})}$ is plotted as a function of $(t - x/c)/t_{ch}$.

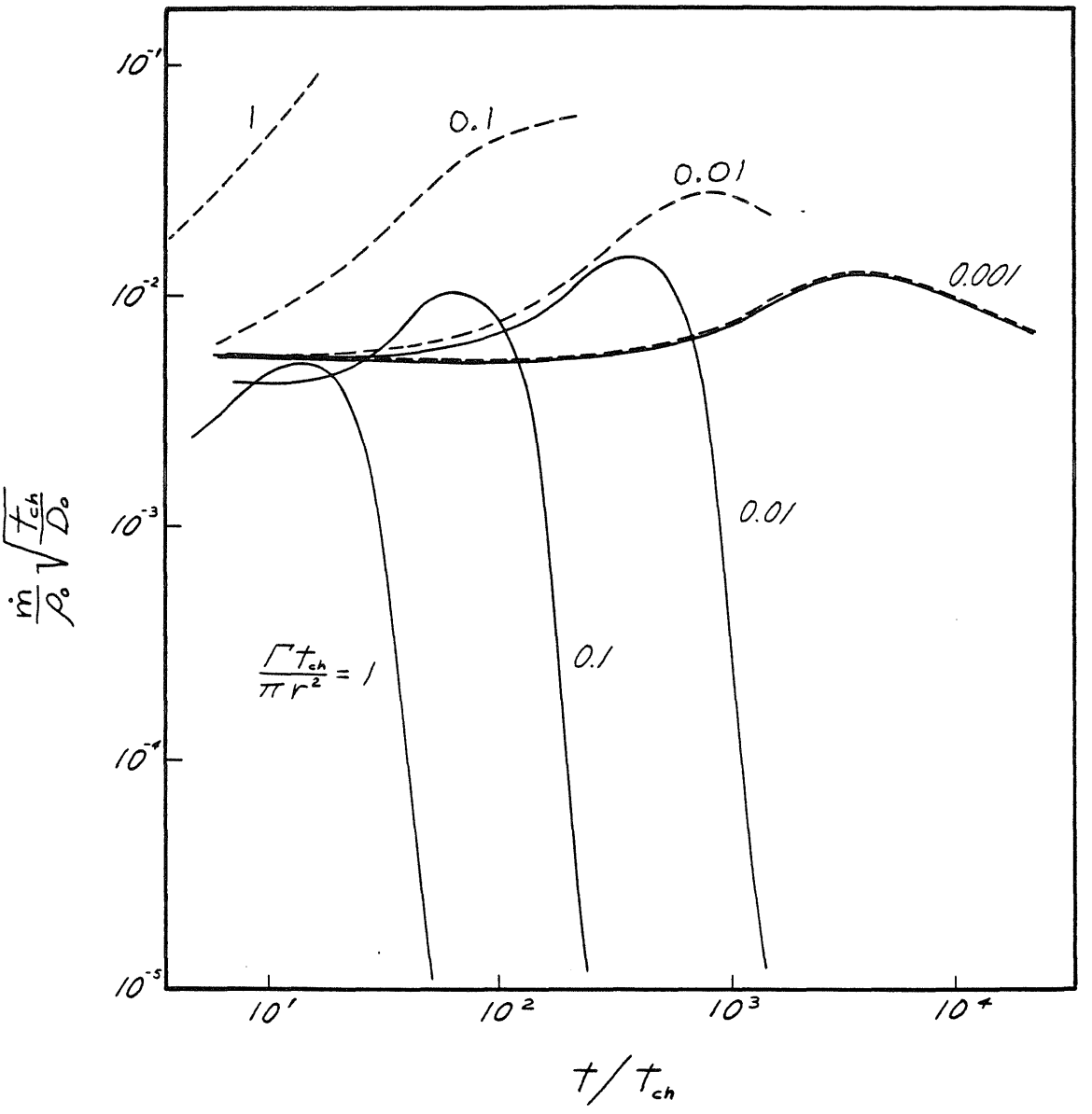

Figure 8.1 The fuel consumption rate per unit flame area is a function of time for a flame which has developed for a time t_0 and is then strained according to equation 2.13. The BLOTTNER results are shown as solid lines, in dimensionless form, with $\dot{m}/\rho_0\sqrt{t_{ch}/D_0}$ plotted against t/t_{ch} for several values of $(\Gamma t_{ch})/(\pi r^2)$. The initial age of the flame, t_0, was equal to $10^4\, t_{ch}$ for all cases. The fuel consumption rates predicted by equation 3.24b are shown as dashed lines.

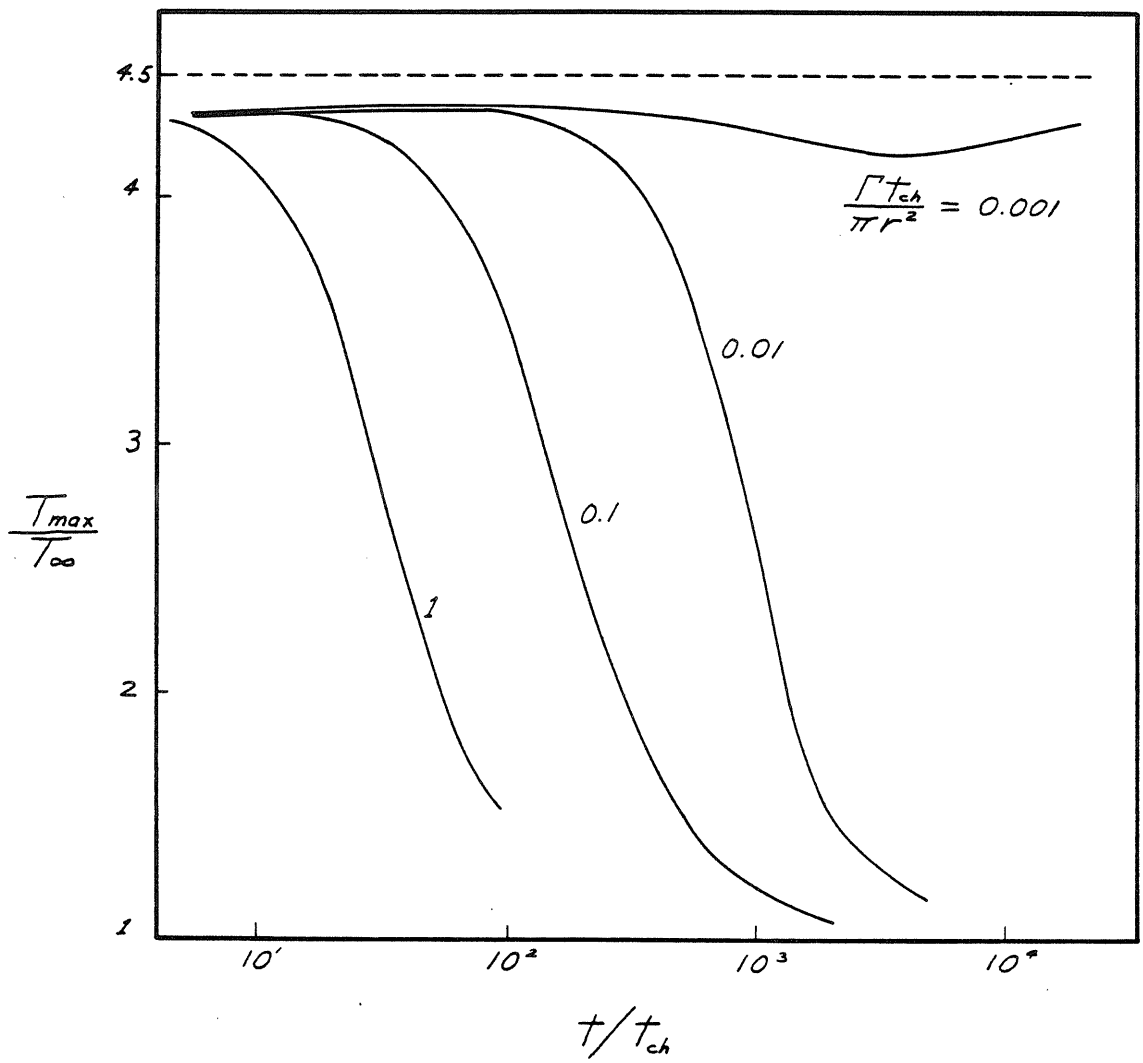

Figure 8.2 Here, the maximum temperature which occurs in the middle of the flame is shown as a function of time. If the Burke-Schumann solution were exactly valid, then T_{max} would be equal to the adiabatic flame temperature, which is $4.5 T_\infty$ in this example.

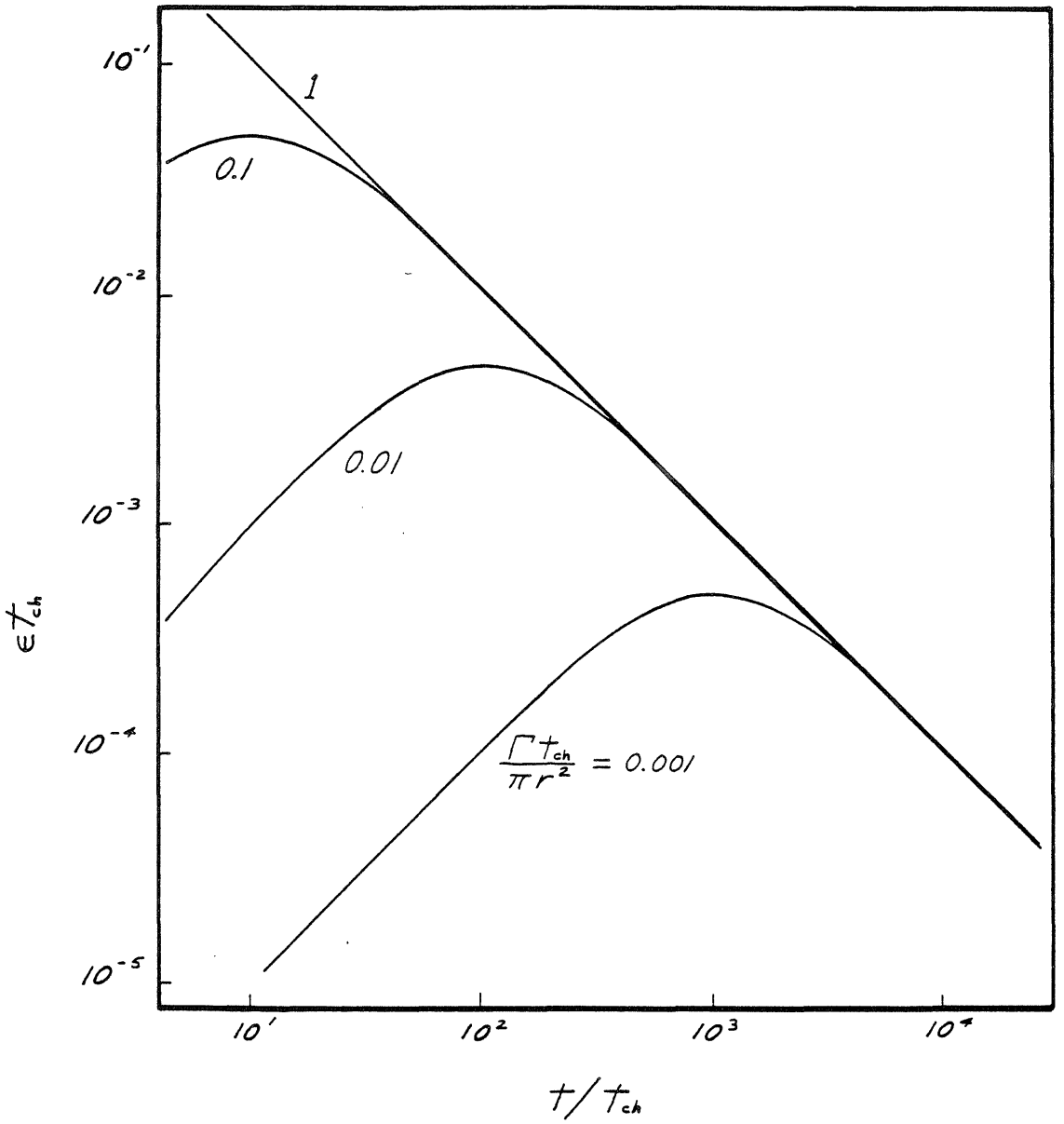

Figure 8.3 The dimensionless strain rate εt_{ch} from equation 2.13 is shown as a function of t/t_{ch}. The BLOTTNER solutions for the strain rates shown here have been given in the previous two figures.

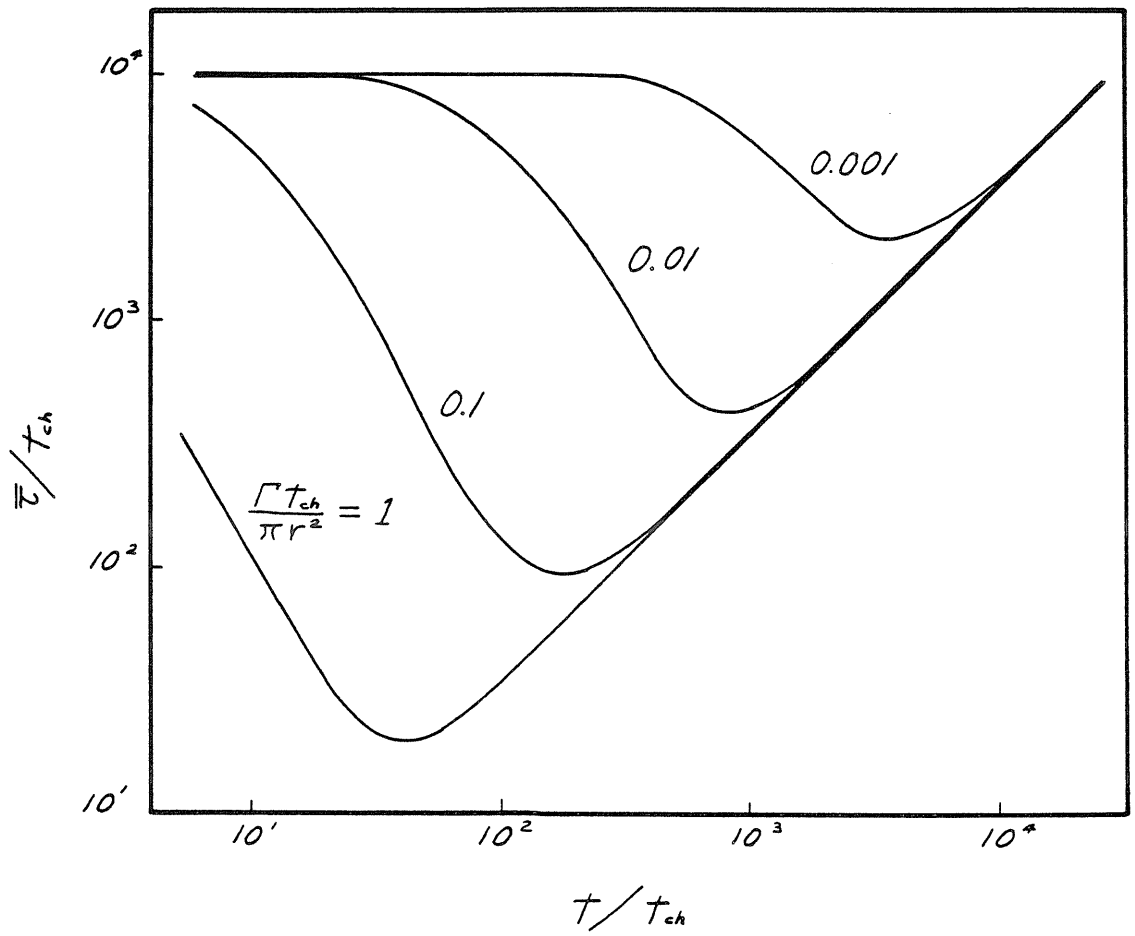

Figure 8.4 For the strain rates shown in the previous figure, equation 8.16 was used to find $\bar{\tau}$ as a function of time. Shown in dimensionless form, $\bar{\tau}/t_{ch}$ is a function of t/t_{ch}.